Technische Universität München
TUM School of Engineering and Design

Development of Comprehensive Methodology for Uncertainty Analyses of Neutron Noise Simulations

Soobeen Yum

Vollständiger Abdruck der von der TUM School of Engineering and Design der Technischen Universität München zur Erlangung des akademischen Grades einer

Doktorin der Ingenieurwissenschaften (Dr.-Ing.)

genehmigten Dissertation.

Vorsitz:	Prof. Dr. Phaedon-Stelios Koutsourelakis
Prüfer der Dissertation:	1. Prof. Dr. Rafael Macián-Juan
	2. Prof. Dr. Christophe Demazière

Die Dissertation wurde am 09.02.2023 bei der Technischen Universität München eingereicht und durch die TUM School of Engineering and Design am 19.10.2023 angenommen.

Acknowledgments

I owe a profound debt of gratitude towards all those who have stood with me and helped to achieve this PhD work. It would not have been possible without all the academic collaborations and moral supports.

- Prof. Dr. Rafael Macián-Juan, I appreciate you giving me an opportunity to work in this chair as a PhD student and for your constant support. Especially the freedom you have given to me encouraged my self-confidence on scientific research.

- Prof. Dr. Christophe Demazière, it was my great pleasure to have worked with you within CORTEX project for last four years. Thank you for all the knowledge you have conveyed and also your hospitality you have shown to me whenever I asked for help, which always made me feel safe.

- I want to thank Dr. Harald Breitkreutz, for being my mentor and your enormous help in preparing all the documents when I started my work in TUM.

- I was very honored to have worked with Dr. Mathieu Hursin, you have always inspired me with your guidance and scientific idea. I appreciate our fruitful discussions we have made almost every week and also your manifold advice. It's no exaggeration to say that my work wouldn't have been this valuable in scientific point of view without your help.

- Prof. Dr. Paolo Vinai and Dr. Antonios Mylonakis, the conversation with you were always pleasant regardless of the topics. Thank you for your kind help whenever I came up with scientific questions, and more importantly, your very good humors!

- I appreciate all the members within CORTEX project where I have learned the power of collaborations. The excellent collaboration with great people has trained me as an independent researcher.

- Special thanks to Prof. Dr. Hojin Park, for letting me question about nuclear physics without hesitation and for your kind and detailed explanation in spite of a time difference between Korea and Germany.

  호진옹 많이 고마워요!

- I also appreciate to all the people in the chair of nuclear technology for making nice atmosphere at work.

- To all my Korean friends from SNU Nuclear Engineering and previous co-workers in KAERI, which are too many to even list their names, I am grateful for all the nice moments we have shared in Seoul and Daejeon which made me today.

- My precious Munich-friends, Peter, Félix, Petter, Sebastian, Zara, Kåre, Mina and Zahra, thank you for every experience we have shared together, you have made my time in Munich so enjoyable.

- To my family, mom and dad, and also my brother, I cannot thank you enough for your unconditional love and supports which always have been the shoulder that I could lean on, and for having shared your wisdom that inspired me to push beyond my limits.

- Finally, Christian, the best friend of my life, thank you so much for coming into my life although it has required you to have immense patience to face all my ups-and-downs. You always raise me up. Now, I can only say, “we made it together”.

Abstract

The interest on neutron noise in the reactors has risen gradually across the nuclear industries, which leads to an increase of related researches. This PhD work is motivated by the fact that there has been little attempt to carry out uncertainty analyses under the neutron noise condition despite of its potential importance on reactor operation.

The main objective of the present PhD research is to establish a comprehensive uncertainty analysis methodology for the modeling of stationary neutron flux oscillations. The methodology includes uncertainty propagation and sensitivity analysis. Both the uncertainty propagation and the sensitivity analysis commonly use a large part of the entire analysis process, from the selection of uncertain parameters to the actual code simulations. The methodology has been structured at a small-sized zero-power reactor and optimized by a series of analyses with various events inducing neutron noise. In order to confirm an applicability of developed methodology and its limitations which need to be improved, the entire processes developed at zero-power reactor were adopted to an analysis of neutron noise at power plant.

The first part of the PhD research is to build a fundamental structure of methodology. This was done at the CROCUS zero-power reactor with considering a hypothetical noise source. This section has an introductory character, with focusing on investigation and discussion of options which can be chosen at each stage.

In the second part, the methodologies established in the previous section have been applied to the analysis of the neutron noise experiments which are conducted at zero-power reactors. This part can be subdivided into two parts by considered reactor, CROCUS and AKR-2. The entire process has been discretized and optimized from its preliminary stage. The entire uncertainty analyses have been made based on actual experimental condition, thus, both quality and

quantity of available reactor data have been improved. Accordingly, the reliability as well as the applicability of obtained results from the analyses have been enhanced. The uncertainty of neutron noise was calculated at installed detector locations through the uncertainty propagation. The sensitivity analysis has identified the most influential input parameter to an output uncertainty qualitatively and quantitatively.

The third part involves a sensitivity analysis of neutron noise at power plant (Swiss 3-loop Konvoi reactor) with adopting the methodology developed and tested at small-sized zero-power reactors. It was assumed that the neutron noise was induced by one fuel assembly vibration. The sensitivity analysis was repeated with identical processes in three different core conditions (i.e., fuel loading pattern and fuel enrichment), in order to investigate the effect of core condition to the result of sensitivity analysis. As a result, the pre-developed methodology was confirmed as being applicable to a case at a power plant, and the main contributors to the neutron noise were identified properly at a level of preliminary research.

The entire processes and outcomes of this PhD work are valuable since they provide general information on how to perform the uncertainty analyses for neutron noise simulations, as well as quantitative estimates of the computational uncertainty required for the validation of the computer programs under development for the simulation of neutron noise.

Contents

List of Figures

List of Tables

List of Acronyms

AKR-2	Ausbildungskernreaktor 2
APSD	Auto-Power Spectral Density
ARI	All Rods In
ARO	All Rods Out
BEPU	Best Estimate Plus Uncertainty
BOC	Beginning Of Cycle
CFR	Code of Federal Regulation
CIAU	Code with capability of Internal Assessment of Uncertainty
CIC	Compensated Ion Chamber
COLIBRI	CROCUS Oscillator for Lateral Increase Between u-metal Rods and Inner zone
CORTEX	Core Monitoring Techniques and Experimental Validation and Demonstration
CPSD	Cross-Power Spectral Density
CSAU	Code Scaling, Applicability, and Uncertainty
DTU	Technical University of Denmark

EOC	End Of Cycle
EPFL	École Polytechnique Fédérale de Lausanne
FA	Fuel Assembly
FC	Fission Chamber
FP	Full Power
GRS	Gesellschaft für Anlagen und Reaktorsicherheit
HFIR	High Flux Isotope Reactor
KKG	Kernkraftwerk Gösgen
KKU	Kernkraftwerk Unterweser
LARS	Least Angle Regression Selection
LRZ	Leibniz Supercomputing Centre
MATLAB	MATtrix LABoratory
MOC	Middle Of Cycle
MSE	Mean Squared Error
NUSS	Nuclear data Uncertainty Stochastic Sampling
OAT	One At a Time
ORR	Oak Ridge National Laboratory Research Reactor
PC	Proportional Counters

PCC Pearson Correlation Coefficient

PCE Polynomial Chaos Expansions

PC-Kriging Polynomial Chaos Expansions-Kriging

PDF Probability Density Function

PSI Paul Scherrer Institute

PWR Pressurized Water Reactor

QoI Quantity of Interest

SA Sensitivity Analysis

SCC Spearman Correlation Coefficient

SI Sensitivity Index

SPCC Spearman's Partial Correlation Coefficient

SPND Self-Powered Neutron Detector

SRS Simple Random Sampling

TUD Technical University of Dresden

UC Uncertainty Characterization

UMAE Uncertainty Methodology based upon Accuracy Extrapolation

UP Uncertainty Propagation

VCM Variance-Covariance Matrix

ZPTF Zero-Power reactor Transfer Function

Chapter 1

Introduction

1.1 Backgrounds

Since USA Code of Federal Regulation (CFR) allowed from 10 CFR 50.46 either to use a best estimate code plus identification and quantification of uncertainties, or the conservative option using conservative computer code models listed in Appendix K of the CFR, Title 10, Part 50, the interest on Best Estimate Plus Uncertainty (BEPU) has been increased gradually across the nuclear field. The uncertainty analyses associated with BEPU approach is mainly composed of two subsections, uncertainty propagation and sensitivity analysis. The aim of the uncertainty propagation is to identify and quantify all potentially important uncertain parameters. Through the computer code calculations, the pre-identified uncertainty parameters are propagated, and this propagation results in the probability distributions and ranges for the code results. The sensitivity analysis is the way to evaluate sensitivity measures of the importance of parameter uncertainties for the uncertainties of the results. This information provides the guidance as to where to improve the state of knowledge to reduce the output uncertainties most effectively, or where to improve the modeling of the computer code [1].

Small, stationary neutron flux fluctuations around the expected mean value are known as neutron noise. The need for more extensive research on the neutron noise behavior has arisen in the past few years after unexpected evolution of neutron noise was found in several European power plants. Neutronic noise with

magnitudes of up to 10 % of the reactor power have been observed in some pressurized water reactors (PWRs) in Europe. In December 2010, the German PWR KKU (Kernkraftwerk Unterweser) went through a sudden increase of the measured neutron flux signal corresponding to 108 %FP (Full Power) and this activated the reactor scram [2]. Likewise, the Spanish PWR Trillo had to be operated under 93 %FP condition to avoid the actuation of the reactor trip by the neutron noise [3]. These examples represent a clear influence of neutron noise on the plant operations. In this context, the CORTEX (Core Monitoring Techniques and Experimental Validation and Demonstration) project was launched in 2017 in the framework of the EU-Program Horizon 2020 [4]. The main aim of CORTEX was to address these challenges by developing an innovative core monitoring technique that allows detecting anomalies in nuclear reactors. The technique is mainly based on using the inherent fluctuations in the neutron flux recorded by in-core and ex-core instrumentation, from which the anomalies can be differentiated depending on their type, location, and physical characteristics. This unfolding is performed using machine learning, for which the training and validation data are provided by simulations of the neutron noise induced by postulated anomalies. In order to investigate the neutron noise behavior under the various conditions more precisely, noise simulators relying on different computational schemes were developed within the framework of the CORTEX project. Accordingly, a series of uncertainty analyses are required to support the validation of the newly developed simulators.

There have been numerous investigations on uncertainty analyses for the nuclear reactor physics applications including criticality and burnup calculations as well as reactor transient (mainly safety related abnormal conditions) calculations [5-11], by using dedicated modules and tools such as XSUSA [5], NUDUNA [6], TMC [12], SANDY [13], SAMPLER (which is available with SCALE 6.2) [14] and SHARK-X [15]. However, there has been little attempt [16] to carry out uncertainty analyses under specific neutron noise conditions (the condition belongs to the normal operation of the reactor) in spite of its potential importance on the reactor operation.

In this respect, CORTEX project has involved the uncertainty analyses at various neutron noise conditions as one of the tasks, which corresponds to a main theme

of this PhD thesis. Thanks to the intensive collaborations among the counter partners in the project, it was encouraged to consider various reactors with their design/operational information and calculation models in different codes, and the experimental data obtained from neutron noise experiments at each reactor. Throughout the PhD work, the comprehensive methodology of uncertainty analyses is developed and well-structured at zero-power reactors, by using a noise simulator developed within CORTEX project. Additionally, an uncertainty analysis at a commercial power plant is conducted, proving that the developed methodology is not confined to an analysis at zero-power reactors.

1.2 Objectives

The main objective is to establish a comprehensive methodology of uncertainty analyses for the modeling of stationary neutron flux oscillations. This can be achieved by two sub tasks. First, a fundamental methodology of uncertainty analyses is established considering one hypothetical event, which induces neutron noise, at a zero-power reactor. Second, the methodology is modified and optimized by being adopted to various conditions (reactor types and noise sources) in order to guarantee its future applicability. The uncertainty analyses here involve the uncertainty propagation and the sensitivity analysis. It should be noted that the current work is not about noise techniques in reactors but focuses on the simulation of the response of a nuclear system to various noise sources.

The developed methodology will give an appropriate guideline how to conduct the uncertainty analyses under the various neutron flux oscillating conditions. This guideline involves detailed descriptions on necessary procedures from a preparation of the analysis to an interpretation of the simulation results. Furthermore, the entire uncertainty analyses have been made based on the parameters with their actual or most realistic uncertainties under the given condition, thus, assure a high reliability as well as an applicability of the outcomes.

The uncertainty quantification in this study is made by a stochastic sampling-based method, that is, the uncertainty of the neutron noise is calculated by simultaneous perturbations of all input uncertainties. The obtained neutron noise

uncertainties at the installed detector locations can be compared to the relevant uncertainties from experiments for a validation of noise simulator. The following sensitivity analysis is used to determine the input parameters responsible for the output uncertainties, and it eventually helps to reduce uncertainties of neutron noise efficiently if necessary.

1.3 Research Outlines

The works carried out within this PhD thesis consist of six main chapters—an introduction, four chapters with analyses at different noise sources and reactor types, and conclusion.

Chapter 1 provides an overview of the thesis and all necessary backgrounds. The reactors and events inducing neutron noise, which are considered for the analyses in the thesis, are introduced in connection with noise simulations. A general explanation about the available approaches for uncertainty propagation and sensitivity analysis is made, and this is followed by an introduction about the software and tools used for data generation and simulation.

The second part (Chapter 2) aims to build a fundamental structure of uncertainty propagation and sensitivity analysis under a neutron noise condition at CROCUS zero-power reactor [17]. A hypothetical event from a category of "absorber of variable strength" is designed arbitrarily as a target event, due to its simplicity on modeling. This event corresponds to an oscillation of UO_2 fuel density between $100\,\%$ and $120\,\%$, at a frequency of $1\,\mathrm{Hz}$. The behavior of neutron noise is simulated using a noise simulator, CORE SIM [18]. This chapter involves an instruction of analyses with stepwise approach that introduces detailed objective and tasks at each stage. Accordingly, various options in the analysis (e.g., approaches to quantify output uncertainty, sensitivity measures) are investigated and their pros and cons are discussed to identify the most relevant one for the further analyses.

In the following two chapters (Chapter 3 and Chapter 4), the methodologies established in the previous chapter are applied to the analysis of the neutron noise

experiments which are conducted at zero-power reactors, CROCUS and AKR-2 [17, 19]. Both reactors retain their own experimental facilities specialized to conduct various neutron noise experiments, thus, their relevant experiments are considered as target events. The simulation of neutron noise is carried out with CORE SIM+ [20], which capitalizes former CORE SIM tool. In Chapter 3, a series of uncertainty analyses are performed when a neutron noise is induced by fuel rods vibration at CROCUS reactor. The neutron noise is induced by simultaneous oscillation of 18 metallic uranium fuel rods with oscillating amplitude and frequency of 2 mm and 1 Hz, respectively. Most procedures of the analysis are based on the steps structured in previous chapter. However, it is more optimized and concretized by enhancing quantity and quality of available reactor information (i.e., nuclear data uncertainties and uncertainties related to a description of the noise source) and incorporating actual experimental condition. By adopting stochastic sampling-based method, an optimum solution to perturb all input uncertainties simultaneously is discussed. The inclusion of nuclear data into the analysis brings about an issue of "large number of correlated parameters" especially for sensitivity analysis. Thus, all input parameters are grouped according to their similarities, and a calculation scheme using multiple correlation coefficient is adopted. A following chapter (Chapter 4) deals with neutron noises at AKR-2 reactor, where the considered noise source are "rotating absorber" and "vibrating absorber". The analyses process as well as the considered input parameters are similar to those in Chapter 3. However, due to a complexity in AKR-2 reactor model using CORE SIM+, a computational cost becomes more expensive than CROCUS reactor model, resulting in a limited number of code executions. Accordingly, the analyses that demand large number of code calculation to represent a population behavior (among the analyses carried out in Chapter 3) are excluded in this chapter, but only the simplified approaches are selected for the analyses. In Chapter 3 and Chapter 4, output data obtained from noise simulation are converted into specific quantity of interest (QoI), which are determined within CORTEX project. This conversion is made to synchronize various outputs (neutron noise) from both experiments and simulations into one unified measure for the validation process of neutron noise simulator. Through the analysis with actual experiments carried out at two zero-power reactors, the methodology which is developed in the first chapter is modified and optimized properly.

The developed and optimized methodology at zero-power reactors is adopted to an analysis of neutron noise at a power plant in Chapter 5. The study is limited to the sensitivity analysis and is carried out under "fuel assembly (FA) vibration" at Swiss 3-loop pre-Konvoi reactor. The analysis is repeated at three different core conditions with respect to fuel burnups and fuel loading patterns, while the considered input parameters at each condition remain identical. Accordingly, an effect of core condition to a sensitivity of input parameter is investigated. This chapter is made to confirm an applicability of developed methodology to a power plant and also to figure out remaining limitations and future works.

The last chapter (Chapter 6) summarizes the works performed in this PhD thesis and suggests the future tasks based on the confirmed limitations in analyses.

1.4 Reactors of Interest

1.4.1 CROCUS Zero-Power Reactor

CROCUS is a research reactor at École Polytechnique Fédérale de Lausanne (EPFL), a research institute and university in Lausanne, Switzerland [17]. CROCUS is an experimental zero-power reactor, uranium fueled, and water moderated, mainly dedicated to teaching radiation and reactor physics. It is licensed for operating at $100\,\mathrm{W}$, or a neutron flux of $\sim 2.5 \times 10^{9}\,\mathrm{cm^{-2} \cdot s^{-1}}$ at the core center. Power is controlled either by changing the core's water level using a spillway, or by two B_4C absorber control rods, with an accuracy of $\pm 0.1\,\mathrm{mm}$ (equivalent to approximately $\pm 4\,\mathrm{pcm}$) and $\pm 1\,\mathrm{mm}$, respectively. CROCUS operates at room temperature using a controlled water loop with secondary and tertiary circuits, two heat exchangers and an electrical heater.

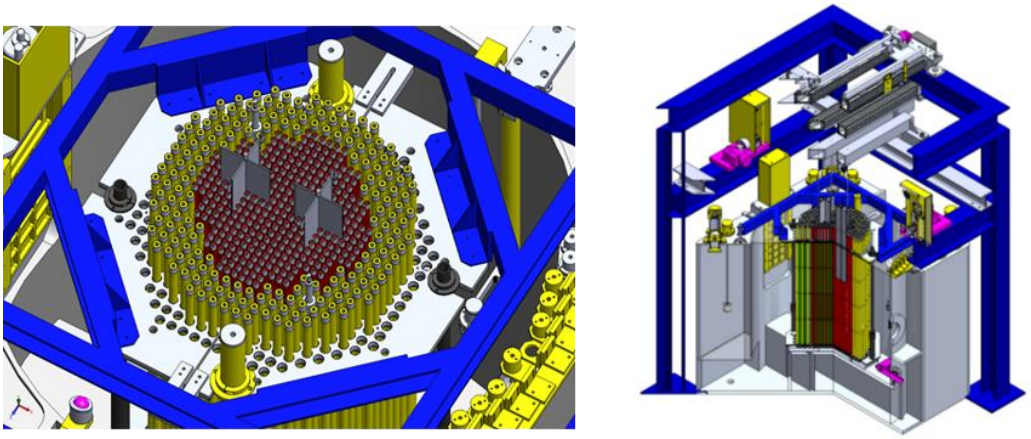

Figure 1.1: Top view of CROCUS core with fuel rods and systems such as cruciform safety blade and control rods (left), cross-section view of the full reactor with core and structures (right)

The core is located in an aluminum vessel of 130 cm diameter and 1.2 cm thickness, and its active part has the approximate shape of a cylinder of about 60 cm in diameter and 1 m in height, as illustrated in Figure 1.1 [17]. It consists of two interlocked fuel zones with square lattices of different pitches: an inner zone of 336 UO_2 rods and an outer zone of 172 U_{metal} rods. The six independent safety systems consist of two cruciform-shaped cadmium blades and four expansion tanks. The safety blades are held by electromagnets for top to bottom gravity insertion. The expansion tanks trap air when valves are closed, allowing a fast drop of the water level when opened. Any of these systems allow shutdown within less than a second.

Since CROCUS became the only zero-power reactor in Switzerland in 2011, Paul Scherrer Institute (PSI) and EPFL agreed upon developing new research experimental programs in the CROCUS reactor. In 2015, an extensive review of possible experiments was carried out and resulted in the selection of three experimental programs [22].

The first one aims for the investigation of mechanical noise induced by fuel rod vibration using the COLIBRI in-core device (CROCUS Oscillator for Lateral Increase Between u-metal Rods and Inner zone). This experiment is going to be

introduced as one of the target events in this study. The details of experiment are explained in Chapter 1.5.2.2.

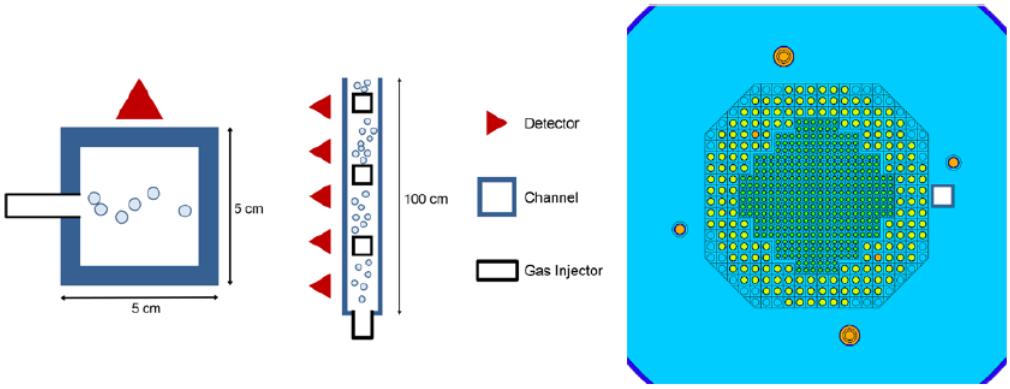

Figure 1.2: VOID experiment: top and side view of bubbling channel (left) and the location in the reflector of the CROCUS reactor (right)

The second one is VOID experiment. A main objective is to reconstruct axial void and velocity profiles in BWR through neutron noise measurements of in-core detectors. The experimental setup is depicted in Figure 1.2 [22].

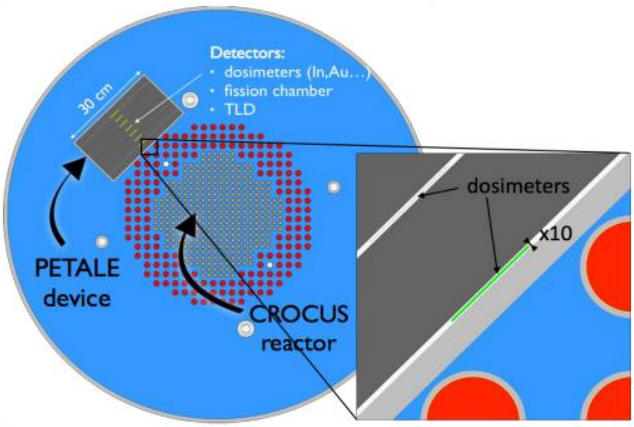

Figure 1.3: Illustration of the PETALE experimental set up

The last one is PETALE experimental program which is planned to be carried out at the CROCUS reactor. This program aims at measuring neutron penetration

in slabs made of materials composing typical LWR reactor pressure vessel. A sketch of the experimental configuration is illustrated in Figure 1.3 [23].

1.4.2 AKR-2 Zero-Power Reactor

The training and research reactor AKR-2 (from the German Ausbildungskernreaktor) has been operated at the Technical University of Dresden (TUD) since 2005 [24]. The reactor is a thermal, homogeneous, solid moderated zero-power reactor with maximum continuous (thermal) power of 2 W. This extremely low nuclear power allows effects of temperature, fuel burnup, formation of nuclear waste, activation of structural materials, Xe-poisoning and others to be neglected. The reactor is the last nuclear facility in Germany to have received an operating license.

Precursor of the AKR-2 was the AKR-1. The AKR-1 training and research reactor of the TUD was put into operation in 1978 based on the concept of the proven training reactor SUR-100 from SIEMENS company. For more than 25 years, the AKR-1 was successfully used for training and education of students, for nuclear research projects, and as an information center for the public.

The design of the reactor is shown in Figure 1.4 and Figure 1.9 [21, 24]. The cylindrical core has a diameter of 250 mm and a critical height of 275 mm. The disk-shaped fuel elements consist of a homogeneous dispersion of polythene and uranium oxide (19.8 % enriched in ^{235}U, O/U ratio 2.27). The core is completely surrounded by a graphite reflector.

For safety reasons, the core consists of two separable sections. The fuel elements of each section are enclosed in a hermetically sealed aluminum container. A second, larger gas-tight reactor tank encloses both, core sections and parts of the reflector. The pressure inside the reactor tank is lowered by (8 ... 18) kPa compared to the ambient atmospheric pressure. This subatmospheric pressure barrier prevents an uncontrolled leakage of radioactive fission products. The reactor is controlled by the three cadmium absorber plates. These plates are designed as combined control and safety rods.

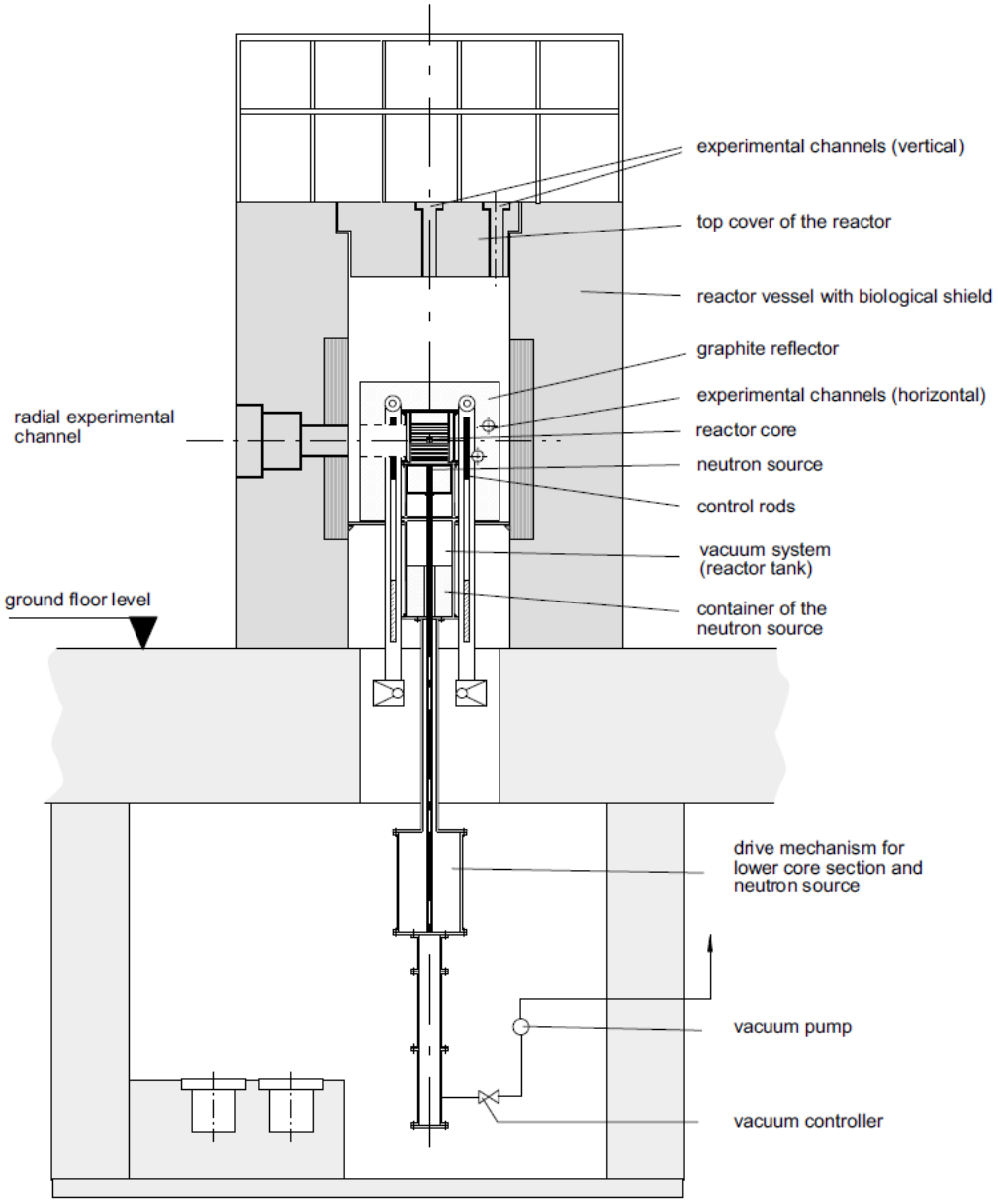

Figure 1.4: Vertical cross-section of the AKR-2

There are total four horizontal and two vertical experimental channels with different diameters and shapes. These channels provide adequate in-pile irradiation volume with different neutron spectra. The experiments at the AKR-2 reactor consist in introducing two different sources of periodic reactivity perturbations

that induce neutron flux oscillations [21]. The first experiment corresponds to a rotating neutron absorber that has a varying absorption cross-section with respect to the rotation angle. The second type of perturbation is generated by a linearly oscillating absorber that is moved back and forth inside the reactor core (vibrating absorber). The details of experiments are introduced in Chapter 1.5.1 and Chapter 1.5.3, respectively.

1.4.3 Swiss 3-Loop Pre-Konvoi Reactor

The Swiss 3-loop Pre-Konvoi reactor corresponds to Gösgen Nuclear Power Plant (official name is "Kernkraftwerk Gösgen (KKG)"), which is located in the Däniken municipality, in Switzerland. It is operated by the ad hoc society Kernkraftwerk Gösgen-Däniken AG, which started its operation in 1979 [25]. The reactor is licensed to operate at a nominal thermal power of 3002 MW.

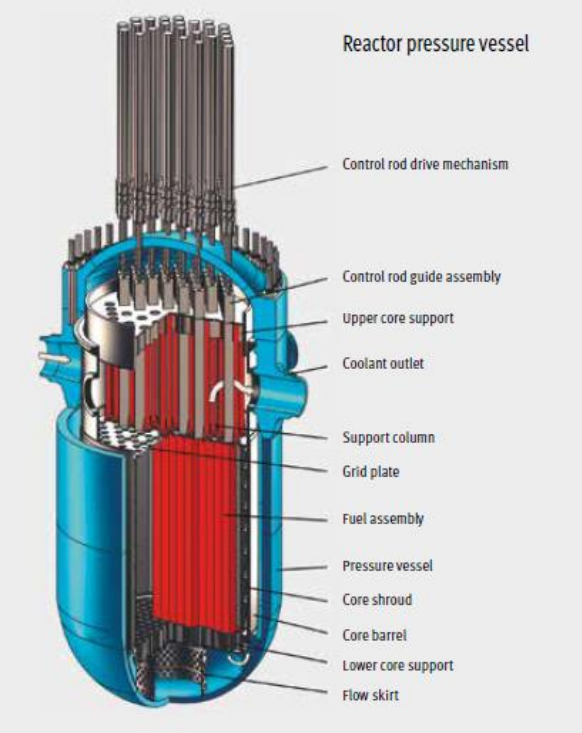

Figure 1.5: The composition of reactor pressure vessel in KKG [25]

The KKG possess a pressurized water reactor delivered by German Kraftwerk Union AG. It contains 177 fuel assemblies, while 48 of them are equipped with control assemblies. Each fuel assembly contains 205 fuel rods, which consist of enriched UO_2 with fissile ^{235}U or MOX fuel elements (uranium-plutonium mixed oxide fuel elements) with a proportion of fissile plutonium. However, MOX fuel has not been used since 2012. Inside each fuel rod, a column of fuel pellets is enclosed in a gas-tight and pressure-resistant-welded Zircaloy cladding tube. The control rods are activated by electromagnetic ratchet jack drive units which are located on the pressure vessel closure head. To adjust the reactor power, the control rods can be moved into the reactor core to a greater or lesser depth. When a fast reactor shutdown is necessary, all the rods are fully inserted into the reactor core. This is done by switching off the current in the electromagnetic restraining coils.

The inner axial flux distribution of KKG is monitored via six axially equally distributed in-core Self-Powered Neutron Detectors (SPNDs), while the four radial ex-core channels contain two compensated ionization chambers, i.e., upper and lower core regions (see Figure 1.6) [26].

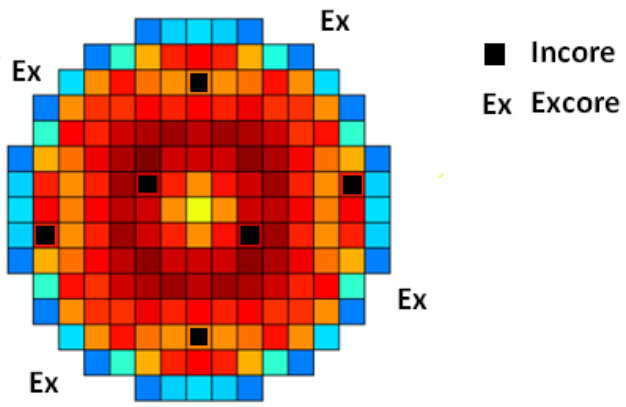

Figure 1.6: Schematic representation of the 3-Loop KKG core and the radial positions of the in-core and ex-core neutron flux detectors

1.5 Neutron Noise

The reactor noise is the neutron fluctuations which are induced by the fluctuations or oscillations of the reactor properties, e.g., displacement of core components, temperature, or density variations. These kinds of reactor composition changings result in the changes of the corresponding cross-sections. And the cross-sections are coefficients of the pertinent transport or diffusion equations. The identified sources of neutron noise, which are especially selected for the further analyses, are discussed in this chapter.

1.5.1 Absorber of Variable Strength

1.5.1.1 Description of Scenario

Absorber of variable strength can be represented as fluctuations in the macroscopic absorption cross-sections at a given fixed location r_0 and the corresponding noise source expressed as,

$$\delta\sum_a(r,\omega) = \gamma(\omega)\delta(r - r_0), \tag{1.1}$$

where $\gamma(\omega)$ is the noise source strength, which might be frequency-dependent in the most general case. Even though the terminology here refers to absorbers, these types of noise sources encompass all kinds of cross-sections, that is, absorption, fission, and scattering [27]. This scenario is particularly important since it constitutes the basis for estimating the reactor Green's function, on which the modeling of the effect of all other types of noise sources can be carried out [28]. Since the mathematical treatment as well as modeling of this case are very straightforward, absorber of variable strength is regarded as simplest noise source one can model.

1.5.1.2 Relevant Experimental Program

The experimental facility which is specialized to generate two different sources of periodic reactivity perturbations inducing neutron flux oscillations is available at the AKR-2 reactor. The first type of perturbation is generated by a rotating neutron absorber that has a varying absorption cross-section with respect to the rotation angle, which is explained hereafter, while the second one by a linearly oscillating absorber that is moved back and forth inside the reactor core. The second perturbation will be discussed in Chapter 1.5.3.2. The tangential line of channel 3-4 as illustrated in Figure 1.7 is the rotating absorber shaft in AKR-2 reactor. In order to maximize the perturbation induced to the neutron flux, it is located where the gradient of the neutron flux is maximum. The absorber which is rotating is natural cadmium sheet and has dimensions of $25\ \text{cm} \times 2\ \text{cm} \times 0.02\ \text{cm}$. Figure 1.8 shows two section views of the rotating absorber (AA and BB) and the geometrical details.

In the first experimental campaign, the measurements were taken with varying the rotation speed which corresponds to the rotation frequency between $0.2 \sim 2$ Hz.

Within the framework of CORTEX project, total two experimental campaigns have been carried out in the AKR-2 reactor. The first experimental campaign in the AKR-2 reactor took place from 6 to 14 March 2018 [29] and the second experimental campaign was held from 6 to 10 July 2020 [30].

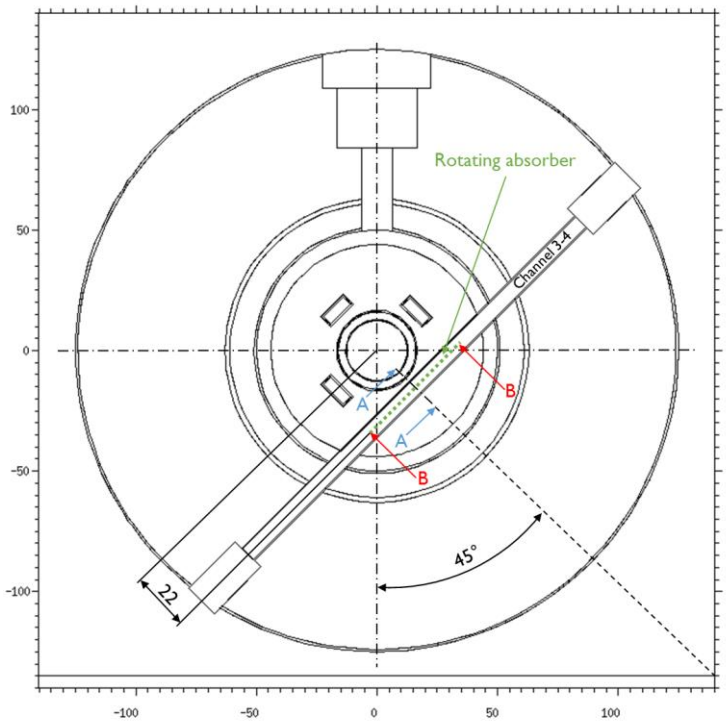

Figure 1.7: Absorber location in rotating absorber experiments [29]

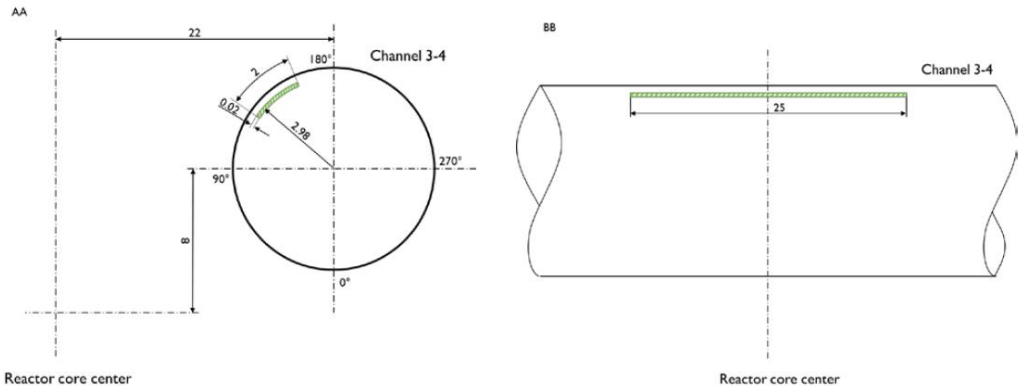

Figure 1.8: Geometrical description of rotating absorber [29]. Cross (left) and longitudinal (right) views, units in cm.

Compared with the first campaign, some advancements were realized, mainly based on the feedback of the modelers (simulator developers and analyzers

within CORTEX project). The main changes in second experimental campaign are as follows [30].

1) Two more detectors were in operation, with one fission chamber and the three miniature scintillators places closer to the center of the reactor.
2) A new high precision linear motor axis was used as a vibrating absorber, allowing for a sinusoidal driving profile with a more flexible amplitude.
3) The reactivity input was lowered by the use of indium foils as absorbing material instead of the cadmium foils used in the first experimental campaign.
4) The experimental channel 7 (see Figure 1.9) was blocked with polyethylene to facilitate the modeling with diffusion codes.
5) Two new data acquisition systems were used to record parts of the data.

Figure 1.9 and Figure 1.10 show the experimental setup of detectors in AKR-2 reactor in first and second experimental campaigns, respectively.

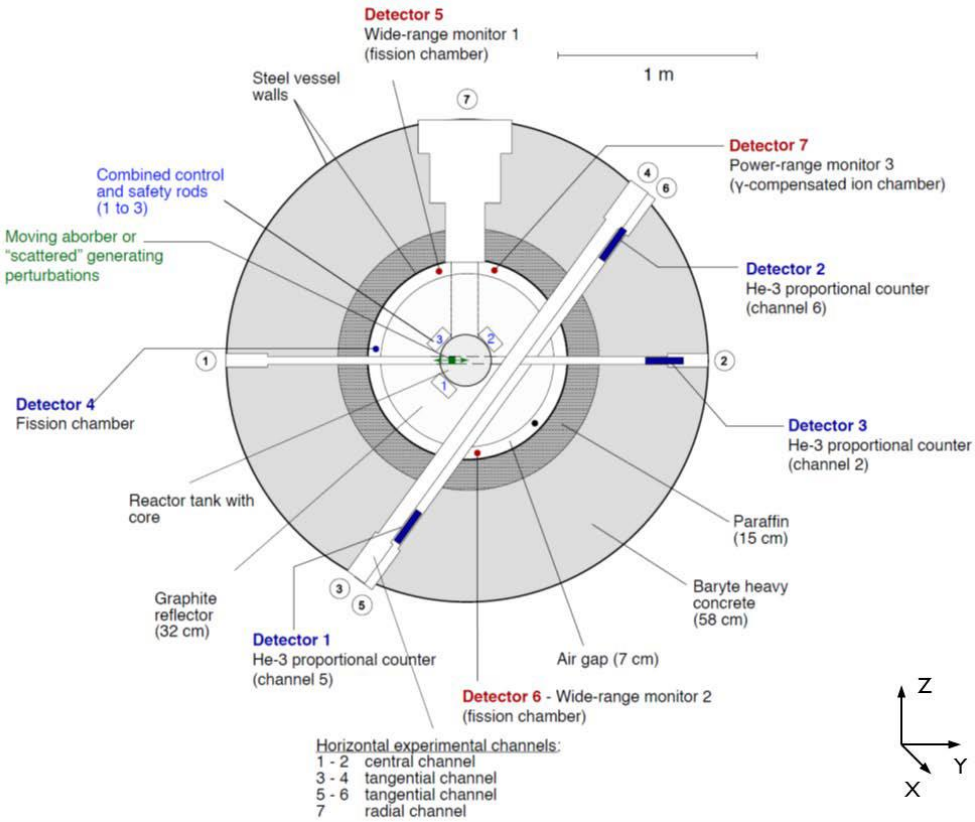

Figure 1.9: Horizontal cross-section of the AKR-2 reactor at core level [29]

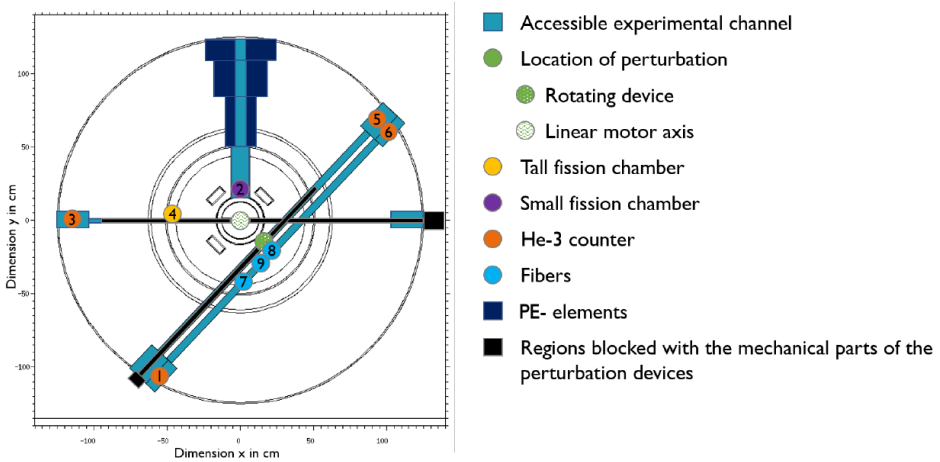

Figure 1.10: Overview of the setup of the second experimental campaign [30]

1.5.2 Fuel Rods Vibration

1.5.2.1 Description of Scenario

In the scenario "fuel rods vibration", a fuel assembly is assumed to vibrate in the $x-$ and/or $y-$ direction (radial direction) of the reactor core. Here, the three well-known vibrations modes can be included [28]: cantilevered beam, simply supported on both sides and cantilevered beam and simply supported.

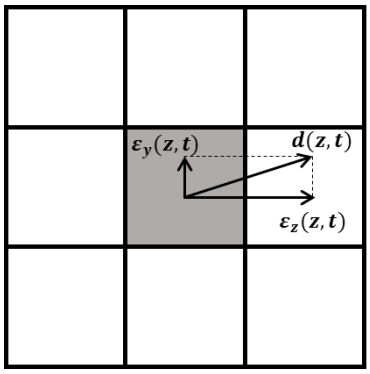

Figure 1.11: Decomposition of the lateral displacement of a vibrating fuel assembly into $x-$ component and $y-$ component

At a given axial level z, the displacement $d(z,t)$ can be decomposed as a displacement $\varepsilon_x(z,t)$ along the $x-$ direction only and a displacement $\varepsilon_y(z,t)$ along the $y-$ direction only, as shown in Figure 1.11 [28]. The squares in the figure represent the fuel assemblies, while the vibrating fuel assembly is described in grey. When considering one direction at a time, the movement of the vibrating fuel assembly can be described in the following manner. The vibration of one fuel assembly along the $x-$ direction can be illustrated as Figure 1.12, with three homogeneous regions due to the homogenization of the macroscopic cross-sections in CORE SIM (CORE SIM+) modeling.

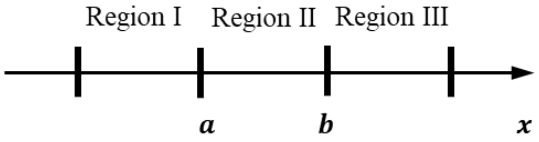

Figure 1.12: Representation of three neighboring fuel assemblies with respect to the $x-$ direction [28, 31]

Considering for the time being Region II and Region III, the spatial distribution of the static macroscopic cross-section for the reaction type α in the energy group g can be represented as,

$$\sum_{\alpha,g}^{x}(x) = [1 - \Theta(x-b)]\sum_{\alpha,g,II} + \Theta(x-b)\sum_{\alpha,g,III}, \tag{1.2}$$

where $\Theta(x-b)$ is the Heaviside function, i.e.,

$$\begin{cases} \Theta(x-b) = 0 \; if \; x < b \\ \Theta(x-b) = 1 \; if \; x \geq b. \end{cases} \tag{1.3}$$

In Equation (1.2), $\sum_{\alpha,g,II}$ represents the macroscopic cross-section of region II, whereas $\sum_{\alpha,g,III}$ represents the macroscopic cross-section of region III. In case of vibrations of the fuel assembly II with respect to the fuel assembly III with a displacement $\varepsilon_x(z,t)$, the position of the boundary between region II and III is time-dependent, and is given as,

$$b(z,t) = b_0 + \varepsilon_x(z,t), \tag{1.4}$$

where b_0 represents the static position of the boundary between regions II and III. To find a right format of the noise source in the frequency-domain corresponding to fluctuations of the position of the boundary between the regions II and III, we put the Equation (1.4) into Equation (1.2), use a first-order Taylor expansion and consider the static macroscopic cross-section (when $\varepsilon_x(z,t) = 0$) and change the expression into frequency-domain. The final expression for the noise source becomes as below.

$$\delta\sum_{\alpha,g}^{x}(x,z,\omega) = \varepsilon_x(z,\omega)\delta(x-b_0)\left[\sum_{\alpha,g,II} - \sum_{\alpha,g,III}\right]. \qquad (1.5)$$

The noise source corresponding to the vibrations of a fuel assembly with respect to its two neighbors is described by two Dirac-like perturbations located at the static boundary of the vibrating fuel assembly.

1.5.2.2 Relevant Experimental Program

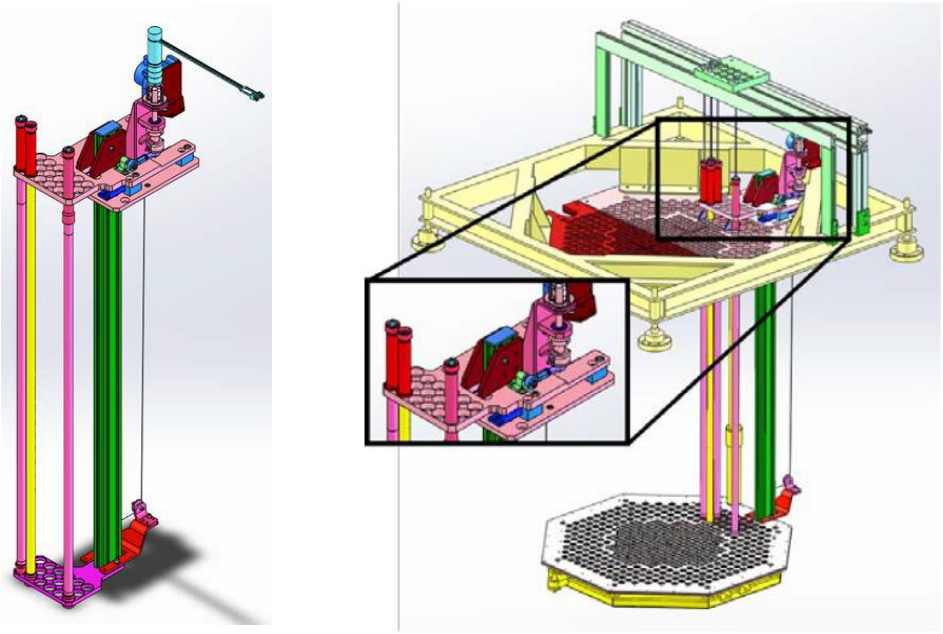

Figure 1.13: COLIBRI fuel rods oscillator alone (left) and with core structures (right), and a few rods inserted in the device [30]

Following the experimental campaign at the CROCUS reactor, the vibrating fuel rods experiments have been carried out using the COLIBRI in-core device that was specifically developed for that purpose [17]. The COLIBRI fuel rods oscillator is designed to oscillate simultaneously any of 18 metallic uranium fuel rods laterally in the west region of the core periphery zone and it consists in two moving plates set above and below the core grids, which are rigidly connected by an

aluminium beam. Each moving plate carries an extremity of the fuel rods, top and bottom, respectively.

Like AKR-2 reactor, total two experimental campaigns have been carried out in the CROCUS reactor for COLIBRI experiments. The first experimental campaign took place from 17 to 21 September 2018 [29] and the second experimental campaign was held from 9 to 22 July 2019 [30].

The second experimental campaign focused on the reduction of uncertainties as compared to the first campaign. The main changes in second experimental campaign are as follows [30].

1) The power increased from $100\ \mathrm{mW}$ to $1\ \mathrm{W}$ to increase the statistical significance.
2) The first experimental campaign with COLIBRI was carried out in 2018 with 20 times of measurements, while varying the oscillating amplitude and frequency: the oscillating amplitude varies between $\pm 0.5 \sim 2.0\ \mathrm{mm}$, while the oscillating frequency varies between $0.1 \sim 2.0$ Hz. In the second campaign, specific conditions of experiments were selected and focused to enable the long experiments (up to 4 hours continuously) with repeatability (amplitude and frequency of oscillation: $1.5\ \mathrm{mm}$, and $0.1\ \mathrm{Hz}$ and $1.0\ \mathrm{Hz}$ only).
3) The additional detectors comprised two more large fission chambers, which allow high statistics and robust measurements, and two proportional counters made sensitive to the fast neutron component.
4) More static and dynamic experiments were conducted without oscillations to allow for reference values.

Figure 1.14 and Figure 1.15 show the experimental setup of detectors in CROCUS reactor in first and second experimental campaigns, respectively.

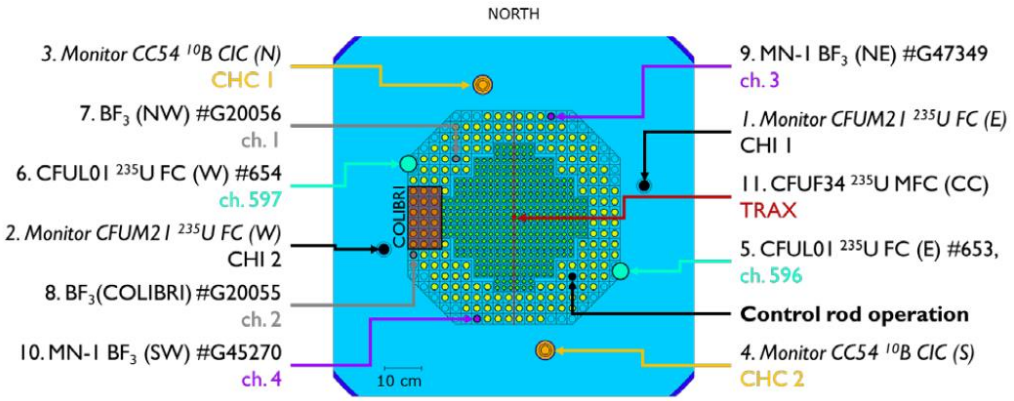

Figure 1.14: Radial view of reactor core with the information of installed detectors [21]

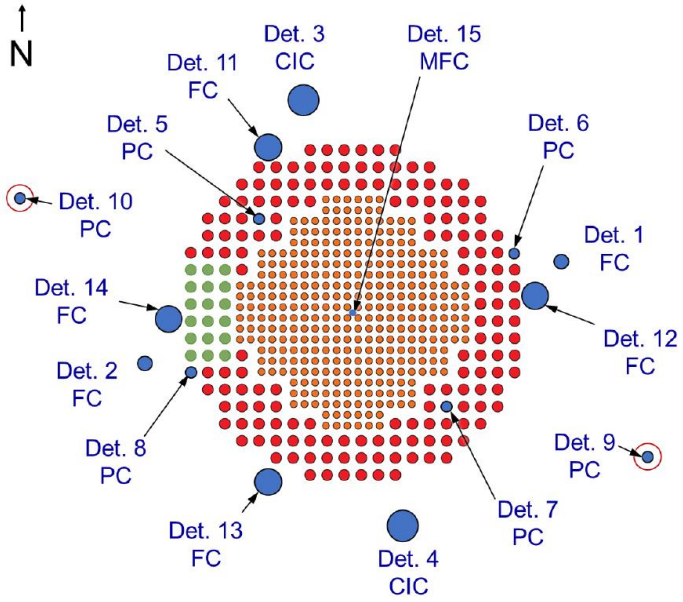

Figure 1.15: Experimental setup of detectors in second experimental campaign [30]

1.5.3 Vibrating Absorber

1.5.3.1 Description of Scenario

The fact that a vibrating control rod leads to a detectable neutron noise is well known from the Oak Ridge National Laboratory Research Reactor (ORR) and High Flux Isotope Reactor (HFIR). Later it turned out that control rod vibrations can occur even in power reactors. Since excessive vibration always signifies a beginning of malfunction, detecting and locating vibrations by neutron noise methods became an interesting task [27]. The vibration of control rod is assumed to be described by a one-dimensional structure along the $z-$ direction (axial direction of the reactor core) vibrating perpendicularly to the two-dimensional (x, y) plane. Furthermore, the vibrating rod is assumed to always remain parallel to itself and to have the most significant effect on the thermal macroscopic absorption cross-section. In these conditions, the vibration of the rod will create a perturbation of the absorption cross-section that is represented as,

$$\delta\sum_a(\boldsymbol{r},t) = \gamma\Theta(z-z_0)\Big[\delta\left(\boldsymbol{r}_{xy}-\boldsymbol{r}_{p,xy}-\varepsilon(t)\right) - \delta\left(\boldsymbol{r}_{xy}-\boldsymbol{r}_{p,xy}\right)\Big], \tag{1.6}$$

where γ is the strength of the perturbation, $\boldsymbol{r}_{p,xy}$ is the equilibrium position of the rod in the (x, y) plane, $\varepsilon(t)$ is a vector representing the displacement of the rod from its equilibrium position in the (x, y) plane, and z_0 represents the axial elevation at which the rod is inserted (insertion from the top of the core). $\Theta(z-z_0)$ is the Heaviside function as below.

$$\begin{cases}\Theta(z-z_0)=0\ if\ z<z_0\\ \Theta(z-z_0)=1\ if\ z\geq z_0.\end{cases} \tag{1.7}$$

After using a one-term Taylor expansion for Equation (1.6), we can get the expression in the frequency-domain as Equation (1.8).

$$\delta\sum_a(\boldsymbol{r},\omega) = -\gamma\Theta(z-z_0)\varepsilon(\omega)\cdot\delta'\left(\boldsymbol{r}_{xy}-\boldsymbol{r}_{p,xy}\right). \tag{1.8}$$

1.5.3.2 Relevant Experimental Program

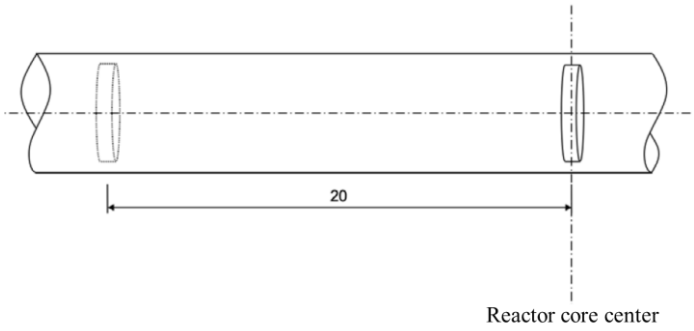

Figure 1.16: Absorber motion path inside channel 1-2. Side view. Unit in cm. [21]

The neutron noise induced by vibrating absorber in this study is specifically targeting the experimental program at AKR-2 reactor [21]. In case of vibrating absorber experiments, the absorber is moved along the experimental channel 1-2 in Figure 1.9, between a position inside the core and a position outside the core for the vibrating experiments.

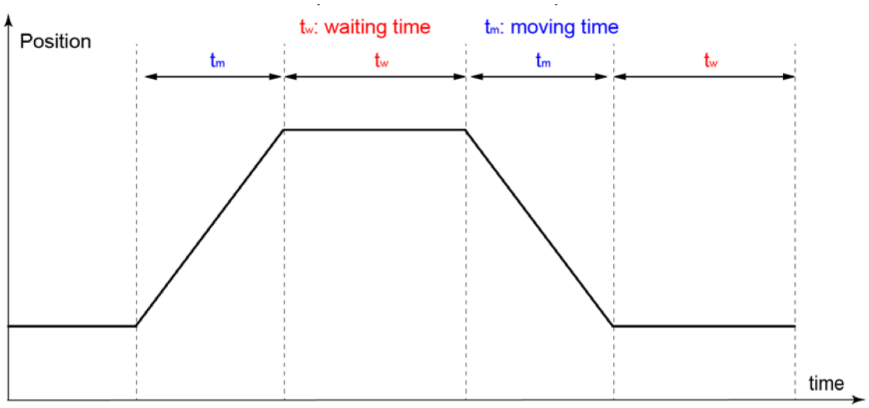

Figure 1.17: Trapezoidal motion followed by absorber in vibrating absorber experiments [21]

The vibrating absorber has a thickness and a diameter of 1.016 mm and 12.7 mm, respectively. The periodic motion of the vibrating absorber is defined by two main parameters: the waiting and moving times as shown in Figure 1.17. The pneumatic system allows to modify the absorbers motion by varying the moving time (t_m) from 0.4 to 2.0 seconds, and/or the waiting time (t_w) from 0.1 to 4.0 seconds.

1.6 Quantity of Interest

This thesis is rooted in CORTEX project, therefore, a QoI at each reactor which is designated within the project is selected as output variable in this thesis. Table 1.1 summarizes the QoIs considered at different reactor types and events [32, 33].

Reactor type	Event	QoI	Corresponding chapter
CROCUS	Absorber of variable strength	Absolute neutron noise (amplitude and phase of fast and thermal neutron noise)	2.3, 2.4
	Fuel rods vibration	Amplitude: APSD normalized by CPSD at the reference detector location (Detector 5)[1] Phase: CPSD phase	3.2, 3.4, 3.5

[1] Detector 5 is relevant to the first experimental campaign, and the second experimental campaign considers another detector (Detector 12) as reference detector. However, only the first experimental campaign is treated in this thesis at the CROCUS reactor.

AKR-2	Rotating absorber	Amplitude: APSD normalized by CPSD at the reference detector location (Detector 1 or 8)[2] Phase: CPSD phase[3]	4.2.4, 4.4.2, 4.5.3
	Vibrating absorber	Amplitude: APSD normalized by CPSD at the reference detector location (Detector 1 or 8) Phase: CPSD phase	4.2.4, 4.4.3, 4.5.4
Swiss 3-Loop pre-Konvoi reactor	Fuel rods (one fuel assembly) vibration	Absolute neutron noise (amplitude and phase of thermal neutron noise)	5.4

Table 1.1: QoIs in different reactors and events

In CROCUS and AKR-2, a reference detector is selected in consideration of generating the most meaningful information as a combination with the rest detectors. Here, the relative location of a detector from the noise source is working as a major consideration.

[2] Detector 1 for first experimental campaign and Detector 8 for second experimental campaign

[3] QoI-phase is calculated with identical reference detector as QoI-amplitude.

The absolute noise amplitude here describes the magnitude of neutron noise, which is directly converted from the original complex quantity obtained from CORE SIM+ computation.

The APSD (Auto-Power Spectral Density) and the CPSD (Cross-Power Spectral Density) are transformations of the neutron flux through the Fourier Transform of the autocorrelation function and the cross correlation between two signals, respectively [34].

$$\begin{aligned} \mathrm{APSD(f)} &= \int_{-\infty}^{\infty} \mathrm{C_{xx}}(\tau) \mathrm{e}^{-\mathrm{j}2\pi \mathrm{f}\tau} \mathrm{d}\tau \\ \mathrm{CPSD(f)} &= \int_{-\infty}^{\infty} \mathrm{C_{xy}}(\tau) \mathrm{e}^{-\mathrm{j}2\pi \mathrm{f}\tau} \mathrm{d}\tau, \end{aligned} \tag{1.9}$$

where τ is the lag used to estimate the autocorrelation function of the sensor output signal and $\mathrm{C_{xx}}$ and $\mathrm{C_{xy}}$ are calculated with Equation (1.10).

$$\begin{aligned} \mathrm{C_{xx}}(\tau) &= \mathrm{E}[\mathrm{x}(\tau) x(\mathrm{t}+\tau)] \\ \mathrm{C_{xy}}(\tau) &= \mathrm{E}[\mathrm{x}(\tau) y(\mathrm{t}+\tau)], \end{aligned} \tag{1.10}$$

where E is the expected value and $\mathrm{x(t)}$ is the sensor output signal. In CORTEX project, APSDs are derived from the thermal neutron noise calculated at the locations of the detectors. The obtained APSDs from the experiments are then normalized by CPSD at the reference detector location [32]. The APSD and the CPSD of the frequency domain neutron noise ($\delta\phi$) at the location i with the reference detector at the location j are calculated with the following relation [20]:

$$\mathrm{APSD}_i = \left(\frac{\delta\phi}{\phi_0}\right)_i \left(\frac{\delta\phi}{\phi_0}\right)_i^{\dagger} \tag{1.11}$$

$$\mathrm{CPSD}_{i,j} = \left(\frac{\delta\phi}{\phi_0}\right)_i \left(\frac{\delta\phi}{\phi_0}\right)_j^{\dagger},$$

where ϕ_0 is the static flux and † symbolizes the complex conjugate.

1.7 Uncertainty Analyses

Throughout the engineering fields, the study of uncertainty has become one important aspect to assessing a model credibility. The parameters, especially in the model of nuclear physics, are often uncertain due to the measurement uncertainty and/or the natural variability. Uncertainty propagation (UP) and sensitivity analysis (SA) are two related tasks for studying uncertainty. UP and SA share the stage named uncertainty characterization (UC), which should be done prior to the main uncertainty analyses. UC is the quantification of the uncertainty in model inputs [35]. Here, "inputs" is a broad term for any quantity in the model whose value is based on real-world data. This includes model parameters, boundary and initial conditions. The aim of UC is to determine probability distributions describing each of the inputs. This is generally a data-driven task that can be especially difficult for complex models with large number of parameters, where even estimating mean values can be challenging. The detailed process of UC will be introduced in Chapter 2. UP and SA are complementary activities: UC is performed first, then UP calculates the output uncertainty and SA identifies which inputs are responsible for that output uncertainty [36].

1.7.1 Approaches for Uncertainty Quantification

For uncertainty quantification, there are two main approaches available, namely the deterministic method and the stochastic sampling-based method [37, 38]. This deterministic method is based on the "propagation of moments" applied to the truncated first-order Taylor series. The variance (σ_R^2) of the system response R, i.e., the second central moment of the linearized R, is computed as:

$$\sigma_R^2 = \vec{S}_\alpha \boldsymbol{V}_\alpha \vec{S}_\alpha^T, \tag{1.12}$$

where $\vec{S}_\alpha = \left[S_{\alpha_1}, S_{\alpha_2}, \ldots\right] = \left[\frac{\partial R}{\partial \alpha_1}, \frac{\partial R}{\partial \alpha_2}, \ldots\right]$ is called the sensitivity coefficient of R with respect to inputs $\vec{\alpha}$, and $\boldsymbol{V}$ is the covariance matrix of the inputs.

This deterministic method, colloquially known as the "Sandwich Rule" method, computes first-order sensitivity coefficients of the output parameters of interest and then combines the sensitivities with the covariance matrix of the input data. This method is not easily applicable to non-linear behavior and requires the calculation of analytical sensitivities in the form of derivatives.

The stochastic sampling-based method does not have these constrains and is based on the perturbation of the uncertain input data as random variables following their uncertainty distributions. The variance of the output parameter corresponds to the contributions of the input parameters' uncertainty.

Among these two approaches, the stochastic sampling-based method is selected due to its advantages in the current work. This method involves the straightforward implementation and implicit treatment of model non-linearity by computing the output uncertainty through the simultaneous consideration of all input uncertainties. Moreover, different from the deterministic method, the stochastic sampling-based method does not require an earlier computation of sensitivity coefficients for the uncertainty quantification. Therefore, this approach becomes suitable, especially in case of involving the perturbation of the complicated groupwise nuclear data with resulting in accuracy enhancement of the obtained neutron noise uncertainties.

1.7.2 Normality Test

Checking a normality of the output distribution plays a key role in understanding a computational relation between the considered inputs and outputs. Finding this relation (such as linear or non-linear relationship) enables to predict a behavior

of output uncertainty and to determine a proper approach for a sensitivity analysis (e.g., correlation-based approach or variance-based approach).

The Shapiro-Wilk test is selected in this thesis to examine if a variable is normally distributed in some population [39, 40]. The Shapiro-Wilk test precisely answers a question "how likely is the observed distribution if the given data are exactly normally distributed in the entire population?". One example of output data distribution is shown in Figure 1.18-a.

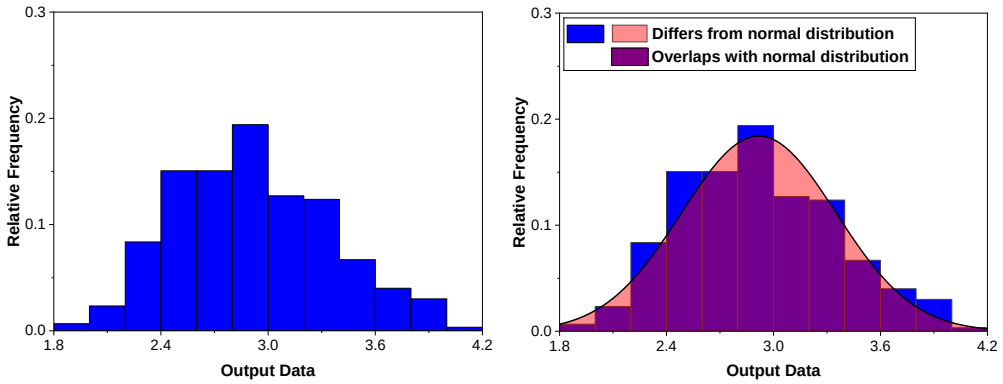

a. Histogram of output data

b. Fitted normal distribution curve

Figure 1.18: Example of histogram and fitted normal distribution curve of output data

The Shapiro-Wilk test first quantifies the similarity between the observed and normal distributions as a single number: it superimposes a normal curve over the observed distribution as shown in Figure 1.18-b. It then computes which percentage of our sample overlaps with it: a similarity percentage. Finally, the test computes the probability of finding this observed, or a smaller, similarity percentage. It does so under the assumption that the population distribution is exactly normal, which is "null hypothesis". The null hypothesis for the Shapiro Wilk test is that a variable is normally distributed in some population. As a rule of thumb, we reject the null hypothesis if p-value is smaller than 0.05. Namely, in this case it can be concluded that our variable is "not" normally distributed.

1.7.3 Uncertainty Propagation

UP replaces a traditional deterministic approach to modeling where inputs and outputs take fixed values, with a probabilistic approach in which uncertainty in inputs and outputs are known, thereby providing a deeper understanding of system behavior. For example, UP in weather forecasting leads to probabilities of weather events (e.g., probability of rain) being presented to the public, which is much more useful than simple predictions (e.g., “will rain”/ “will not rain”) [35]. The key results from UP are error bands that bound the best-estimate predictions, by propagating the input uncertainty through the model to derive the resultant uncertainty in important model outputs.

Since the first uncertainty framework was proposed by U.S. NRC and denominated Code Scaling, Applicability, and Uncertainty (CSAU), a number of uncertainty methodologies have been created in other countries. Even though these methods share a common goal with CSAU, they use different techniques and procedures to obtain the uncertainties on key calculated quantities [41]. CSAU and GRS (from the German, Gesellschaft für Anlagen und Reaktorsicherheit) methods propagate the input uncertainties for the uncertainty evaluation, while UMAE (Uncertainty Methodology based upon Accuracy Extrapolation), CIAU (Code with capability of Internal Assessment of Uncertainty) and Simens methods are extrapolating the output uncertainties. For the “extrapolation of output uncertainty” approach, uncertainty is obtained from the output uncertainty based on comparison between calculation results and significant experimental data [42].

The current thesis aims at the output uncertainty evaluation by the propagation of input uncertainties. Therefore, the GRS method is selected for the further analyses due to the irrelevance between the number of input parameters and the required total number of code runs, which secures the flexibility on analyses at various conditions. Additionally, the Monte Carlo method is employed as a comparison target of GRS method.

1.7.3.1 GRS Method

The key features of GRS method can be summarized as below.

1) The uncertainty space of input parameters (defined by their uncertainty ranges) is sampled at random according to the combined probability distribution of the uncertain parameters. Code calculations are performed by sampled sets of parameters.
2) The number of code calculations is determined by the requirement to estimate a tolerance and confidence interval for the quantity of interest. Following a proposal by GRS in 1990s, Wilks' formula is used to determine the number of calculations to obtain the uncertainty bands [43].
3) Statistical evaluations are performed to determine the sensitivities of input parameter uncertainties on the uncertainties of key results (parameter importance analysis).

Here, the tolerance interval signifies the interval which covers a specified proportion of the population for a given confidence level, while the confidence level is the likelihood that a tolerance interval will actually cover the minimum percentage we state. Tolerance intervals can be one-sided (a range where one limit is either negative infinity or positive infinity) or two-sided (a range with a specified minimum and maximum).

The equations below describe Wilks' formula for one-sided (upper) tolerance limit and two-sided tolerance limit, respectively:

$$\sum_{j=0}^{m-1} \binom{N}{j} q^{N-j}(1-q)^{j} \leq 1-\alpha \tag{1.13}$$

$$\sum_{i=0}^{r+m-1} \binom{N}{i} (1-q)^{i} q^{N-i} \leq 1-\alpha, \tag{1.14}$$

where α is the confidence level, q is a tolerance limit, N is a size of samples, r and m are the numbers related to the elements in an ordered sample. The minimum number of calculations for both cases especially in first-order prediction can be found in Table 1.2. The order states the number of code runs expected to lie in the "tail" of the distribution (i.e., beyond the q percentile value chosen by the user), and therefore the m^{th} (or r^{th}) largest, or smallest, output value is chosen as the limiting value. This is intended to reduce the sampling error inherent in first-order Wilks' predictions (i.e., where $m = 1$, or $m = r = 1$) [44]. Higher order tolerance limits correspond to values of the ranked output samples away from the maximum and minimum values. They approach progressively with a lower variance, as the order increases, the $q \times 100\,\%$ and $(1 - q) \times 100\,\%$ quantiles of the true output uncertainty distribution and give a better estimate of these values. The decrease in the variance requires a larger output sample and, therefore a larger number of code executions.

		One-sided statistical tolerance limits			Two-sided statistical tolerance limits		
		q (quantile)					
		0.90	0.95	0.99	0.90	0.95	0.99
α (confidence level)	0.90	22	45	230	38	77	388
	0.95	29	59	299	46	93	473
	0.99	44	90	459	64	130	662

Table 1.2: Minimum number of calculations for one-sided and two-sided statistical tolerance limits

Following the U.S. NRC regulatory guide 1.105, it is highly recommended to use $95\,\%/95\,\%$ tolerance limit for combining uncertainties [45]. In addition to this, one of the previous uncertainty studies for best-estimate nuclear system codes, the BEMUSE analysis of the LOFT L2-5 test, indicated that applying Wilks' formula to the 4th or 5th order usually produced a more satisfactory tolerance, at the price of some additional code runs [46].

1.7.3.2 Brute Force Monte Carlo Method

Brute force Monte Carlo method has been selected as a comparison target of the GRS method. This method is well-known as an alternative to the more cumbersome perturbation methods used so far extensively over the world (see Figure 1.19). This takes advantage of the large computational power available nowadays [47].

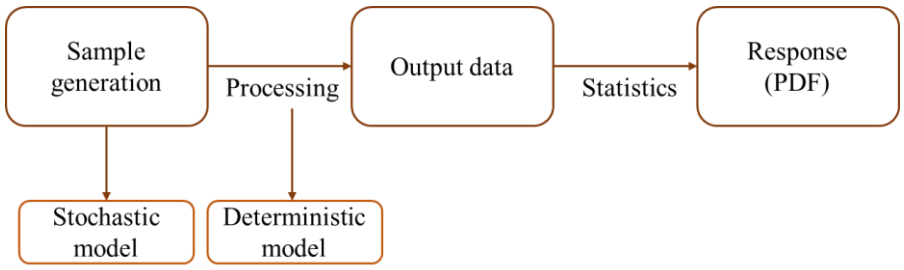

Figure 1.19: General overview of Brute force Monte Carlo algorithm

The advantages of the Brute force Monte Carlo approach can be boiled down to two items. First, the result of the uncertainty propagation shows more realistic values with a large number of sample runs. Especially, this can be a competitive edge when compared to the results from GRS method using Wilks' formula, which cover the required probability (95 % to 5 %) with a certain confidence level for any case. Another point is that this approach can yield the full Probability Density Function (PDF) of the value of interest. Once a PDF is defined, we can expect that whichever sample runs we make, the result will have the same distribution as we obtained earlier. In other words, we can be always safe when making the parametric assumptions about the sampling distribution, regardless of the sample size [48].

1.7.4 Sensitivity Analysis

According to [36], the sensitivity is "the study of how the variation in the output of a model (numerical or otherwise) can be apportioned, qualitatively or quantitatively, to different sources of variation, and of how the given model depends

upon the information fed into it.". Furthermore, "Sensitivity analysis studies the relationships between information flowing in and out of the model.". These definitions imply that the parameter values that characterize both (and only) the boundary and initial conditions, e.g., representative of a system, and the numerical structure of a correlation embedded into the model (or code) constitute the typical objective of a SA [41].

The key result from SA is the influence of input parameters upon selected output quantities and the evaluation of the relative influence of input parameters.

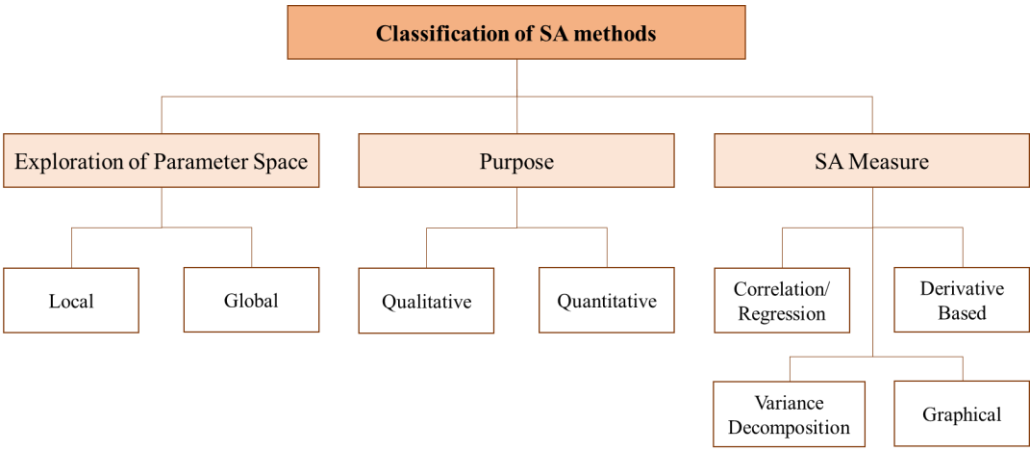

Figure 1.20: Classification of SA methods

A variety of SA measures and methods have been used widely, and each has its own advantages and disadvantages. Figure 1.20 summarizes SA methods classification [49]. The "exploration of the parameter space" is the most widely recognized classification. When SA is performed by varying individual parameters in a small vicinity of a base point, the method is classified as local. One example of "local" sensitivity analysis is "One at a Time (OAT)", which changes one parameter at a time while keeping all other parameters fixed at their base values. On the other hand, if SA is carried out by varying all parameters within their entire uncertainty ranges simultaneously, the method is classified as global. In computational point of view, the local methods are more efficient, however, has lower reliability since they cannot account for model nonlinearity, non-monotonicity and parameter interactions.

Another way for classifying SA methods is based on "purpose of the application". The qualitative way is identifying the influential parameters by screening or other low computational cost methods, and this is often used to reduce the burden on further model analysis [50]. Meanwhile, quantitative methods quantify the contributions of individual parameters to output variance, however, often at a very high computational cost.

The third way of classifying SA methods is based on "sensitivity measure", which ranges from simple visual inspection of input vs. output plots to robust and sophisticated variance-based sensitivity indices. In this chapter, the two most representative and widely used approaches within this classification, correlation-based and variance-based approaches, are compared to each other to figure out the optimal solution in our specific analysis condition.

1.7.4.1 Correlation-based Approach

The use of correlation-based coefficients, as well as regression-based coefficients as sensitivity indices are traditional approaches extensively used to assess the strength of the association between two factors due to their relatively simple statistical theories.

Pearson Correlation Coefficient

Pearson Correlation Coefficient (PCC) is the most familiar measure of dependence between two quantities [51, 52]. PCC is a measure of the strength of the linear association between X and Y and obtained by dividing the covariance of the two variables by the product of their standard deviations. Let a generic model function $Y = f(X)$ with an input vector $X = (X_1, \dots, X_n)$ where X is a random variable with a continuous probability distribution function (PDF) $p(X_1, \dots, X_n)$. The Pearson coefficient is computed using Equation (1.15).

$$r_p(X,Y) = \frac{cov(X,Y)}{\sigma_X \sigma_Y}, \tag{1.15}$$

where σ_X and σ_Y are the standard deviations of the variables and $cov(X,Y)$ is the covariance of the variables.

This means that if X and Y have a perfect direct (increasing) linear relationship (correlation), PCC will equal or be close to $+1.0$, or -1.0 in the case of a perfect decreasing (inverse) linear relationship (anticorrelation). Therefore, there is less of a relationship if the coefficient approaches zero.

Spearman Correlation Coefficient

Spearman Correlation Coefficient (SCC) is a nonparametric measure of rank correlation. It describes how well the relationship between two variables can be described using a monotonic function. SCC between two variables is equal to PCC between the rank values of those two variables and can be calculated using Equation (1.16).

$$r_s(X,Y) = \rho_{R(X),R(Y)} = \frac{cov(R(X),R(Y))}{\sigma_{R(X)}\sigma_{R(Y)}}, \tag{1.16}$$

where $\sigma_{R(X)}$ and $\sigma_{R(Y)}$ are the standard deviations of the rank variables and $cov(R(X),R(Y))$ is the covariance of the rank variables. If there are no ties, a perfect SCC of $+1.0$, or -1.0 occurs when each of the variables is a perfect monotone function of the other.

Critical value of Correlation Coefficient

While an amplitude of coefficient indicates the strength of the correlation, it is important to set a "criterion" to prove the validity of calculated coefficient in statistic point of view. The criterion, which is called as a critical value, is the value that a test statistic must exceed in order for the null hypothesis (H_0) to be rejected. Here, the null hypothesis states that the two random variables are mutually independent. Therefore, when $|r|$ exceeds the critical value, we can reject the H_0 hypothesis at the certain significance level (α) we defined. The correlation coefficient has the following test statistic [51],

$$w_p = \frac{z_p}{\sqrt{n-1}}, \tag{1.17}$$

with z_p is the standard normal (1- α/2) quantile. The formula above tells how to approximate the pth quantile of ρ, when the sample size is larger than 30.

As an example, if we have 1000 samples and want to consider the significance level of 0.05, the critical value is obtained as 0.06. It means that when the coefficient is larger than 0.06, the two random variables can be regarded as "correlated" with 5 % probability that this correlation is not true [53].

Square of the Correlation Coefficient

The squared coefficient evaluates the scatter of the data points around the fitted regression line. It is also called the coefficient of determination, or the coefficient of multiple determination for multiple regression [54]. For the same data set, higher squared coefficient values represent smaller differences between the observed data and the fitted values. The squared coefficient is the percentage of the dependent variable variation that a linear model explains.

$$Squared\ Coefficient^2 = \frac{Variance\ explained\ by\ the\ model}{Total\ Variance}. \tag{1.18}$$

1.7.4.2 Multiple Correlation Coefficient

When the multiple input parameters are correlated (e.g., nuclear data input parameters), the correlation coefficients should be calculated in a distinct manner in order to measure the effect of large number of correlated input parameters efficiently. r_p^2 in Equation (1.15) can be interpreted as the "coefficient of determination" of the relationship between Y and X_i assuming a linear model between Y and X_i. This demonstrates the fraction of the variance of Y which is explained from approximating Y by a linear combination of the X_i. This interpretation can be used to estimate the first order sensitivity index of the input parameter X_i,

$$S_{X_i} = r_p^2. \quad (1.19)$$

Those first order sensitivity indices can be regarded as multiple correlation coefficients which correspond to groups of input parameters [55, 56]. The multiple correlation coefficient of group 1 ($X_{(1)} = (X_1, \dots, X_k)$) is calculated following the equation below.

$$R_{(1)}^2 = \left(r_p(Y, X_1), \dots, r_p(Y, X_k)\right) \sum_{X_{(1)}}^{-1} (r_p(Y, X_1), \dots, r_p(Y, X_k))^T, \quad (1.20)$$

where $r_p(Y, X_i)$ is the correlation coefficient between Y and X_i, and $\sum_{X_{(1)}}^{-1}$ is the inverse of the variance-covariance matrix (VCM).

In this work, a "Moore-Penrose pseudo inverse (Pseudoinverse)", which is a built-in MATLAB function (the function named as ***pinv***), is used to inverse the obtained VCM [57, 58]. Pseudoinverse is frequently used to solve a system of linear equations when the system does not have a unique solution or has many solutions. Especially when a target matrix (VCM) is not square or is square and singular, Pseudoinverse can help to find the inverse matrix. Additionally, compared to another function finding an inverse matrix implemented in MATLAB (the function named as ***inv***), Pseudoinverse has a strength in its capability of avoiding nonfinite values (*Inf* or *NaN*) in the calculated inverse of matrix.

PSI implemented the calculating module of the aforementioned multiple correlation coefficient into their own developed tool, which is dedicated for the uncertainty analyses, named SHARK-X [58]. SHARK-X is a set of Perl-based tools build around the deterministic neutron transport code CASMO-5, used to perform uncertainty quantification for lattice calculations at the PSI.

1.7.4.3 Variance-based Approach

In many variance-based sensitivity analysis methods, the variance is used as an indicator of the importance of an input variable. Among many methods for analysing the decomposition of variance as a sensitivity measure, the method

developed by Sobol is the most well-established and widely used one [59]. Following Sobol's method, we can obtain the first order sensitivity index (S_i) and the total sensitivity index (S_{T_i}). The first order index represents the main effect contribution of each input parameter to the variance of the output. Meanwhile, the total sensitivity index measures the contribution to the output variance of input parameter including all the interactions with other input variables. These indices can be obtained following the equations below,

$$S_i = \frac{V(E(Y|X_i))}{V(Y)} \tag{1.21}$$

$$S_{T_i} = \frac{E(V(Y|X_{\sim i}))}{V(Y)} = 1 - \frac{V(E(Y|X_{\sim i}))}{V(Y)}, \tag{1.22}$$

where X_i is i^{th} input parameter, Y is a model output and $X_{\sim i}$ means $N \times (k-1)$ matrix of all factors but X_i, with N the sample size and k the number of samples.

The $V(E(Y|X_i))$ for S_i and $E(V(Y|X_{\sim i}))$ for S_{T_i} can be calculated with the formulas below.

$$V(E(Y|X_i)) = \frac{1}{N}\sum_{j=1}^{N} f(A)_j f\left(B_A^{(i)}\right)_j - f_0^2 \tag{1.23}$$

$$E(V(Y|X_{\sim i})) = \frac{1}{N}\sum_{j=1}^{N} f(A)_j \left(f(A)_j - f\left(A_B^{(i)}\right)_j\right), \tag{1.24}$$

where $A_B^{(i)}$ is a matrix, column i comes from matrix $\boldsymbol{B}$ and all other $k-1$ columns come from matrix $\boldsymbol{A}$.

The detailed information on calculating Sobol's sensitivity indices using the decomposition of variance can be found in [60]. To get the precise estimates on the

sensitivity indices, this approach is costly in terms of the number of model cells. In common practice, the value of 10^4 model evaluations can be required to estimate the Sobol's index with a statistical error of $10\ \%$ [61].

There have been many attempts to find more efficient ways to compute the first order and total sensitivity indices. Among them, Jansen's formula is considered as the best way especially for estimating the total effect [62]. The improved estimator for both S_i and S_{T_i} are given by the formulas described below [63].

$$V(E(Y|X_i)) = V(Y) - \frac{1}{2N}\sum_{j=1}^{N}(f(B)_j - f\left(A_B^{(i)}\right)_j)^2 \tag{1.25}$$

$$E(V(Y|X_{\sim i})) = \frac{1}{2N}\sum_{j=1}^{N}\left(f(A)_j - f\left(A_B^{(i)}\right)_j\right)^2. \tag{1.26}$$

Moreover, Jansen's formula requires $N \times (k+2)$ model evaluations rather than $N \times (2k+1)$ from the original Sobol's formula, resulting in improved computational costs. In addition, it was proven that Jansen's approach has even less statistical error compared to Sobol's approach, as shown in Figure 1.21. When the sampling size becomes larger, the statistical error of Jansen's approach decreases dramatically while that of Sobol's approach becomes saturated at some point and maintains this value as depicted in Figure 1.21 [64].

However, variance-based approach requires a large number of model evaluations, e.g., sufficiently large number (500 or higher number) of samples are required on computing the sensitivity indices, which are often unacceptable for time expensive computer codes [62]. The solution on this consists in substituting the physical model M with a mathematical approximation $\widehat{M}$ built from a set of data samples. Such an approximation is referred to as various names depending on a field of research considered, e.g., surrogates, metamodels, response surface models or approximation models, etc., and the details are introduced in Chapter 1.8.4, accordingly.

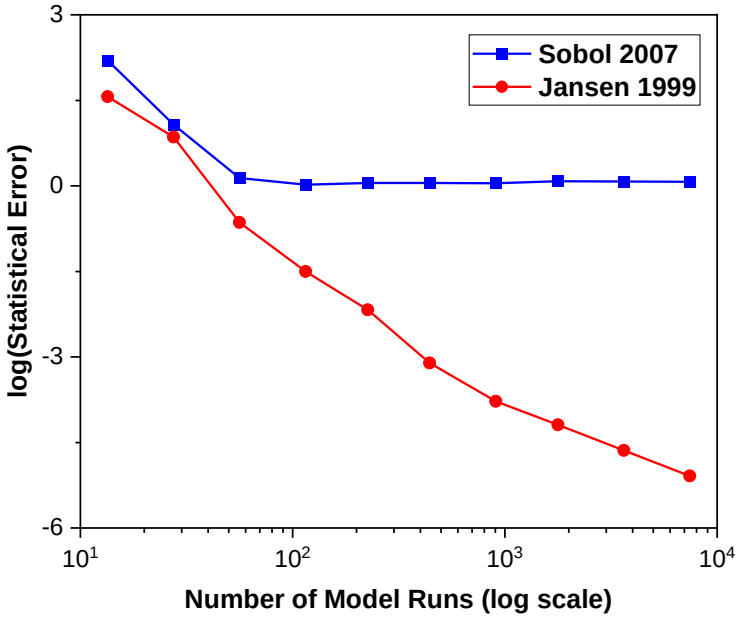

Figure 1.21: Comparison of statistical error from “Jansen 1999” and “Sobol 2007” at increasing number of model runs [64]

1.7.4.4 Comparison of Approaches

The pros and cons of correlation-based (or regression-based) approach and variance-based approach can be summarized as Table 1.3 [65].

	Pros	Cons
Correlation-based approach (or Regression-based approach)	- The concept is easily understandable. - It is computationally cheap. - When the variables are “linearly” related, it can provide “true” quantitative information. - It can detect a “direction” of influence.	- When the variables are not “linearly” related, the accurate prediction is not guaranteed.

Variance-based approach	- It is appropriate for all kinds of models. - It can provide “true” quantitative sensitivity measure. - It can provide information about orders of parameter influence (interaction among the variables)	- The concept is mathematically complicated. - It is computationally expensive. - It cannot detect a “direction” of influence.

Table 1.3: Comparison between correlation-based approach and variance-based approach

1.8 Software and Tools for Analyses

1.8.1 MATLAB

MATLAB (MATtrix LABoratory) is a proprietary multi-paradigm programming language and numeric computing environment developed by MathWorks [66], which was first released in late 1970s. MATLAB allows matrix manipulations, plotting of functions and data, implementation of algorithms, creation of user interfaces, and interfacing with programs written in other languages.

In this study, MATLAB is used for the following purposes.

1) Sample generation for simulation using Serpent and CORE SIM (CORE SIM+)
2) Performing batch computation for CORE SIM (CORE SIM+)
3) Data extraction and conversion
4) Statistical analyses

Especially, the implemented numerical algorithm in MATLAB enhances an efficiency on statistical analyses, e.g., sampling methods, normality tests and calculation of sensitivity coefficients.

1.8.2 Serpent

Serpent is a multi-purpose three-dimensional continuous-energy Monte Carlo particle transport code, developed at VTT Technical Research Centre of Finland, Ltd. The applications can be roughly divided into three categories as below [67].

1) Traditional reactor physics applications, including spatial homogenization, criticality calculations, fuel cycle studies, research reactor modeling, validation of deterministic transport codes, etc.
2) Multi-physics simulations, i.e., coupled calculations with thermal-hydraulics, CFD and fuel performance codes.
3) Neutron and photon transport simulations for radiation dose rate calculations, shielding, fusion research and medical physics.

The suggested applications of Serpent include, among other applications, the spatial homogenization and constant group generation for deterministic reactor calculations and the validation of deterministic lattice transport codes [68].

Serpent is used to generate two-groups constants and their uncertainties at the area of interest for the further neutron noise simulations. The Serpent is mainly running in Linux operative system and the computational cost of Serpent is very high with reasonable computational error. Therefore, a series of Serpent computations are made by the aid of Linux clusters in Leibniz Supercomputing Centre (LRZ) [69].

1.8.3 CORE SIM / CORE SIM+

1.8.3.1 CORE SIM

CORE SIM is a numerical tool for reactor noise analysis, more specifically, is a dynamic core simulator as well as static core simulator relying on the two-group diffusion approximation [70]. This tool uses sets of macroscopic cross-sections as input parameters. Since the thermal-hydraulic variables directly affect the macroscopic cross-sections, the change in thermal-hydraulic condition can be introduced by the equivalent change in cross-sections. This way of defining the input parameters allows a high degree of flexibility in the use of the tool compared to coupled neutron kinetics/thermal-hydraulics tools [18].

The CORE SIM is based on diffusion theory with two energy groups and one group of delayed neutrons. In this formalism, the time- and space-dependent fast neutron flux, thermal neutron flux, and precursor density, can be expressed, respectively, as below [18].

$$\begin{aligned}\frac{1}{\nu_1}\frac{\partial}{\partial t}\phi_1(\boldsymbol{r},t) &= \nabla\cdot\left[D_{1,0}(\boldsymbol{r})\nabla\phi_1(\boldsymbol{r},t)\right]\\ &+\left[(1-\beta)\upsilon\Sigma_{f,1}(\boldsymbol{r},t)-\Sigma_{a,1}(\boldsymbol{r},t)\right.\\ &\left.-\Sigma_r(\boldsymbol{r},t)\right]\phi_1(\boldsymbol{r},t)+(1-\beta)\upsilon\Sigma_{f,2}(\boldsymbol{r},t)\phi_2(\boldsymbol{r},t)\\ &+\lambda C(\boldsymbol{r},t)+S_1(\boldsymbol{r},t)\end{aligned} \tag{1.27}$$

$$\begin{aligned}\frac{1}{\nu_2}\frac{\partial}{\partial t}\phi_2(\boldsymbol{r},t) &= \nabla\cdot\left[D_{2,0}(\boldsymbol{r})\nabla\phi_2(\boldsymbol{r},t)\right]+\Sigma_r(\boldsymbol{r},t)\phi_1(\boldsymbol{r},t)\\ &-\Sigma_{a,2}(\boldsymbol{r},t)\phi_2(\boldsymbol{r},t)+S_2(\boldsymbol{r},t)\end{aligned} \tag{1.28}$$

$$\begin{aligned}\frac{\partial}{\partial t}C(\boldsymbol{r},t) &= \beta\upsilon\Sigma_{f,1}(\boldsymbol{r},t)\phi_1(\boldsymbol{r},t)+\beta\upsilon\Sigma_{f,2}(\boldsymbol{r},t)\phi_2(\boldsymbol{r},t)\\ &-\lambda C(\boldsymbol{r},t),\end{aligned} \tag{1.29}$$

where the macroscopic removal cross-section is defined as:

$$\Sigma_r(\boldsymbol{r},t) = \Sigma_{s0,1\to2}(\boldsymbol{r},t) - \frac{\Sigma_{s0,2\to1}(\boldsymbol{r},t)\phi_2(\boldsymbol{r},t)}{\phi_1(\boldsymbol{r},t)}. \tag{1.30}$$

Here, ϕ_1 and ϕ_2 represent the fast neutron flux the thermal neutron flux, respectively. In case of non-steady-state conditions, the time-dependent terms, generically expresses as $X(\boldsymbol{r},t)$, can be split into a mean value $X_0(\boldsymbol{r})$ (corresponding to the steady-state configuration of the system) and a fluctuating part $\delta X(\boldsymbol{r},t)$ around the mean value as:

$$X(\boldsymbol{r},t) = X_0(\boldsymbol{r}) + \delta X(\boldsymbol{r},t). \tag{1.31}$$

If the neutron noise is induced by perturbations of the macroscopic cross-sections and if there is no external neutron source, then splitting the time-dependent parameters into mean values and fluctuations according to Equation (1.31), performing a temporal Fourier-transform, and neglecting second-order terms (linear theory), the following matrix equation is obtained.

$$\begin{aligned}\left[\nabla\cdot\bar{\bar{D}}(\boldsymbol{r})\nabla + \bar{\bar{\Sigma}}_{dyn}^{crit}(\boldsymbol{r},\omega)\right]\times\begin{bmatrix}\delta\phi_1(\boldsymbol{r},\omega)\\ \delta\phi_2(\boldsymbol{r},\omega)\end{bmatrix}&\\ = \bar{\phi}_r(\boldsymbol{r})\delta\Sigma_r(\boldsymbol{r},\omega) + \bar{\bar{\phi}}_a(\boldsymbol{r})\begin{bmatrix}\delta\Sigma_{a,1}(\boldsymbol{r},\omega)\\ \delta\Sigma_{a,2}(\boldsymbol{r},\omega)\end{bmatrix}&\\ + \bar{\bar{\phi}}_f^{crit}(\boldsymbol{r},\omega)\begin{bmatrix}\delta\upsilon\Sigma_{f,1}(\boldsymbol{r},\omega)\\ \delta\upsilon\Sigma_{f,2}(\boldsymbol{r},\omega)\end{bmatrix},&\end{aligned} \tag{1.32}$$

where

$$\bar{\phi}_r(\boldsymbol{r}) = \begin{bmatrix}\phi_{1,0}(\boldsymbol{r})\\ -\phi_{1,0}(\boldsymbol{r})\end{bmatrix} \tag{1.33}$$

$$\bar{\bar{\phi}}_a(\boldsymbol{r}) = \begin{bmatrix}\phi_{1,0}(\boldsymbol{r}) & 0\\ 0 & \phi_{2,0}(\boldsymbol{r})\end{bmatrix}. \tag{1.34}$$

The matrix $\bar{\bar{\Sigma}}_{dyn}^{crit}$ is defined as:

$$\bar{\bar{\Sigma}}_{dyn}^{crit}(\boldsymbol{r},\omega)=\begin{bmatrix}-\Sigma_1^{crit}(\boldsymbol{r},\omega) & \frac{\upsilon\Sigma_{f,2,0}(\boldsymbol{r})}{k_{eff}}(1-\frac{i\omega\beta}{i\omega+\lambda})\\ \Sigma_{r,0}(\boldsymbol{r}) & -(\Sigma_{a,2,0}(\boldsymbol{r})+\frac{i\omega}{\nu_2})\end{bmatrix}, \tag{1.35}$$

with

$$\begin{aligned}\Sigma_1^{crit}(\boldsymbol{r},\omega)=\Sigma_{a,1,0}(\boldsymbol{r})+\frac{i\omega}{\nu_1}+\Sigma_{r,0}(\boldsymbol{r})\\ -\frac{\upsilon\Sigma_{f,1,0}(\boldsymbol{r})}{k_{eff}}\left(1-\frac{i\omega\beta}{i\omega+\lambda}\right).\end{aligned} \tag{1.36}$$

And the matrix $\bar{\bar{\phi}}_f^{crit}$ is given as:

$$\begin{aligned}&\bar{\bar{\phi}}_f^{crit}(\boldsymbol{r},\omega)\\ &=\begin{bmatrix}-\frac{\phi_{1,0}(\boldsymbol{r})}{k_{eff}}(1-\frac{i\omega\beta}{i\omega+\lambda}) & -\frac{\phi_{2,0}(\boldsymbol{r})}{k_{eff}}(1-\frac{i\omega\beta}{i\omega+\lambda})\\ 0 & 0\end{bmatrix}.\end{aligned} \tag{1.37}$$

For the uncertainty analysis using CORE SIM, the following variables in Table 1.4 need to be defined in each input file.

Input file name	Variable name	Description of the variable	Dimension of the variable	unit
XS_data.mat	ABS1	Fast macroscopic absorption cross-section	3	cm^{-1}
	ABS2	Thermal macroscopic absorption cross-section	3	cm^{-1}
	D1	Fast diffusion coefficient	3	cm^{-1}
	D2	Thermal diffusion coefficient	3	cm^{-1}
	NUFIS1	Fast macroscopic fission cross-section multiplied by the average number of neutrons released per fission event	3	cm^{-1}
	NUFIS2	Thermal macroscopic fission cross-section multiplied by the average number of neutrons released per fission event	3	cm^{-1}
	REM	Macroscopic removal cross-section	3	cm^{-1}
GEOM_data.mat	DX	Size of an elementary node in the x-direction	0	cm
	DY	Size of an elementary node in the y-direction	0	cm
	DZ	Size of an elementary node in the z-direction	0	cm

DYN_data.mat	Beff	Effective fraction of delayed neutrons (one group of delayed neutrons)	0	1
	f	Frequency at which the noise calculations have to be performed	0	Hz
	l	Decay constant of the neutron precursors (one group of delayed neutrons)	0	s^{-1}
	V1	Average neutron speed in the fast group	0	$cm.s^{-1}$
	V2	Average neutron speed in the thermal group	0	$cm.s^{-1}$
dS_data.mat	dABS1	Fast macroscopic absorption cross-section	3	cm^{-1}
	dABS2	Thermal macroscopic absorption cross-section	3	cm^{-1}
	dNUFIS1	Fast macroscopic fission cross-section multiplied by the average number of neutrons released per fission event	3	cm^{-1}
	dNUFIS2	Thermal macroscopic fission cross-section multiplied by the average number of neutrons released per fission event	3	cm^{-1}

	dREM	Macroscopic removal cross-section	3	cm^{-1}

Table 1.4: Content of the input files considered in current uncertainty analyses

CORE SIM has an obvious competitive edge compared to other existing noise simulators: first, it is calculating the neutron noise in the frequency domain, therefore, there is no need to time discretization of the neutron noise equations. Additionally, since the first-order neutron noise can be expressed as a source problem, the calculation of the neutron noise is a lot simpler than the calculation of the static flux involved in an eigenvalue problem [71].

1.8.3.2 CORE SIM+

CORE SIM+ is capitalized on the former experience of the CORE SIM tool [20, 72]. The calculation process consists of two steps: the steady-state neutron flux calculation and the neutron noise calculation in the frequency domain, respectively. CORE SIM+ includes new features to optimize both steps of a neutron noise simulation. This allows the modeling of a wide range of neutron noise source in an efficient manner.

One of the options implemented in CORE SIM+ are the efficient matrix/vector construction, the efficient numerical solvers combined with acceleration methods and the automated generation of the reactor Green's function.

Additionally, in CORE SIM+, the physical system is discretized using a rectilinear grid whose node sizes are provided by the user as input information. This choice has the advantage that a finer resolution can be defined for specific regions, e.g., area where perturbations are defined, and the gradient of the neutron flux is strong. While coarser cells are held for those regions where the spatial variation of the system properties and of the neutron flux is less remarkable. This allows optimizing the computational effort, as compared to the case of uniform fine mesh applied to systems with sharp heterogeneities both in static and dynamic data.

The required inputs for CORE SIM+ calculation are identical to those for CORE SIM, as listed in Table 1.4.

1.8.4 Surrogate Models

As introduced in Chapter 1.7, several techniques for uncertainty analyses require large number of simulations which is computationally demanding, as is often the case with modern computer codes. The surrogate modeling can become a proper remedy to this problem, which mimics the model response within the chosen parameter bounds but is computationally inexpensive [73].

Popular surrogate modeling approaches widely used are as follows: kriging, polynomial response surface, radial basis function, support vector machines, space mapping, artificial neutral networks and Bayesian networks. However, the nature of true function is not known a priori for some problems, it is not clear which surrogate model is most accurate. Moreover, each model has its own optimal condition to enhance the accuracy, e.g., input dimension, complexity of the model. Especially, in case of considering large input dimension, the following two surrogate models are generally recommended: Kriging interpolation and support vector machines [74]. In this PhD work, we are focusing on Kriging interpolation and additionally Polynomial Chaos Expansions-Kriging (PC-Kriging), a combined version of two models to enhance the accuracy.

1.8.4.1 Kriging Interpolation

The Kriging approach is an optimal interpolation based on regression against observed values of surrounding data points, weighted according to spatial covariance values (Figure 1.22) [75]. The Kriging interpolation model effectively represents the response Y as the sum of a realization of a regression model F and the result of a stochastic process z.

$$Y = F(\beta, x) + z(x) \tag{1.38}$$

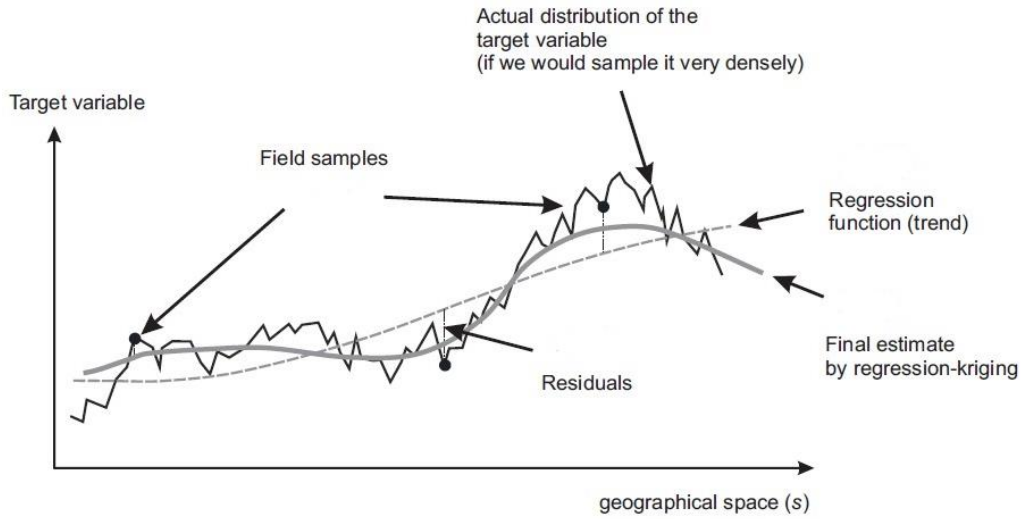

Figure 1.22: A schematic example of Kriging concept

However, the use of $z(x)$ as a stochastic process does not mean that the responses are treated as being stochastic. Rather, the model uses the result of a stochastic process to explain deviations from the regression model. Further explanations on each model are as below:

The regression model

The regression model represents the general trend of the samples and is modeled with a low order polynomial. The importance of the regression model varies with the density of the samples, if samples are close, then the effect of correlation from the samples will dominate the appearance of the model. The better the regression model fits the data, the less the correlation model is exploited to explain global behavior [76].

The correlation model

The correlation model parameters are closely interlaced with the regression parameters. The effect of the correlation model is to explain deviations from the general trend. This model can be one of these functions: exponential, general exponential, Gaussian, linear, spherical, cubic, spline. If the underlying

phenomenon is continuously differentiable, the correlation function will likely show a parabolic behavior near the origin, which means that choosing the Gaussian, the cubic or the spline function would be recommended.

The Kriging approach suffers from some well-known drawbacks in high dimension, which may be due to multiple causes [77]. For starters, the size of the covariance matrix of the kriging model may increase dramatically if the model requires a large number of sample points. As a result, inverting the covariance matrix is computationally expensive. The second drawback is the optimization of the subproblem, which involves estimating the hyperparameters for the covariance matrix. This is a complex problem that requires inverting the covariance matrix several times.

However, the Kriging model has become increasingly popular due to its ability to estimate the error of the predictor and its flexibility in accurately imitating the dynamics of computationally expensive simulations, which helps to compensate for the effects of data clustering, assigning individual points within a cluster less weight than isolated data points.

Technical University of Denmark (DTU) has developed the software package DACE (Design and Analysis of Computer Experiment), which is a MATLAB toolbox for working with kriging approximations to computer models [78]. This software enables to build a kriging approximation model so that it could be used as a surrogate for the computer model. By implementing various correlation functions and high dimensional options for regression models, the prediction of kriging approximation with higher precision becomes possible.

1.8.4.2 Polynomial Chaos Expansions (PCE)

PCE is one of the most commonly used methods for the uncertainty quantification, which is able to provide efficient and accurate ways of analyzing the uncertain behavior in a complex system. This method can fall into two categories: intrusive and non-intrusive categories [79]. Intrusive methods substitute the PCE approximations into governing equations and uses a Galerkin technique as well as a discretization scheme to solve for the coefficients in the expansion. Non-

intrusive method evaluates the coefficients in the expansion using a small number of model simulations and requires no manipulation of underlying partial differential equation. That is to say, the latter approaches are easier to implement, therefore, will be considered in this study.

PCE surrogates the computational model with a series of orthonormal polynomials in the input variables where polynomials are chosen in coherency with the probability distributions of those input variables [80]. Consider a random vector with independent components $X \in R^M$ described by the joint PDF f_X. We can also consider a finite variance computational model as a map $Y = M(X)$, with $Y \in R$ such that:

$$E[Y^2] = \int_{D_X} M^2(x) f_X(x) dx < \infty. \tag{1.39}$$

Then the PCE of $M(X)$ is defined as:

$$Y = M(X) = \sum_{\alpha \in N^M} y_\alpha \Psi_\alpha(X), \tag{1.40}$$

where the $\Psi_\alpha(X)$are multivariate polynomials orthonormal with respect to f_X, $\alpha \in N^M$is a multi-index that identifies the components of the multivariate polynomials $\Psi_\alpha$and the $y_\alpha \in R$are the corresponding coefficients (coordinates). In realistic applications, the sum in Equation above needs to be truncated to a finite sum, by introducing the truncated polynomial chaos expansion:

$$M(X) \approx M^{PC}(X) = \sum_{\alpha \in A} y_\alpha \Psi_\alpha(X), \tag{1.41}$$

where $A \subset N^M$is the set of selected multi-indices of multivariate polynomials.

1.8.4.3 PC-Kriging

The two aforementioned techniques, PCE and Kriging, have been developed more or less in parallel so far with little interactions between the researchers in the two fields. By combining these two models, which is called as PC-Kriging, a sparse set of orthonormal polynomials (PCE) approximates the global behavior of the computational model whereas Kriging manages the local variability of the model output. The optimal sparse set of polynomials are determined by an adaptive algorithm similar to the least angle regression algorithm. From the numerical investigations, it is concluded that PC-Kriging performs better than or at least as good as the two distinct meta-modeling techniques. Moreover, when the experimental design has a limited size, a larger gain in accuracy is also confirmed [81].

Thanks to ETH Zurich, who has been developing open-source scientific modules to carry out various uncertainty quantification, the software UQLab is available, and this enables to perform surrogate modeling with PC-Kriging method [82].

Chapter 2

Establishing Fundamental Methodology

This chapter describes a process to prepare a fundamental and comprehensive methodology for the uncertainty analyses. It should be noted that building a skeleton of integrated methodology for both uncertainty propagation and sensitivity analysis is a main aim in this chapter. Therefore, the work does not involve detailed analyses considering precise reactor data since validating a noise simulator or prioritizing the input uncertain parameters to enhance reactor operation is not the main purpose.

The methodology is tested on a hypothetical case of "absorber of variable strength" at CROCUS zero-power reactor [83]. The nuclear data needed for the modeling of the reactor core are generated with the Monte Carlo code Serpent [67] and the neutron noise simulations are performed using the neutron noise tool CORE SIM [18].

2.1 Description of Target Experiment

2.1.1 Target Reactor

The CROCUS zero-power reactor is selected as a target reactor (see Chapter 1.4.1). The initial position of control rod is set to "all rods in (ARI)".

2.1.2 Target Event

A case of an absorber of variable strength is selected as an event which induces neutron noise into the core. An absorber of variable strength corresponds to the fluctuation of the neutron absorptions at selected locations in the system and is modeled with the fluctuation of the neutron macroscopic cross-sections at the location of the neutron noise source. Since the mathematical treatment as well as modeling of this case are easier than those of other sources, it is then selected as an initial trial case to develop the basic methodologies.

Here, an arbitrary event is considered in which the UO_2 fuel density oscillates between 100 % and 120 % of its nominal value at a frequency of 1 Hz. This event describes the density change in all the 336 UO_2 fuel rods.

2.2 Preparation for the Analysis

2.2.1 Process of Analysis

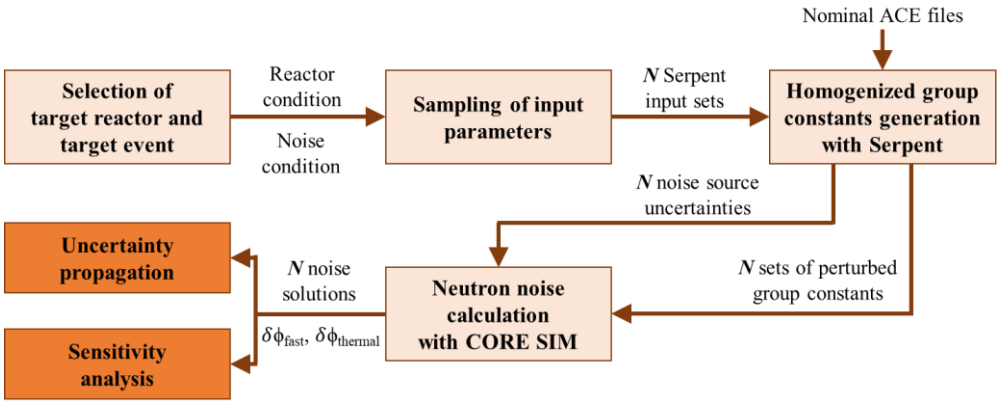

Figure 2.1: Flow chart for the uncertainty analyses

Figure 2.1 shows a schematic flow chart of the developed methodology. Both the uncertainty propagation and the sensitivity analysis commonly use a large part

of the entire analysis process, from the selection of uncertain parameters to the actual code simulations, which will be described in Chapter 2.2.2 to Chapter 2.2.5. Afterwards, Chapter 2.3 and Chapter 2.4 will cover the detailed process on UP and SA, respectively.

2.2.2 Listing Input Parameters

A phenomena identification is a systematic and documented way of gathering information on a specific subject, in order to determine what has the priority for the research on that subject. The "Phenomena" here can actually be the condition of a particular reactor, system, component, a physical or engineering approximation, a reactor parameter, or anything else that might influence the figure-of-merit [84].

The neutron noise balance equation implemented in CORE SIM and CORE SIM+ is written in a matrix form as reported below [70, 18].

$$\boldsymbol{L}\delta\phi = \delta S, \tag{2.1}$$

where $\boldsymbol{L}$ is the diffusion approximation of the transport operator, which depends on the neutron diffusion coefficients, the kinetics parameters, the effective multiplication factor of the system and the static cross-sections of the system. The noise source term, δS, refers to the neutron noise source resulting from the fluctuations of the cross-sections as described in the Chapter 1.8.3.

Table 2.1 summarizes the remarkable phenomena at the given condition and input parameters that can influence each phenomenon, which are selected based on expert judgement. For $\boldsymbol{L}$, the uncertainties in the design and operating parameters can be considered as influential and possibly correlated parameters [85].

<table>
<tr><th colspan="3">Phenomenon Description</th><th>Key Parameters</th></tr>
<tr><td colspan="3">Diffusion coefficients</td><td>Initial pool temperature</td></tr>
<tr><td colspan="3" rowspan="5">Effective delayed neutron fraction/
Decay constant</td><td>^{235}U homogeneity</td></tr>
<tr><td>^{235}U loading per rod</td></tr>
<tr><td>Control rod displacement</td></tr>
<tr><td>Water level</td></tr>
<tr><td>Control rod chemical composition</td></tr>
<tr><td colspan="2" rowspan="5">Initial static flux</td><td>Total power</td></tr>
<tr><td>Fuel heated area</td></tr>
<tr><td rowspan="2">Peaking factor</td><td>Control rod displacement
(radial direction)</td></tr>
<tr><td>Control rod displacement
(axial direction)</td></tr>
<tr><td rowspan="2">Isotopic composition
(Manufacturing tolerance)</td><td>^{235}U homogeneity</td></tr>
<tr><td>^{235}U loading per rod</td></tr>
<tr><td rowspan="3">Neutron energy flux spectrum[4]</td><td rowspan="3">Factors in six factor formula</td><td rowspan="3">Thermal utilization factor ($\boldsymbol{f}$)</td><td>Water level</td></tr>
<tr><td>Initial position of control rods</td></tr>
<tr><td>Control rods chemical composition</td></tr>
</table>

[4] Here, the neutron energy flux spectrum is considered as one of the main phenomena because of its contribution to the condensation of the cross-sections (Σ_X).

			Water level
			^{235}U homogeneity
			^{235}U loading per rod
			Fuel burnup (^{235}U content during whole cycle)
		Resonance escape probability ($\boldsymbol{p}$)	Fuel diameter
			Cladding thickness
			Filler gap thickness
		Fast fission factor ($\boldsymbol{\varepsilon}$)	Fuel diameter
			Cladding thickness
			Filler gap thickness
			^{235}U enrichment
		Reproduction factor (η)	Composition of the fuel (Ratio between ^{235}U and ^{238}U)
	Neutron speed (Average fast neutron speed/ Average thermal neutron speed)		Total power
			Initial pool temperature
Noise source			Depends on the target event (Void generation, fuel rods displacement, etc)

Table 2.1: Main phenomena and high priority parameters affecting the neutron noise [83]

Meanwhile, the noise source defined here is a change in UO_2 fuel density, namely, the parameters related to the δS are already considered as one of the

components in $\boldsymbol{L}$. Table 2.2 summarizes the selected 26 parameters with their distribution information: 10 of 26 parameters are correlated and sampled accordingly, while the remaining 16 parameters are sampled independently.

No.	**Parameter**		**Distribution**	**Unit**	**Mean**	**Standard deviation (Lower /Upper limit[5])**	**Correlation with other parameters[6]**
1	Water level		Normal	cm	95.22	0.01	
2	Initial pool temperature		Normal	°C	20.0	0.02	
3	Initial pool density		-	g/ cm^3			-2E-4* <**2**> + 1.0023
4	Fuel density	UO_2	Normal	g/ cm^3	10.556	0.034	
5		U_{metal}	Normal	g/ cm^3	18.677	0.044	
6	Nuclide mass fraction	^{235}U of UO_2	Normal	-	1.806E-2	7E-6	
7		^{238}U of UO_2	-	-			0.881513 - <**6**>
8		^{235}U of U_{metal}	Normal	-	9.470E-3	7E-6	

[5] This column shows the value of lower and upper limit in case of having uniform distribution.

[6] This column shows the correlated parameters which are composing the corresponding parameter in case of having no specific distribution information (<***k***> represents the parameter consistently with the ID numbers given in the first column).

9		^{238}U of UO_2	-	-			1 - <**8**>
10	Active fuel length		Normal	cm	100.0	0.02	
11	Relative axial location	Bottom of upper Grid	-	cm			<**10**> + 0.5
12		Bottom of upper Cd	-	cm			<**10**> + 1.0
13		Top of upper Cd	-	cm			<**10**> + 1.05
14		Top of upper Grid	-	cm			<**10**> + 2.55
15		Fuel rod top spring	-	cm			<**10**> + 1.47
16	Fuel diameter	Fuel rod outer surface of UO_2	Normal	cm	0.526	8.5E-4	

17		Cladding outer surface of UO_2	Normal	cm	0.63	5E-3	
18		Fuel rod outer surface of U_{metal}	Normal	cm	0.85	1E-3	
19		Cladding outer surface of U_{metal}	Uniform	cm	0.965	0.965 / 0.97	
20	Cladding thickness	UO_2	Normal	cm	0.085	5E-3	
21		U_{metal}	Normal	cm	0.1	5E-3	
22	Inner surface of cladding	UO_2	-	cm			<**17**> - <**20**>
23		U_{metal}	-	cm			<**19**> - <**21**>
24	Square pitch	UO_2	Normal	cm	1.837	2E-4	
25		U_{metal}	Normal	cm	2.917	2E-4	
26	Initial position of control rod		Uniform	cm	0.0	0.0 / 0.01	

Table 2.2: The distribution information of uncertain parameters considered for the case of “absorber of variable strength” [83]

2.2.3 Neutron Noise Calculation using CORE SIM

The core of the CROCUS reactor is approximately cylindrical in shape with a radius of about 65 cm including reflector area and a height of 100 cm. In CORE SIM, the core is modeled with a three-dimensional mesh of $43 \times 43 \times 30$ cells, in the $x-$, $y-$ and $z-$ directions of the core, respectively. The modeled reactor core, at the mid-point of the height, is depicted in Figure 2.2.

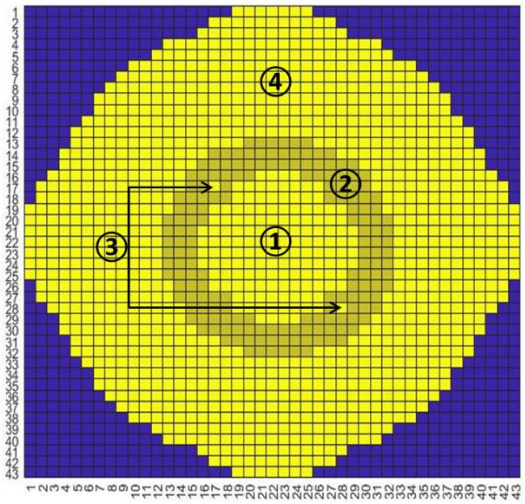

Figure 2.2: Modeled reactor core in CORE SIM (①: Central zone with UO_2, ②: Peripheral zone with U_{metal}, ③: Control rods, ④: Reflector)

The core is divided into four regions in the radial direction, and it is assumed that each region has homogeneous cross-sections as well as other kinetic data. The nuclear data required by CORE SIM are extracted from the Serpent output and assigned to the corresponding nodes of the nodalization scheme automatically by a MATLAB script developed in the course of this work.

Since the water level is lower than the height of fuel elements, around 5 cm of the fuel end-part is exposed to air. Therefore, it is clear that the neutron behavior at the region under the water and above the water must show different trends.

The neutron oscillating behavior becomes more remarkable at a region having higher static-flux, therefore, the mid-point of the height is chosen as an area of interest because of its high static flux. Additionally, when considering the initial control rods location as fully inserted, the axial neutron flux likely has a bottom skewed shape. In other words, the air exposed region has a relatively lower static flux compared to that of the core region under the water, which results in less influence on a spot having the highest flux. Hence, the fuel end-part above the water level is assumed to have the same kinetic values of that under the water to simplify the core modeling procedure. Nevertheless, to assure the acceptability of this assumption, the neutron noise uncertainty data at the core center region have been compared with and without modeling the air-exposed region. The maximum discrepancy between the two different approaches is 0.15 % and 0.23 % for the amplitude and the phase of neutron noise, respectively. In other words, the discrepancy is small enough to be neglected and, therefore, it justifies the assumption in this study.

Since CORE SIM performs the calculations in the frequency domain, the resulting neutron noise is a complex quantity. Therefore, the amplitude and the phase of the neutron noise are derived from a post-process.

2.2.4 Homogenized Group Constant with Serpent

The Serpent model of the CROCUS reactor has been built specifically for cross-section generation purposes [86]. The two-energy group cross-sections are generated with Serpent v2.1.30 for 8 universes in the reactor core: four in the radial direction (UO_2 region, U_{metal} region, control rods region and reflector region, as described in Figure 2.3 [87]) and two in the axial direction (regions under and above the water level)[7]. The calculation is performed using the JEFF-3.1.1 nuclear data base, with 150 active cycles of $5 \cdot 10^5$ source neutrons, skipping the first

[7] However, as it is introduced in previous chapter, the group constants from four universes under the water level are utilized for the further noise simulation.

100 cycles. At the same time, the effective kinetic parameters at the equivalent reactor conditions are generated through the Serpent computation [88].

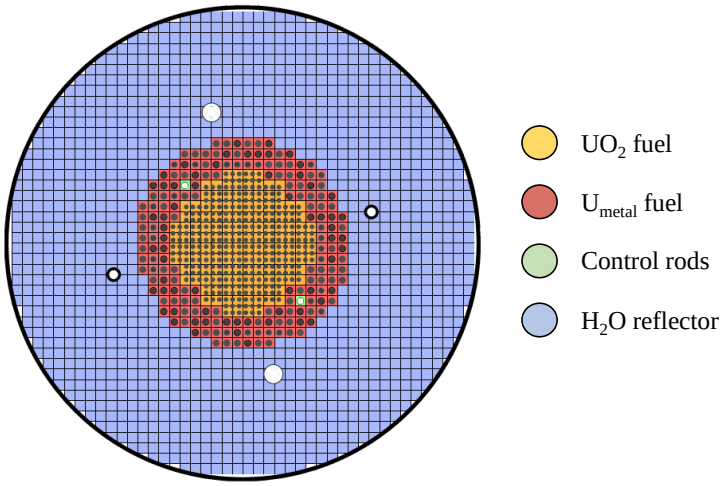

Figure 2.3: Radial nodalization for the region of the core

2.2.5 Output Uncertainty Treatment

2.2.5.1 Combining Uncertainties

Serpent is a Monte Carlo particle transport code, which provides an output as probability distribution with its mean value and the relative error. Therefore, a proper uncertainty treatment must be carried out in case of an arithmetic operation with the output values.

Post-processing with fission cross-section data

In CORE SIM, the perturbation of the macroscopic fission cross-section ($\delta\Sigma_f$) is multiplied by the average number of neutrons released per fission event (ν). Serpent provides the error distributions for both $\delta\Sigma_f$ and ν. Such information are combined to obtain an error distribution for the multiplication of two parameters as described below [89].

$$z = xy \tag{2.2}$$

$$\Delta z = |xy| \sqrt{(\frac{\Delta x}{x})^2 + (\frac{\Delta y}{y})^2}, \tag{2.3}$$

where x and y denote the mean values, and Δx, Δy denote the relative errors.

Perturbation of macroscopic cross-sections for an absorber of variable strength

The perturbation of a generic macroscopic cross-section ($\delta\Sigma_X$) is a crucial input for the neutron noise simulation with CORE SIM. In the case of an absorber of variable strength, the amplitude of the perturbation can be taken as the difference between two values: the one in perturbed conditions and the one in unperturbed conditions. Since both values have their own distributions from the Serpent computation, an additional error propagation is required to get the distribution for the difference of the two values and it is described below [89].

$$z = x - y \tag{2.4}$$

$$\Delta z = \sqrt{(\Delta x)^2 + (\Delta y)^2} \tag{2.5}$$

2.2.5.2 Resampling Output Data for Noise Simulation with CORE SIM

The nuclear data obtained from Serpent computation are not discrete values but have distributions with mean and error values. Therefore, it is necessary to define one representative value for the further CORE SIM computation.

A normal distribution is made using MATLAB with the Serpent-calculated mean and error values for all data of interest. Afterwards, one random value within this

distribution is sampled using Simple Random Sampling (SRS) method and saved in an appropriate format for CORE SIM computation.

2.3 Neutron Noise under the Unperturbed Condition

The behavior of static fluxes and thermal neutron noise under the nominal condition in radial direction of the core are investigated as shown in Figure 2.4 and Figure 2.5. The nominal behavior in static and dynamic condition can play a role as a reference point which helps us to understand the results from further uncertainty analyses. The static fluxes in both energy groups show similar tendency that the values increase when it gets close to the core center. The amplitude of neutron noise shows similar pattern with static flux, while the phase of neutron noise is spatially homogeneous. Neutron noise data in Figure 2.5 correspond to the absolute noise amplitude and phase, respectively, which are directly converted from the original complex quantity obtained from CORE SIM computation.

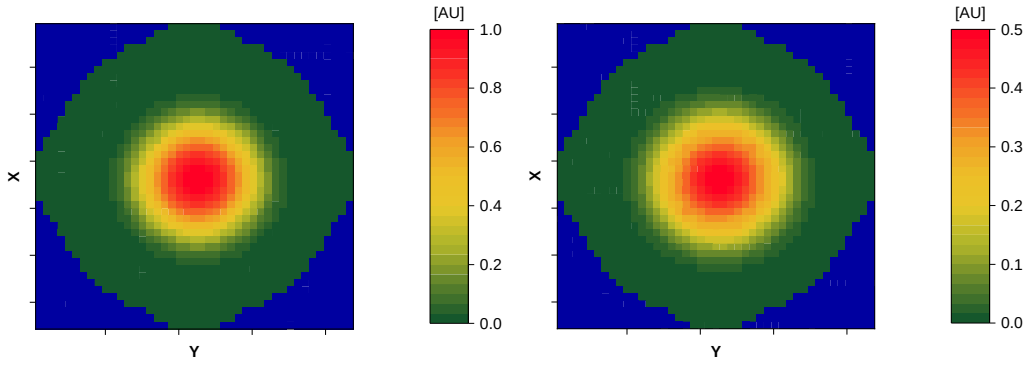

a. Fast static flux b. Thermal static flux

Figure 2.4: Static flux behavior in the mid-height of the core

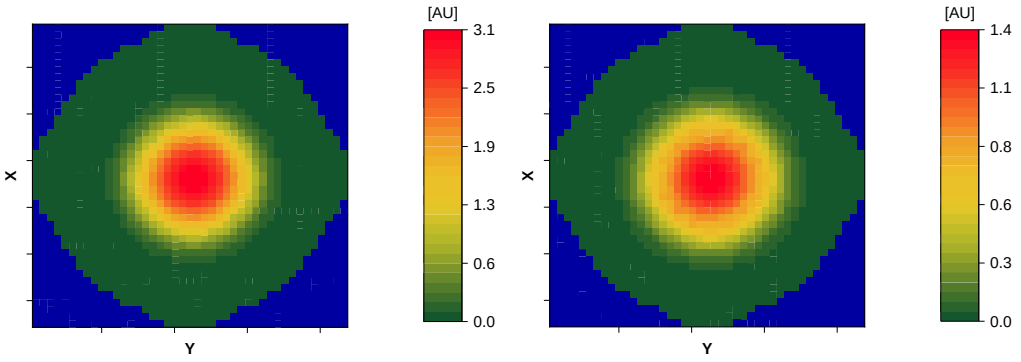

a. Amplitude of fast neutron noise

b. Amplitude of thermal neutron noise

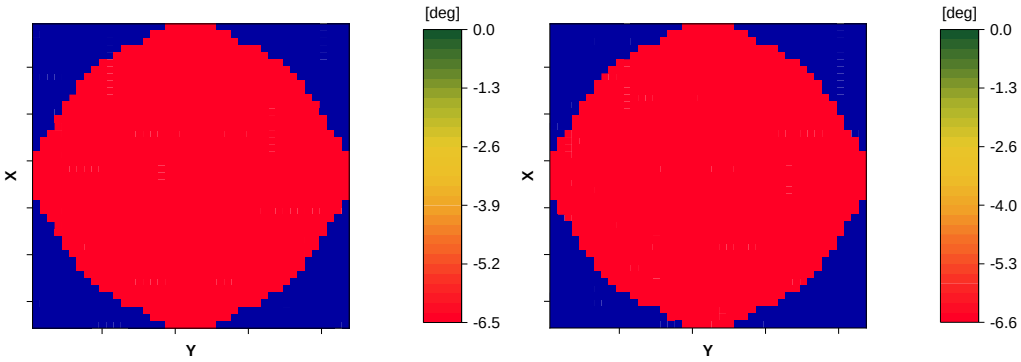

c. Phase of fast neutron noise

d. Phase of thermal neutron noise

Figure 2.5: Neutron noise behavior in the mid-height of the core

2.4 Uncertainty Analysis

This chapter describes the process of uncertainty propagation and sensitivity analysis. As it is aforesaid, the main purpose is building a basic structure of comprehensive methodology, which can become a foundation of further studies with various reactors and noise inducing events. The following work involves a discussion regarding the available approaches and a confirmation of their compatibilities in analyzing neutron noise behavior.

As it is earlier introduced in Figure 2.1, a sample generation of input parameters is made first. This is done by SRS, and the sampled inputs are used for group constants generation with Serpent. It is followed by noise simulation with CORE SIM and the obtained neutron noise data are used as outputs for uncertainty propagation and sensitivity analysis. When the analysis is carried out locally, the neutron noise corresponds to the value at the center position of the reactor core.

The uncertainties of neutron noise are determined by GRS methodology using Wilks' formula and brute force Monte Carlo method. Through the comparisons of processes and results, the pros and cons of each methodology is discussed. The following sensitivity analyses are carried out with two different approaches: correlation-based and variable-based approaches. The suitability of approaches in this study is discussed in terms of their functions in identifying the input parameters which are responsible for the output (neutron noise) uncertainties.

2.4.1 Generation of Random Samples

Considering the character and the condition of the target reactor, the applicable parameters are condensed and tabulated with their distribution data in Table 2.2. The parameters under normal distribution are considered as having a truncated normal distribution within the upper and lower design boundary values.

A total of 500 different sets of values for the uncertain parameters are generated with the SRS method using a program developed in MATLAB. These sets are then used as inputs for a series of computations with Serpent in order to create sets of two-energy group macroscopic cross-sections needed for the CORE SIM calculations.

Once all the 500 input sets are generated, a batch computation with CORE SIM is performed. Since CORE SIM performs the calculations in the frequency domain, the obtained neutron noise is a complex quantity, with an amplitude and a phase. Both values characterizing the neutron noise are calculated in an additional post-processing step.

2.4.2 Uncertainty Propagation

Two different approaches using GRS method and brute force Monte Carlo method are considered for a comparison in uncertainty propagation. GRS method is utilized by considering 1st order and 4th order Wilks' formula for 95 %/95 % tolerance limits. Meanwhile, the brute force Monte Carlo method demands a large sample size to ensure a realistic estimation, therefore, a surrogate modeling is used to increase sample size from 500 to 20,000.

2.4.2.1 GRS Methodology using Wilks' Formula

For the 1st order and 4th order Wilks' formula for two-sided tolerance limits, 93 times and 260 times of code calculation are required, respectively [90]. In case of the 1st order Wilks' formula, the largest and the lowest values among 93 calculation results credit the uncertainty propagation result to satisfy the 95 %/95 % criterion. Similarly, the relevant values are the 4th largest and the 4th smallest values for the case of 4th order Wilks' formula.

2.4.2.2 Brute Force Monte Carlo Method

In order to increase the sample size to build a faithful PDF of output data (neutron noise), a Kriging approximation included in DACE package (see Chapter 1.8.4.1) is used as a surrogate model.

In this study, considering the complexity underlying the neutron noise behavior, the second order polynomial and the Gaussian function are selected as a regression model and a correlation model, respectively. The mean squared errors (MSE) of the predictor are obtained as 7E-4 for the amplitude of the noise and 1E-4 for the phase of the noise, where 20,000 cases are predicted based on 500 results from actual code simulation.

As it can be seen in Figure 2.6, a histogram as well as a PDF is made for each neutron noise data. A series of normality tests are performed with Shapiro-Wilk test and the obtained p-values are summarized in Table 2.3. Since all p-values are

large enough (typically > 0.05), the hypothesis of normality for the outputs cannot be rejected at a significance level of 5 %.

Parameter	p-value
Amplitude of fast neutron noise	0.0698
Amplitude of thermal neutron noise	0.1005
Phase of fast neutron noise	0.6492
Phase of thermal neutron noise	0.8818

Table 2.3: Shapiro-Wilks test for normality p-value for neutron noise data

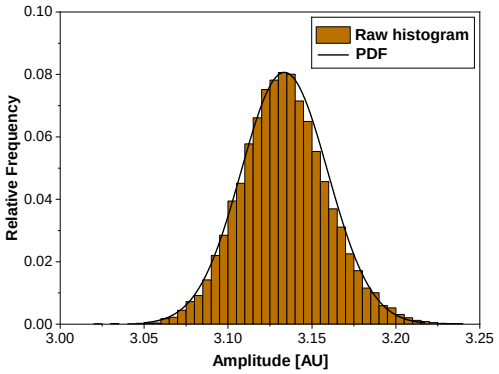

a. Amplitude of fast neutron noise

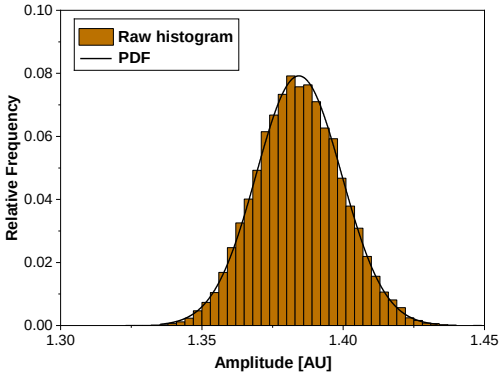

b. Amplitude of thermal neutron noise

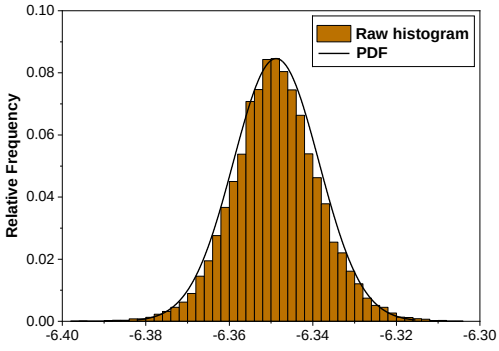

c. Phase of fast neutron noise

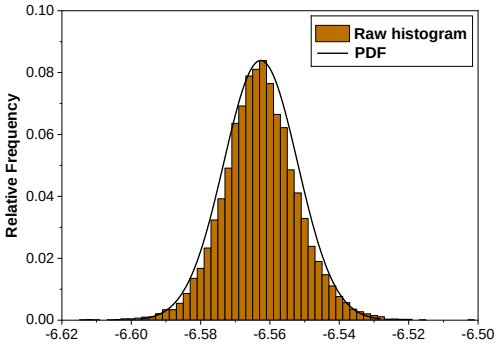

d. Phase of thermal neutron noise

Figure 2.6: Probability density function of neutron noise

After increasing the sample size by surrogate modeling, the 95 % upper and lower limits are identified, which correspond to 95 % and 5 % population level, respectively.

2.4.2.3 Comparison of Methodologies

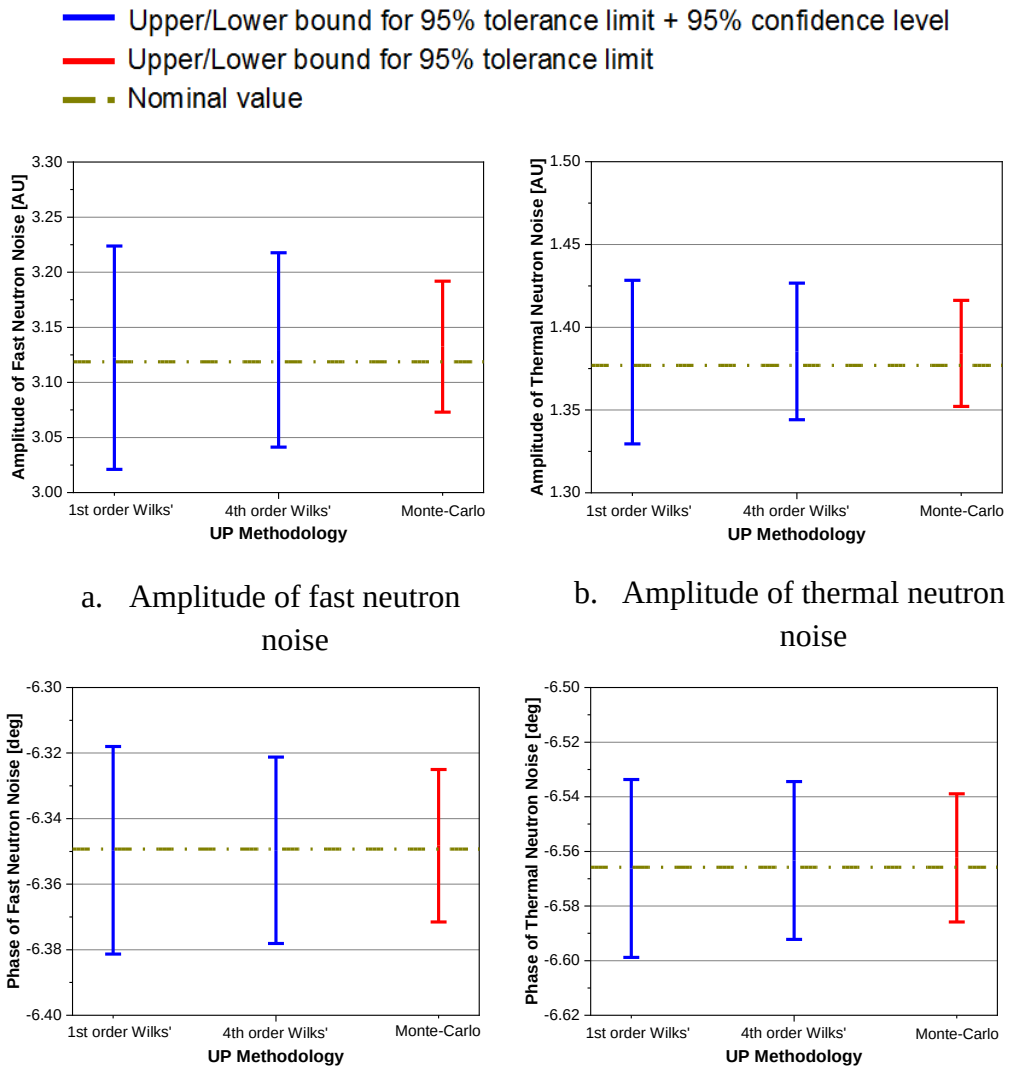

a. Amplitude of fast neutron noise

b. Amplitude of thermal neutron noise

c. Phase of fast neutron noise

d. Phase of thermal neutron noise

Figure 2.7: Uncertainty range estimated with different methodologies

Figure 2.7 shows the comparison of the results from two methods. The nominal value signifies an output data calculated from nominal conditions where all input parameters take their nominal values (see Table 2.2) and no uncertainty is considered.

Above all, when using the 1st order or the 4th order of Wilks' formula, the uncertainties become larger than that from Monte Carlo approach, therefore, more conservative results are drawn. When the result from using 1st order Wilks' formula is compared to that from using 4th order Wilks' formula, the 1st order Wilks' formula tends to give more conservative range, because of the less accurate estimate of the percentiles. Since the tolerance limit is an approximation to the true population, there is an inherent conservatism in the typical prediction as in the Equation (1.14). In case of $N = 93$, which is the minimum size of samples for 1st order Wilks' formula, there is a tendency to strongly over-estimate the 95th quantile of the population and under-estimate the 5th quantile of the population. However, the conservatism diminishes as the sample size increases. Therefore, the result from 4th order Wilks' formula shows a smaller uncertainty range, which is more realistic outcome than the result from 1st order Wilks' formula.

2.4.2.4 Spatial Distribution of Neutron Noise Uncertainty

As an example of the spatial distribution of the output uncertainties, the plane at mid-elevation of the reactor core is taken. Figure 2.8 depict the results for both amplitude and phase of neutron noise.

The magnitude of the neutron noise uncertainty has a spatial dependency for both the fast and the thermal neutron noise, while the uncertainty in the phase is approximately constant. In Figure 2.8-a and -b, the values become larger as the location gets closer to the center of the core. For a better understanding, the uncertainties of the neutron noise amplitudes are normalized by a static neutron flux as shown in Figure 2.9. Here the normalized uncertainties show a uniform value throughout the core region. This implies that the neutron noise uncertainty is highly correlated with the static flux. Meanwhile, the uncertainty of the phase shows no strong spatial dependency as shown in Figure 2.8-c and -d, because all the fuel rods in the central part of the core are perturbed at the same time and in

the same manner. Moreover, since the reactor core is relatively small, the point-kinetic component of the system response to the perturbation is overwhelming. The amplitude of the neutron noise thus follows the static flux, whereas the phase of the neutron noise is spatially homogeneous.

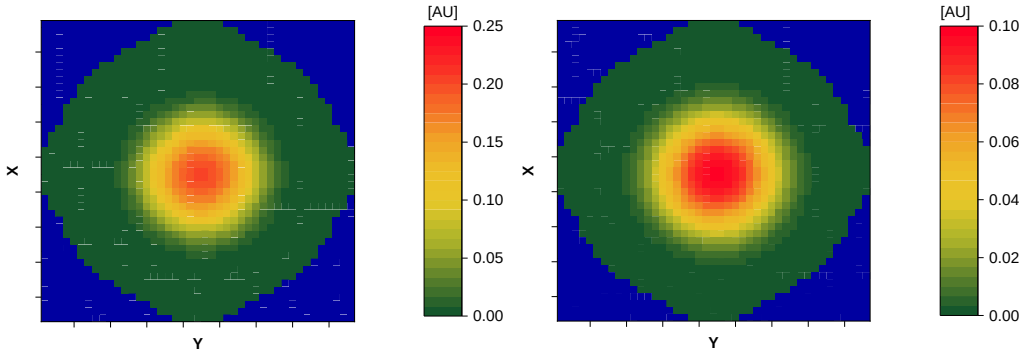

a. Amplitude of fast neutron noise

b. Amplitude of thermal neutron noise

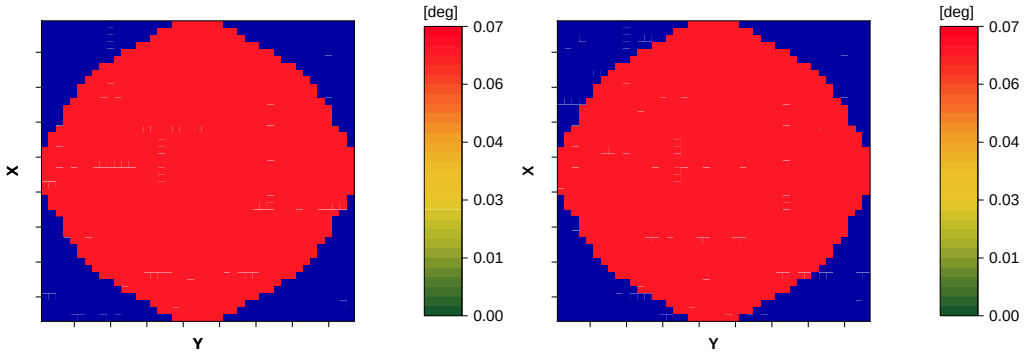

c. Phase of fast neutron noise

d. Phase of thermal neutron noise

Figure 2.8: The magnitude of the neutron noise uncertainty in radial direction of the core (mid-height of the core)

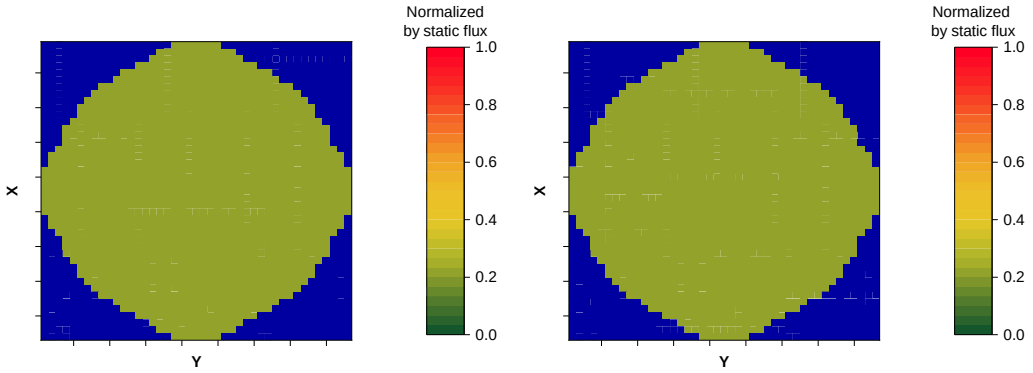

a. Amplitude of fast neutron noise

b. Amplitude of thermal neutron noise

Figure 2.9: Amplitude of neutron noise normalized by static flux

2.4.3 Sensitivity Analysis

This chapter aims to compare the performance of different approaches (i.e., correlation-based approach and the variance-based approach) in sensitivity analysis and to discuss the outcome in relation to pros and cons that each approach has.

2.4.3.1 Correlation-based Approach

Backgrounds

The SCC is selected as a representative sensitivity measure in correlation-based approach. The SCC has been extensively used in sensitivity analyses due to its advantage of simplicity and ease of use. However, it has a drawback that it can draw only a limited conclusion in the case of general nonlinear and non-monotonic models. In addition to this, SCC cannot be used to say anything about a cause-and-effect relationship. It can be only concluded that input parameter and output value are related by examining the value of SCC. However, the same value of SCC does not tell us if the input parameter influences the output value or the other way around. That is, the correlation-based coefficient should not be the

primary tool used to study causation, because of the problem with the influence of third variables.

In this regard, calculating the Spearman's Partial Correlation Coefficient (SPCC) can be helpful to check the direct effect of each input parameter on the output value. The SPCC provides a measure of strength of the correlation between the individual input parameter and output value when the effect of all of the other parameters is removed [51].

In the case of one explained output value Y and two explicative input parameters X_1 and X_2 (in case of Spearman correlation coefficient, X_i represents the rank variable), the partial correlation coefficient can be estimated as follows:

$$r_{Y,X_1|X_2} = \frac{r_{Y,X_1} - r_{Y,X_2} r_{X_1,X_2}}{\left(1 - r_{Y,X_2}^2\right)^{\frac{1}{2}} \left(1 - r_{X_1,X_2}^2\right)^{\frac{1}{2}}}. \tag{2.6}$$

The recursive formula in the general case is provided in the following equation:

$$r_{Y,X_j|X_{\sim j}} = \frac{r_{Y,X_j|X_{1,2,\ldots,j-1,j+1,\ldots,N-1}} - r_{Y,X_N|X_{1,2,\ldots,N-1}} r_{X_j,X_N|X_{1,2,\ldots,j-1,j+1,\ldots,N-1}}}{\left(1 - r_{Y,X_N|X_{1,2,\ldots,N-1}}^2\right)^{\frac{1}{2}} \left(1 - r_{X_j,X_N|X_{1,2,\ldots,j-1,j+1,\ldots,N-1}}^2\right)^{\frac{1}{2}}}, \tag{2.7}$$

where $X_{\sim j} = X_{1,2,\ldots,j-1,j+1,\ldots,N}$.

However, apart from its applicability to checking the individual effect on output value, SPCCs do not yield any relevant information regarding the relative importance of the explicative variables. In other words, SPCCs will be used in this study only to check the degree of the collaboration between the parameters, not to find the most influencing input parameters on neutron noise uncertainty which corresponds to the original purpose of the sensitivity analysis.

Results

Figure 2.10 illustrates SCC and SPCC which are calculated from 500 samples. These are estimated for 16 out of the 26 input parameters listed in in Table 2.2. Since the other 10 parameters are dependent on the selected 16 parameters according to the correlations described in the Table 2.2, their sensitivity coefficients are directly correlated to those of selected parameters. Therefore, the 16 main parameters leading the phenomenon are regarded as having a higher priority and only considered in this analysis.

Following the guidelines described in Chapter 1.7.4.1, a critical value of correlation coefficient with 500 samples and significance level of 0.05 becomes 0.1, approximately. Therefore, we can say that the phase of neutron noise is not correlated to specific input parameters but correlated to all parameters in a similar level. The same goes for the amplitude of neutron noise except the 9th input parameter, which stands for "fuel rod outer diameter of the cladding" —a diameter of the fuel rod.

In terms of the SPCCs, the results can be translated as follows:

If SPCC is larger than SCC, the input parameter (X_j) has a direct effect to the output result (Y). However, the contribution of X_j is screened because of its relatively small initial uncertainty range or small weighting factor applied to this parameter compared to other parameters ($X_k,\ j \neq k$). That is to say, the collaboration with other parameters works towards decreasing the amount of effect on Y. If SPCC is smaller than SCC, X_j increases its influence by the cooperation with other parameters.

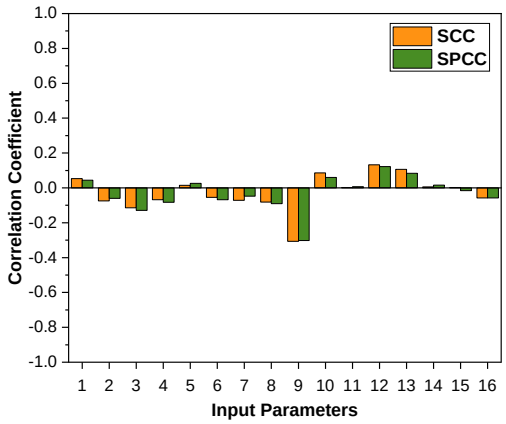

a. Amplitude of fast neutron noise

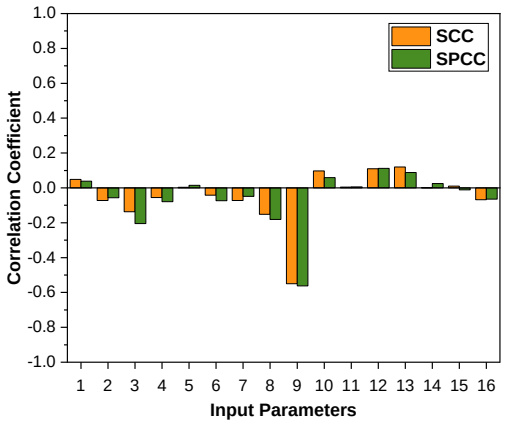

b. Amplitude of thermal neutron noise

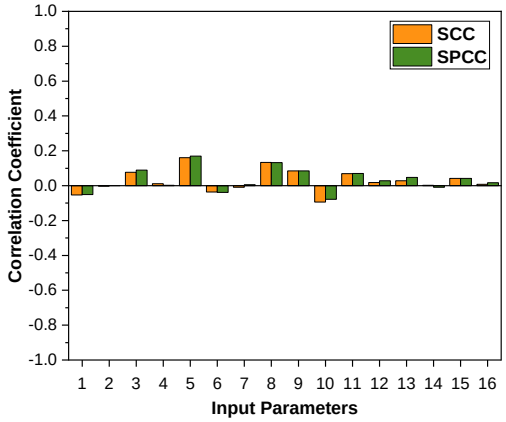

c. Phase of fast neutron noise

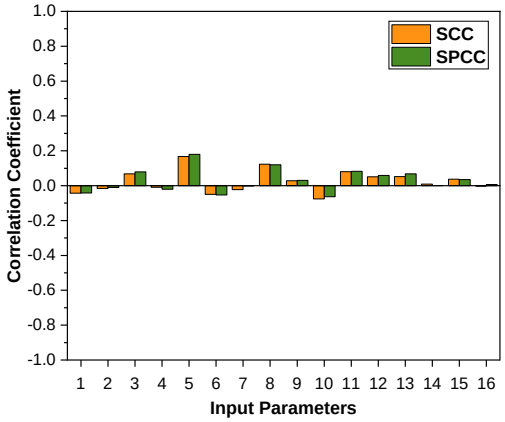

d. Phase of thermal neutron noise

No.	Input parameter	No.	Input parameter
1	Water level	9	Fuel rod outer diameter of cladding (UO_2)
2	Initial pool temperature	10	Fuel rod outer diameter (U_{metal})
3	Fuel density (UO_2)	11	Fuel rod outer diameter of cladding (U_{metal})
4	Fuel density (U_{metal})	12	Cladding thickness (UO_2)
5	Enrichment (UO_2)	13	Cladding thickness (U_{metal})
6	Enrichment (U_{metal})	14	Square pitch (UO_2)

7	Active fuel length	15	Square pitch (U_{metal})
8	Fuel rod outer diameter (UO_2)	16	Initial position of control rod

Figure 2.10: SCC and SPCC of input parameters

However, as depicted in Figure 2.10, there is no remarkable difference between the results from SCC and SPCC, and this result implies that no strong collaboration among the input parameters is detected. Nevertheless, it is hard to conclude that the input parameters showing negligible correlation here have actually no effect on the output data. Since the SCC detects monotonic relationship between the input and the output variables, there is a possibility that the real correlation is concealed due to its non-monotonic relationship. Therefore, it is worthwhile to check the true correlation through an additional analysis using variance-based approaches.

2.4.3.2 Variance-based Approach

Backgrounds

Considering its higher precision and relatively cheaper computational cost compared to the analysis using Sobol's approach (see Chapter 1.7.4.3), Jansen's formula is used for the following sensitivity analysis with variance-based approach. The first order and total sensitivity indices are calculated based on 20,000 samples, whose simulation results are predicted by Kriging interpolation using 500 data sets from actual code execution.

Results

Figure 2.11 with sensitivity indices larger than 0.1 can be regarded as "highly sensitive" and the indices between 0.01 and 0.1 can be classified into "sensitive" [91].

In case of first order sensitivity indices, the 9^{th} input parameter has a dominant effect on the amplitude of neutron noise and there is no remarkable parameter

affecting the phase of neutron noise. These findings are identical to the results from the correlation-based sensitivity analysis.

The total sensitivity indices of all parameters are larger than the first order sensitivity indices, since the total index represents the effect that a parameter of interest can make by itself as well as with other parameters. In case of the amplitude of neutron noise, the 9th parameter still remains as the most influential parameter and it is followed by the 5th and 6th parameters (enrichment of the fuel). Meanwhile, there is no clearly dominant parameter on the phase of the neutron noise, even though all the total sensitivity indices become larger than the first order indices. Hence, it can be concluded that each input parameter is affecting the phase of the neutron noise not only by itself, but also by the collaboration with other parameters and the influence of each parameter is about the same.

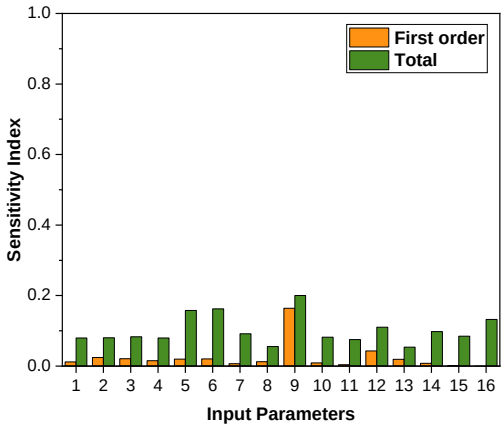

a. Amplitude of fast neutron noise

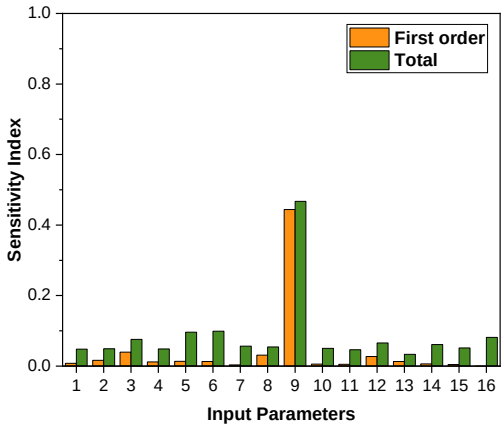

b. Amplitude of thermal neutron noise

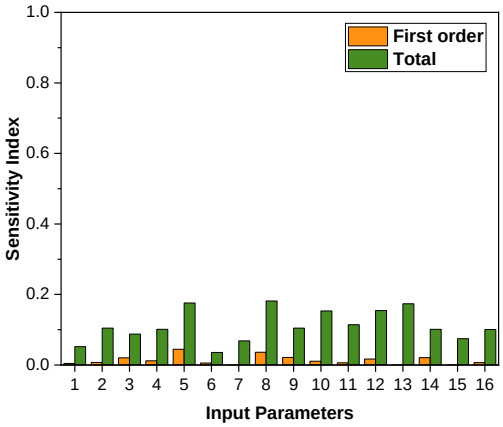

c. Phase of fast neutron noise

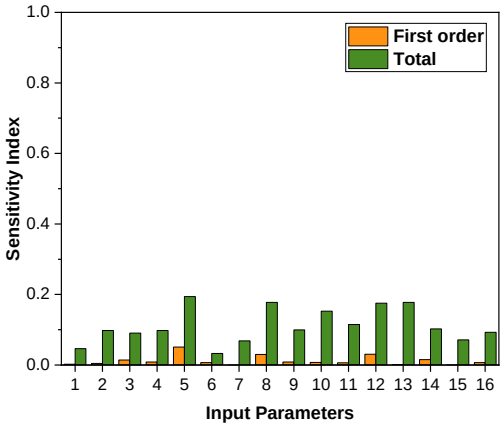

d. Phase of thermal neutron noise

No.	Input parameter	No.	Input parameter
1	Water level	9	Fuel rod outer diameter of cladding (UO_2)
2	Initial pool temperature	10	Fuel rod outer diameter (U_{metal})
3	Fuel density (UO_2)	11	Fuel rod outer diameter of cladding (U_{metal})
4	Fuel density (U_{metal})	12	Cladding thickness (UO_2)
5	Enrichment (UO_2)	13	Cladding thickness (U_{metal})
6	Enrichment (U_{metal})	14	Square pitch (UO_2)
7	Active fuel length	15	Square pitch (U_{metal})
8	Fuel rod outer diameter (UO_2)	16	Initial position of control rod

Figure 2.11: First order and total sensitivity indices of input parameters

2.4.3.3 Discussions

As described in the two chapters above, the UO_2 fuel rod outer diameter (9^{th} parameter) shows the maximum effect on the amplitude of the neutron noise. Since this parameter directly affects the area occupied by the fuel inside of the core, it contributes to the changes on moderator-to-fuel ratio. In other words, the increased fuel rod outer diameter results in the decrease of the resonance escape probability and the increase of the thermal utilization factor. Therefore, it

changes the effective neutron multiplication factor (k_{eff}), which affects the static and dynamic behavior of the neutron flux and ultimately the neutron noise.

It is also an interesting point that only the outer diameter of UO_2 has a remarkable effect on neutron noise whereas the outer diameter of U_{metal} has no strong effect. It is inferred that this difference stems from the followings: the differences on initial uncertainties and the total number of fuel rods. The outer diameter of UO_2 has an uncertainty which is two times larger than that of U_{metal}. Plus, there are 336 rods for UO_2 fuels and 176 rods for U_{metal} fuels. Therefore, the uniform change of cladding thickness of UO_2 fuels results in a bigger decline of the moderator-to-fuel ratio than by the change of U_{metal} fuels. In addition, the perturbation introduced in the system and inducing the neutron noise is directly associated with the UO_2 fuel rods.

When the results from two different approaches are compared to each other, the main findings can be summarized as follows.

1) The total sensitivity index makes it possible to predict the hidden collaboration between the parameters, which is invisible with the correlation-based approach.
2) In terms of the ranking parameters, more precisely “finding out the most influential parameter to the neutron noise”, both correlation-based approach and variance-based approach predict the same results under the current analysis condition. However, for the sake of higher precision, additional discussion regarding the convergence of the sensitivity indices and the accuracy of surrogate modeling needs to be made. This will be dealt with accordingly in Chapter 3.5.

Chapter 3

Application of the Methodology to CROCUS Zero-Power Reactor

A further analysis is carried out based on the fundamental methodologies established in the previous chapter, with considering an existing experimental condition. This chapter is based on an experimental program at CROCUS reactor, which was conducted in the framework of CORTEX project. Through the analyses, it is expected that the pre-developed methodologies in Chapter 2 are validated and concretized with enhanced accuracy.

3.1 Description of Target Experiment

3.1.1 Target Reactor

The CROCUS zero-power reactor is considered as a target reactor also in this chapter. The initial operating condition of the reactor is identical to those described in Chapter 2, except the position of control rod which is changed into "fully withdrawn" according to a setup of given experiment [21, 87].

3.1.2 Target Event

Following the experimental campaign at the CROCUS reactor, the experiment carried out with COLIBRI fuel rods oscillator (see Chapter 1.5.2.2) is selected as

a target event in this section. The experimental condition considered in two sequential experimental campaigns with COLIBRI is almost identical except oscillation specification (oscillating amplitude and frequency) and detector installations. Therefore, this chapter focuses on first experimental campaign and its experimental condition is used in the analysis.

Among the experiments performed under the first experimental campaign, one representative case with oscillating amplitude and frequency of $2\ \mathrm{mm}$ and $1\ \mathrm{Hz}$, respectively, is selected as a target condition in this work. In the context of the CORTEX project, the output behavior at the location of 8 detectors (Detector 3 ~ Detector 10, see Figure 1.14) are mainly discussed with respect to the validation of the modeling tools. Therefore, the uncertainty analyses at the local points are going to be performed at these identical detector locations. Additionally, the noise behavior of fast neutrons is excluded from discussion for the sake of applicability of obtained results, since the in-core detectors detect only thermal neutrons.

3.2 Description of Computational Method and Quantities of Interest

3.2.1 CORE SIM+ Model of CROCUS

The core is modeled with a three-dimensional mesh of $44 \times 156 \times 54$ cells, in the $x-$, $y-$ and $z-$ directions of the core, respectively. The area around the neutron noise source is modeled with the fine meshes with the size of $2\ \mathrm{mm}$, whereas the remaining area is modeled with coarser meshes with a size of $3\ \mathrm{cm}$. The relevant description on modeling of noise source in CORE SIM+ computation is described in Chapter 1.5.2. Figure 3.1 shows the modeled reactor core at mid-core elevation. The two red lines at the boundaries of different regions

represent the location where the noise sources are assigned for the noise simulation[8]. The homogenized nuclear data are assigned to the corresponding meshes of the model through a MATLAB script developed in the course of this work. Different from the preliminary analysis in Chapter 2, the reactor core regions above the water level are added to the modeling to enhance an accuracy of modeled reactor core.

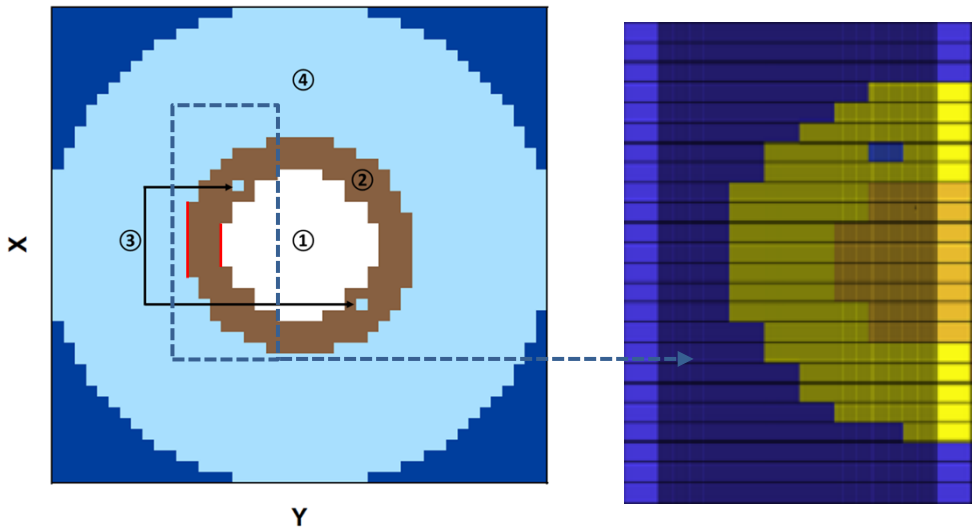

Figure 3.1: Modeled reactor core in CORE SIM+ (left) and the area around oscillating fuel rods modeled with fine meshes (right) (①: Central zone with UO_2, ②: Peripheral zone with U_{metal}, ③: Control rods, ④: Reflector)

[8] The modeled oscillating boundary which is closer to the core center (right-side red line in Figure 3.1) is shorter than the left side boundary although the actual two boundaries have same length as shown in Figure 1.14. This is because CORE SIM+ builds the noise source associated with the vibration from the differences between the cross-sections of the regions on the left and on the right sides of the moving boundaries (see Equation (1.5)). Thus, the parts of the moving boundaries that are between regions with the same cross-sections are not shown since their perturbation is zero.

3.2.2 Homogenized Group Constant with Serpent

The Serpent model which was built for cross-section generation in Chapter 2.2.4 is modified with different initial position of control rods (i.e., all rods out (ARO)) and adopted to this chapter for same purpose.

Due to convergence issues, the fast and thermal diffusion coefficients and the removal cross-section in reflector region above the water and the removal cross-section in control rod region above the water are set to small, constant non-zero values. As demonstrated in Chapter 2.2.3, the nuclear data changes in the region of “above water level” has little impact on neutron noise, this simplification of nuclear data does not affect the accuracy of the model.

3.2.3 Neutron Noise under the Unperturbed Condition

In the experiments carried out within the CORTEX project, the detector time series are converted into the frequency domain for the purpose of validating the noise simulators [32]. The conversion is made through the Fourier transform of auto- and cross-correlation functions, which are so-called APSD and CPSD, as early introduced in Chapter 1.6. In the same context, the simulation result from CORE SIM+ are used to derive APSD and CPSD following the Equation (1.11), with using Detector 5 as a reference detector.

The spatial distribution of static fluxes and thermal neutron noise at mid-height of the core, in nominal conditions where all input parameters take their nominal values and no uncertainty is considered (see Table 2.2 and Table 3.1), are shown in Figure 3.2 ~ Figure 3.4 The neutron noise is shown in two different quantities: the absolute noise (Figure 3.3) and QoI (Figure 3.4). The nominal behavior in static and dynamic condition can play a role as a reference point which helps to understand the results from further uncertainty analyses. The static fluxes in both energy groups show similar tendency that the values increase as it gets close to the core center.

Compared to the absolute (original) noise whose behavior is almost following the pattern of fundamental flux as shown in Figure 3.3-a, the QoI amplitude (Figure 3.4-a) filters out the point kinetic component and magnifies the spatial component of the neutron noise. Compared to the phase of absolute neutron noise, the variation of QoI phase becomes more visible in Figure 3.4-b, since the value at the reference location (Detector 5) is calibrated to zero.

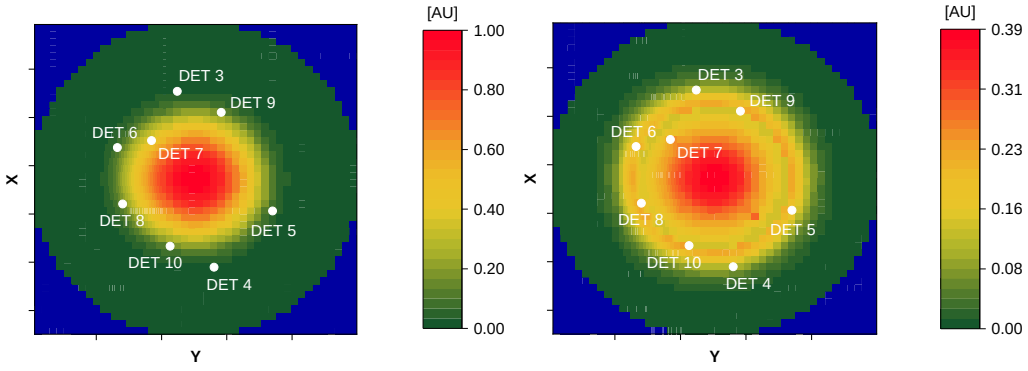

a. Fast static flux b. Thermal static flux

Figure 3.2: Static flux behavior in the mid-height of the core

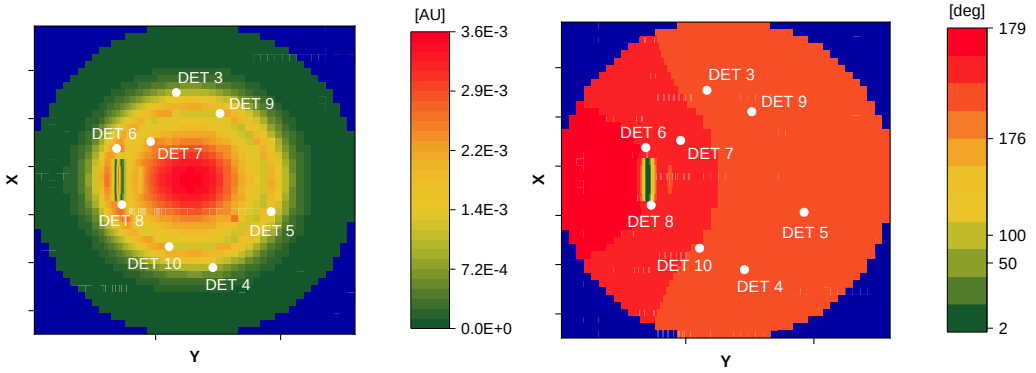

a. Amplitude b. Phase

Figure 3.3: Absolute neutron noise behavior in the mid-height of the core

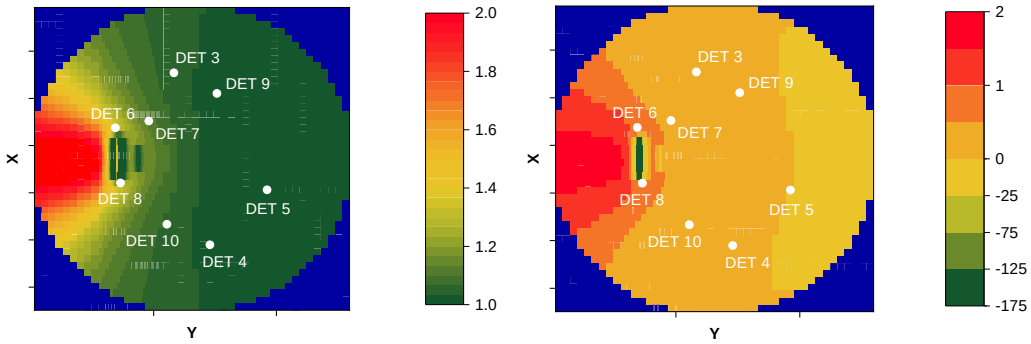

a. Amplitude b. Phase

Figure 3.4: QoI behavior in the mid-height of the core

3.3 Preparation for the Analysis

3.3.1 Process of Analysis

Figure 3.5 shows a schematic flow chart of the developed methodology, including the expected outcomes from each step. The subchapters below describe the important points involved in the various steps. Both uncertainty propagation and sensitivity analysis commonly consider the initial five steps from the selection of the "target reactor" and "target event" to the "neutron noise calculation". Here, the reactor and the condition inducing neutron noise are introduced and the relevant input parameters are listed. Based on the distribution information of each input parameter, all the parameters are sampled for N times for the group constant generation using Serpent. The CORE SIM+ uses obtained two-energy group macroscopic cross-sections as inputs and a batch computation is made for N times for both static and dynamic reactor conditions, resulting in N neutron noises. The obtained N neutron noise are then used for both uncertainty propagation and sensitivity analysis.

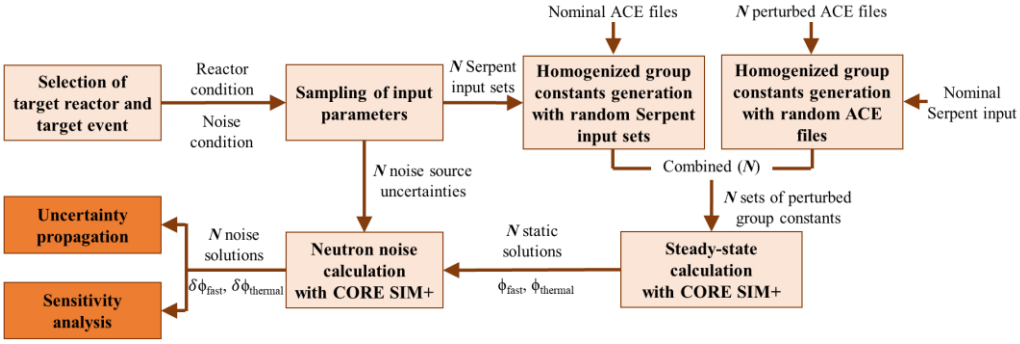

Figure 3.5: Flow chart for the uncertainty analyses

3.3.2 Listing Uncertain Parameters

The reactor design and operating parameters listed in Table 2.2 remain as uncertain parameters for group constant generation using Serpent, while the initial position of control rods is removed from the consideration. Additionally, the nuclear data uncertainties generated from perturbed set of ACE formatted files are further considered as a component in ***L***. The nuclear data uncertainties are treated in a distinct manner owing to their inherent correlations. The detailed information on a treatment process is described in Chapter 3.3.3.

Several parameters related to a description of noise source (δS) are also taken into consideration additionally: the oscillating amplitude, the oscillating frequency, and the location of noise source. The oscillating amplitude and frequency are assumed to perturb within ± 5 % from their nominal values. Since the location of the noise source can only be perturbed within a discrete number of meshes, it is designed to be perturbed with three values along the oscillating direction, -1, 0 and +1: -1 signifies the movement of 1 mesh away from the core center, while +1 means the movement of 1 mesh towards the center. The uncertainty parameters which are added from the list introduced in Table 2.2 are summarized in Table 3.1.

No.	Parameter	Distribution	Unit	Nominal value	Standard deviation (Lower/ Upper limit[9])
1~748	Nuclear data uncertainties[10]				
749	Oscillating amplitude	Normal	cm	0.2	0.01
750	Oscillating frequency	Normal	Hz	1	0.05
751	Location of noise source	Uniform	Mesh	Ideal oscillation boundary	-1/+1

Table 3.1: The distribution information of uncertain parameters additionally selected for the event of "fuel rods vibration"

3.3.3 Generation of Random Samples

Random sets of perturbed input parameters are generated based on the distribution information with a SRS method using a specifically designed MATLAB script. The eventual correlations are taken into account. The resulting input data sets are then used in a series of computations with Serpent in order to create the sets of two-energy group macroscopic cross-sections needed for the CORE SIM+ calculations.

The sampling of nuclear data, needed for generating group constants uncertainties, deserves further explanation, as it usually involves many correlated inputs.

[9] This column shows the value of lower and upper limit in case of having uniform distribution.

[10] Nuclear data uncertainties are treated in a distinct manner and the detailed information on a treatment process is described in Chapter 3.3.3.

The generation of the perturbed set of nuclear data is done through the sampling of multigroup covariances by using the PSI tool "NUSS (Nuclear data Uncertainty Stochastic Sampling)" [92]. NUSS is used in the present work to generate a perturbed set of the ACE formatted file, which will be used in the Serpent calculations required to produce the random sets of two-group constants needed for CORE SIM+. The Serpent calculations were performed with Serpent v2.1.29, using its native ENDF/B-VII.0 ACE files and ENDF/B-VII.1 covariances and the Scale 6.0 energy group structure [93]. The microscopic data for U-235, U-238, H-1 and O-16 are considered while the following reaction types are perturbed: (n, el), (n, inl), (n, 2n), (n, capture), (n, f), $\bar{\nu}$ and χ. The relevant propagated nuclear data consist of diffusion coefficient (D), absorption cross-section (Σ_{abs}), nu-fission cross-section ($\nu\Sigma_{fiss}$), and removal cross-section (Σ_{rem}) of two-energy groups in 8 reactor core regions as described in Chapter 2.2.4. The obtained group constants are summarized as a form of histogram in Appendix A.1.

It should be noted that, even though the kinetic parameters are perturbed in CORE SIM+, their uncertainties do not include uncertainties in their physical values, only the effect of nuclear data perturbations on the effective quantities determined by Serpent.

At the preliminary study carried out in Chapter 2, the uncertainties of homogenized group constants are propagated solely from the perturbation of design and operating parameters, and the analysis does not involve a perturbation of microscopic data. Accordingly, an inclusion of additional nuclear data uncertainties in this chapter raises questions about how to combine new uncertainties into the existing uncertainties (two-group constants uncertainties from design and operating parameters).

The most ideal solution is propagating uncertainties of two-group constants by perturbing all input parameters simultaneously as shown in Figure 3.6-a. However, a list of input parameters has been constantly modified while the CORTEX project was underway, thus, a possibility of including additional input parameters was kept open. Moreover, an availability of NUSS was unclear at the early stage of the project.

On the premise that there could be additional modification on microscopic data perturbation using NUSS, it is decided to make two separate Serpent computation as depicted in Figure 3.6-b. Thus, it becomes necessary to find a proper way to combine two outputs from two separate Serpent computations. Additionally, since the initial parameters perturb non-simultaneously, this process arises a question if it can guarantee the same outputs as the one unified approach (Figure 3.6-a) generates. The relevant discussions on aforementioned two questions are made in the following chapters.

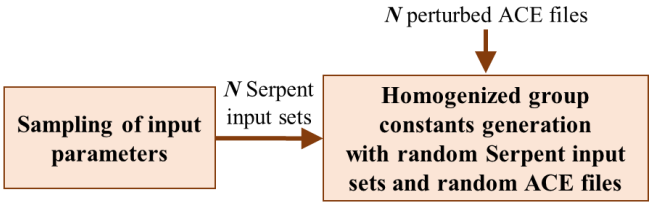

a. Propagating uncertainties with one unified Serpent computation

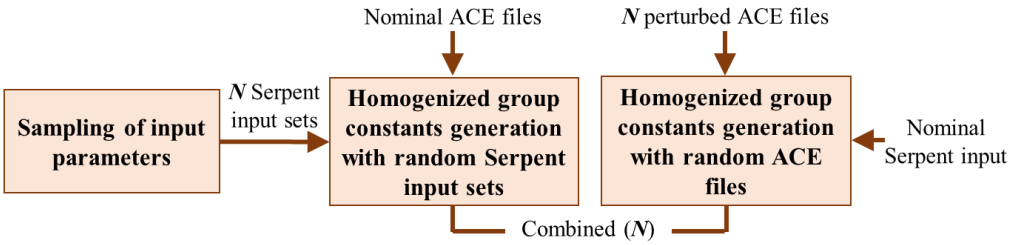

b. Propagating uncertainties with separate Serpent computations

Figure 3.6: Two variations for propagating nuclear data uncertainties

3.3.4 Investigation on Approaches for Group Constants Uncertainty Treatment

As it is demonstrated in the previous chapter, it is required to figure out the proper methodology for combining the nuclear data uncertainties with the nuclear data propagated from design and operating parameters. This becomes critical when considering the limited samples size and the impact of the selected methodology

to the accuracy of the output. In this respect, we introduce the three probable approaches and analyze the pros and cons from various angles.

1st approach: Resampling nuclear data from the new distribution

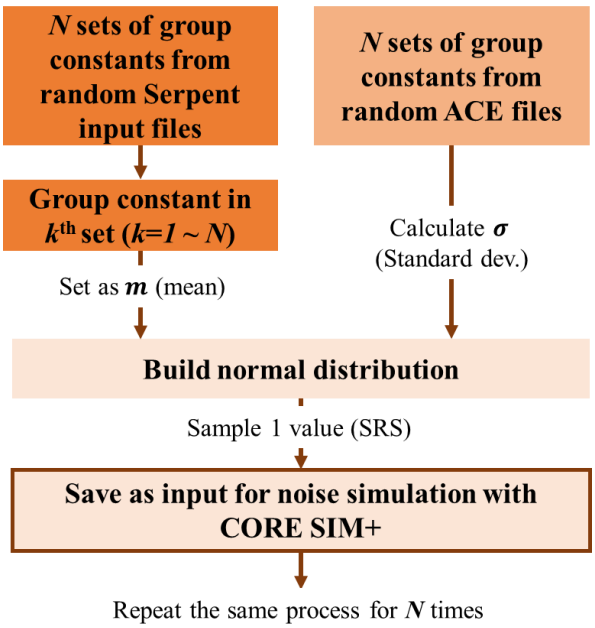

Figure 3.7: The procedure on nuclear data uncertainty treatment at 1st approach

The first approach described in Figure 3.7 assumes that group constants are having normal distribution: each data obtained from random Serpent input files is regarded as mean value while a standard deviation is calculated within the N group constants from random ACE files. Accordingly, normal distribution is built with calculated mean value and standard deviation. One value from each distribution is selected by SRS and directly saved as input for the further CORE SIM+ computation. For each nuclear data at different core region (8 universes shown in Figure 2.3), the same process is repeated for N times.

2nd approach: Rebuilding nuclear data by considering covariance information

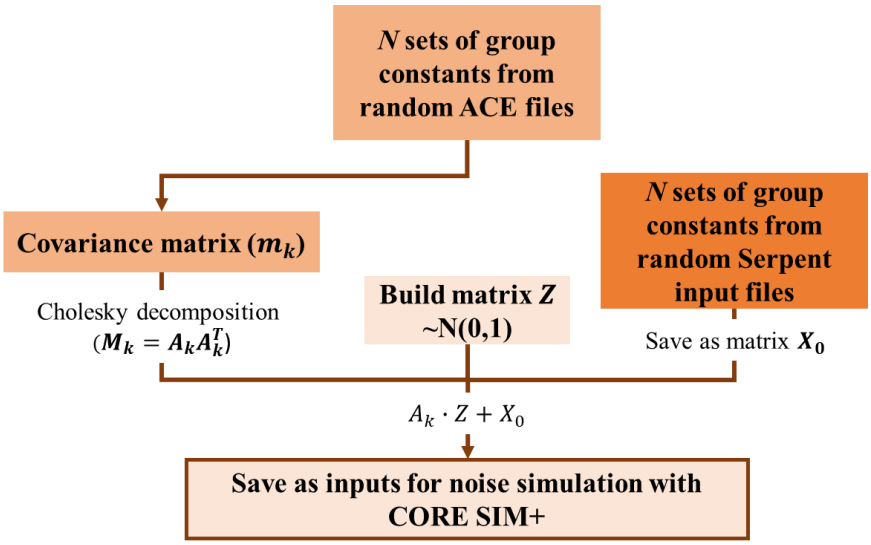

Figure 3.8: The procedure on nuclear data uncertainty treatment at 2nd approach

Despite the simplicity that the first approach has, the correlations among the nuclear data are ignored by the independent sampling processes at each nuclear data, thus, an accuracy of the outputs is not guaranteed. The second approach involves a standard random sampling scheme with a covariance matrix obtained from the perturbed nuclear data samples [94]. Each covariance matrix decomposes into a lower triangular matrix and its conjugate transpose by the Cholesky decomposition–a widely used method for manipulating the covariance matrix of an uncertain quantity [37, 95]. The Cholesky decomposition is mainly used for a numerical solution of linear equation, and this is highly reputed for its contribution to the superior efficiency and the numerical stability [96]. The detailed process to combine two nuclear data sets is as follows [37].

1) Find the covariance matrices (M_k, $k = 1{\sim}8$) among the nuclear data (data sets from random ACE files) in 8 core regions.
2) Decompose the covariance matrices ($M_k = A_k A_k^T$) by using Cholesky decomposition.
3) Build matrix Z with the dimension $[K \times N]$, here, K corresponds to the number of nuclear data we consider, while N represents the number of samples we want to generate.

$$Z = \begin{pmatrix} \overrightarrow{Z_1} \\ \overrightarrow{Z_2} \\ \vdots \\ \overrightarrow{Z_K} \end{pmatrix} = \begin{pmatrix} z_{1,1} & z_{1,2} & \cdots & z_{1,N} \\ z_{2,1} & z_{2,2} & \cdots & z_{2,N} \\ \vdots & \vdots & \ddots & \vdots \\ z_{K,1} & z_{K,2} & \cdots & z_{K,N} \end{pmatrix} \tag{3.1}$$

In the above matrix, all row vectors $\vec{Z}$ are independent and identically distributed random variables, meaning they have the same probability distribution and mutually independent. Particularly, the probability distribution is standard normal (mean=0 and standard deviation=1).

4) The new samples of nuclear data (X') are calculated as follows.

$$X' = A_k \cdot Z + X_0, \tag{3.2}$$

where X_0, which has the dimension $[K \times N]$, contains the raw nuclear data from Serpent computation.

The covariance matrices are built based on the 300 data sets and are shown in Figure 3.9. As one can notice from the figure, the correlation coefficients does not reflect a correct relationship between different nuclear data (e.g., a negative relationship between absorption and nu-fission cross-sections is found although a positive relationship is expected). When we consider the rule of thumb in statistics, this poor prediction stems from the small sample size ($N = 300$) which cannot draw a correct population behavior.

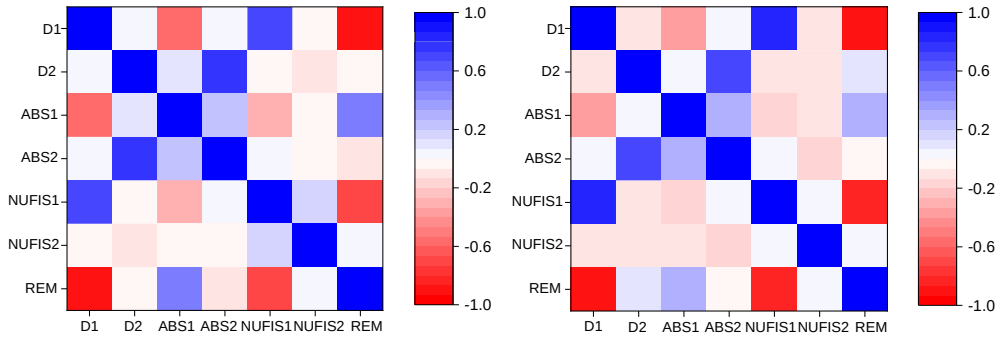

a. Inner fuel region under the water level

b. Outer fuel region under the water level

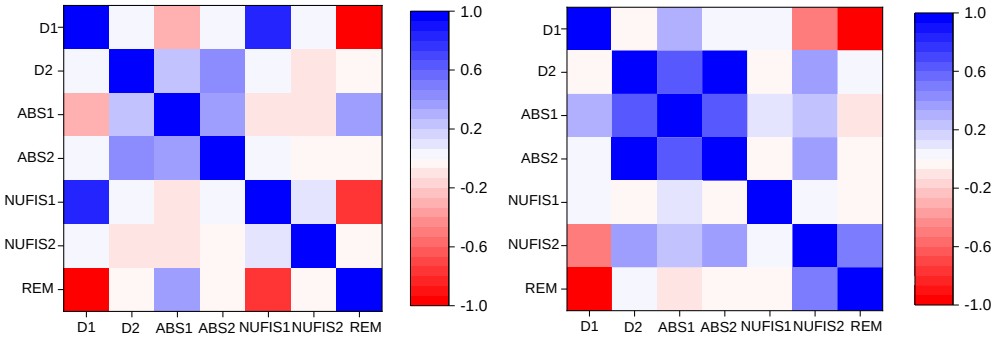

c. Control rods region under the water level

d. Reflector region under the water level

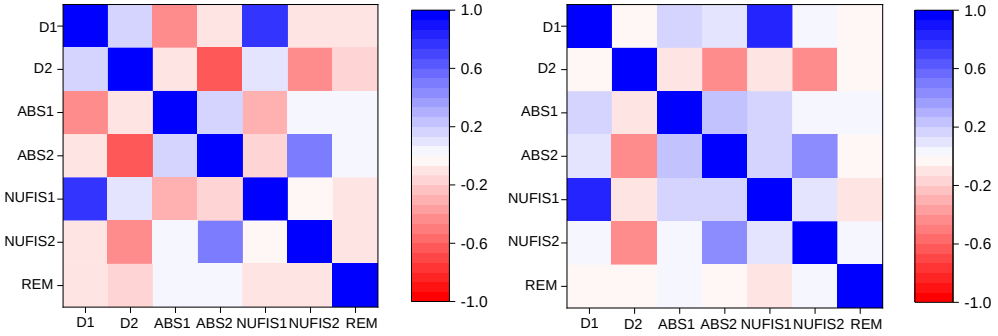

e. Inner fuel region above the water level

f. Outer fuel region above the water level

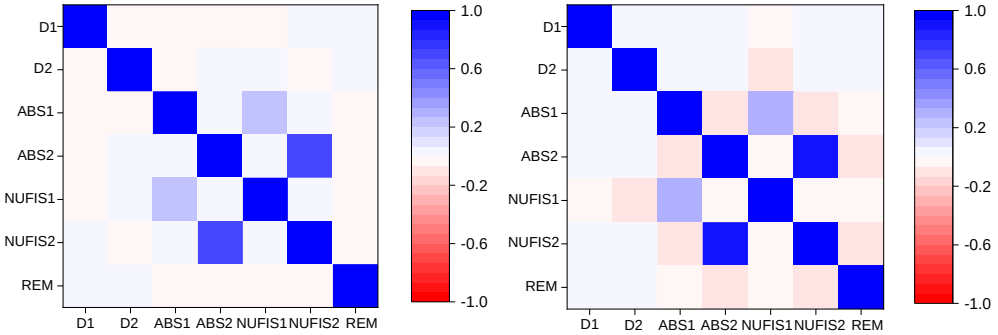

g. Control rods region above the water level

h. Reflector region above the water level

Figure 3.9: Correlation coefficients matrix of two-group constants

3rd approach: Direct use of distribution information of group constants sets

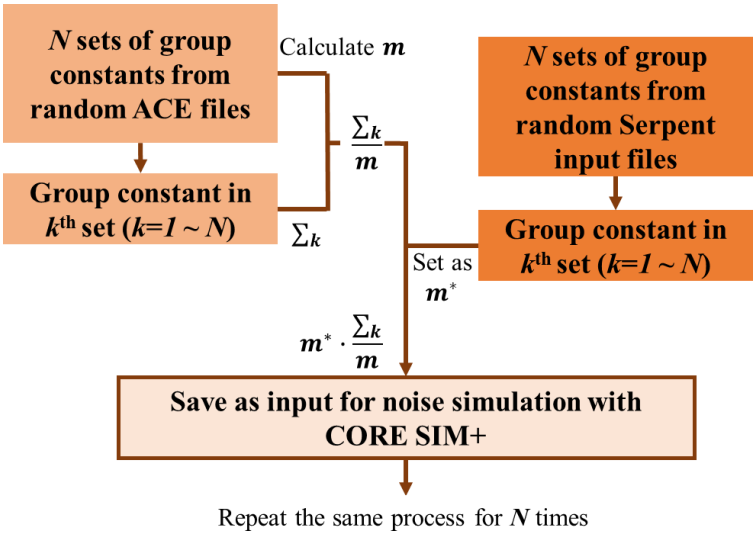

Figure 3.10: The procedure on nuclear data uncertainty treatment at 3rd approach

The main aim of this approach (see Figure 3.10) is excluding the subjective judgements as much as possible which lowers the accuracy but directly importing the actual distributional patterns which exist in N sets of data. The procedure is as follows.

1) Calculate a mean value of group constants from random ACE files in different core regions based on N data samples.
2) With a corresponding group constant in k^{th} data set ($\Sigma_{ACE,k,region\ A,data\ X}$), calculate a ratio with the obtained mean value using Equation (3.3).

$$Ratio_{region\ A,data\ X} = \frac{\Sigma_{ACE,k,region\ A,data\ X}}{mean_{region\ A,data\ X}}, \tag{3.3}$$

where k is a sample number (1~N), $region\ A$ is divided reactor core region (1~8) and $data\ X$ refers nuclear data (total, nu-fission, absorption and removal cross-sections).

3) Multiply this ratio to a corresponding group constant in k^{th} data set from random Serpent input files ($\Sigma_{Serpent,k,region\ A,data\ X}$) and obtain the final combined data ($\Sigma_{k,region\ A,data\ X}$). This is to combine the data from random ACE files to the data from random Serpent input files by their distribution information (i.e., ratio between mean value and each data).

$$Ratio_{region\ A,data\ X} = \frac{\Sigma_{k,region\ A,data\ X}}{\Sigma_{Serpent,k,region\ A,data\ X}} \tag{3.4}$$

4) For each nuclear data at different core region (8 universes), the same process is repeated for N times.

As it is described above, a total number of group constants sets after combination is limited to the sample size we already have. Therefore, this is expected to become a problematic point if a flexibility of sample generation (a total number of samples which can be produced) is required.

Discussions

The three introduced approaches can be discussed mainly in three different aspects, namely, applicability, accuracy, and conservatism. The "applicability" signifies an ease use of approach and a flexibility in sample generation, which is confirmed at 1st approach. However, the 2nd approach obliges to perform Cholesky decomposition which can become tricky when the covariance matrix is not positive definite, additionally, the number of samples which can be generated with 3rd approach is limited. On the contrary, the 2nd and 3rd approach assure the "accuracy" in terms that the correlations among group constants are preserved, which is not expected in 1st approach. However, the accuracy at 2nd approach is guaranteed only with a faithful covariance matrix. Thus, a large sample size is required for a reliable representation of matrix, which results in higher computational cost. The "conservatism" is not always crucial as the two aforementioned points, however, becomes important when defining upper/lower bound of output uncertainties and comparing these bounds to other relevant values (e.g., experimental data or safety limits).

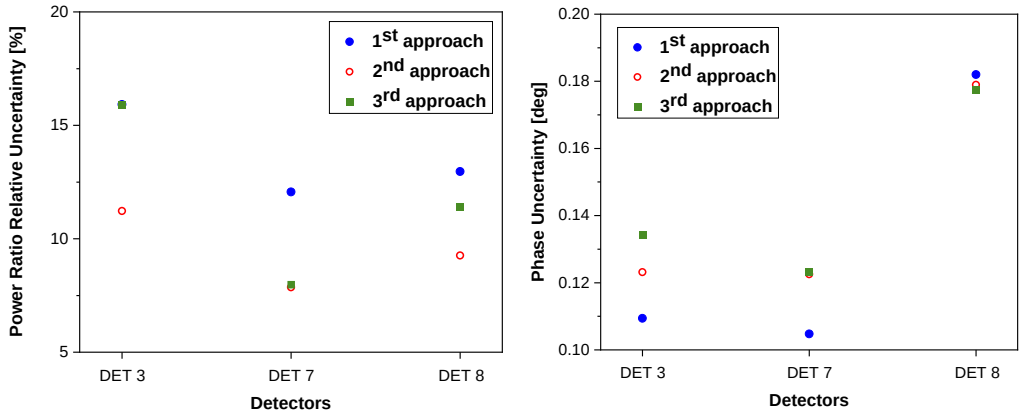

a. Amplitude of thermal neutron noise

b. Phase of thermal neutron noise

Figure 3.11: Comparison of neutron noise perturbation among three different approaches

Figure 3.11 compares the uncertainties of neutron noise (absolute noise) propagated from selected uncertain parameters using three different approaches. Only the results at three different detector locations (Detectors 3, 7 and 8) are dealt with, owing to their non-overlapping static and dynamic behavior, as shown in Figure 3.3.

	1st approach	**2nd approach**	**3rd approach**
Applicability	High	Low	Low
Accuracy	Low	Medium[11]	High
Conservatism	High	Low	High

Table 3.2: Ranking three approaches in different aspects

[11] it guarantees high accuracy theoretically, but not with small sample size as we currently consider in this study. Therefore, it is compromised as “medium” here.

It can be said that at most detector locations, 1st and 3rd approaches predict similarly large uncertainties for both amplitude and phase of noise–thus, guarantee high conservatism in result. By bringing all the characteristics discussed above, the three approaches can be ranked as Table 3.2. Here, both 1st and 3rd approaches get the highest score as having two "high". However, considering the main aim of PhD work, which is establishing a comprehensive methodology for future analyses (such as, simulator validation or optimization of experimental (or operational) condition), the "accuracy" can get a higher priority than the "applicability". Accordingly, the uncertainties of group constants are treated with the 3rd approach hereafter.

3.3.5 Justification of Current Group Constants Treatment

The introduced methodology to determine the final uncertainties of nuclear data doubles the necessary number of code runs; since the uncertainties from design/operating parameters (namely, Serpent inputs) and microscopic data (ACE files) are propagated non-simultaneously by separate Serpent computation. In order to confirm that this separate treatment of group constants can estimate the "correct" values for noise simulation, a comparison between the calculated group constants from the separate steps and one unified step (i.e., considering simultaneous perturbation of all parameters) is carried out.

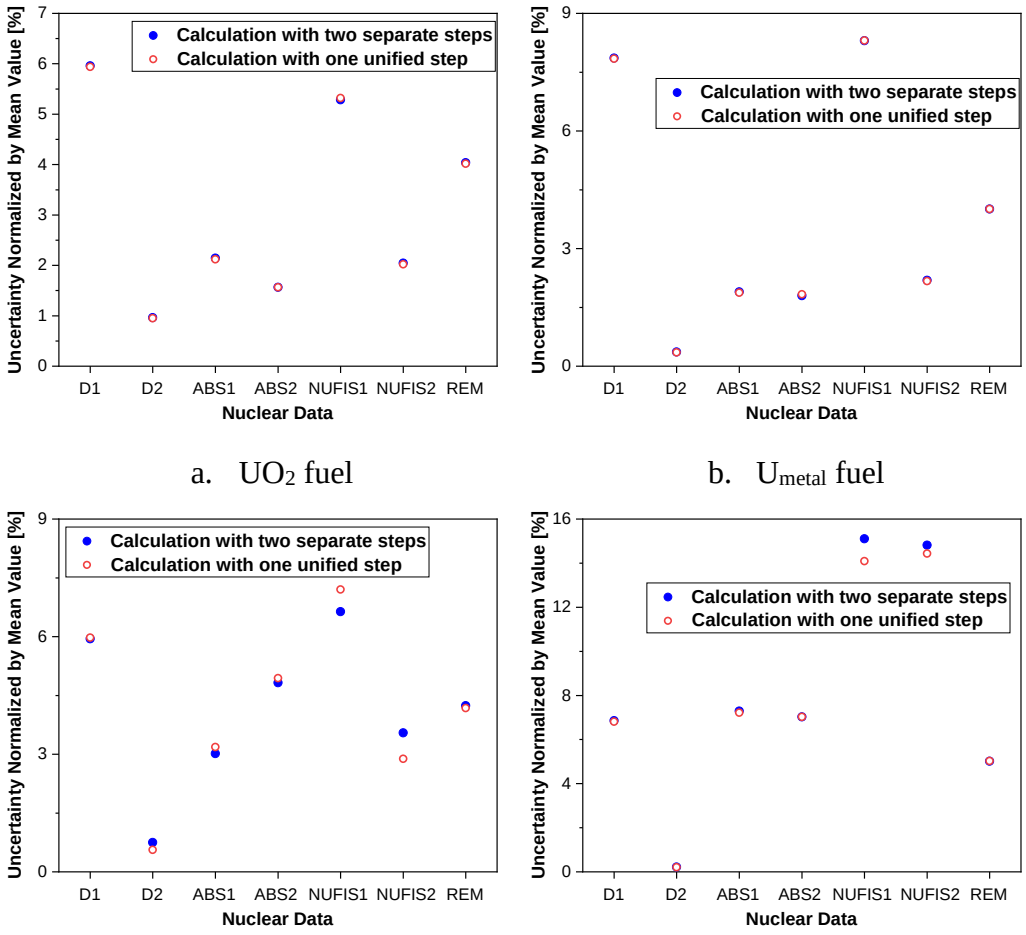

a. UO_2 fuel

b. U_{metal} fuel

c. Control rods

d. Reflector

Figure 3.12: Comparison of uncertainties of nuclear data between two different approaches (under the water level)[12]

Figure 3.12 compares the final uncertainties of nuclear data calculated from the two approaches at different core regions, based on 300 data sets. Except the nuclear data whose values are relatively small, therefore having inherently large

[12] The full name of nuclear data written in x-axis of the graphs correspond to the description in Table 1.4.

statistical uncertainties (e.g., nu-fission cross-sections at control rods and reflector area), the rest nuclear data show negligible discrepancies between two different calculation schemes, which is smaller than 0.2 %. It can be said that the approach with two separate steps propagates the uncertainties of relevant parameters to the two-group constants properly regardless of a non-simultaneous perturbation of the considered parameters, hence, the suitability of the approach for the further analysis is justified.

Finally, a total of 300 input sets are generated for the statistical uncertainty propagation using CORE SIM+, considering all input parameters introduced. A batch computation with CORE SIM+ is performed for both static and dynamic reactor conditions. Since CORE SIM+ performs the calculations in the frequency domain, the obtained neutron noise is a complex quantity, with an amplitude and a phase. The QoI in this work are post-processed accordingly (see Equation (1.11)).

3.4 Uncertainty Propagation

Based on 300 output samples, the radial distribution of QoI uncertainties is analyzed to gain a better understanding of its spatial variation, especially with respect to the distance to the noise source. Next, the QoI uncertainties at the detector locations are analyzed. This analysis involves an investigation of correlated behavior among the QoIs at the detector locations. Additionally, the influence of the Monte Carlo uncertainty on the QoI uncertainties is considered. Finally, the linearity of the current calculational scheme is investigated using the distribution characteristics of the output samples.

3.4.1 Uncertainties Associated to the Induced Neutron Noise

In order to gain an overview of the output variability, its values in the radial direction of the core have been determined at the core mid-height, where all the detectors are installed, and the results are depicted in Figure 3.13 [103]. This map

is obtained from 260 radial maps of the QoIs, whose number corresponds to the required number of code runs for the 4th order Wilks' formula for two-sided limits. The 260 outputs are extracted randomly from the 300 simulated cases. The value at the specific local point is calculated as follows: first, the QoIs (amplitude and phase) at this location from the prepared 260 radial maps are extracted. Second, the difference between the 4th largest and the 4th smallest among these 260 values is calculated. Third, this difference value is normalized by the mean value of 260 data at this local point.

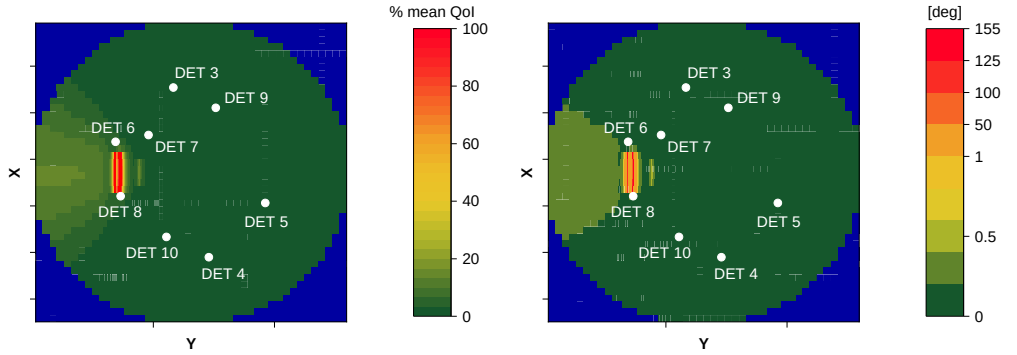

a. QoI-amplitude b. QoI-phase

Figure 3.13: The magnitude of QoI uncertainty in radial direction of the core (mid-height of the core)

The uncertainties of both amplitude and phase are highly localized in the area of the oscillating fuel rods. With the exception of this area, the magnitude of uncertainty is lower throughout the core, while the neighboring area of the oscillating fuel rods still shows a larger uncertainty than the remaining core area. This separation of the reactor core into two regions (neighboring area of the noise source and the rest) can also be observed in the correlations between the neutron noise calculated at the detector locations shown in Figure 3.14-a and -b. These figures represent correlation matrices for two QoIs of neutron noise (amplitude and phase), at the different detector locations based on 300 random outputs. The correlation information helps to perform groupwise uncertainty analyses by grouping correlated data, which simplifies the entire analysis. Detectors 6 and 8, which are closest to the noise source, are strongly correlated together and less correlated

to the others. The other detectors are also very strongly correlated among each other.

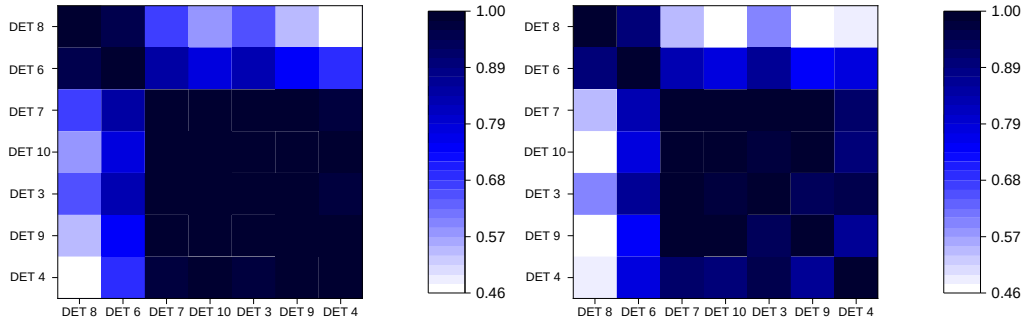

a. QoI-amplitude b. QoI-phase

Figure 3.14: The correlated behavior among the QoIs at the detector locations

Figure 3.15 compares the QoI uncertainties (amplitude and phase) between the simulation results and the actual experimental results from the first experimental campaign performed with the COLIBRI device [98]. Two simulation cases are presented, i.e., the case that propagates both the uncertainties associated with the 776 input parameters in Table 2.2 and Table 3.1 and the statistical error of the Monte Carlo estimation of the nuclear data, and the case that takes only into account the Monte Carlo statistical error of the nuclear data.

At all detector locations, the experimental uncertainties are much larger than the computational uncertainties in general. The statistical uncertainty shown in Figure 3.15 results from the Monte Carlo nature of the two-energy group cross-sections generation process performed with Serpent. The uncertainties of noise amplitude with and without considering the uncertain parameters (as listed in Table 2.2 and Table 3.1) are compared in this figure. Only the statistical uncertainty from the Serpent computation is included in the case of “with statistical uncertainty”. In all detector locations in Figure 3.15, the uncertainties of neutron noise involving the perturbation of uncertain parameters is around 100 times larger than those calculated without uncertain parameters. Therefore, the statistical uncertainty stemming from the Monte Carlo simulations themselves is confirmed as negligible and will not be discussed further in this PhD work.

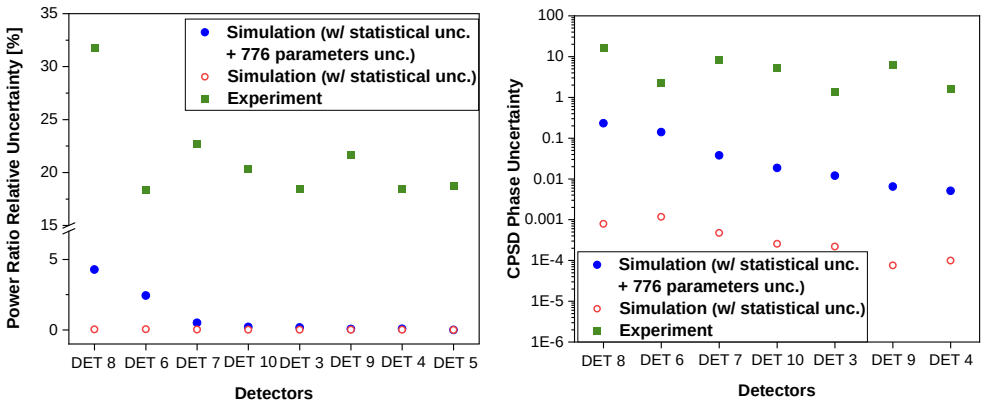

a. QoI-amplitude b. QoI-phase

Figure 3.15: Comparison of QoI uncertainties

3.4.2 Distribution of the Considered Responses

Additionally, the distribution information of 300 neutron noise simulations (the absolute noise and the QoI) is collected to investigate the linearity of the current calculational scheme when propagating uncertainties. In this respect, a series of normality tests are performed with the Shapiro-Wilks approach (see Chapter 1.7.2), considering as output samples, the real and imaginary part of the absolute noise and the QoIs (amplitude and phase) at the detector locations. Table 3.3 summarizes the obtained p-values. A linear approximation for the solution of the neutron noise balance equations is implemented in CORE SIM+, which neglects second-order perturbation terms for the neutron noise. There is nevertheless a non-linearity in the noise source, when both the uncertainty in the amplitude of the displacement and the uncertainties in the static cross-sections are considered, as Equation (1.5) demonstrates. Since the current study considers both uncertainties, there is a possibility that the calculation process of absolute neutron noise becomes non-linear. Meanwhile, by nature, the APSD and CPSD involve the product of two complex numbers as described in Equation (1.11), and, as such, are non-linear functions of the neutron noise.

In Table 3.3, both real and imaginary parts of the absolute noise are confirmed as having large p-values, which validates the normality of the data. Since most input parameters have a normal distribution as described in Table 2.2 and Table 3.1, the output data is also expected to be characterized by a normal distribution if it results from a linear combination of the inputs. The large p-values suggest indeed that the simultaneous perturbation of the "amplitude of the displacement" and the "static cross-sections" does not result in any significant non-linearity. The following sensitivity analysis (in Chapter 3.5) will confirm that this assumption is correct. On the other hand, the QoIs have smaller p-values in general due to the conversion process from the absolute noise to the APSD and CPSD, which are non-linear.

Parameter	**p-value**						
	DET 8	DET 6	DET 7	DET 10	DET 3	DET 9	DET 4
Real part	0.45	0.72	0.82	0.93	0.82	0.93	0.82
Imaginary part	0.49	0.76	0.27	0.53	0.60	0.53	0.61
QoI (Amplitude)	1E-13	1E-5	0.18	0.29	0.19	0.33	0.35
QoI (Phase)	1E-10	0.03	0.51	0.34	0.53	0.37	0.69

Table 3.3: p-values of neutron noise calculated from Shapiro-Wilk test

Confirming the linearity between inputs and outputs when propagating uncertainty plays a key role in choosing a proper approach for the sensitivity analysis (e.g., the possibility of using PCC). The compatibility of the different approaches for the sensitivity analysis is discussed later in Chapter 3.5.3.2, to identify and choose the most appropriate direction for further analysis.

Next, we investigate what the main contributors to the considered response uncertainty are.

3.5 Sensitivity Analysis

This section consists of three parts. In the first part, a use of correlation-based approach for the further analyses is justified through a comparison between the sensitivity indices predicted by correlation-based approach and variance-based approach, as an extension of the previous validation carried out in Chapter 2.4.3. The following section involves a convergence test of sensitivity indices with different sample sizes. This is to determine the minimum sample size required for a reliable quantitative estimate of the sensitivity indices. In the last section, the main sensitivity analyses using two different approaches are carried out. The first one is a simplified approach which ranks the parameters by means of the QoI uncertainties propagated by perturbing the independent groups of input parameters separately. In the second approach, the exact level of contribution of the input parameters is measured by calculating the sensitivity indices. This process involves a calculation of multiple correlation coefficients within the grouped parameters to perform a groupwise sensitivity analysis. Accordingly, the most influential group (group of parameters or individual parameters) for the different detector locations is identified.

3.5.1 Justification of Using Correlation-based Approach

In Chapter 2.4.3, it is described that a use of variance-based approach in sensitivity analysis can draw more precise results especially when the physical processes are complicated, such as, at a condition of neutron noise. Variational methods can handle both linearity and non-linearity in the solution of differential equations, thus, can be also applied to the analysis where the simulation is based on time-dependent neutron diffusion equations with thermal-hydraulic feedbacks. CORE SIM+, however, solves the linearized neutron oscillation problem in the frequency domain without considering any thermal-hydraulic feedback. The second-order perturbation terms are neglected and as such all possible induced non-linearities in the solution of the neutron noise equations [99]. This simplifies the mathematical treatment without significantly affecting the physical accuracy in the case of weak non-linear effects. This linear approximation allows us to

consider other statistically based approaches for sensitivity analysis, which avoids the need to modify the code to introduce the variational techniques mentioned above (e.g., regression or correlation-based approaches[13]).

Accordingly, a series of validations are carried out to confirm whether the correlation-based approach can be a reliable substitute for the variance-based approach, as it is presumed by the characteristics of CORE SIM+. SCC and Jansen's formula are selected as representative methods for correlation-based and variance-based analyses, respectively. Figure 3.16 describes a planned validation process.

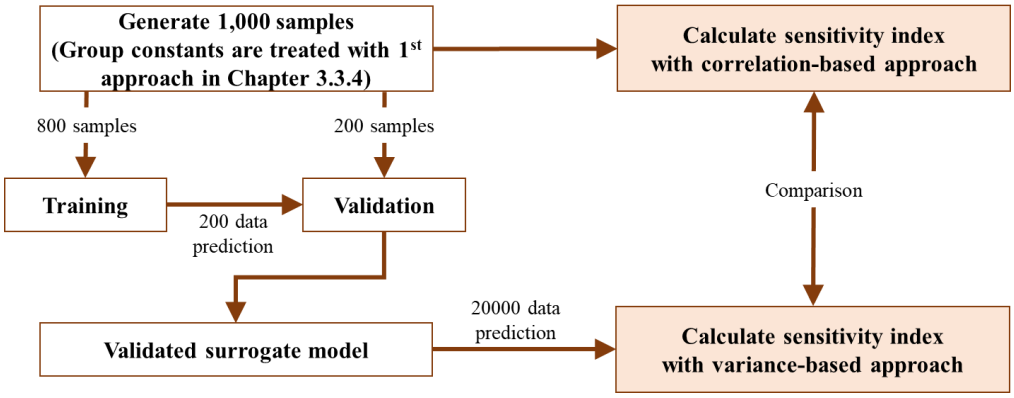

Figure 3.16: Flow chart for a comparison of sensitivity indices calculated from correlation-based and variance-based approaches

[13] For a use of regression or correlation-based approach, the condition of the data without bifurcations or sudden discontinuities is required. One input parameter in this study named "location of noise source" perturbs within discrete values due to the nature of CORE SIM+ model. However, this parameter is continuous in nature, thus, sampling within discrete values should not impact on predicting a linear correlation with output variable.

The neutron noise data (absolute noise) at the location of Detector 8 are used for the present validation. The details of each step are as follows.

1) As it is demonstrated in Chapter 1.7.4.3, sensitivity analysis using variance-based approach demands a large number of model evaluations. Therefore, a use of surrogate model is required to predict the response for untried input sets. However, a precision of surrogate model is also affected by sample size which is used for training the model, hence, a sample size of 1000 is considered in this validation. The uncertainties of two-group constants are treated with using 1st approach introduced in Chapter 3.3.4. This modification from 3rd to 1st approach is limited to this validation, because of a flexibility that the 1st approach has especially on sample generation, which the 3rd approach does not have. This validation is made only for comparing the performances between two approaches at an identical condition, hence, a temporary modification within this chapter is acceptable. Considering the input parameters listed in Table 2.2 and Table 3.1, a total of 1000 input sets are generated and a batch computation with CORE SIM+ is performed for both static and dynamic reactor conditions.

2) The surrogate model PC-Kriging is selected and PCE is set to have a degree-adaptive Least Angle Regression Selection (LARS) of degrees one to five. 800 samples out of 1000 samples from the actual cod runs are used to train a surrogate model. Afterwards, the trained model is used to predict the neutron noise behavior for the rest 200 cases. The predicted results by the surrogate model are compared to the results from actual simulation as shown in Figure 3.17. The maximum errors are less than $2\,\%$ and $0.02\,\%$ for the amplitude and the phase of neutron noise, respectively. Therefore, this result represents a good agreement between actual and predicted results, and the trained surrogate model is qualified for the further prediction.

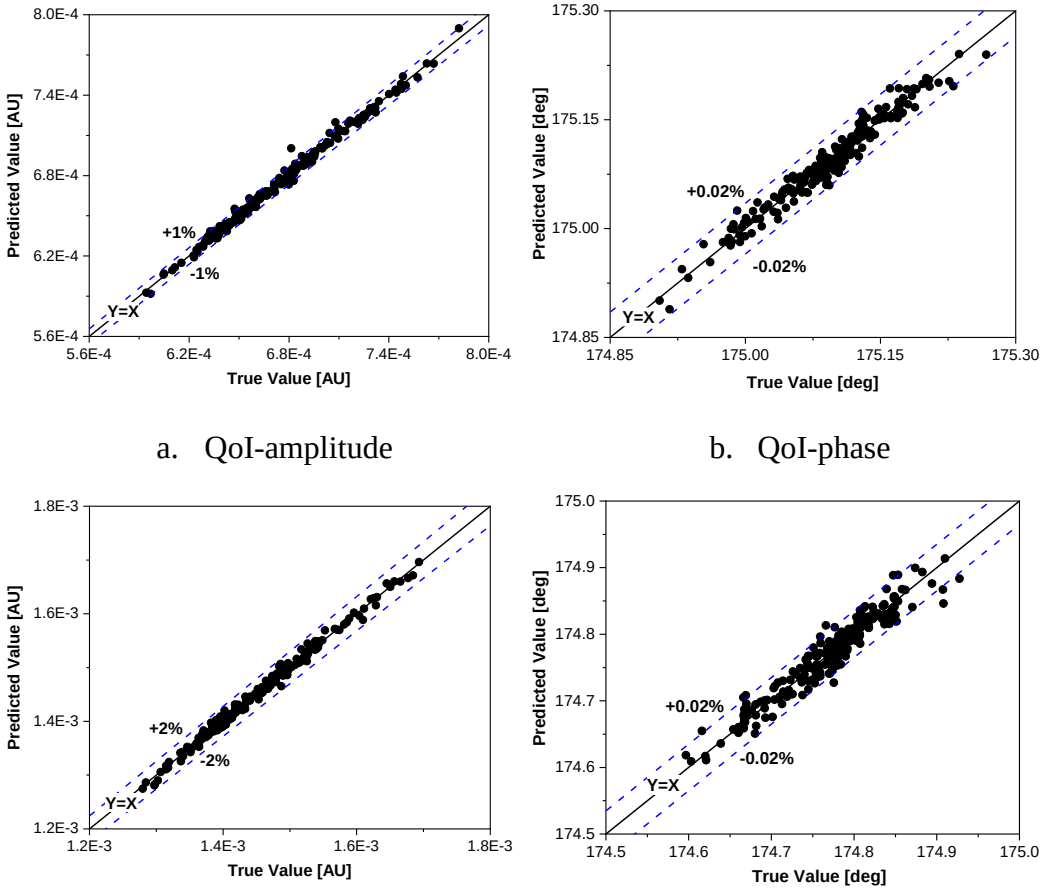

a. QoI-amplitude

b. QoI-phase

c. Amplitude of thermal neutron noise

d. Phase of thermal neutron noise

Figure 3.17: Validation of trained surrogate model

3) The trained model predicts the noise behavior for 20,000 untried cases (input sets). Table 3.4 summarizes the leave-one-out (LOO) error (ε_{LOO}), which is an estimate of the mean-square error between the original model and the surrogate model.

   The first-order sensitivity indices with Jansen's formula are calculated based on 20,000 inputs and output results.

	Fast neutron noise		Thermal neutron noise	
	Amplitude	Phase	Amplitude	Phase
ε_{LOO}	0.004	0.009	0.050	0.050

Table 3.4: Leave-one-out error in surrogate modeling

4) Spearman correlation coefficients are calculated between input parameters and output data (amplitude and phase of fast and thermal neutron noise) based on 1000 samples obtained at the Step 1). Afterwards, the calculated coefficient is squared to represent the sensitivity index.

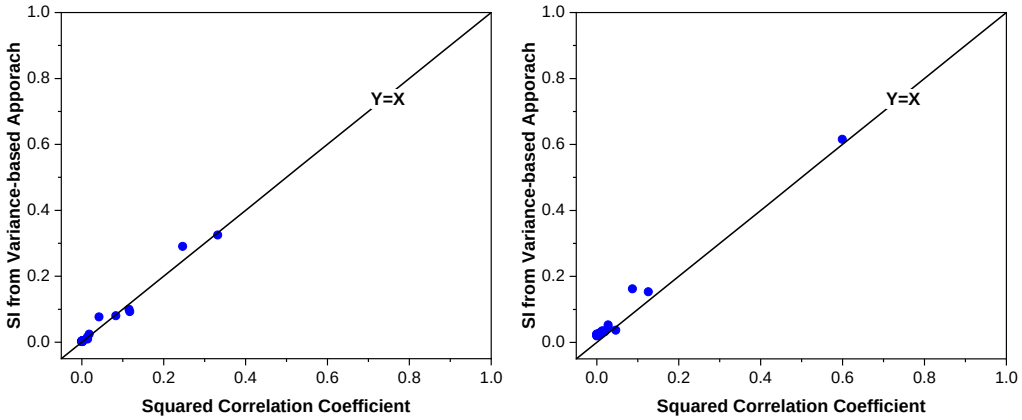

a. Amplitude of thermal neutron noise

b. Phase of thermal neutron noise

Figure 3.18: Comparison between sensitivity indices calculated from correlation-based and variance-based approaches ("SI" denotes "sensitivity index".)

5) The results from two different approaches are compared in Figure 3.18. This comparison is made only with thermal neutron noise, whose behavior is a main concern within CORTEX project. For the sake of conciseness, only 21 input parameters whose indices are larger than 0.05 are selected in this comparison by considering a criterion on a correlation with 1000 samples at a significance level of 5 % (see Chapter 1.7.4.1). In Figure 3.18, it is found that two different approaches predict the similar

results, since there is no strong dispersion around the line $y = x$. Therefore, the replacement of the variance-based approach with correlation-based approach for the further analysis is justified.

3.5.2 Convergence on the Sensitivity Indices with the Number of Samples

A series of convergence tests with different sample sizes are performed to define the proper sample size for further analyses which guarantees the "convergence". Here, "convergence" means that the sensitivity index is similar across replications under the same sample size by using a bootstrap approach [100]. The sensitivity indices considered for the convergence assessment are calculated between two input parameters and the QoI at the location of Detector 8. Parameters with a small (U-238 elastic scattering cross-section of energy-group 9) and large sensitivity (location of noise source) are chosen to cover all possible convergence behavior. The tests are carried out with different sample sizes between 10 to 1000, which are sampled randomly from 1000 existing data sets. The sampling of equivalent sample size is repeated 1000 times using bootstrapping with replacement [101]. Afterwards, to compute 95 % confidence intervals, the 2.5^{th} and 97.5^{th} percentiles of the index distribution (1000 indices at each sample size) obtained by bootstrapping are identified. The sensitivity indices and their confidence intervals at different sample size are given by the convergence plots in Figure 3.19.

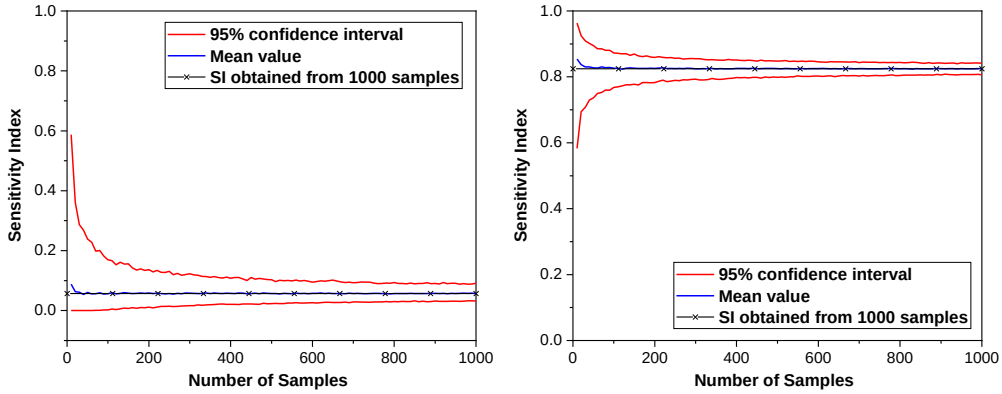

a. U-238 elastic scattering cross-section

b. Location of noise source

Figure 3.19: Convergence plots of sensitivity indices with 95 % confidence interval

3.5.3 Sensitivity Analyses at the Detector Locations

Due to the fact that nuclear data input parameters are both numerous and correlated, a methodology is adopted to measure the effect of large number of correlated input parameters efficiently [97], through the determination of a correlation coefficient for a group of input parameters (see Chapter 1.7.4.2).

In the sensitivity analysis, the input parameters are divided in three groups which are not correlated among each other. Group 1 consists of the parameters related to the reactor design and operation (parameters no.1 to no. 25 listed in Table 2.2) and is named as “group of design and operating parameters”. Group 2 is composed of all the nuclear data parameters. It is referred to as “group of nuclear data” later on. Groups 3 is made up of the input parameters related to the description of the noise source (parameters no. 749 to no. 751 in Table 3.1) and referred to as “group of noise source data”. The relative contributions of three groups are compared through the two different approaches in the following sensitivity analysis: the main focus of the first approach is to compare the QoI uncertainties at the detector locations perturbing one group of input parameters at a time. The

second approach, however, measures the exact amount of contribution of each group to the neutron noise by means of the sensitivity index.

3.5.3.1 Simplified Approach for Parameter Ranking

The relative effects of the different groups of parameters (namely, group of design/operating parameters, group of nuclear data and group of noise source data) are investigated by comparing the uncertainties propagated from the different groups as shown in Figure 3.20. The uncertainties are obtained following a 1st order Wilks' formula for two-sided limits to reduce the number of samples and consequently the computational cost of such analysis. As the main objective of this study is a qualitative ranking of the groups, the use of a lower order Wilks' formula is acceptable.

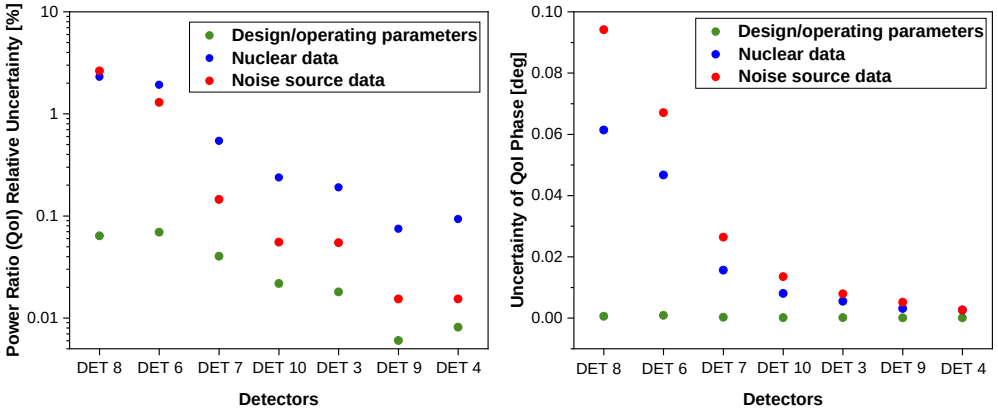

a. Amplitude of neutron noise b. Phase of neutron noise

Figure 3.20: Comparison of neutron noise uncertainties obtained from the different groups of input parameters

The effect of group of design and operating parameters is confirmed as negligible in all detector locations for both amplitude and phase. At the detector locations near the noise source (Detectors 8 and 6), the uncertainties of amplitude are strongly driven by the combination of group of noise source data and the group of nuclear data. However, the uncertainties of phase are dominantly affected by the group of noise source data. When the detector is located further away from the noise source, the uncertainties of amplitude are influenced by the group of

nuclear data while the group of noise source data remains as the most influential group to the phase of neutron noise.

3.5.3.2 Analysis using Groupwise Sensitivity Indices

The uncertainty due to the group of design and operating input parameters is excluded from now on due to its negligible effect as confirmed in Figure 3.20. The approach described in Chapter 1.7.4.2 is used to calculate the multiple correlation coefficients of the groups. This requires an estimation of the correlation among the parameters belonging to a same group (see Equation (1.20)). In this study, the analysis using groupwise sensitivity indices is repeated twice with different grouped parameters. The first trial is carried out with two groups: the group of nuclear data and the group of noise source data. In the second analysis, the group of nuclear data is subdivided into four nuclide groups (all nuclide reaction pair of a given nuclide are grouped together) while the group of noise source data is separated into three individual parameters (oscillating amplitude, oscillating frequency and location of noise source). Additionally, this calculation scheme using a multiple correlation coefficient requires a large number of samples, hence, a sample size of 1000 is considered in this section.

Meanwhile, despite of its suitability in the current calculational scheme, the PCC might not provide significant information since the input and output (QoI) parameters considered in this study are not linearly related. Therefore, the applicability of the PCC in the current analysis condition is discussed in the following section.

Assessment of Pearson correlation coefficient

Current work handles a large number of input parameters, where an analysis with grouping input parameters can be efficient especially when the parameters are correlated. A sensitivity analysis with grouping parameters requires a use of PCC since it deals with correlation coefficient between inputs and outputs, not a rank variable, as introduced in Chapter 1.7.4.1.

In order to use PCC, a “linear model” between the output data and input parameters belonging to a same group should be guaranteed. However, the output data in this study (QoI) is a combination of APSD and CPSD at the reference detector location, whose calculation process is non-linear but monotonous as confirmed in Table 3.3. Under these circumstances, a series of tests are carried out to confirm whether the PCC can be still used as a sensitivity measure between input parameters and QoI.

These tests are conducted by comparing PCC and SCC[14] calculated between inputs and two different output data which are the results from “linear” and “non-linear” processes. A good agreement in between can ultimately assure an applicability of PCC to a current sensitivity analysis with grouping parameters. The first calculation involves linearly related input and output parameters, for which PCC should be an accurate measure of sensitivity. The next calculation involves input and output parameters, which are not linearly related. It is intended to check that the PCC can provide the proper input ranking. According to the normality test introduced in Table 3.3, the output data from the linear and non-linear processes correspond to the absolute neutron noise (real and imaginary parts) and the QoIs (both amplitude and phase), respectively.

Figure 3.21 compares the results from two different approaches for four different output data at the location of Detector 8.

[14] The SCC relies on the correlation between the “rank values” of two parameters [40]. Therefore, it can detect the monotonic relationship (linear or non-linear) between the parameters and can be used to verify that the PCC provides a reasonable measure of sensitivity even with a non-linear model.

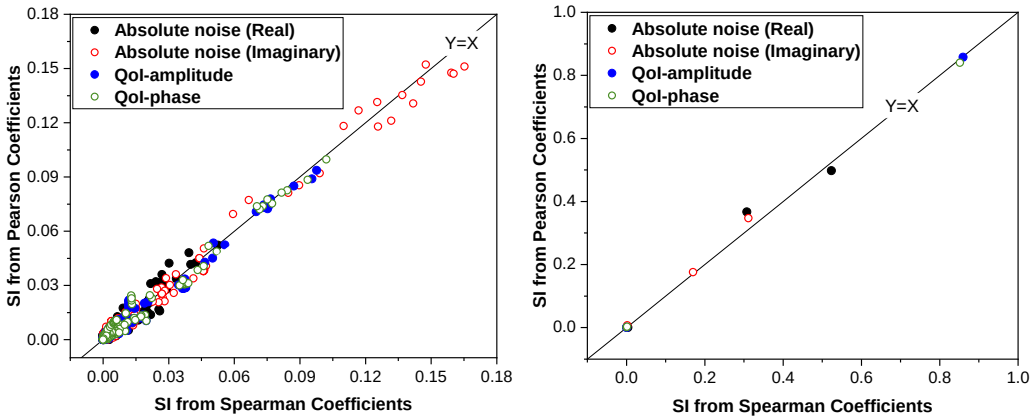

a. Nuclear data b. Noise source data

Figure 3.21: The comparison of sensitivity indices calculated from Spearman and Pearson correlation coefficients (Output data: real and imaginary part of absolute noise and QoIs)

There is no strong dispersion around the line $y = x$ in Figure 3.21 for all outputs. It can be concluded that the PCC produces reliable sensitivity indices for both absolute noise and QoI. Therefore, the PCC is used for ranking the importance of the input parameters (both individual parameters and grouped parameters).

Estimation of groupwise sensitivity indices

The sensitivity indices of two groups (group of nuclear data and group of noise source data) for different detector locations are shown in Figure 3.22. A similarity with the results from simplified approach (see Figure 3.20) can be found, in terms of the level of contribution of each group at different detector locations. The group of noise source data dominates at the locations close to the noise source. However, its effect to noise amplitude becomes negligible as the detector location gets further away from the noise source and the group of nuclear data becomes dominant instead, while no such a remarkable change is found in noise phase. Meanwhile, considering that the sensitivity index here is identical to the first order sensitivity indices (see Equation (1.19)), the sum of sensitivity indices of two different groups is expected to become unity when they are uncorrelated with each other. However, the actual sums of the results shown in Figure 3.22 are

larger than 1.0 at all detector locations. This is due to the low number of samples ($n = 1000$) considered here, which does not allow a faithful representation of the covariance matrix in Equation (1.20).

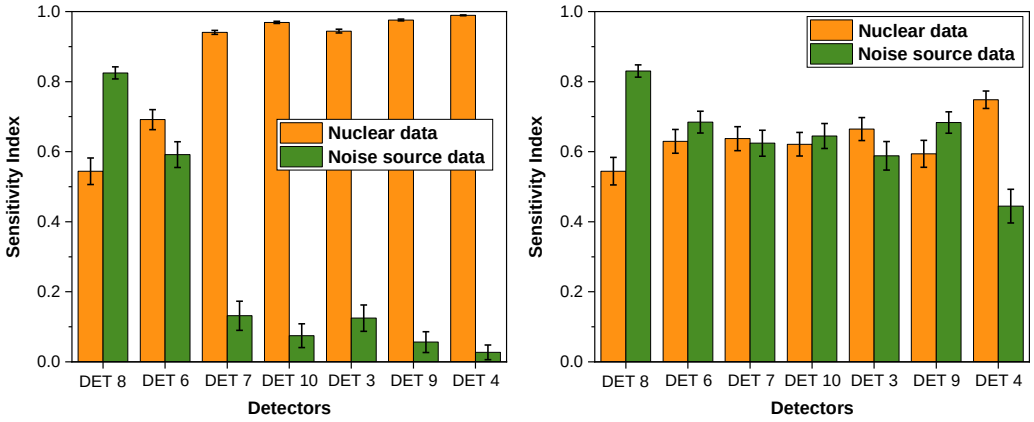

a. Amplitude of neutron noise b. Phase of neutron noise

Figure 3.22: The sensitivity indices and the 95 % confidence intervals between grouped parameters (nuclear data group and noise source data group, and QoIs at different detector locations

To support this statement, a series of sensitivity tests with different samples sizes are carried out. Figure 3.23 represents the sensitivity indices of two groups for the QoI amplitude at the location of Detector 8, which vary with the sample size. In case of “Group of noise source data”, the sensitivity index as well as the confidence intervals converge quickly with the increasing number of samples.

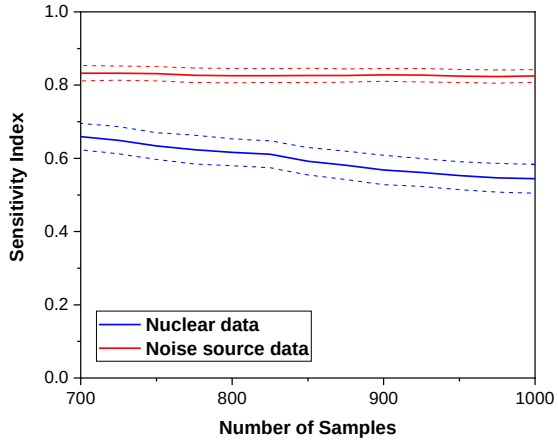

Figure 3.23: The sensitivity indices of two groups with 95 % confidence intervals varying with sample size (The straight line and the dashed line signify "mean value" and "95 % confidence intervals", respectively.)

On the other hand, the sensitivity index of "Group of nuclear data" decreases gradually, while the confidence interval remains constant. Since only three parameters are included in "Group of noise source data", the covariance matrix to estimate in Equation (1.20) is small and its components converge quickly. However, "Group of nuclear data" consists of 748 correlated parameters, thus, an accurate estimation of its component will require a much larger number of samples; this explains the slow convergence of the associated sensitivity index. Therefore, it is expected that the sum of two groups sensitivity indices can become 1.0 eventually, when the sample size becomes large enough to result in a precise covariance matrix of "Group of nuclear data".

Any further sample size increment to confirm this speculation is not carried out within this study, however, a sample size which fulfills the convergence of sensitivity indices can be suggested as depicted in Figure 3.24. In this figure, a trend of sensitivity index for a group of nuclear data is extrapolated with logarithm function. Since the sensitivity index for a group of noise source data is obtained as 0.83 in Figure 3.23, the sum of all group indices is expected to become 1.0 at a sample size larger than 2200.

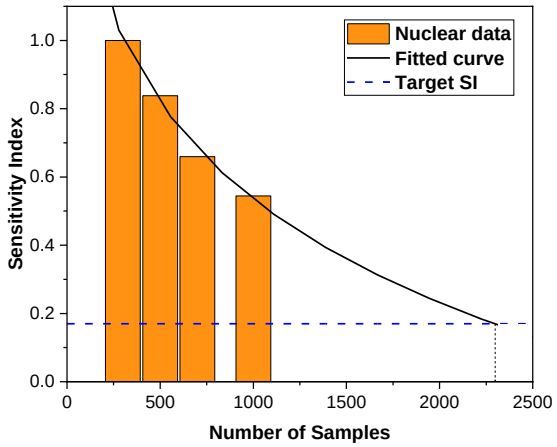

Figure 3.24: Prediction of sample size for convergence of sensitivity index within nuclear data

Nevertheless, when comparing the relative contributions of groups to the output uncertainty shown in Figure 3.20, the "ranks between the two groups (groups of nuclear data and noise source data)" are identical to what can be seen in Figure 3.22. Accordingly, it can be said that the qualitative ranks of the groups, which are obtained in this study with 1000 samples, are still reliable even though the quantitative estimates are not reliable.

Finally, the group of nuclear data is further divided by isotopes (^{1}H, ^{16}O, ^{235}U and ^{238}U) as shown in Figure 3.25. Additionally, the group of noise source data is divided into its individual parameters (oscillating amplitude, oscillating frequency, and location of noise source). At the location of Detectors 6 and 8, both QoI amplitude and phase are strongly driven by the location of noise source. At the remaining detector locations, the groups of ^{235}U and ^{238}U are the largest contributor to the uncertainty of QoI amplitude, while the oscillating frequency becomes most influential to the uncertainty of QoI phase.

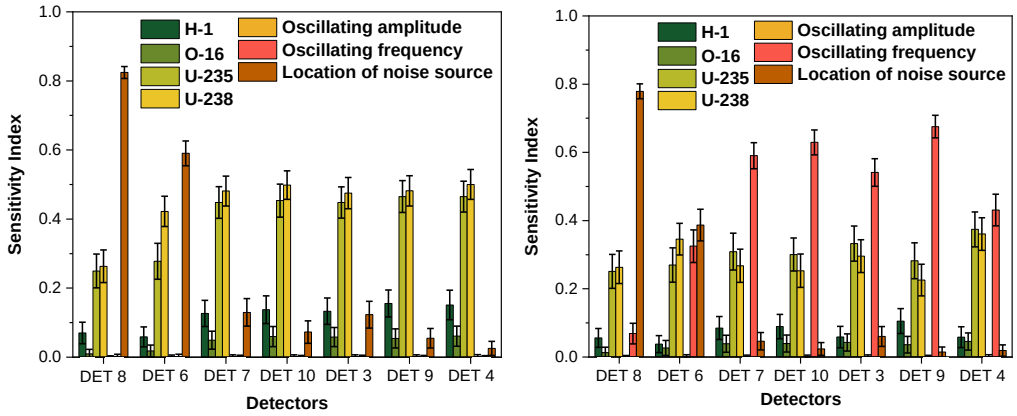

a. Amplitude of neutron noise b. Phase of neutron noise

Figure 3.25: The sensitivity indices and the 95 % confidence intervals between grouped parameters (nuclear data group (four isotope groups) and noise source data group (three independent parameters)), and QoIs at different detector locations

Another finding is the irrelevance of the oscillating frequency for the amplitude of neutron noise. This can be explained by the Zero-Power reactor Transfer Function (ZPTF). Since CROCUS is a small-sized zero-power reactor, the dynamic behavior of the reactor is overwhelmingly driven by point-kinetics. In this condition, the reactor response is given by the ZPTF, whose "plateau region" exists in the specific frequency range of [27],

$$\lambda \ll \omega \ll \frac{\beta}{\Lambda_0}. \tag{3.5}$$

In this "plateau region", the oscillating frequency has very little impact on the reactor response and the amplitude of the neutron noise is nearly constant. Approximately, this range corresponds to the oscillating frequency between 0.01 Hz and 20 Hz, considering the characteristics of the CROCUS reactor [85]. That is to say, the oscillating frequency in this study, 1 Hz, belongs to the plateau region and this backs up the little effect on the QoI.

Chapter 4

Application of the Methodology to AKR-2 Zero-Power Reactor

Another small-sized zero-power reactor, AKR-2, is considered for additional uncertainty analyses following the experimental programs conducted within CORTEX project (i.e., rotating absorber and vibrating absorber). The comprehensive methodology which has been developed with CROCUS reactor is directly adopted to the analysis at AKR-2 reactor.

4.1 Description of Target Experiment

4.1.1 Target Reactor

The AKR-2 zero-power reactor is selected as a target reactor (see Chapter 1.4.2).

4.1.2 Target Event

In the context of the CORTEX project, two neutron noise experiments are conducted at AKR-2 reactor: rotating absorber, which is equivalent to an absorber of variable strength, and vibrating absorber. In COLIBRI experiment, the experimental condition in first and second experimental campaigns are very similar, therefore, do not demand any specific modification in code simulations. This similarity enables to focus on only one experimental campaign. However,

different from COLIBRI experiments, the experiments carried out in AKR-2 reactor went through major modification from first to second experimental campaign. These modifications affect applicable input parameters as well as modeling of noise source. Therefore, both experimental campaigns need to be analysed independently. The detailed experimental condition of two target events at two experimental campaigns are summarized in Table 4.1 [30]. The experimental condition described here correspond to the condition selected for the validation of noise simulators which are under development in CORTEX project.

	First experimental campaign		**Second experimental campaign**	
Rotating absorber	Oscillating frequency	1 Hz	Oscillating frequency	2 Hz
Vibrating absorber	Moving time	1 second	Oscillating frequency	2 Hz
	Waiting time	0.1 second		

Table 4.1: Experiments specification

4.2 Description of Computational Method and Quantities of Interest

4.2.1 CORE SIM+ Model of AKR-2

First campaign

The core is modeled with a three-dimensional mesh of $109 \times 109 \times 64$ cells, in the $x-$, $y-$ and $z-$ directions of the core, respectively. Compared to the CROCUS reactor, AKR-2 has more complex core composition and the two different sources of reactivity perturbations are located in different orientation, therefore, this complexity hinders from modeling the reactor core in

straightforward way especially around the noise source regions. In this regard, the interesting area has to be modeled with finer meshes in all $x-$, $y-$ and $z-$ directions. In radial direction of the core, $x-$ and $y-$ directions of the meshes around the noise source are modeled with a size of 1 cm, while the rest area is modeled with 8 cm. Meanwhile, the meshes in axial direction are modeled with a size of 5 mm while the rest area are modeled with the size of 5 cm and 10 cm for the convenience of modeling. The modeled reactor core, at the height of 130 cm, is depicted in Figure 4.1: the radial direction of the core is modeled with 45 degree rotation in clockwise direction from the orientation shown in Figure 1.9.

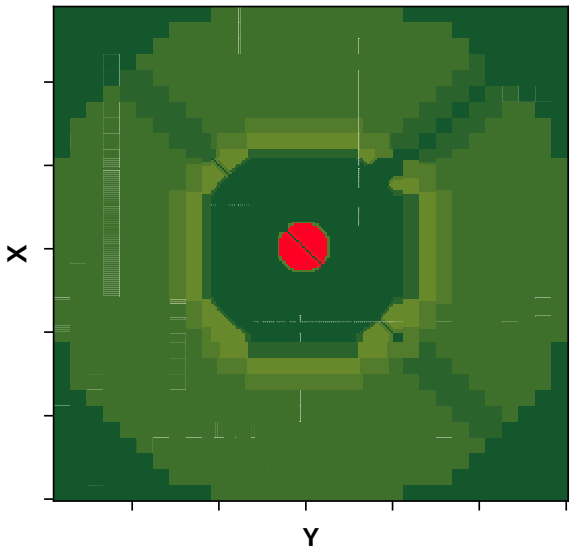

Figure 4.1: Modeled reactor core with CORE SIM+

Second campaign

The reactor models which are used in first experimental campaign are improved for the simulations, by incorporating even finer spatial meshes than those used in previous campaign on the region where the noise source is located. Different core model is developed for each experiment [32], which has fine meshes around the location of relevant noise source. The core is modeled with a three-dimensional mesh of $205 \times 169 \times 88$ cells for rotating absorber and $208 \times 208 \times 64$ cells for vibrating absorber, in the $x-$, $y-$ and $z-$ directions of the core,

respectively. The fine meshes around rotating absorber are modeled with a mesh size of 1 mm, while the meshes around vibrating absorber have a size of 3 to 4 mm.

4.2.2 Homogenized Group Constant with Serpent

Considering the complex composition of the reactor core with various experimental channels inside, the core is divided into 20 different regions for both group constants generation (using Serpent) and neutron noise simulation (using CORE SIM+). In Serpent, the specific region which is defined for group constants generation is called as "universe". Figure 4.2 shows the defined 20 universes at AKR-2 reactor [102]. For the sake of conciseness, a description of divided reactor core regions is made with universe numbers hereafter in the analyses.

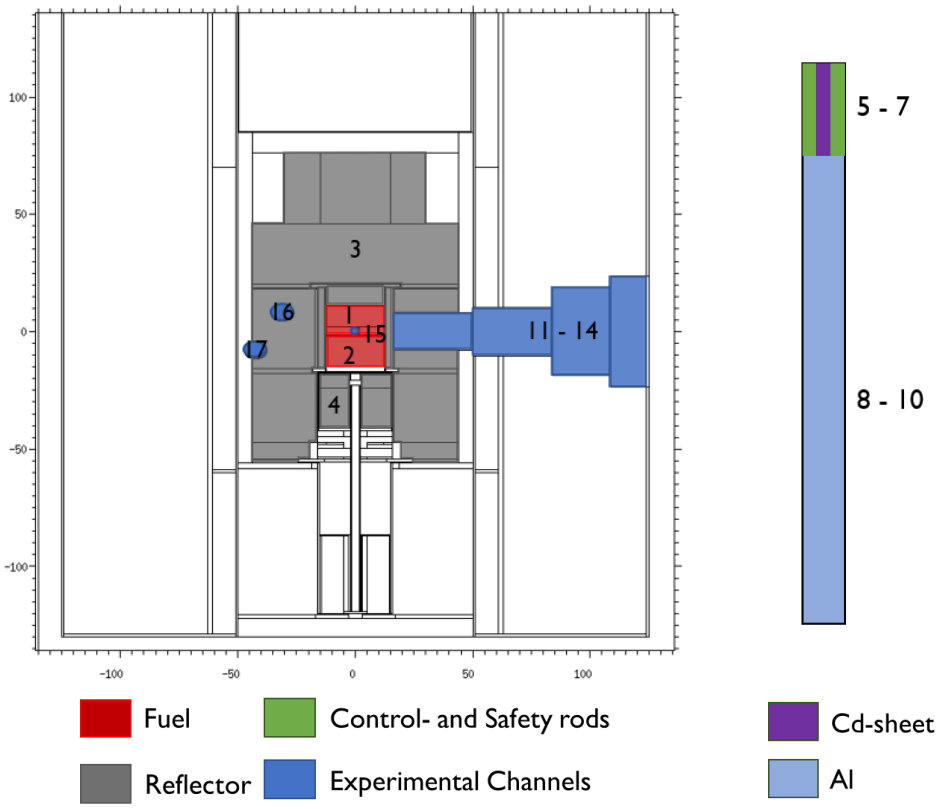

Description	Universe no.	Description	Universe no.
Fuel zone #1	1	Small central channel (1-2)	15
Fuel zone #2	2	Tangential channel (3-4)	16
Reflector zone #1	3	Tangential channel (5-6)	17
Reflector zone #2	4	Concrete	18
CSR[15]without Al + air	5, 6, 7	Paraffine	19
CSR	8, 9, 10	Air gap	20
Tall central channel (7)	11, 12, 13, 14		

Figure 4.2: Universe defined for group-constants generation in Serpent computation

4.2.3 Neutron Noise Source Modeling in CORE SIM+

Different from the noise sources introduced in Chapter 2 and Chapter 3, whose perturbation characteristics are relatively straightforward, “rotating absorber” and “vibrating absorber” have different mechanisms and should be modeled by incorporating their specific moving characteristics. In the first campaign, the perturbation of absorption cross-sections in fast and thermal energy groups and removal cross-sections in fast energy group are modeled as noise sources for both experimental cases (rotating and vibrating absorber). The rotating absorber considers the same types of perturbing cross-sections at the second experimental campaign, however, the vibrating absorber considers only absorption cross-sections in thermal energy group for a simplicity in modeling.

[15] Control and safety rods

First campaign: Rotating absorber

The perturbing cross-sections of a reaction x at rotating absorber can be obtained by the following expansion [32].

$$\delta\sum_x(r,\omega) = 2\pi \sum_{k=-\infty}^{+\infty} c_k \delta(\omega - k\omega_0), \tag{4.1}$$

where ω_0 is an angular frequency of vibration and c_k can be calculated following the equations below.

$$c_k = \frac{\Delta}{2\pi k}[i \cdot cos(k\omega_0 t) + sin(k\omega_0 t)]_{t=a}^{t=b} \tag{4.2}$$

$$a = \frac{R\theta}{v} - \frac{T}{2} \tag{4.3}$$

$$b = \frac{R\theta}{v} + t_d - \frac{T}{2} \tag{4.4}$$

$$t_d = \frac{Length\ of\ Cd\ sheet}{v} \tag{4.5}$$

In equations above, Δ signifies the macroscopic cross-section of Cd, while v and T indicate the velocity of absorber and the period, respectively. R and θ are defined as shown in Figure 4.3.

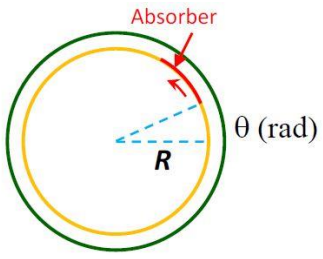

Figure 4.3: Rotating absorber [32]

Figure 4.4 shows an example of modeled perturbing cross-sections in fundamental mode ($k = 1$) when the rotation frequency is 1 Hz.

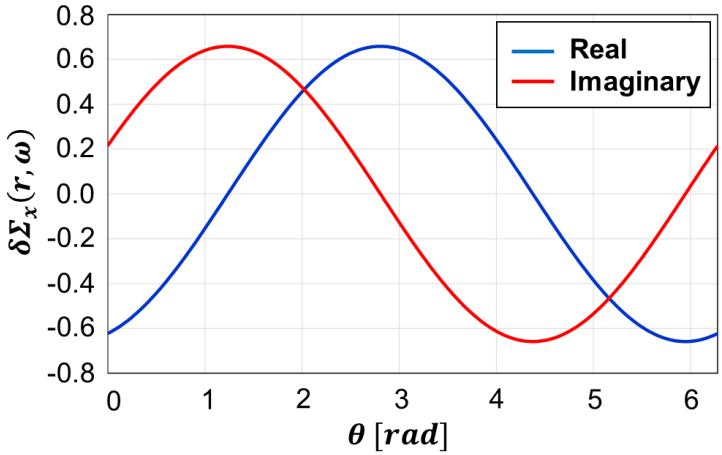

Figure 4.4: Modeled perturbing cross-sections for both real and imaginary parts in fundamental mode ($k = 1$) [32]

First campaign: Vibrating absorber

The frequency domain cross-section fluctuations of a reaction x at vibrating absorber can be obtained by the identical equation considered at rotating absorber (see Equation (4.1)). However, in case of vibrating absorber, the perturbing cross-sections are defined differently depending on a relative location of absorber in the channel [32]. The three classifications of absorber location are as follows.

1) when the distance to the left end of vibration region is shorter than the thickness of the absorber ($0 < x < D$)
2) when the distance to the right end of vibration region is shorter than the thickness of the absorber ($W - D < x < W$)
3) when the absorber is located between 1) and 2)

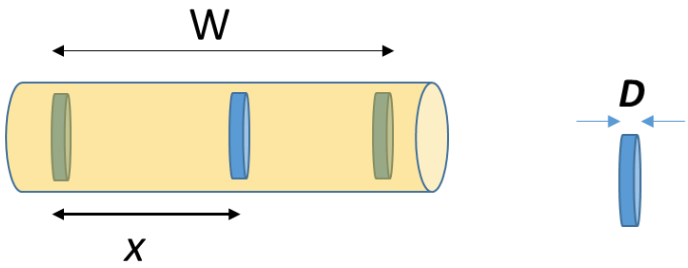

Figure 4.5: Absorber (blue) moving along the experimental channel (yellow) [32]

The perturbing cross-section at the three different regions can be calculated as follows. When the absorber is located in 1), c_k is given the Equation (4.6).

$$c_k = \frac{\Delta}{2\pi k}[i \cdot cos(k\omega_0 t) + si\,n(\,k\omega_0 t)]_{t=a}^{t=b}, \tag{4.6}$$

where $a = -x/v$ and $b = t_w + x/v$.

When the absorber moves the middle of the vibrating channel, which corresponds to the case 2), c_k is obtained by the Equation (4.7).

$$\begin{aligned} c_k = \frac{\Delta}{2\pi k}\{&[i \cdot cos(k\omega_0 t) + si\,n(\,k\omega_0 t)]_{t=a}^{t=b} \\ &+ [i \cdot cos(k\omega_0 t) + si\,n(\,k\omega_0 t)]_{t=c}^{t=d}\}, \end{aligned} \tag{4.7}$$

where $a = -x/v$, $b = D/v + x/v$, $c = t_w + x/v - D/v$ and $d = t_w + x/v$.

At the location of case 3), the perturbing cross-sections can be calculated with the same Equation for the case 3), but with $a = -T/2$, $b = W/v - x/v - t_m$, $c = t_w + x/v - D/v$ and $d = T/2$.

Figure 4.6 shows an example of modeled perturbing cross-sections in fundamental mode ($k = 1$) when the moving and waiting time of the absorber are 1 second and 0.1 second, respectively.

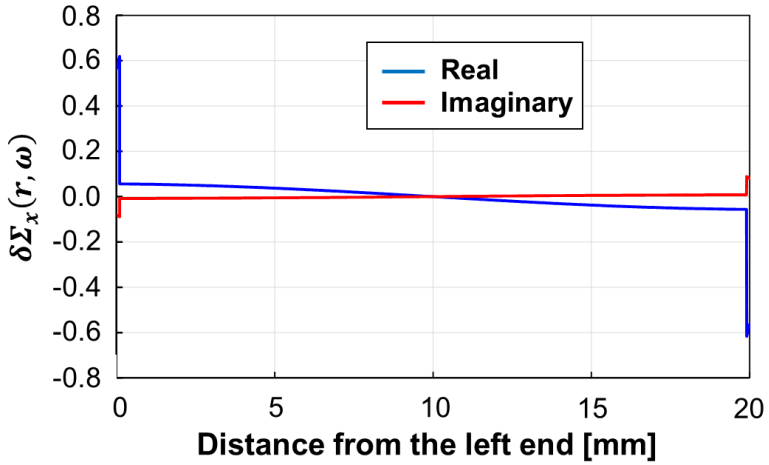

Figure 4.6: Modeled perturbing cross-sections for both real and imaginary parts in fundamental mode ($k = 1$) [32]

Second campaign: Rotating absorber

The modeling of neutron noise source in case of "rotating absorber" remains constant from that at the first campaign.

Second campaign: Vibrating absorber

The location and motion of the vibrating absorber have been changed in the second campaign [32]. Here, the vibration is assumed to be completely sinusoidal. The cross-section fluctuation in the frequency domain is expressed by Equation (4.1). The expansion coefficients, c_k, are given as below.

When $0 < x < W$,

$$c_k = -\frac{\Delta}{\pi k}\left(k\left(cos^{-1}\left(\frac{x}{A}-1\right)\right)\right), \tag{4.8}$$

where Δ signifies the cross-section of the absorber, A and W are the amplitude and the thickness of the absorber, respectively.

When $W < x < 2A$,

$$c_k = \frac{\Delta}{2\pi k}\{[sin(k\omega_0 t)]_{t=a}^{t=b} + [sin(k\omega_0 t)]_{t=c}^{t=d}\}, \tag{4.9}$$

where $a = -\frac{T}{2\pi}\left(cos^{-1}\left(\frac{x-W}{A}-1\right)\right)$, $b = -\frac{T}{2\pi}\left(cos^{-1}\left(\frac{x}{A}-1\right)\right)$, $c = \frac{T}{2\pi}\left(cos^{-1}\left(\frac{W}{A}-1\right)\right)$ and $d = \frac{T}{2\pi}\left(cos^{-1}\left(\frac{x-W}{A}-1\right)\right)$.

When $2A < x < 2A + W$,

$$c_k = \frac{\Delta}{\pi k}\sin(k\omega_0 a), \tag{4.10}$$

where $a = \frac{T}{2\pi}\left(\pi - cos^{-1}\left(1-\frac{x-W}{A}\right)\right)$.

Figure 4.7 shows a schematic view of vibrating absorber and Figure 4.8 depicts real part of perturbing cross-section ($Re[\delta\sum(x,\omega)]$) as a function of x under a vibration with frequency of 2 Hz and amplitude of 3 cm. Unlike the first campaign, imaginary part of perturbing cross-section ($Im[\delta\sum(x,\omega)]$) is modeled as zero.

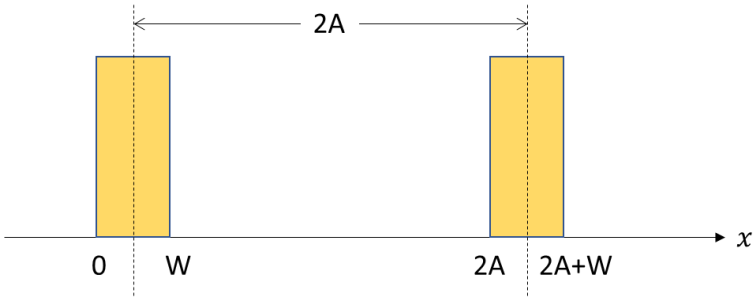

Figure 4.7: Schematic view of vibrating absorber [32]

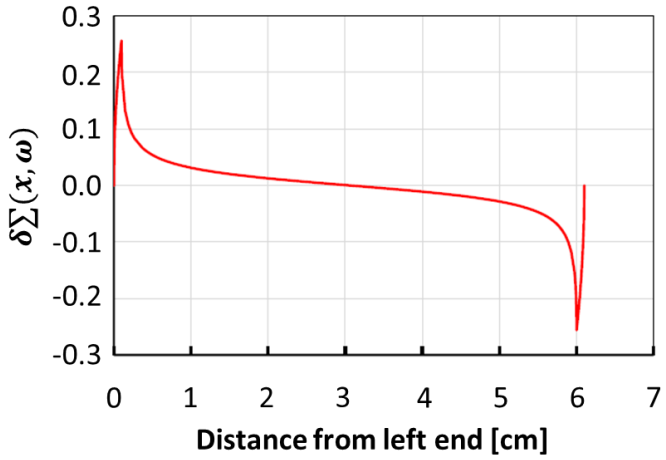

Figure 4.8: Modeled perturbing cross-section for real part in fundamental mode ($k = 1$) under a vibration with frequency of 2 Hz and amplitude of 3 cm [32]

4.2.4 Neutron Noise under the Unperturbed Condition

The behavior of static fluxes under the unperturbed condition in radial direction of the core are shown in Figure 4.9 and Figure 4.10, for rotating absorber and vibrating absorber, respectively. Two events are sharing the identical static flux distributions for the further noise calculation. Figure 4.9 and Figure 4.10 are the radial static flux distribution at two different heights of the core, in order to represent the static behavior at the axial level where the target noise source (rotating and vibrating absorber) is located.

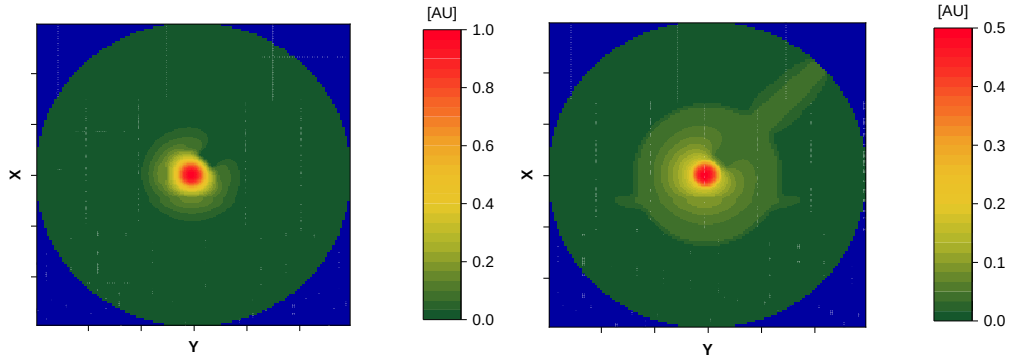

a. Fast static flux b. Thermal static flux

Figure 4.9: Static fluxes behavior at the 21 cm below the axial mid-point (the identical axial location where the rotating absorber is located)

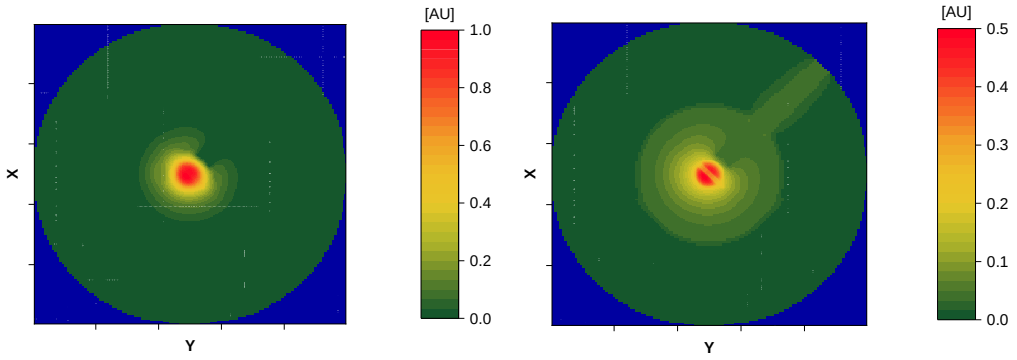

a. Fast static flux b. Thermal static flux

Figure 4.10: Static fluxes behavior at the 43 cm below the axial mid-point (the identical axial location where the vibrating absorber is located)

The static fluxes in both energy groups show similar tendency that the values increase when it gets close to the core center.

The behavior of neutron noise under the nominal condition in radial direction of the core are confirmed as shown in Figure 4.11 (rotating absorber) and Figure 4.12 (vibrating absorber) in two different quantities: absolute noise (thermal neutron noise) and QoIs. As it is already confirmed in Chapter 3.2.3, the amplitude of absolute neutron noise shows similar pattern with static flux, while the

amplitude of QoI reveals the spatial component of the neutron noise. Whereas the phase of neutron noise shows similar distribution in both formats. This is because the distribution of the phase of neutron noise is mostly homogeneous except at the location of noise source having a steep gradient. Therefore, converting the absolute neutron noise into QoI can barely magnify the spatial component, resulting in the similar patterns between the absolute value and QoI.

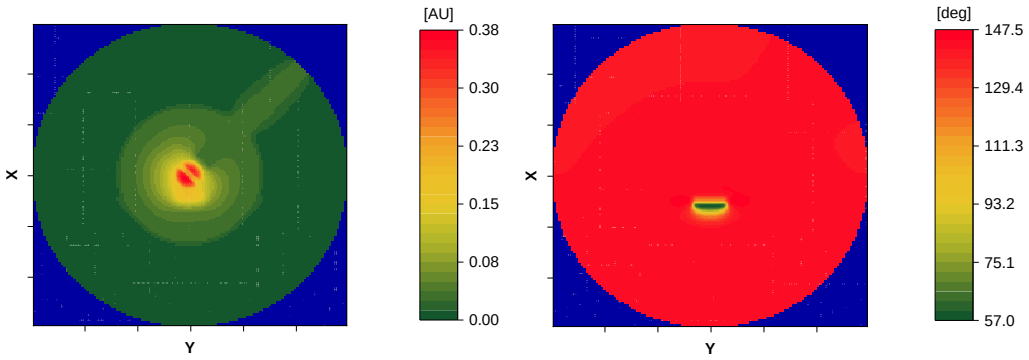

a. Amplitude of absolute neutron noise

b. Phase of absolute neutron noise

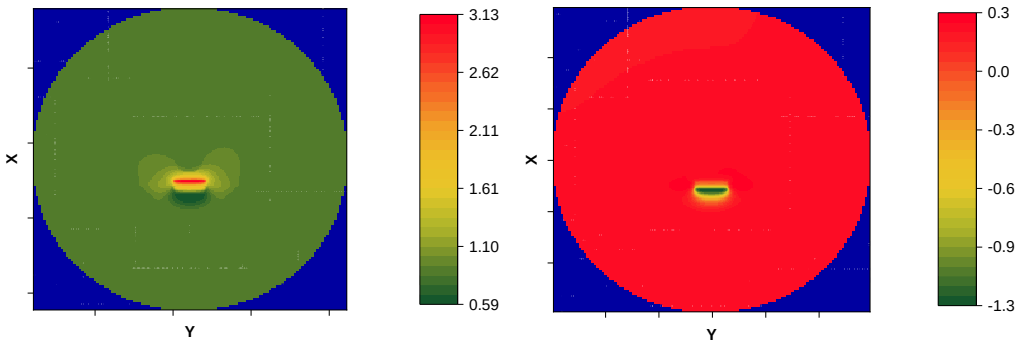

c. Amplitude of QoI

d. Phase of QoI

Figure 4.11: Neutron noise behavior at “rotating absorber” at the axial location of noise source

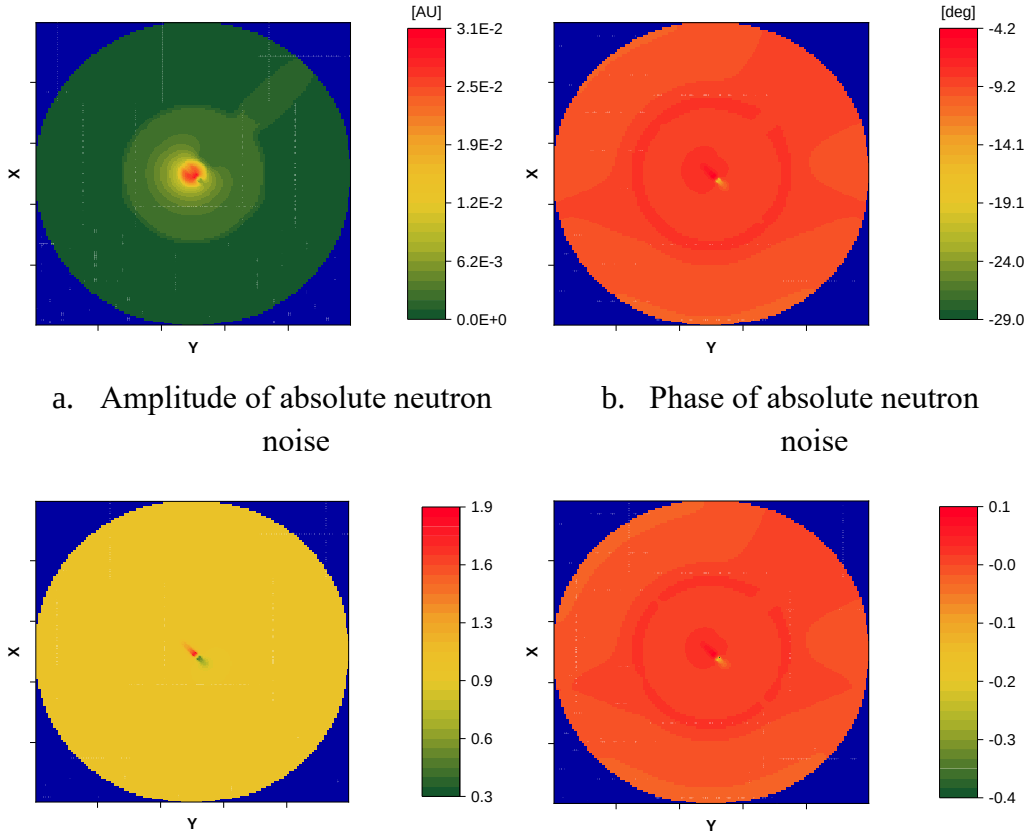

a. Amplitude of absolute neutron noise

b. Phase of absolute neutron noise

c. Amplitude of QoI

d. Phase of QoI

Figure 4.12: Neutron noise behavior at "vibrating absorber" at the axial location of noise source

4.3 Preparation for the Analysis

4.3.1 Process of Analysis

Since AKR-2 is based on AKR-1 which was designed in 1970s, there is a lack of design information regarding operational uncertainties and manufacturing tolerances of reactor components. Accordingly, the analyses are carried out mainly based on the process developed at CROCUS reactor as described in Figure 3.5,

while the perturbation of design and operating parameters is excluded from consideration.

The modified flow chart is illustrated in Figure 4.13 and Figure 4.14 for first and second experimental campaign, respectively.

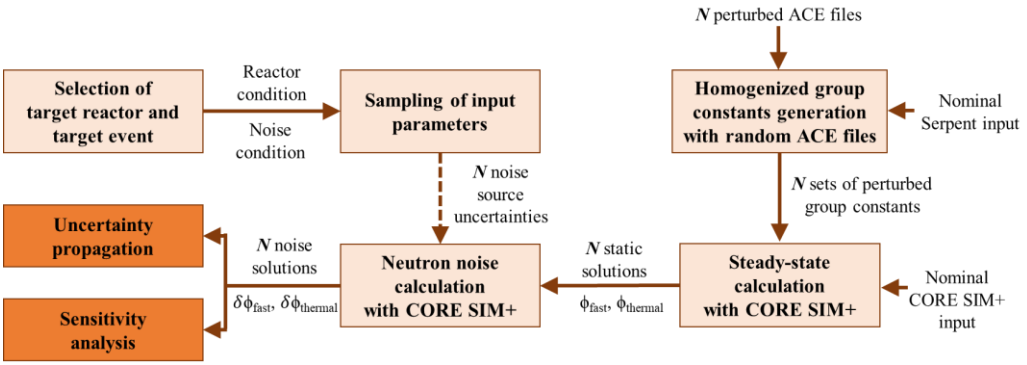

Figure 4.13: Flow chart for the uncertainty analyses for first experimental campaign

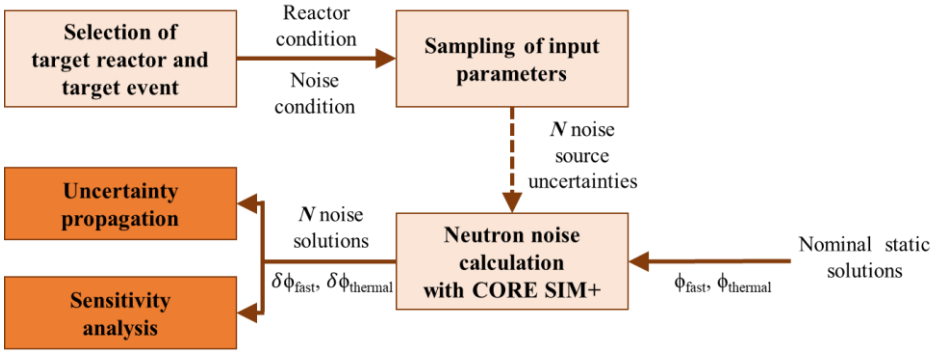

Figure 4.14: Flow chart for the uncertainty analyses for second experimental campaign

4.3.2 Listing Uncertain Parameters

First campaign

No.	Parameter		Distribution	Unit	Nominal value	Lower/ Upper limit
1 ~ 864	Nuclear data uncertainties[16]					
865	Rotating absorber	Frequency	Uniform	Hz	1	0.95/1.05
	Vibrating absorber	Moving time	Uniform	second	1	0.95/1.05
		Waiting time	Uniform	second	0.1	0.095/0.105
866	Location of noise source (along the core center direction)		Uniform	Mesh	Ideal oscillating boundary	-1/+1[17] ($-\sqrt{2}/+\sqrt{2}$)[18]
867	Location of noise source (along the lateral direction of experimental channel)		Uniform	Mesh	Ideal oscillating boundary	-1/+1 ($-\sqrt{2}/+\sqrt{2}$)

Table 4.2: The distribution information of uncertainty parameters considered in the first campaign

As it is aforementioned above, the information on design and operating parameters of AKR-2 are fairly limited, therefore, these parameters are excluded from consideration. Meanwhile, the nuclear data uncertainties and the uncertainties of noise source description remain as uncertainty parameters for the consistency with the preceding analyses at the CROCUS reactor. The uncertainties of

[16] The detailed information on nuclear data uncertainties is described in Chapter 4.3.4.

[17] -1/+1 correspond to -1/+1 cm.

[18] In case of vibrating absorber, the experimental channel is modeled in a diagonal direction in x-y plane, therefore, the location is perturbed within $\pm\sqrt{2}$ mesh and this corresponds to -1.4/+1.4 cm.

frequency for both experiments are set as 5 % around their mean values by expert judgement.

Second campaign

No.	Parameter		Distribution	Unit	Nominal value	Standard deviation (Lower/ Upper limit[19])
1	Frequency		Normal	Hz	2	5 %
2	Location of noise source	Along the experimental channel	Uniform	Mesh	Ideal location	-1/+1[20]
3		Along the core center line	Uniform	Mesh	Ideal location	-1/+1[21]

Table 4.3: The distribution information of uncertainty parameters considered in the second campaign

From the analysis conducted at a condition of first experimental campaign (Chapter 4.5), it is confirmed that the effect driven by the nuclear data uncertainties is less remarkable than the effect from the noise source parameters (the frequency and the location of noise source). Therefore, for the sake of conciseness

[19] Standard deviation in the case of a normal distribution or lower and upper limits in the case of a uniform distribution.

[20] -1/+1 correspond to -0.47/+0.47 cm for the vibrating absorber and -1/+1 cm for the rotating absorber.

[21] -1/+1 correspond to -0.47/+0.47 cm for vibrating absorber. This parameter is not considered in the case of the rotating absorber.

of the calculational process, the nuclear data uncertainties are not considered in the analysis for second experimental campaign. This enables us to skip a series of static calculations and to focus on noise calculation with considering only the noise source parameters, thus, saves computational cost remarkably. The new core model prepared with CORE SIM+ [32] for an analysis at rotating absorber has non-uniform mesh composition along the core center direction, thus, a perturbation of noise source location does not guarantee a relocation of identical amount of noise source (perturbing cross-sections). Accordingly, the location of noise source along the core center line is excluded from the analysis of "rotating absorber" as shown in Table 4.3.

4.3.3 Generation of Random Samples

A total of 93 input sets are generated following the identical procedure introduced in Chapter 3.3.3, these input sets involve the perturbation of parameters except the nuclear data. The uncertainties of nuclear data are treated independently in the following chapter.

4.3.4 Nuclear Data Uncertainty Treatment

For the propagation of nuclear data uncertainties at AKR-2 reactor to the two-group constants, 93 times of Serpent calculations were performed with Serpent v2.1.31, using its native ENDF/B-VII.0 ACE files and ENDF/B-VII.1 covariances obtained from njoy2012 COVR module and Scale 6.0 energy group structure [103]. The microscopic data for ^{235}U, ^{238}U, ^{1}H, ^{12}C and ^{16}O are considered while the following reaction types are perturbed: (n, el), (n, inl), (n, 2n), (n, capture), (n, f), $\bar{\nu}$ and χ. The relevantly propagated nuclear data consist of diffusion coefficient (D), absorption cross-section (Σ_{abs}), nu-fission cross-section ($\nu\Sigma_{fiss}$) and removal cross-section (Σ_{rem}) of two-energy group in 20 reactor core regions as described in Figure 4.2. The obtained group constants are summarized as a form of histogram in Appendix A.2.

4.4 Uncertainty Propagation

4.4.1 Uncertainty Propagation Method

In the first experimental campaign, there are three He-3 Proportional Counters (PC), three Fission Chambers (FC) and one ^{10}B-coated Compensated Ion Chamber (CIC) as shown in Figure 1.9 [21]. The detection of the data in the second experimental campaign is made by two FCs, four PCs and three optical fiber based scintillator detectors (see Figure 1.10). Different from the CROCUS reactor, the neutron detectors at AKR-2 are not installed at the same axial height but with differences of up to $10\ \mathrm{cm}$ and $16\ \mathrm{cm}$ at the first and second experimental campaigns, respectively. Therefore, the further analysis in this chapter focuses on the behavior at the installed detector locations and excludes the core-wise analyses at certain axial level.

The uncertainty propagation is carried out following 1st order Wilks' formula for two-sided limits by considering a computational cost which is more expensive than at the CROCUS reactor. Therefore, we need to perform 93 times of code execution to credit that the largest and the lowest values among the results are satisfying the $95\ \%/95\ \%$ criterion.

4.4.2 Rotating Absorber

First campaign

Figure 4.15 shows the QoI uncertainties at the installed detector locations in the first experimental campaign, where Detector 1 is set as reference detector. One remarkable point here is that the nominal value is biased to one uncertainty boundary, which is different from an expectation that the nominal value is close to a mean value of two extremes.

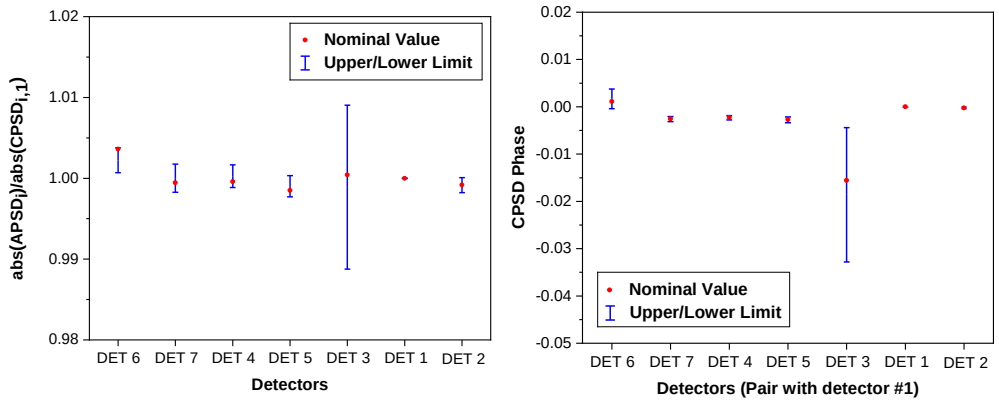

a. APSD amplitude b. CPSD phase

Figure 4.15: The perturbation of thermal neutron noise (QoI)

This can be explained by a combination of the noise source and the static flux. As it is introduced in Table 4.2, the location of noise source is perturbed along the core center direction within ± 1 mesh. Meanwhile, the position of experimental channel for the rotating absorber in Figure 1.7 tells us that if the location of the channel is perturbed, it moves either toward the core center or away from the center. When the absorber approaches to the core center, the channel is positioned at the location of higher static flux. The neutron noise is a product of a noise source and a static flux (see Equation (1.32)) and the gradient of the static flux across the core center is not linear as shown in Figure 4.16. Namely, an increment of the neutron noise can vary depending on a gradient of static flux.

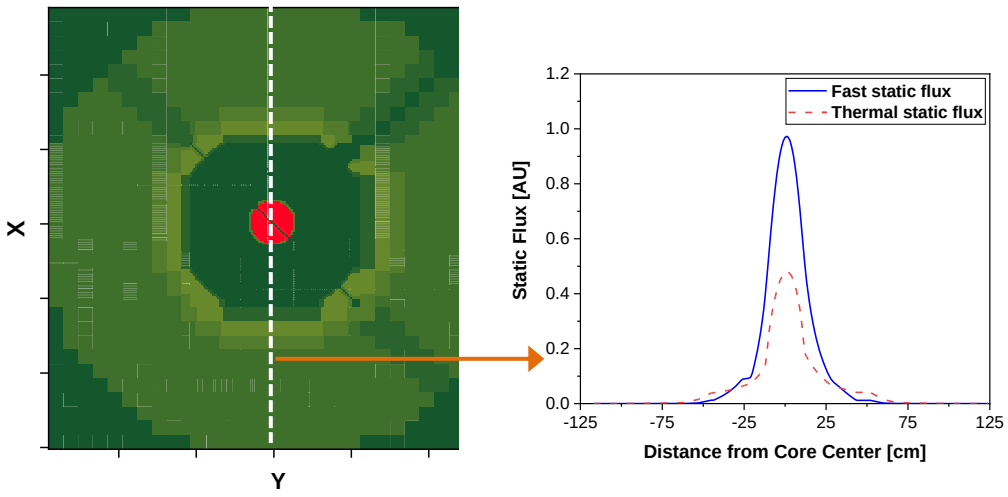

Figure 4.16: Static flux distribution across the core center (along the white line in left figure)

The increment of neutron noise when the experimental channel approaches to the core center becomes larger than the decrement of neutron noise when the channel moves away from the core center, and this tendency generates the biased result confirmed in Figure 4.15. Additionally, we can infer the relative importance of "location of noise source along the core center direction" on neutron noise from the biased state. Several detecting locations including Detector 6 show strong bias, which can imply that the "location of noise source along the core center direction" is a main driver to the neutron noise. However, this is one of the expected outcomes from the sensitivity analysis and the relevant discussion is made in Chapter 4.5, accordingly.

Second campaign

Figure 4.17 shows the QoI uncertainties at the installed detector locations in the second experimental campaign, where Detector 8 is set as reference detector. Since the location of noise source is not perturbed along the core center line in this analysis, the biased nominal values confirmed in the first experimental campaign are not found in the figures.

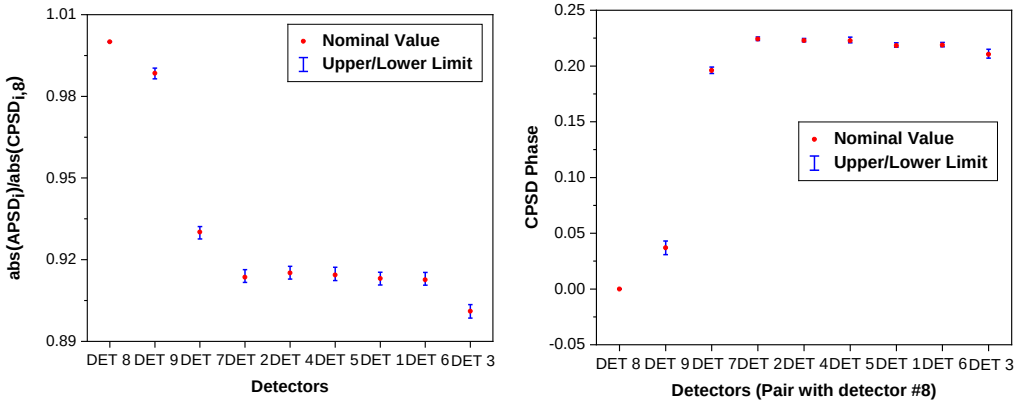

a. APSD amplitude b. CPSD phase

Figure 4.17: The perturbation of thermal neutron noise in the format of QoI

4.4.3 Vibrating Absorber

First campaign

The uncertainties of neutron noise obtained at the event of vibrating absorber is depicted in Figure 4.18. The uncertainties in all detector location are much smaller compared to those at rotating absorber. This stems from different magnitudes of noise sources: in case of "rotating absorber", the magnitude of perturbing cross-section is around 20 times bigger than that of "vibrating absorber". Therefore, the neutron noise is less affected by smaller magnitude of noise source, resulting in smaller uncertainties. Meanwhile, the nominal value is not biased as it is at the rotating absorber. Because the experimental channel is originally penetrating the core center, the ± 1 mesh perturbation along the core center direction does not generate any difference with respect to the increment on static flux, therefore no additional contribution to the neutron noise.

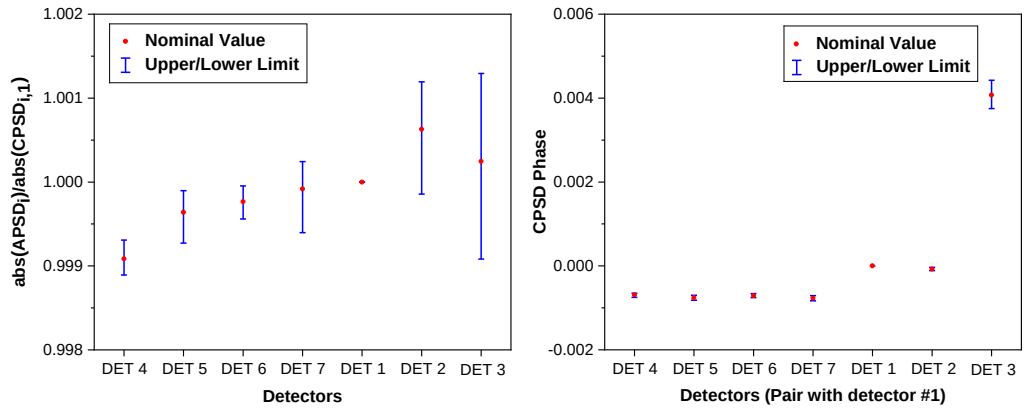

a. APSD amplitude b. CPSD phase

Figure 4.18: The perturbation of thermal neutron noise in the format of QoI

Second campaign

Figure 4.19 shows the uncertainties of QoIs in second experimental campaign. The uncertainties of QoI-amplitude shown in Figure 4.19-a are even larger than those at the first campaign, while there is no remarkable change in QoI-phase. In the following chapter, we investigate what the main contributors to the considered response uncertainty are.

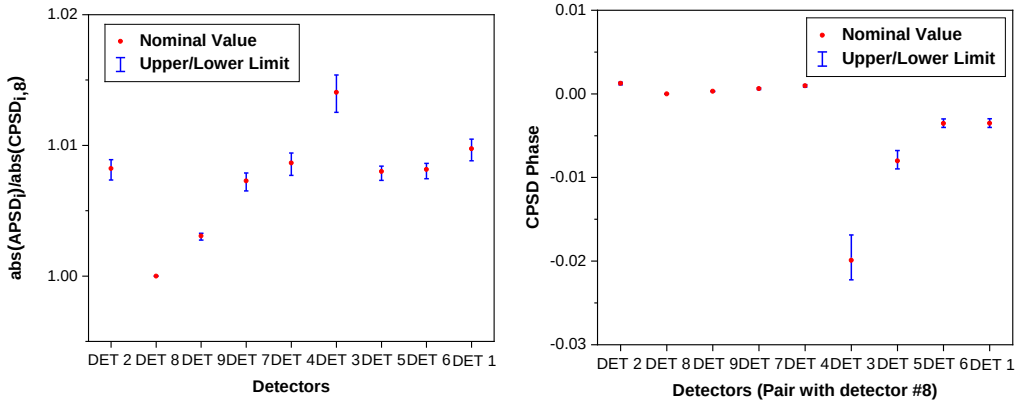

a. APSD amplitude b. CPSD phase

Figure 4.19: The perturbation of thermal neutron noise in the format of QoI

4.5 Sensitivity Analysis

4.5.1 Sensitivity Analysis Method

The sensitivity analyses are made based only on the first experimental campaign, in order to involve more input parameters into consideration. In accordance with the process carried out in Chapter 3.5 with CROCUS reactor, the sensitivity analysis is conducted with both qualitative and quantitative ways.

The analysis using qualitative approach begins with grouping input parameters into two groups, namely, group of nuclear data and group of noise source data. The definition of each group is identical to that described in Chapter 3.5.3: group of nuclear data and group of noise source data include the parameters no. 1 to no. 864 and the parameters no. 865 to no. 867 in Table 4.2, respectively. The neutron noise uncertainties at the installed detector locations from two groups are compared and the relative importance of groups is discussed.

The following sensitivity analysis with quantitative approach is carried out using Pearson correlation coefficient, which is an identical methodology considered in the analyses under the “fuel rods vibration (see Chapter 3.5.3.2)”. Due to a small sample size (93) obtained from noise simulations, a criterion of the correlation is increased compared to that at the previous analyses at CROCUS reactor: according to the Z test, we can regard that the two random variables are “correlated” with 5 % probability that this correlation is not true, when the absolute value of calculated coefficient based on 93 samples becomes larger than 0.21.

4.5.2 Convergence of the Sensitivity Indices with the Number of Samples

A series of convergence tests with different sample sizes are performed to confirm whether the current sample size (93) can guarantee the “convergence” in

this study. The overall procedure is identical to the one used in “Fuel rods vibration (see Chapter 3.5.2)”. The sensitivity indices considered for the convergence assessment are calculated between two input parameters and the QoI-amplitude at the location of Detector 7 during “rotating absorber”. Parameters having a small (frequency) and large sensitivity (location of noise source (along the core center direction)) to QoI-amplitude are chosen to cover all possible convergence behavior. The tests are carried out with different sample sizes between 10 to 93, which are sampled randomly from 93 existing data sets. The sampling of equivalent sample size is repeated 500 times using bootstrapping with replacement [101]. Afterwards, to compute 95 % confidence intervals, the 2.5th and 97.5th percentiles of the index distribution (500 indices at each sample size) obtained by bootstrapping are identified. The sensitivity indices and their confidence intervals at different sample size is given by the convergence plot found in Figure 4.20.

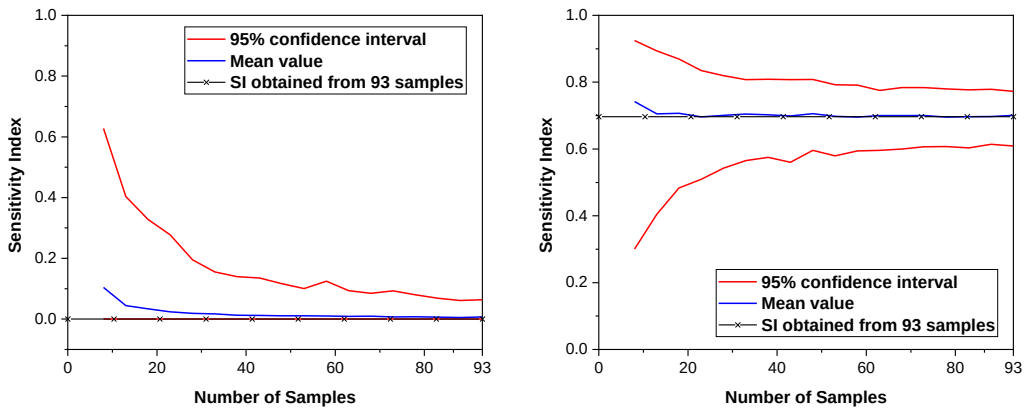

a. Frequency

b. Location of noise source (center)

Figure 4.20: Convergence plots of sensitivity indices with 95 % confidence interval

The confidence interval decreases as the sample size increases. The mean values of sensitivity indices are nearly saturated when the sample size is getting larger. However, the confidence intervals are not fully saturated and seem larger than those in “fuel rods vibration” which was carried out with 1000 samples. Considering the large confidence interval, which is not fully converged, identifying a

dominantly influencing parameters to output noise should be a main goal in this study and a discussion about the rest parameters will not be made.

4.5.3 Rotating Absorber

4.5.3.1 Correlations in QoIs

As it is confirmed in the previous analysis at “fuel rods vibration”, identifying the correlated behavior among the neutron noises at the installed detector locations helps to get a better understanding in uncertainty analyses by grouping the correlated signals. Figure 4.21-a shows the QoI-amplitudes which are separated into two groups: Detector 2 is nearly independent from other detectors, while the rest detectors are strongly correlated among each other. The QoI-amplitude under the rotating absorber is APSD amplitude normalized by CPSD amplitude using Detector 1 location as the reference location. Since Detector 2 is located on a same channel with Detector 1 (see Figure 1.9), the noise behavior becomes similar with that of Detector 1, which results in different tendency with other detectors when normalized by the signal of Detector 1. Meanwhile, all QoI-phases (Figure 4.21-b) are strongly correlated among each other with showing almost perfect linear correlation.

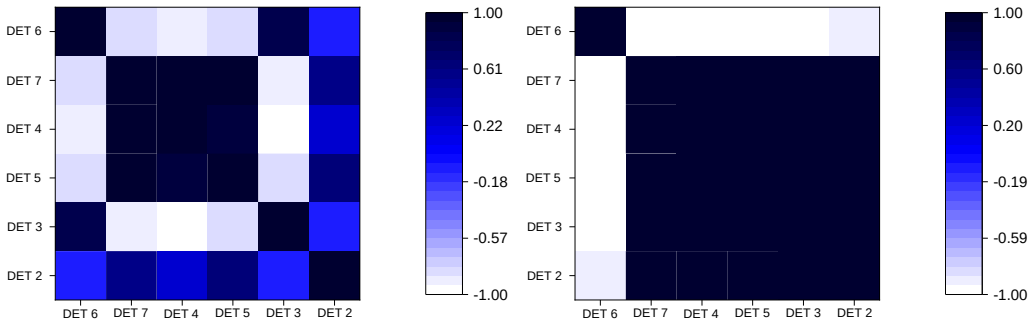

a. QoI-amplitude b. QoI-phase

Figure 4.21: The correlated behavior among the QoIs at the detector locations

In the following section, the sensitivities of input parameters at installed detector locations are explained in connection with the correlated behavior identified above.

4.5.3.2 Sensitivity Analysis with Qualitative Approach

The uncertainties of neutron noise propagated from the two different groups are compared as shown in Figure 4.22, in order to investigate the relative effects of the different groups of parameters (namely, group of nuclear data and group of noise source data). Each uncertainty is calculated with the perturbation of parameters belonging to the considered group of input parameters, while the remaining input parameters are kept at their nominal values. The uncertainties are obtained following the 1st order Wilks' formula for two-sided limits, whose required number of code runs is 93.

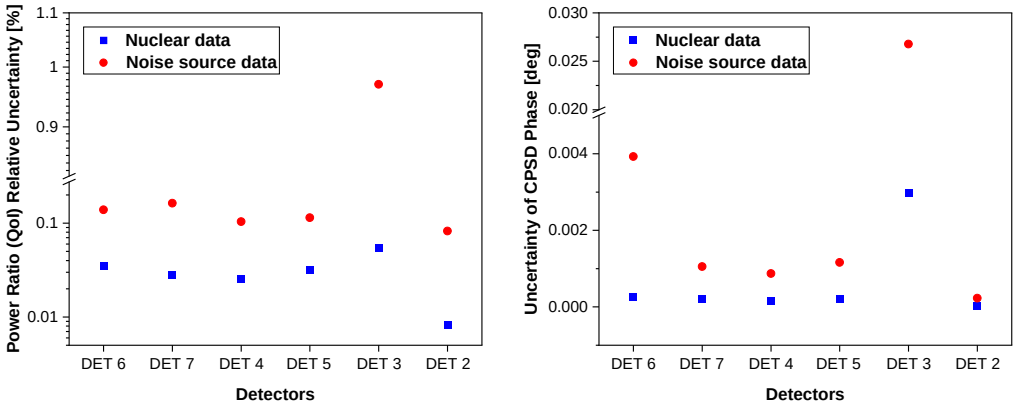

a. QoI-amplitude b. QoI-phase

Figure 4.22: Comparison of neutron noise uncertainties obtained from the different groups of input parameters ("DET" denotes "DETECTOR")

From the results, it is confirmed that both QoI amplitude and phase in all detector locations are strongly driven by the group of noise source data.

4.5.3.3 Sensitivity Analysis with Quantitative Approach

Based on the results from qualitative approach, additional sensitivity analysis using quantitative approach is carried out with focusing on "Group of noise

source data". The calculated sensitivity indices of three parameters included in the group using Pearson correlation coefficient are depicted in Figure 4.23 for the amplitude and the phase of QoIs, respectively. In this figure, two parameters of "location of noise source along core center direction" and "location of noise source along lateral direction of experimental channel" are abbreviated to "Location (Center)" and "Location (Ch 3-4)", respectively.

In Figure 4.23-a, the QoI-amplitude at the location of Detector 2 is strongly affected by the "Location (Ch 3-4)", while the rest QoIs are influenced mainly by the "Location (Center)". This grouped behavior among the detector locations is identical to the findings from correlated behavior confirmed in Figure 4.21-a. Additionally, Figure 4.23-b shows that the QoI-phases at all detector locations are strongly driven by the "Location (Center)", which corresponds to the correlation found in Figure 4.21-b.

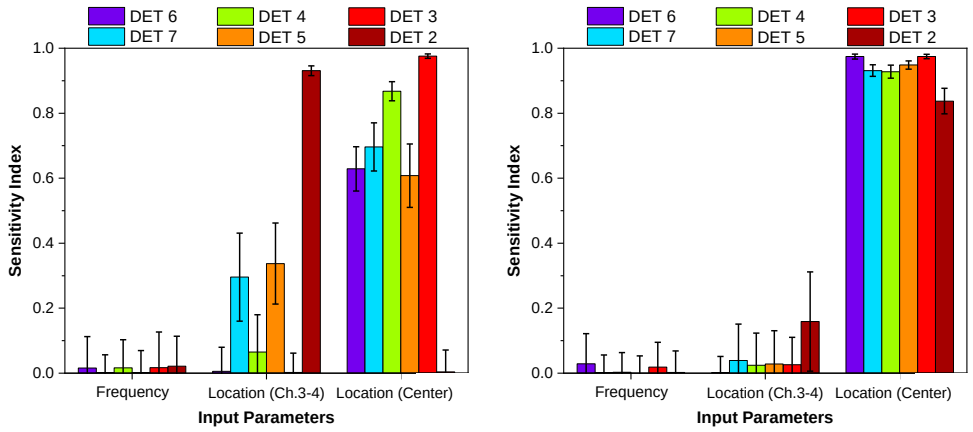

a. QoI-amplitude b. QoI-phase

Figure 4.23: The sensitivity indices and the 95 % confidence intervals between input parameters and QoIs ("DET"denotes "DETECTOR")

4.5.4 Vibrating Absorber

4.5.4.1 Correlations in QoIs

The correlation among the QoIs during "vibrating absorber" is identified and the results are depicted in Figure 4.24. The QoI-amplitudes are separated into two groups: first group consists of Detector 4, 5 and 7, and the second group consists of the rest three detectors. The QoI-phases are also separated into two groups: first group consists of Detector 2, and the second group consists of the rest five detectors.

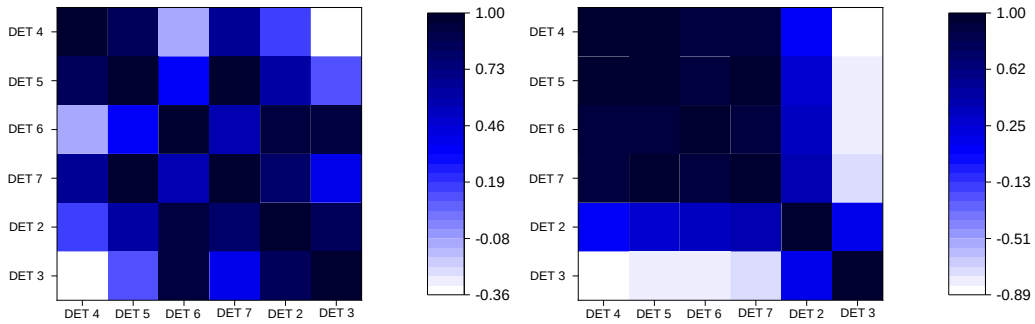

a. QoI-amplitude b. QoI-phase

Figure 4.24: The correlated behavior among the QoIs at the detector locations

Similarly to the previous section, the sensitivities of parameters at different detector locations are investigated in the following section in connection with the correlated behavior identified above.

4.5.4.2 Sensitivity Analysis with Qualitative Approach

The sensitivity analysis using qualitative approach is carried out with two groups of input parameters. The uncertainties of QoI amplitude and phase obtained from the perturbation of each group are shown in Figure 4.25.

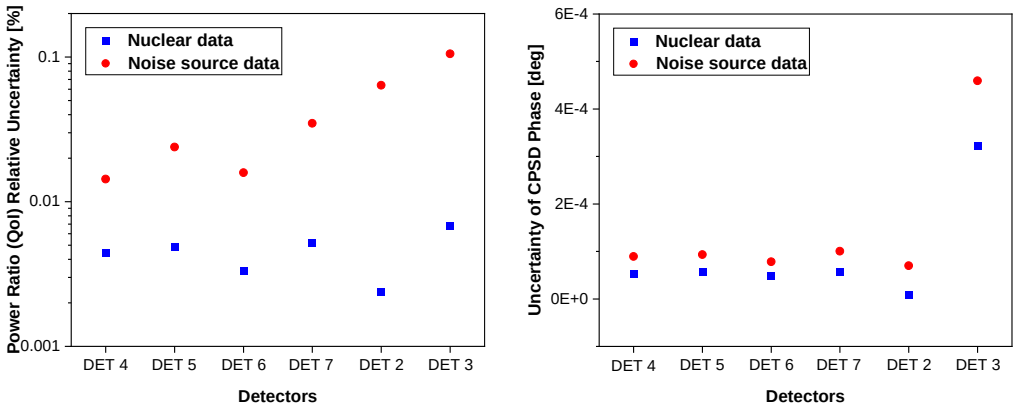

a. QoI-amplitude b. QoI-phase

Figure 4.25: Comparison of neutron noise uncertainties obtained from the different groups of input parameters ("DET" denotes "DETECTOR")

According to the results, the group of noise source data is confirmed as a major contributor to the QoI amplitude and phase at all installed detector locations.

4.5.4.3 Sensitivity Analysis with Quantitative Approach

Considering the results in the previous section, the sensitivity analysis using quantitative approach is performed with focusing on the parameters included in "Group of noise source data". The calculated sensitivity indices of three parameters using Pearson correlation coefficient are depicted in Figure 4.26 for the amplitude and the phase of QoIs. In this figure, the parameter of "location of noise source along lateral direction of experimental channel" is abbreviated to "Location (Ch 1-2)".

In Figure 4.26-a, the QoI-amplitudes at the location of Detector 4, 5 and 7 are affected by the "Location (Center)", while the rest QoI-amplitudes (Detector 6, 2 and 3) are affected mainly by the "Location (Ch 1-2)". This correlation among the signals at the different detector locations is identical to the findings in Figure 4.24-a. The QoI-phase at the installed detector location show the same grouped behavior as confirmed in Figure 4.24-b: the QoI-phase at the location of Detector 2 is strongly driven by the "Location (Ch 1-2)", while the rest QoIs are mainly affected by the vibrating frequency.

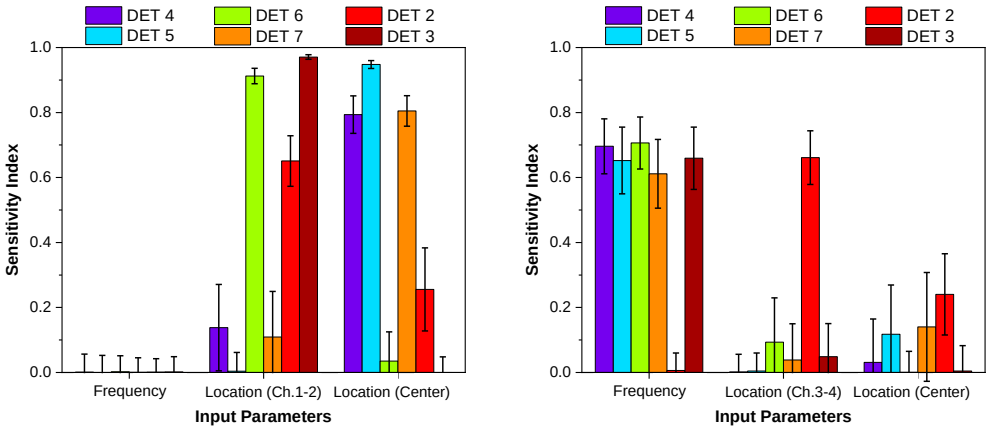

a. QoI-amplitude b. QoI-phase

Figure 4.26: The sensitivity indices and the 95 % confidence intervals between input parameters and QoIs (“DET” denotes “DETECTOR”)

Chapter 5

Investigation of an Applicability of Developed Methodology to a Power Plant

Based on the methodology which has been structured and optimized at two different zero-power reactors in previous sections, an additional uncertainty analysis is conducted at Swiss 3-loop pre-Konvoi reactor. Current study only involves the sensitivity analysis, and the uncertainty propagation is excluded since the validation of the noise simulators is limited to the zero-power reactors (CROCUS and AKR-2) within the CORTEX project.

The neutron noise induced by one fuel assembly vibration is simulated by the noise simulator CORE SIM+ for various core conditions (different fuel burnups and fuel loading patterns). The sensitivity analysis identifies the relative importance of the considered input parameters to the neutron noise at the installed detector locations. Additionally, by the repetition of the identical analysis under different core conditions, the influence of the input parameters which varies depending on the fuel burnup and the fuel loading pattern is also investigated.

5.1 Description of Target Condition

5.1.1 Target Reactor

The target reactor considered here is the Gösgen Nuclear Power Plant (KKG), which is introduced in Chapter 1.4.3.

In the context of the CORTEX project, the PSI provided the necessary core data, which include three-dimensional distribution of the nodal macroscopic cross-sections in two-energy groups and the kinetic parameters of Cycle 39 (MOC and EOC) and Cycle 40 (BOC, MOC and EOC) [104]. Accordingly, the analyses are carried out based on these core conditions.

5.1.2 Target Event

Experimental reactors, such as AKR-2 or CROCUS [17, 19], have their own dedicated experimental facilities, which makes it possible to plan the relevant noise experiments within their capabilities. However, in power plants during normal operation no neutron noise experiments can be performed to get measurements for perturbations which can be precisely reproduced by simulations. Therefore, an event which induces the neutron noise has been selected based on the analyses performed in [105].

The relevant event is a “fuel assembly vibration”, where the size of fuel assembly corresponds to $21.56\,\mathrm{cm} \times 21.56\,\mathrm{cm} \times 358\,\mathrm{cm}$ and the oscillating fuel assembly is located $53.9\,\mathrm{cm}$ away from the core center as shown in Figure 5.1.

It is assumed that the fuel assembly oscillates following the cantilevered beam mode whose oscillating amplitude increases along the axial height as described on the right side in Figure 5.1 [28]. Additionally, the oscillating frequency of the fuel assembly is presumed as 1 Hz.

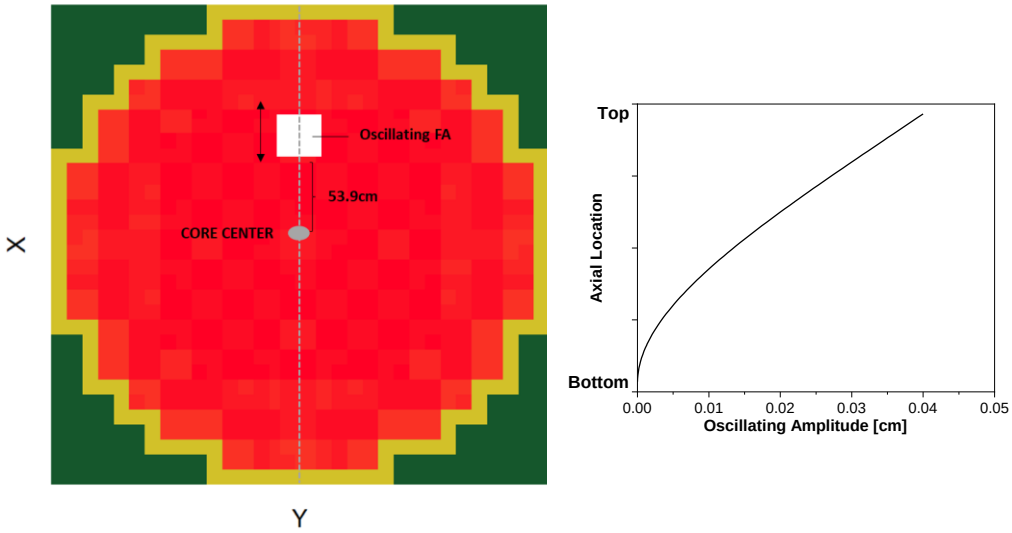

Figure 5.1: Radial location of the considered vibrating assembly (left) and axial shape of the maximum lateral displacement of this assembly

5.2 CORE SIM+ Model of Swiss 3-loop pre-Konvoi Reactor

The reactor core is modeled with a three-dimensional mesh of $76 \times 51 \times 102$ cells, in the $x-$, $y-$ and $z-$ directions of the core, respectively. The area around the neutron noise source is modeled with refined mesh cells of size 4.3 mm, whereas the other parts of the core have mesh sizes varying between 3 and 10 cm. Figure 5.2 shows the nodalization of the core at the axial mid-point.

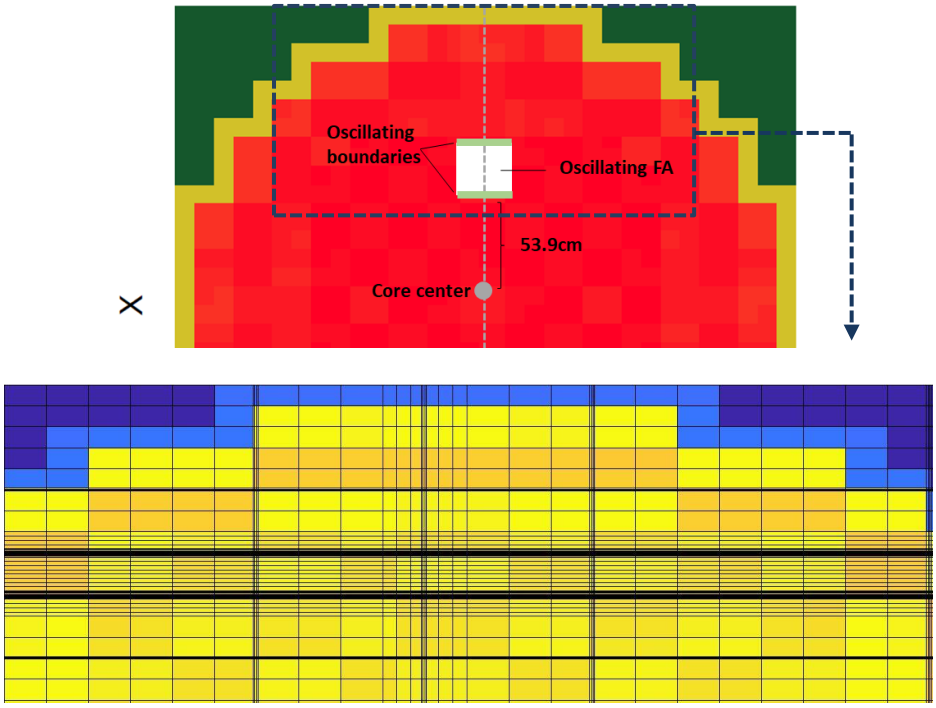

Figure 5.2: Description of the radial nodalization around the noise sources at mid-core elevation

The two green lines at the boundaries of oscillating fuel assembly represent the location where the noise sources are assigned for the noise simulation using CORE SIM+. The lower picture of Figure 5.2 focuses on the meshes modeled around oscillating fuel assembly, showing the finer meshes at the oscillating boundaries compared to the rest area.

5.3 Preparation for the Analysis

5.3.1 Process of Analysis

The workflow chart is depicted in Figure 5.3, which is mostly based on Figure 3.5. The selected input parameters are considered in both steady-state and dynamic calculations using CORE SIM+ as follows. Based on the selected core

condition, the two energy-group cross-sections and the core kinetic parameters are determined, and their corresponding uncertainties are generated. Then N steady-state calculations are carried out with CORE SIM+, resulting in N static solutions. The obtained static fluxes are combined with noise sources which are perturbed within the uncertainty ranges, and used as inputs for noise calculations. The further sensitivity analysis is carried out by using the obtained N neutron noise solutions from CORE SIM+ calculation. The final output (thermal neutron noise) from CORE SIM+ computation is a complex quantity, therefore, the complex values are converted into amplitude and phase of neutron noise via post-processing.

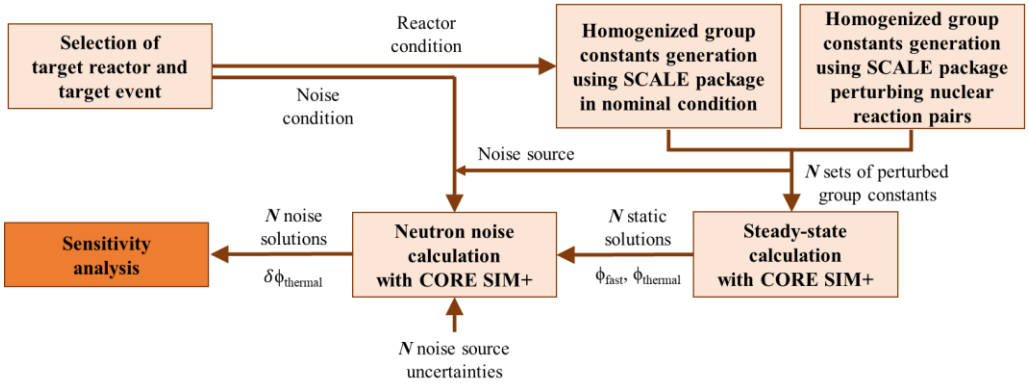

Figure 5.3: Workflow chart for the sensitivity analysis

5.3.2 Listing Uncertain Parameters

The parameters for the target reactor and transient are investigated based on expert judgement as summarized in Table 5.1. The oscillating amplitude and frequency are designed to be perturbed with a standard deviation of 5 % around their nominal values. The number of nuclear data uncertainties is not counted since much larger number of nuclides are involved compared to zero-power reactors (see Chapter 5.3.3), resulting in huge number of uncertain parameters.

No.	Parameter	Distribution	Unit	Mean	Standard deviation[22] (Lower/Upper limit[23])
-	Nuclear data uncertainties[24]				
1	Oscillating amplitude	Normal	cm	Inherent oscillating curve in Figure 5.1	5 %
2	Oscillating frequency	Normal	Hz	1	0.05
3	Location of noise source	Uniform	Mesh	Ideal oscillating boundary	-1/+1[25]
4	Detecting location (x-axis)	Uniform	Mesh	Ideal detecting location	-1/+1
5	Detecting location (y-axis)	Uniform	Mesh	Ideal detecting location	-1/+1
6	Detecting location (z-axis)	Uniform	Mesh	Ideal detecting location	-1/+1

Table 5.1: The information of selected uncertain parameters

[22] This column shows the standard deviation in case of having normal distribution.

[23] This column shows the value of lower and upper limit in case of having uniform distribution.

[24] Nuclear data uncertainties are treated in a distinct manner (see Chapter 5.3.3) as they are propagated to seven parameters: five macroscopic cross-sections as well as two diffusion coefficients.

[25] -1/+1 correspond to -0.43/+0.43 cm.

The Swiss 3-loop pre-Konvoi reactor KKG has a total of 36 in-core detectors. They are installed in 6 different axial positions and each axial position consists of 6 detectors in different radial positions (see Figure 5.4 [106]). The 36 detecting locations are perturbed between -1 mesh and +1 mesh from the ideal locations, in the $x-$, $y-$ and $z-$ directions of the core.

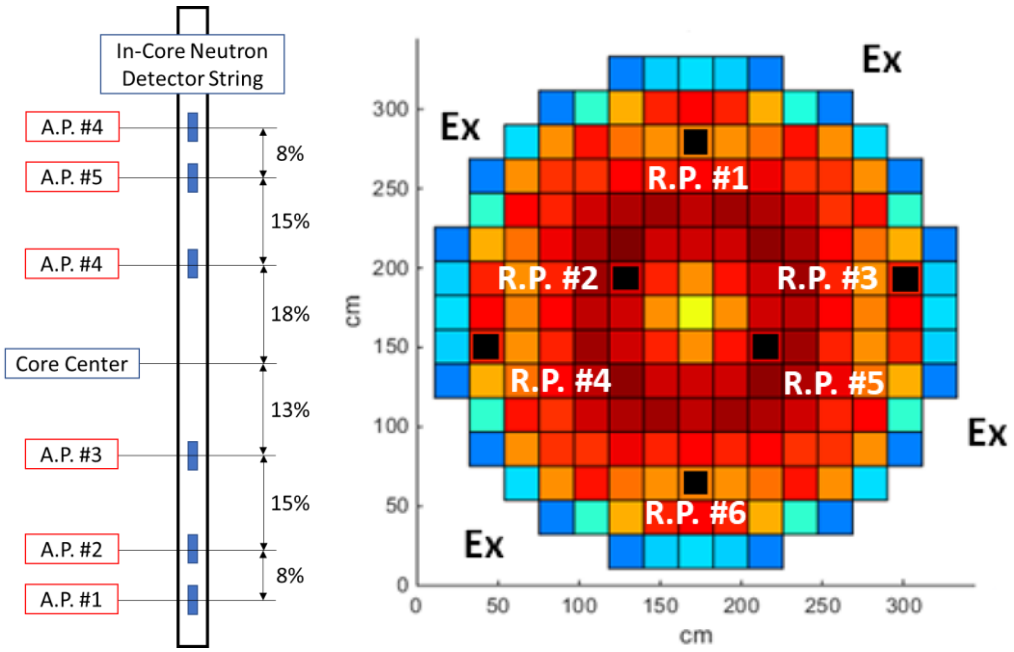

Figure 5.4: Locations of in-core detectors in axial and radial direction of the core. On the left: values in percent (%) indicate "% active fuel length"; "A.P." and "R.P." denote "axial position" and "radial position", respectively.

5.3.3 Generation of Random Samples

A total of 500 input sets are generated for the statistical uncertainty propagation using CORE SIM+. For the input parameters except nuclear data, random sets of perturbed input parameters are generated using the distribution information listed in Table 5.1 using SRS method.

The uncertainties of the nuclear data are propagated to the macroscopic nuclear parameters. This process requires an extra explanation since nuclear data involve

many correlated inputs. SAMPLER is a stochastic uncertainty quantification tool part of the SCALE package (as opposed to TSUNAMI which offers a perturbation theory approach) [107]. It allows the quantification of uncertainty due to uncertainties in:

1) Neutron cross-sections
2) Fission yield and decay data
3) Any user input parameter of a SCALE component.

This study only considers the neutron cross-section uncertainty. This is achieved by using the master sample file included in SCALE. This master file contains 1000 samples of perturbation factors for all energy groups and reactions in all materials. These factors have been pre-computed with the Medusa module of the XSUSA program using the 44-group covariance data provided by SCALE[26]. All SCALE models use thermal-hydraulic conditions representative of core-averaged conditions at Hot Full Power, namely a fuel temperature of 900 K and a moderator density of 707 kg/m^3.

	Fuel burnup effect	
Enrichment effect	5.06 % Enrichment @ 0MWd/t Burnup	5.06 % Enrichment @ 30MWd/t Burnup
	4.9 % Enrichment @ 0MWd/t Burnup	

Table 5.2: Test matrix

Since all the fuel assembly types from these two cycles differ only slightly in enrichment, two fuel assembly SCALE models are considered using the minimum and maximum enrichments (4.9 % and 5.06 %) found in cycles 39 and 40. No information is available regarding the burnup distribution for either cycle.

[26] The default 94 nuclides in the fuel are taken into account, while 2~8 reactions per nuclide and 44 energy groups per reaction are considered [5].

Therefore, the effect of burnup on the neutron cross-section uncertainty is treated by considering fresh fuel and fuel at 30 MWd/t. The test matrix presented in Table 5.2 gives a representation of which parameter combinations are studied.

In total 300 varied macroscopic cross-sections were generated using SAMPLER for each of the 3 cases presented above (see Appendix A.3). From those 300 samples of macroscopic cross-sections, relative variations from the reference version of the nuclear data libraries are computed and are applied to vary the macroscopic cross-sections for CORE SIM+. The standard deviation of ratios between the samples and the reference case is presented in Table 5.3. The standard deviations remain low (maximum < 0.3 %) for all group constants. The effect of the burnup on the standard deviation is larger than the effect of the enrichment.

	Diffusion Coefficient		**Absorption Xsec**		**nu-Fission Xsec**		**Removal Xsec**
	Fast	Thermal	Fast	Thermal	Fast	Thermal	
Case 1 5.06 % @0MWd/t	3.98E-04	9.10E-04	3.88E-03	7.25E-04	2.54E-03	1.37E-03	1.11E-03
Case 2 5.06 % @30MWd/t	4.32E-04	7.92E-04	3.75E-03	7.95E-04	2.08E-03	2.10E-03	1.37E-03
Case 3 4.9 % @0MWd/t	3.99E-04	9.07E-04	3.93E-03	7.20E-04	2.53E-03	1.36E-03	1.11E-03

Table 5.3: Propagation of nuclear data uncertainty to nuclear parameters for CORE SIM+ (standard deviation of ratios between 300 samples and nominal case)

5.4 Sensitivity Analysis

To confirm how the core condition affects the sensitivity of input parameters to the neutron noise, three conditions are selected from the viewpoint of fuel

loading pattern and fuel burn-up: to check the influence of loading pattern, EOC 39 and EOC 40 are selected, while BOC and EOC in cycle 40 are considered to confirm the fuel burn-up effect. For each core condition, the homogenized nuclear data at the corresponding condition are used as nominal (unperturbed condition) data.

5.4.1 Sensitivity Measure

As its applicability to the sensitivity analysis at a neutron noise condition in preceding works, the PCC is selected for sensitivity measure. The calculated coefficient is squared to represent the "sensitivity index".

5.4.2 Setting up the Standards in Analysis

5.4.2.1 Convergence of the Sensitivity Indices with the Number of Samples

A series of convergence tests are performed by varying the sample size. This test is necessary to find out an optimal sample size which strikes a balance between computational cost and reliability of the calculated sensitivity index. The tests are carried out with different sample sizes between 10 to 500, which are sampled randomly from 500 existing data sets, under the conditions of BOC 40. The sampling of equivalent sample size is repeated for 1000 times using bootstrapping with replacement [101]. For each sample size, the sensitivity indices are calculated for 1000 times between the input parameters and the amplitude of thermal neutron noise. Afterwards, the 2.5^{th} and 97.5^{th} percentile of the 1000 sensitivity indices are identified to build 95 % confidence interval. Figure 5.5 shows the converging trend of two representative sensitivity indices to the amplitude of the thermal neutron noise: "detecting location (y-axis)" which has relatively small index and "location of noise source" which has relatively large index at the detector location of A.P. #1 and R.P. #2.

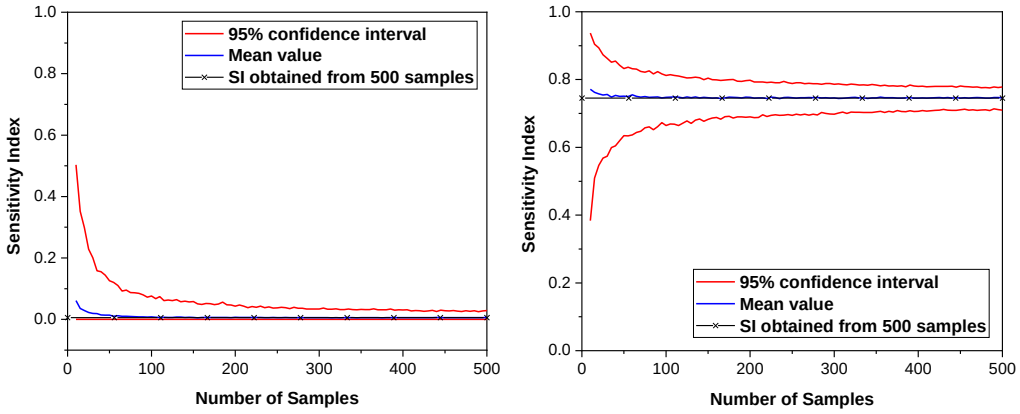

a. Detecting location (y-axis) b. Location of noise source

Figure 5.5: Convergence plots of sensitivity indices with 95 % confidence interval

The confidence interval decreases as the sample size increases. When the sample size is larger than 300, a difference between the calculated confidence interval (with a sample size larger than 300) and the final estimation with 500 samples becomes smaller than 0.15. Considering a small difference with the final estimation, further analyses with different core conditions will be carried out using a sample size of 300. According to the Z test, the critical value of the Pearson correlation coefficient can be obtained as 0.11 at a sample size of 300, with a significance level of 5 % (see Chapter 1.7.4.1).

5.4.2.2 Sensitivity Test on Nuclear Data Uncertainty

The reactor core consists of 177 fuel assemblies whose enrichments and burn-up conditions are different from each other. Therefore, to assure the accuracy of the analysis, the nuclear data uncertainties should be calculated by considering the characteristics of individual fuel assemblies. However, this realistic approach increases the computational cost and also complicates the modeling for the noise calculation. For this reason, a simplified approach is introduced by assuming that all fuel assemblies have identical nuclear data uncertainties which are generated for a specific enrichment and burn-up condition. To study the effect of this simplification, a series of sensitivity analyses are performed with varying the nuclear

data uncertainties calculated from three different core condition as introduced in Table 5.2.

For each case, nuclear data uncertainties are generated for the corresponding core conditions as explained in Chapter 5.3.3 and the obtained set of uncertainties is adopted to all fuel assemblies. The three cases of sensitivity analyses are carried out with the BOC 40 set as the nominal core condition. Therefore, the identical homogenized group constants from BOC 40 are used as nominal values for all three cases.

The main concern of the sensitivity analysis is to identify the major contributors to the noise behavior. Hence, the parameters having relatively large sensitivity indices are used for comparing the results from the three different cases. In this context, the two parameters having the largest sensitivity indices at the installed detector locations are compared between each other: (1) oscillating amplitude and location of noise source for the amplitude of neutron noise, (2) fast absorption cross-section and location of noise source for the phase of neutron noise. Figure 5.6 compares the sensitivity indices calculated for different neutron noise fluxes, which are obtained from the three different nuclear data uncertainties (corresponding to Cases 1, 2 and 3). Figure 5.6-a and -b show the sensitivity indices between the two aforementioned input parameters and the neutron noise (amplitude and phase) at the installed detector locations. Each comparison consists of 72 points: 36 in-core detectors $\times$ 2 input parameters. The $x-$axis represents the sensitivity indices calculated with the Case 1 condition, while the $y-$axes show the indices calculated with Case 2 and Case 3 conditions.

From the comparison, it is found that the three different nuclear data uncertainties obtained from three different fuel conditions do not cause significant differences in results, since there is no strong dispersion around the line $y = x$. This comparison shows that an exact reactor model (core condition, assumption of one-homogenized uncertainties for all FAs/different uncertainty for each FA) used to generate the nuclear data uncertainties does not affect the results in a significant manner. Accordingly, further analyses are carried out with a simplified modeling approach that assumes all the fuel assemblies having identical nuclear data uncertainties.

In the following analyses, the uncertainties from Case 1 are used at the BOC 40, while the uncertainties from Case 2 are used at the EOC 39 and 40. These combinations are made to perform the analysis at the specific core condition with the nuclear data uncertainties generated from the burn-up condition mostly similar to the given core condition within the available options in Table 5.2. Therefore, nuclear data uncertainties generated from "lower burn-up condition" are used at BOC, while the data generated with "higher burn-up condition" are used at EOC. However, as it is confirmed in Figure 5.6, using different nuclear data uncertainties will not bring any remarkable change in results.

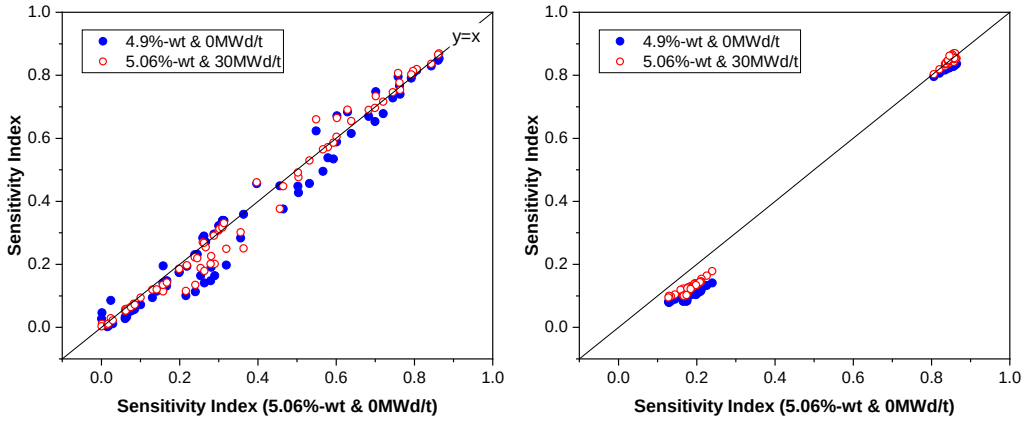

a. Amplitude of thermal neutron noise

b. Phase of thermal neutron noise

Figure 5.6: The comparison of sensitivity indices calculated with different nuclear data uncertainties which are obtained from various fuel condition

5.4.3 Sensitivity Analysis at Various Core Conditions

5.4.3.1 Analysis at BOC 40

Figure 5.7 shows the radial distribution of the thermal neutron noise in the core for the nominal condition without uncertainties.

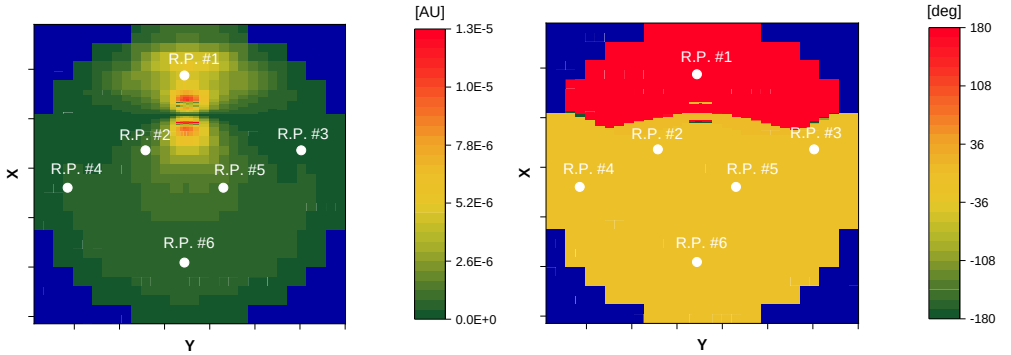

a. Amplitude b. Phase

Figure 5.7: Thermal neutron noise behavior at the axial position #3 in BOC 40

To get a better understanding on the noise behavior at the detector locations, correlation matrices for the amplitude and phase of the thermal neutron noise are calculated based on 300 data sets as shown in Figure 5.8 [33]. This correlation information helps to infer the noise behavior at the specific detector location by reading the signals from the correlated detectors. Additionally, it enables to perform the group-wise uncertainty analyses, which simplifies the interpretation process of the calculation results.

In case of the amplitude of thermal neutron noise, the detectors can be radially divided into three groups according to three different correlations: group 1 consists of the signal at the radial position #1, group 2 consists of the signals at the radial positions #2, #5 and #6, group 3 consists of the signals at the radial positions #3 and #4. Meanwhile, the phase data show simpler correlations than the amplitude data. The data at radial positions #2 to #6 have almost perfect positive linear correlations among each other and have perfect negative linear correlations with the value at radial position #1. The latter is explained by the out-of-phase behavior existing between the radial position #1 and all other radial positions, as shown in Figure 5.7-b.

Since correlations exist between the thermal neutron noise at the detector locations, the uncertainties of the noise (distribution range of the neutron noise) are also expected to show correlated responses at the detector locations.

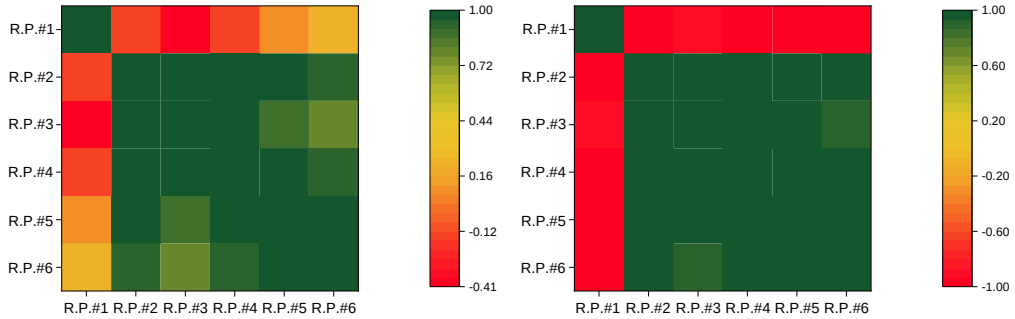

a. Axial position #1 (Amplitude)

b. Axial position #1 (Phase)

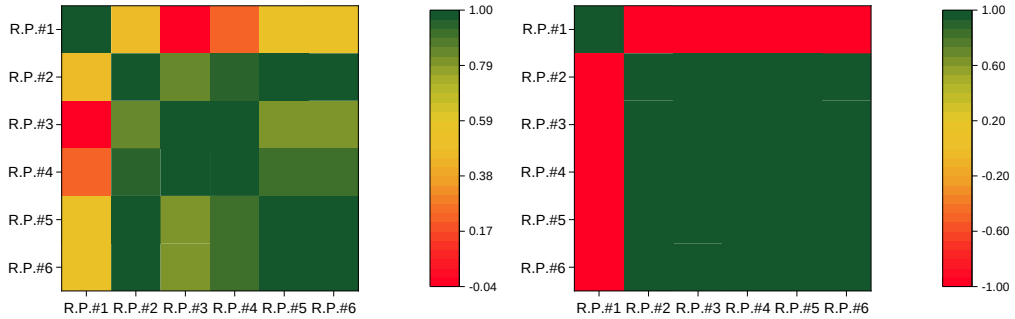

c. Axial position #3 (Amplitude)

d. Axial position #3 (Phase)

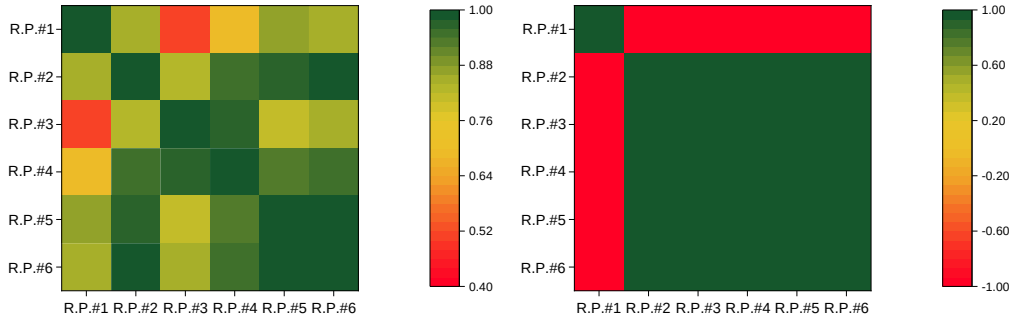

e. Axial position #6 (Amplitude)

f. Axial position #6 (Phase)

Figure 5.8: Correlated behavior between the amplitude and the phase of the thermal neutron noise at the detector locations [33]

That is, when the signals from two detectors are correlated, their uncertainties respond in the same direction, either increase or decrease, as the input parameters are perturbed. As a result, the correlated detector signals are expected to have similar sensitivities to the input parameters, which will be investigated in the following sections.

Simplified approach with grouped parameters

A groupwise sensitivity analysis is conducted to investigate the relative effects of the different groups of parameters. The entire 13 input parameters listed in Table 5.1 are grouped into three groups according to the similarities they have in between: (1) group of nuclear data, (2) group of noise source data, (3) group of detecting location. The group of detector locations includes the perturbation of the location in the $\mathrm{x}-$, $\mathrm{y}-$ and $\mathrm{z}-$ directions. The group of noise source data includes the oscillating amplitude, the oscillating frequency, and the location of the noise source. The uncertainties of thermal neutron noise obtained for the three different groups are compared in Figure 5.9. The neutron noise is calculated with the perturbation of parameters belonging to a given group, while the remaining input parameters are fixed at their nominal values. The neutron noise uncertainties are obtained following 1st order Wilks' formula for two-sided limits, for which the required number of code runs corresponds to 93. The corresponding results are represented as follows.

The graph showing the results for the detector locations consists of 6 blocks along the $x-$ axis (as Figure 5.10), where each block corresponds to each axial position shown in Figure 5.4. Each block contains the values from the 6 radial detectors located in this axial position and the corresponding radial position is represented with ascending order, from position #1 (very left value in the block) to #6 (very right value in the block).

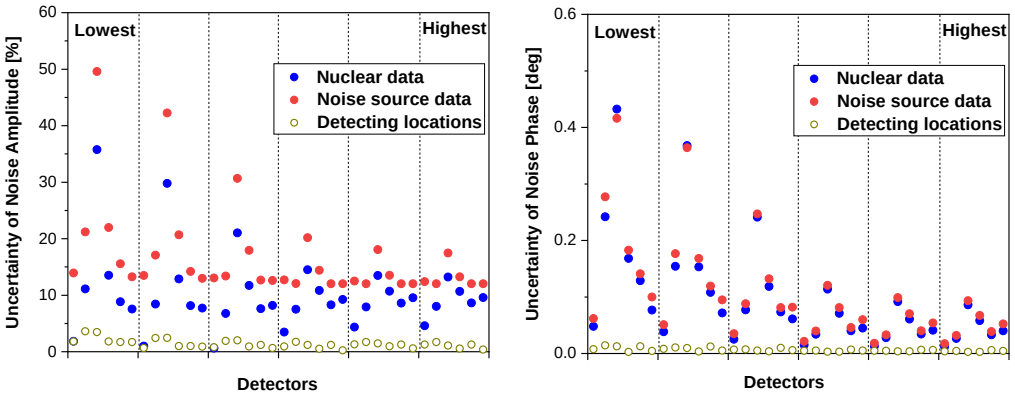

a. Amplitude of thermal neutron noise

b. Phase of thermal neutron noise

Figure 5.9: Comparison of neutron noise uncertainties obtained from the different groups of input parameters

For both the amplitude and phase of the neutron noise, the uncertainties propagated from the group of noise source data show the largest value in all detector locations, while they are followed by the uncertainties from the group of nuclear data. The uncertainties by group of nuclear data become larger at radial position #3 at low axial positions, still, they are not remarkably different from the uncertainties from the group of noise source data.

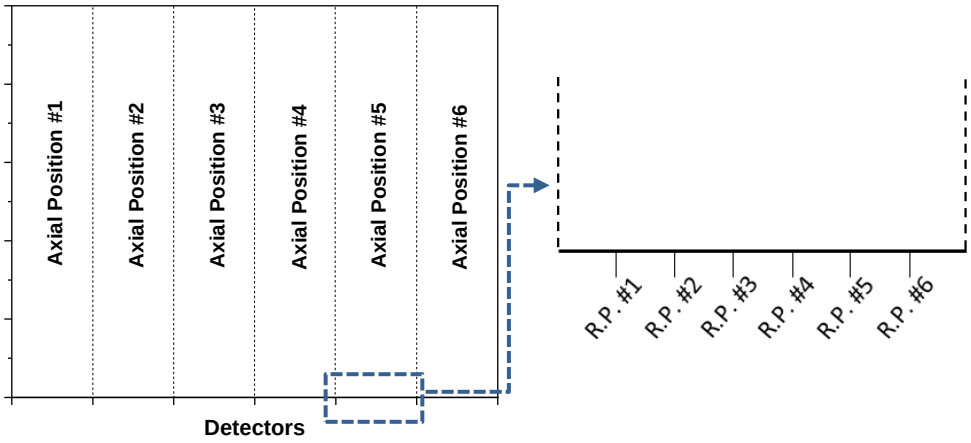

Figure 5.10: The composition of the graph with respect to the detector information ("R.P." denotes "Radial position")

Accordingly, the obtained results can be simply interpreted as the neutron noise being mainly driven by the group of noise source data.

Approach with Quantitative Measure

Based on the results obtained from the simplified approach, an additional analysis with quantitative measure is carried out. Here, the parameter which contributes to the neutron noise the most within the group of noise source data is quantitatively identified. This can be done by calculating the sensitivity indices for each input parameter. The calculated sensitivity indices between the three noise source parameters and the neutron noise are summarized in Figure 5.11 with 95 % confidence intervals.

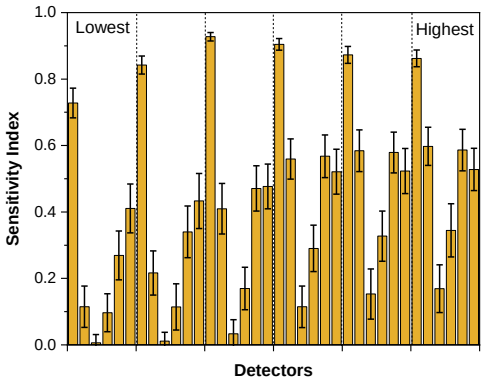

a. Oscillating amplitude (amplitude)

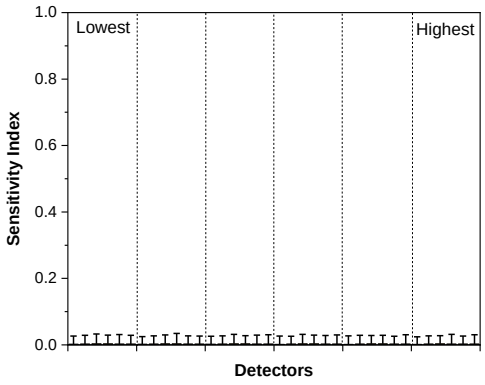

b. Oscillating amplitude (phase)

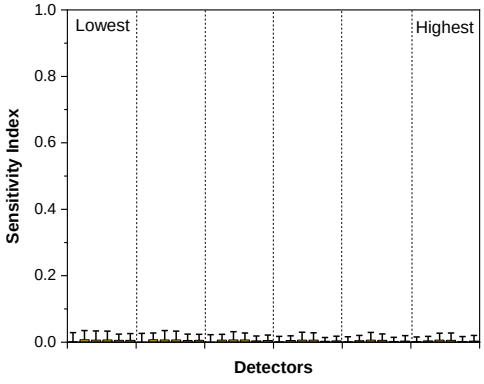

c. Oscillating frequency (amplitude)

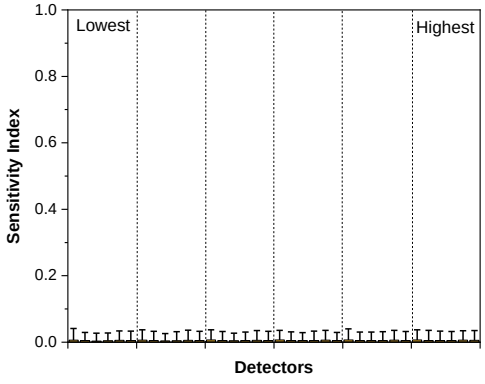

d. Oscillating frequency (phase)

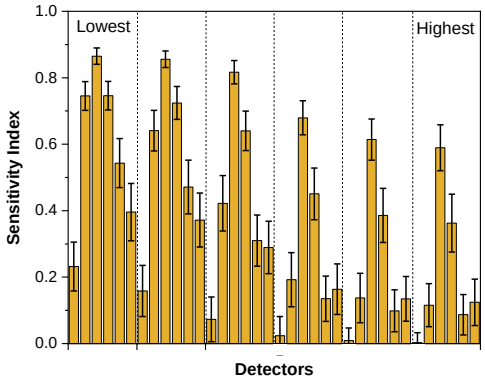

e. Location of noise source (amplitude)

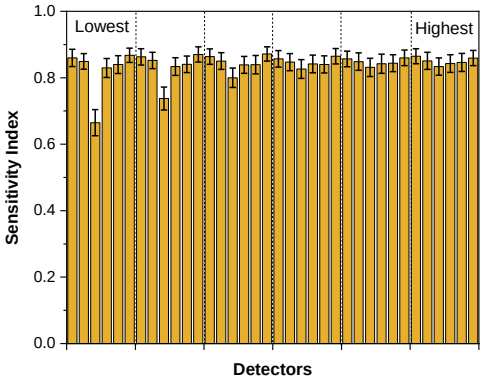

f. Location of noise source (phase)

Figure 5.11: The sensitivity indices and the 95 % confidence intervals between noise source data and thermal neutron noise at different detector locations at BOC 40

The main findings can be explained in connection with the correlation among the detector locations shown in Figure 5.8. For the neutron noise amplitude, the oscillating amplitude dominates in all axial positions at radial position #1, while the location of the noise source is always dominating at radial positions #3 and #4. However, at radial positions #2, #5 and #6, the location of noise source dominates at the lowest position and becomes weaker at higher axial positions. The decreasing effect is caught up by the increased effect of the oscillating amplitude and at higher axial locations, eventually, the oscillating amplitude becomes the main contributor.

The phase data at all detector locations are strongly dependent on the location of noise source, which supports the correlation information shown in Figure 5.8.

5.4.3.2 Analysis at EOC 40

The sensitivity analysis with an identical procedure as the one adopted in previous chapter is repeated at the core conditions of EOC 40. The different core conditions are reflected in the different values of the two-group nuclear data of the core, resulting in different noise behavior as shown in Figure 5.12. The

considered event (one FA oscillation) in this study brings about a larger amplitude of neutron noise at the core condition of EOC 40 than at BOC 40 (see Figure 5.7).

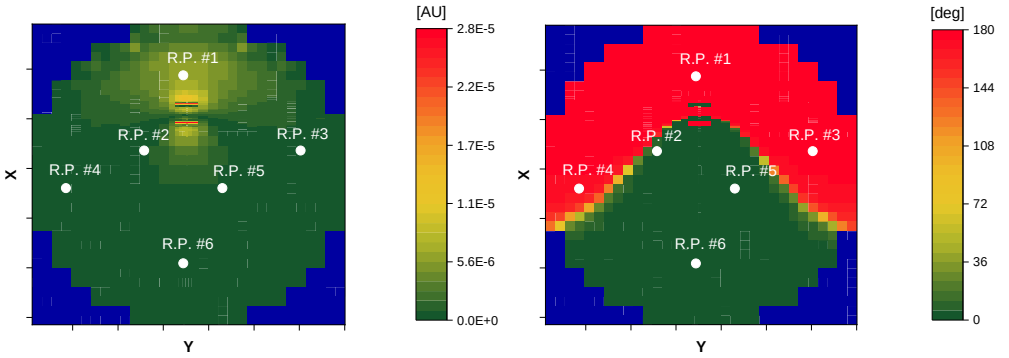

a. Amplitude b. Phase

Figure 5.12: Thermal neutron noise behavior at the axial position #3 in EOC 40

Problematic point in analysis

As shown in Figure 5.7-b and Figure 5.12-b, CORE SIM+ predicts an "out-of-phase" behavior between two core regions because of a vibrating fuel assembly. The boundary of these two regions is determined by the location of the noise source, which is one of the input parameters considered in this study. However, the boundary reacts sensitively to the uncertainty of the noise source location, although this uncertainty corresponds to only ± 4.3 mm. The modification of the boundary can change the phase region that the detector actually sees, therefore, it can affect the phase signal measured by the core detectors. Figure 5.13 and Figure 5.14 show the variation of the boundary according to the perturbation of the noise source location at two axial positions of the detector installations. At the bottom position, radial positions #2, #4 and #5 can belong to two different phase regions depending on the location of noise source, while only radial position #4 changes regions when located at higher axial positions.

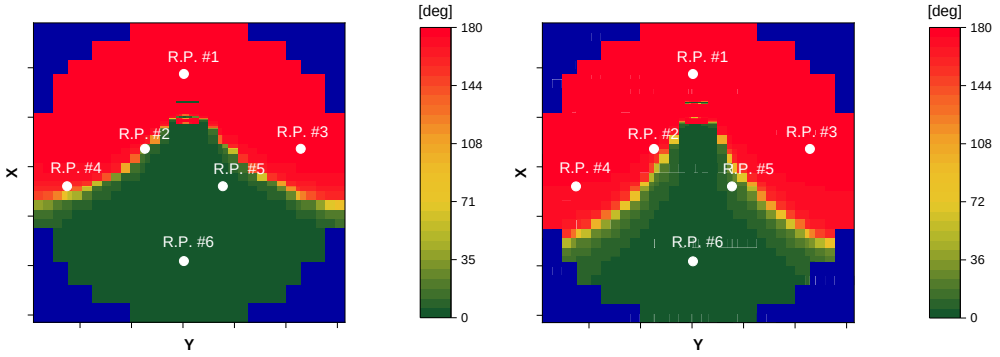

a. 1 mesh toward core periphery

b. Ideal position

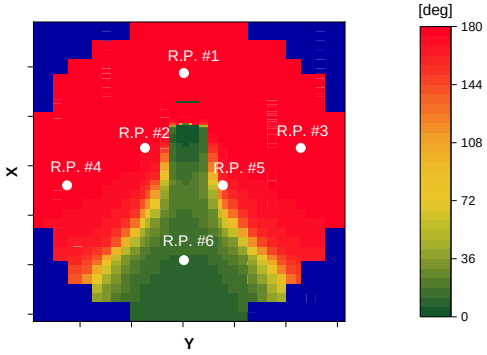

c. 1 mesh toward core center

Figure 5.13: The phase of thermal neutron noise depending on the location of noise source at EOC 40 (at the bottom position of the detector installation)

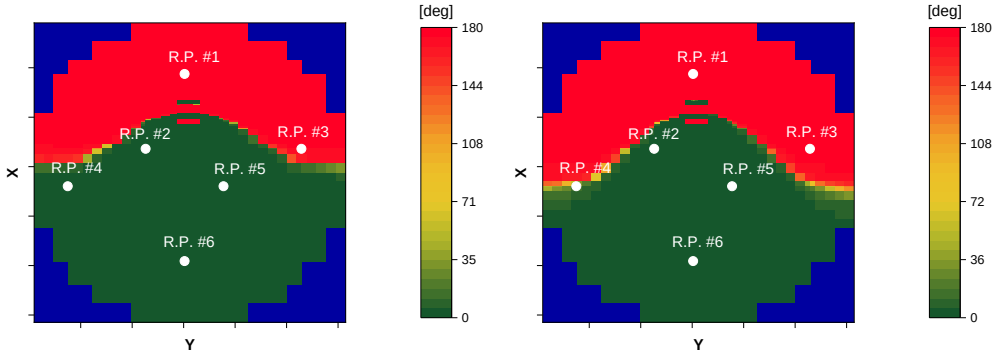

a. 1 mesh toward core periphery

b. Ideal position

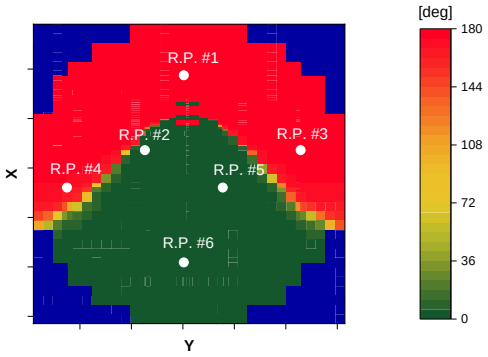

c. 1 mesh toward core center

Figure 5.14: The phase of thermal neutron noise depending on the location of noise source at EOC 40 (at the mid-height position of the detector installation)

Consequently, when the location of noise source is perturbed 300 times within its uncertainty range, the obtained 300 noise solutions at these problematic detectors' locations show a discontinued distribution as shown in Figure 5.15. The histogram of amplitude data confirms that if a certain location may belong to two different phase regions depending on the change of the oscillating boundary, the amplitude also encounters a similar issue, which results in a discontinuity of the calculated data.

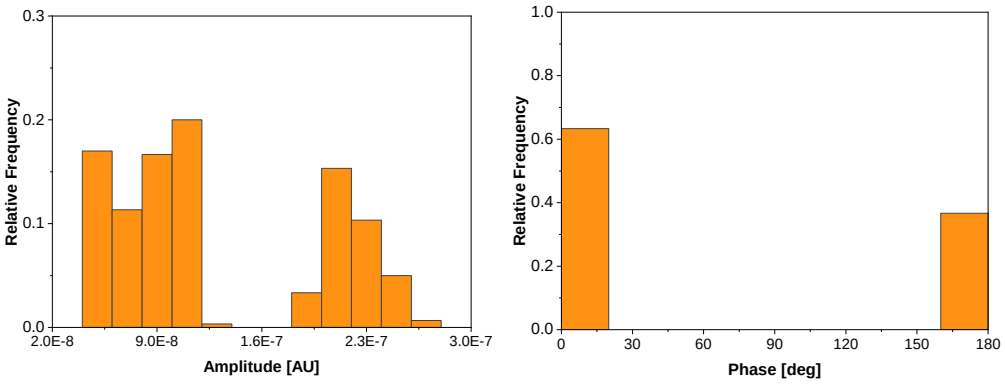

a. Amplitude b. Phase

Figure 5.15: Histogram of 300 thermal neutron noise at the location of Detector 4 (at the mid-height position of the detector installation)

The discontinuity existing among the calculated output data makes it impossible to adopt the regression-based approach for the further sensitivity analysis, since this approach is only valid on the premise that there is a linear relationship between the inputs and the outputs. Accordingly, the following sensitivity analysis is carried out only for the detectors which are not having this property (i.e., radial positions #1, #3 and #6).

Approach with Quantitative Measure

For the sake of conciseness, only the results of the noise source data are dealt with hereafter and discussed. The sensitivity indices are calculated and compared to those at BOC 40 in Figure 5.16 and Figure 5.17, in order to understand the findings in connection with an effect of "fuel burnup". The comparison is made only at the radial locations where the relevant sensitivity indices at EOC 40 are available, namely R.P. #1, #3 and #6.

First of all, the noise signals at the detector locations which are excluded here (radial positions #2, #4 and #5) are more sensitive to the location of the noise source than any other input parameters. That is, despite not carrying out further statistical analysis with the data at the radial positions #2, #4, and #5, the main contributing parameter at these locations can be determined as being the location of noise source.

In Figure 5.16, the oscillating amplitude becomes less influential at EOC, while the effect from the location of the noise source is increased in most detector locations.

Meanwhile, there is no remarkable change in the phase (Figure 5.17), and the location of the noise source still maintains its dominant effect. A possible reason why the influence from the location of the noise source at EOC has been increased will be discussed in Chapter 5.4.4.

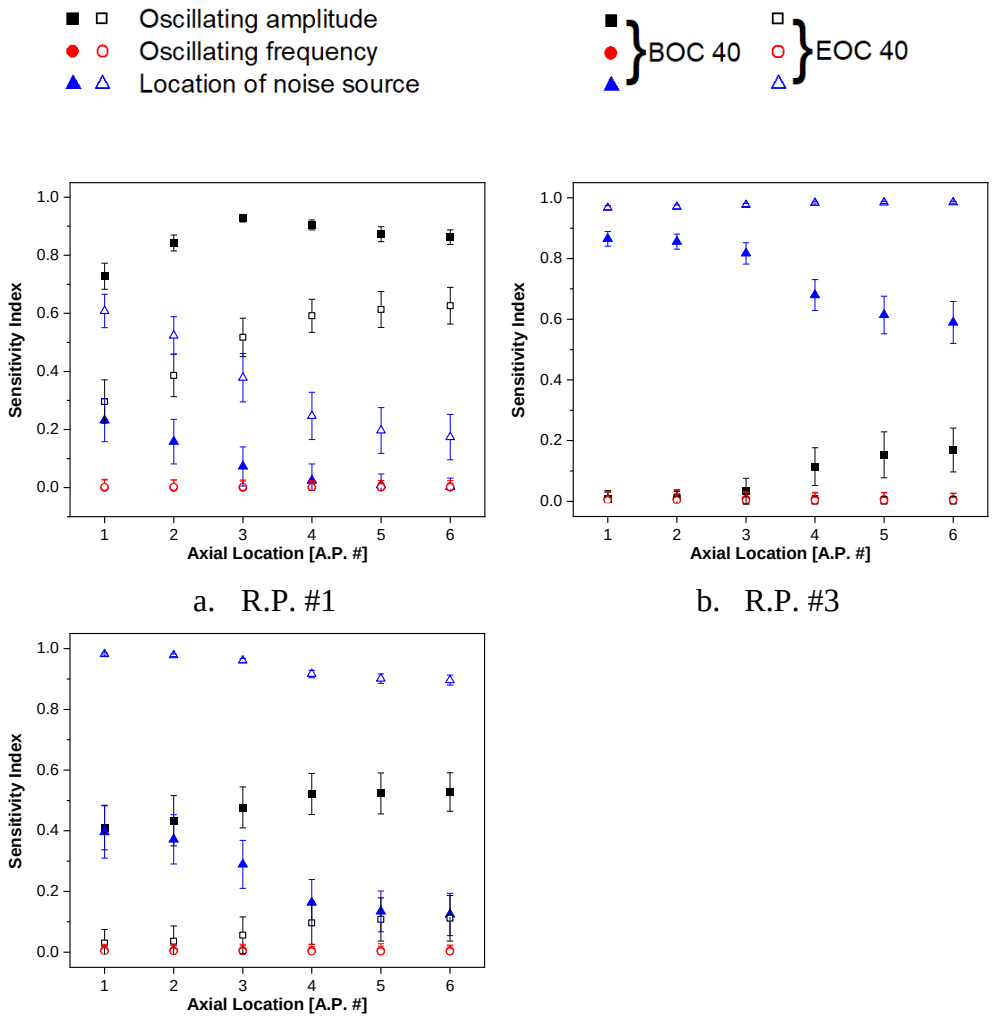

a. R.P. #1

b. R.P. #3

c. R.P. #6

Figure 5.16: Comparison of sensitivity indices and the 95 % confidence intervals at different radial and axial locations between BOC 40 and EOC 40 (amplitude)

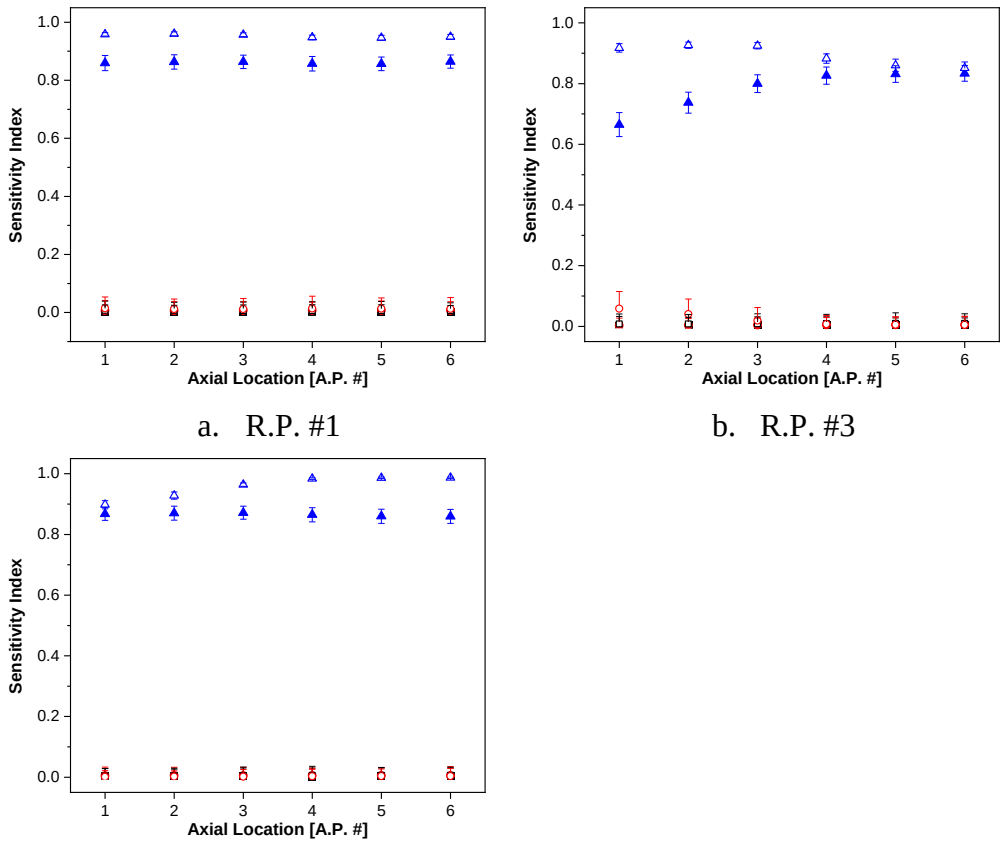

a. R.P. #1

b. R.P. #3

c. R.P. #6

Figure 5.17: Comparison of sensitivity indices and the 95 % confidence intervals at different radial and axial locations between BOC 40 and EOC 40 (phase)

5.4.3.3 Analysis at EOC 39

Figure 5.18 shows the distribution of the thermal neutron noise in the radial core direction under unperturbed conditions.

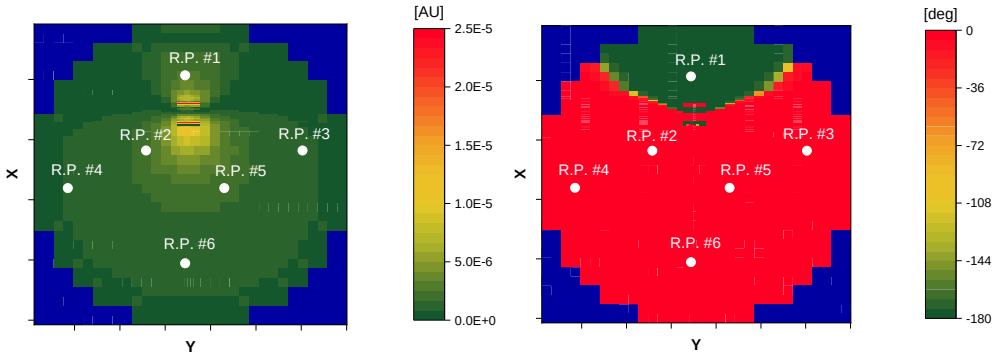

a. Amplitude b. Phase

Figure 5.18: Thermal neutron noise behavior at the axial position #3 in EOC 39

Problematic point in analysis

The same issue as reported at EOC 40 is also found at EOC 39 with a different pattern as shown in Figure 5.19. The problematic point is found at the radial position #1 between the mid-height and the top of the core. Therefore, the following sensitivity analysis is carried out for all detectors except for those at radial position #1.

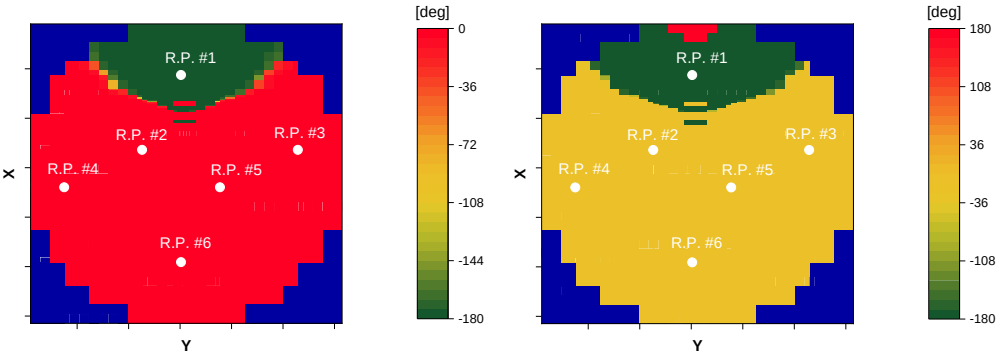

a. 1 mesh toward core periphery b. Ideal position

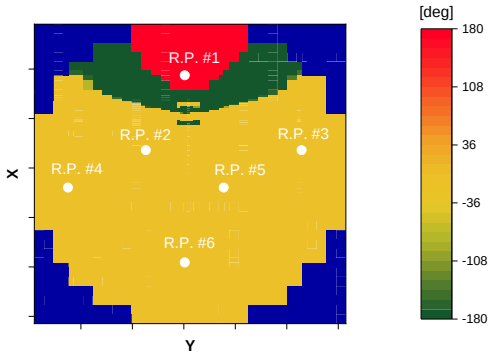

c. 1 mesh toward core center

Figure 5.19: The phase of thermal neutron noise depending on a location of noise source at EOC 39 (at the mid-height position of the detector installation)

Approach with Quantitative Measure

To study the effect of fuel loading pattern, the sensitivity indices obtained for the case of EOC 39 are compared with those for EOC 40. Only the radial locations with relevant sensitivity indices are taken, i.e., R.P. #3 and #6. The results at each axial point are shown in Figure 5.20 and Figure 5.21.

Contrary to the results between different fuel burnup conditions (see Figure 5.16), only monotonous changes are found in Figure 5.20. The oscillating amplitude at EOC 39 affects the amplitude of the noise in a significant manner, nonetheless, the location of noise source maintains its dominant effect at both core conditions. In the case of the phase (see Figure 5.21), the oscillating frequency shows a visible influence at EOC 39, which decreases as the detecting position gets higher axially. However, the phase of neutron noise is mainly driven by the location of noise source at both EOC 39 and EOC 40. The following section discusses why the location of noise source remains as a main contributor to the neutron noise at EOC.

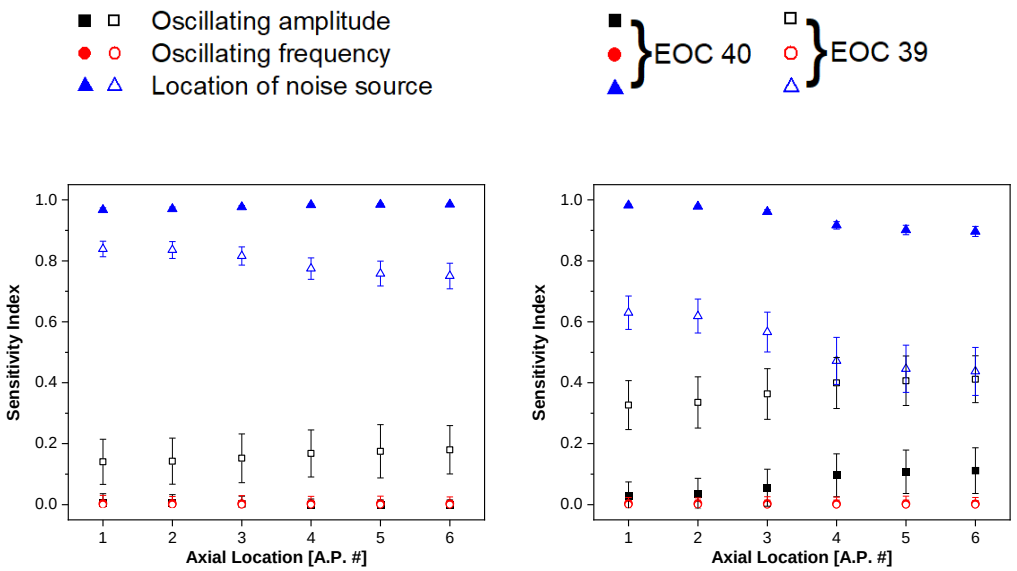

a. R.P. #3 b. R.P. #6

Figure 5.20: Comparison of sensitivity indices and the 95 % confidence intervals at different radial and axial locations between EOC 39 and EOC 40 (amplitude)

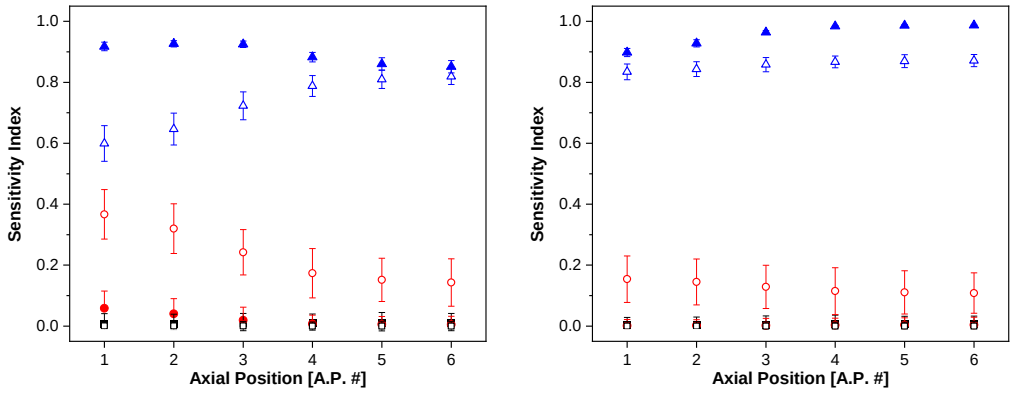

a. R.P. #3 b. R.P. #6

Figure 5.21: Comparison of sensitivity indices and the 95 % confidence intervals at different radial and axial locations between EOC 39 and EOC 40 (phase)

5.4.4 Comparison between Different Cycles and Reasons for Differences

A reason why the location of noise source at EOC has an increased influence on the neutron noise than at BOC can be investigated in relation to the spatial distribution of the static flux. Both the static fast and the static thermal neutron fluxes affect the neutron noise in combination with the noise source. Depending on the position of the noise source, the static flux can provide a different weight because of its spatial distribution. Accordingly, the gradient of the static flux is investigated within the uncertainty range of "location of noise source" in order to compare the "weighting factors" between two different core conditions: BOC and EOC. Figure 5.22-a shows the perturbation of the oscillating boundary in two-dimensional meshes. "0 mesh" indicates the ideal location of the oscillating boundary without uncertainty perturbation, while "-1 mesh" and "+1 mesh" denote the relocation of the oscillating boundary by -1 (to the core periphery) mesh and +1 (to the core center) mesh, respectively. The ratios of static flux gradients between the adjacent two meshes (between -1 mesh and 0 mesh, and between 0 mesh and +1 mesh) are compared in Figure 5.22-b (BOC 40 and EOC 40) and Figure 5.22-c (BOC 40 and EOC 39).

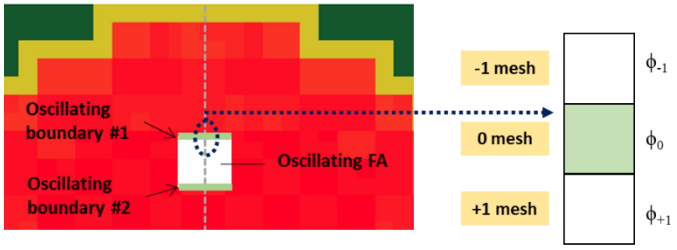

a. Two oscillating boundaries perturbing between -1 and +1 meshes

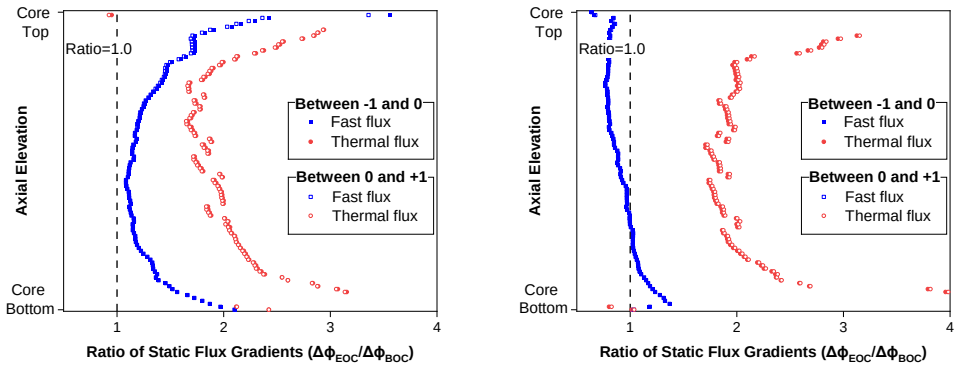

b. Static flux gradients ratio between BOC 40 and EOC 40 (at oscillating boundary #1 (left) and #2 (right))

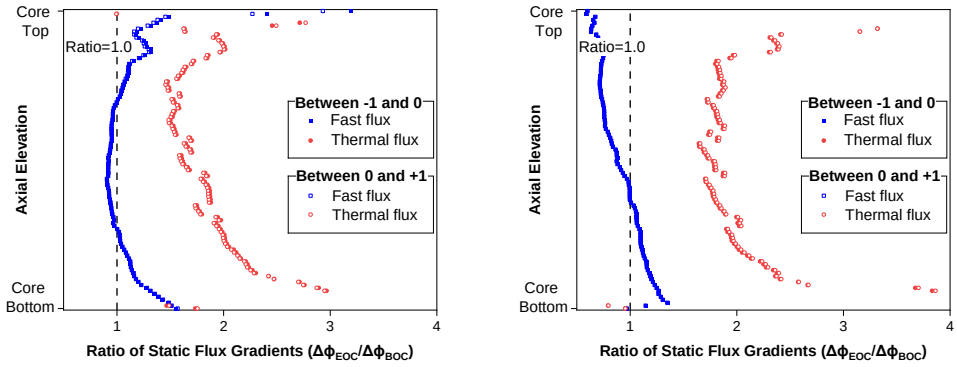

c. Static flux gradients ratio between BOC 40 and EOC 39 (at oscillating boundary #1 (left) and #2 (right))

Figure 5.22: Comparison of ratios of static flux gradients

A value larger than 1.0 signifies that the static flux gradient at EOC (cycle 40 and 39 in Figure 5.22-b and -c, respectively) is larger than that at BOC. In most axial locations, both fast and thermal static fluxes at EOC have steeper gradients around the oscillating boundaries than at BOC 40. Consequently, the noise source at the oscillating boundaries at EOC is weighted more than at BOC 40 when the assigned location is perturbed, which justifies the increased influence of “location of noise source” on the neutron noise.

Chapter 6

Conclusion

In this PhD work, a comprehensive uncertainty analysis methodology has been established for the modeling of neutron flux oscillations induced by various noise sources at zero-power reactors, and its applicability to an analysis at power plant has been demonstrated. The methodology includes uncertainty propagation and sensitivity analysis. The works described in this thesis have been conducted under the framework of the European Horizon 2020 CORTEX project which was launched in 2017 for 48 months duration. Accordingly, the reactors operated or licensed by the collaborators participating CORTEX project (i.e., CROCUS at EPFL, AKR-2 at TUD and Swiss 3-loop Konvoi reactor) are dealt with in this work. In the same context, the identical experimental conditions that are covered within the experimental programs at aforementioned reactors are considered as target condition for the analyses.

This last chapter consists of summary of each chapter, confirmed problematic points which remain as future works, and the final remarks.

6.1 Chapterwise Summary

Chapter 1 has an introductory character, which contains all fundamental information needed to launch further research. First, the objectives and the novelty of present work were introduced in connection with a CORTEX project. It is followed by a research outline, which is a preview of the thesis. The rest of the given

chapter consists of four introductions: 1) the reactors that are considered within this thesis with their ongoing/planned experimental programs. 2) the considered neutron noise types in accordance with their numerical modeling and relevant experimental condition at each reactor. 3) the general information of uncertainty analyses, this involves objectives and definitions of UP as well as SA. Additionally, available UP and SA methods are listed with their pros and cons. 4) the software and tools which are used in this study. This includes a main information of each tool and the specific features used in current analyses.

In Chapter 2, a fundamental methodology of uncertainty analyses was formed with considering one hypothetical event. This section intended to establish a basic structure, which can be used as a basis for the further analyses. A basic flow chart that provides stepwise instruction has been made. Based on a neutron noise balance equation implemented in CORE SIM, uncertain parameters which are worth to consider are listed with their distribution information. The modeling of reactor core (CROCUS reactor) for noise simulation with CORE SIM was introduced while an approximation in core modeling was applied for the sake of conciseness. Due to a nature of Monte Carlo code (Serpent), the obtained group constants have distributions, accordingly, a discussion on their uncertainty treatment for its further consideration in CORE SIM computation is made. The introduction about a preparation for both UP and SA is followed by the detailed explanation of each analysis. This part involves a series of comparisons of various methodologies to investigate the optimum options for the current study. In uncertainty propagation, GRS methodology using Wilks' formula and brute force Monte Carlo method were selected for further comparison. It was confirmed that GRS method using higher order Wilks' formula or brute force Monte Carlo method can make statistically better estimation of the actual 5 %–95 % quantiles of the output's probability distribution, namely, diminish the conservatism. The following sensitivity analysis compared correlation-based approach with variance-based approach, with respect to "ease of use" and "precision of outcome". The variance-based approach often demands large sample size and relies on a use of surrogate modeling, which makes it less attractive despite of its high precision. Thus, the comparison was mainly to confirm whether the correlation-based approach can be an appropriate substitute for variance-based approach in identifying the most influencing parameter in this given neutron noise condition. The

sensitivity indices obtained from two approaches showed good agreement in terms of predicting influential parameters, therefore, a use of correlation-based approach in current analysis has been justified.

Chapter 3 improved and concretized the works which were carried out in previous section, by conducting the analyses with ongoing experimental program (COLIBRI experiment) at CROCUS reactor. This section involved nuclear data uncertainties and their treatment, which aimed to enhance an accuracy of the entire analyses. In addition to this, the output data at the location of installed detectors were mainly treated for the sake of usability of the results against experimental data. According to the agreement made within CORTEX project, a QoI has been designated for the validation of noise simulators and used as output parameter in this work. The uncertainties of QoI were calculated using 4^{th} order Wilks' formula for two-sided limits based on $95\,\%/95\,\%$ criterion and were compared to the experimental uncertainties, as an example of code validation. The correlation matrix among the QoIs at the detector locations was made to confirm correlated pair of detectors in neutron noise behavior (amplitude and phase). As a result, the detectors are grouped into two separated groups by their relative distances from the oscillating fuel rods. The distribution information of neutron noise was collected to investigate the linearity of the current calculation scheme, by means of Shapiro-Wilks approach. Accordingly, a linearity and non-linearity were detected in calculation process of absolute noise and QoI, respectively. The sensitivity analysis was begun with a justification of using correlation-based approach for the given condition as an extension of previous validation in Chapter 2. This was done by a comparison between the sensitivity indices calculated from Spearman correlation coefficient and Jansen's formula. The surrogate model (PC-Kriging) was first validated for its predicting accuracy, and the sensitivity indices having relatively large values (> 0.05) were only considered for a comparison between correlation-based and variance-based approaches. The corresponding results proved that correlation-based approach has a competitive edge over variance-based approach in terms of identifying relatively influencing parameters to the output behavior, with low computational cost. The following sensitivity analyses were carried out with two different approaches, namely, qualitative and quantitative approaches. The entire input parameters were grouped into three independent groups for a convenience of input data treatment,

especially the data being correlated. The qualitative approach ranked the groups of parameters by comparing the neutron noise uncertainties propagated from the simultaneous perturbation of parameters belonging to a same group. It was confirmed that "the group of design and operating parameters" had negligible effect, thus, this group was excluded in the following quantitative analysis. The multiple correlation coefficient was selected for a further groupwise analysis, in order to take a correlation among the parameters into the consideration. It was followed by a justification of a use of Pearson correlation coefficient as a sensitivity measure when the QoI, an outcome of non-linear process, was considered as output data for the sensitivity analysis. It was confirmed that the QoIs at the installed detector locations could be divided by identical two groups, which was confirmed in correlation matrix, depending on their dependency on specific group of input parameters.

In Chapter 4, uncertainty analyses were carried out with an identical methodology used in Chapter 3 at different condition. Another zero-power reactor, AKR-2, was considered when the neutron noise was induced by rotating absorber and vibrating absorber according to the experimental campaigns at the reactor. Different from the COLIBRI experiment at CROCUS reactor, the conditions of experiments at AKR-2 have been modified remarkably through the two experimental campaigns carried out in the context of CORTEX project. Thus, the analyses were repeated twice to cover both experimental campaigns. The nuclear data and noise source data (which are related to the description of the noise source) were considered as input parameters. A complexity of AKR-2 core modeling with CORE SIM+ increased a computational cost, therefore, the smallest sample size (93) which meets the percentile/confidence level criterion of 95 %/95 % for Wilks' formula two-sided limits was considered. Due to the small sample size, the computational scheme using multiple correlation coefficient was excluded, but the sensitivity analysis was carried out with qualitative approach and partial quantitative approach–only with the parameters belonging to a group of noise source data. Throughout the analyses, the uncertainties of QoIs were obtained and the most influential parameters to the QoIs were identified in connection with correlation information among the neutron noises at the installed detector locations.

In Chapter 5, a series of sensitivity analyses were conducted at Swiss pre-Konvoi reactor at a level of preliminary research. This work was aimed to confirm that the pre-developed methodology at small-sized zero-power reactors is applicable to a case in the power plant. An imaginary event that neutron noise is induced by one fuel assembly oscillation was considered at various core conditions (with respect to fuel loading pattern and fuel enrichment). From the analysis using qualitative approach at BOC 40, it was confirmed that the neutron noise was mainly driven by the noise source parameters, that is, oscillating amplitude, oscillating frequency and location of noise source. The following quantitative analysis focused on calculating sensitivity index of these three parameters, this strategy with considering only three parameters is also applied to the analyses at the rest core conditions (EOC 39 and 40). According to the results, the location of noise source increased its contribution to neutron noise remarkably when the fuel burnup was developed, while a modification of fuel loading pattern did not lead to any remarkable change in results. A difference in static flux gradient within the uncertainty range of "location of noise source" was considered as a main reason for the confirmed "fuel burnup" effect, owing to its contribution to the magnitude of noise source as a "weighting factor". Consequently, the methodology structured at zero-power reactors was reasonably well adopted to an analysis at power plant, and a probable future task was suggested based on a detected limitation in current study.

6.2 Future Work

Due to a limited duration of PhD work, a few points remain as "not fully explained" and have to be left behind as future tasks.

In Chapter 3.5.3.2, the groupwise analysis by calculating multiple correlation coefficient was recommended in sensitivity analysis, since a large number of "correlated" parameters are involved. However, because of relatively expensive computational cost taken at group constant generation with Serpent, the total number of sample size which can be generated within a certain time has been limited. The number of samples was not large enough to build a faithful VCM, resulting in a decreased reliability of obtained sensitivity indices. As the

following test in Chapter 3.5.3.2 suggested, increased sample size can predict precise VCM within grouped parameters and enables to make reliable quantitative analysis. The sample size can be increased either by direct increase of a number of code execution with high performance computing or by prediction with machine learning techniques. However, in case of using machine learning, a precision of considered surrogate model should be further discussed.

Another future work is related to a “phase shift” when a fuel assembly vibrates at power plant, which was described in Chapter 5.4.3. By nature, out-of-phase behavior between two core regions around a vibrating fuel assembly was predicted by CORE SIM+. The location of vibrating fuel assembly determined a boundary between two core regions, and its perturbation resulted in a perturbation of boundary with affecting the phase signals at the installed detector locations. This discontinuity within the obtained output data (neutron noise) hindered a further analysis, especially with a selected sensitivity measure in this study. Thus, it is recommended to understand the details of confirmed phenomena and to look for feasible improvements in analyses. First, carrying out a series of experiments can be helpful to verify the confirmed phenomena, by demonstrating that a phase boundary is indeed strongly affected by a perturbation of “location of exact noise source” (other parameters should remain as identical during the process). When the experiments present the identical pattern as it is confirmed from simulation, it can be used as additional evidence that the location of noise source becomes the most influencing parameter at the area near the phase boundary. Additionally, it can be suggested to adopt a reliable uncertainty of “location of vibrating fuel assembly” to the simulation, since the neutron noise is confirmed as reacting sensitively to this parameter. Thus, a design uncertainty of fuel rods’ initial location (along the vibrating direction) can be investigated through the random measurements of installed fuel rods at a stage of experiment preparation. Applying this reliable uncertainty to a simulation is expected to enhance the accuracy of simulated neutron noise behavior at all installed detector locations, consequently, the accuracy of obtained sensitivity index.

The last suggestion on future work is a realistic involvement of reactor design parameters into the simulations. Rather than to the zero-power reactors, this is more relevant to the nuclear power plants where the reactor parameters, such as,

fuel/coolant temperature and fuel compositions, are changing dynamically during the operation. By using other types of noise simulator which can model the feedback effects and varying spatial power distributions in a core (i.e., radial and axial peaking factor), the effect of reactor design parameters to the neutron noise can be reflected properly. However, this task requires a proper simulator and appropriate data post-processing. For example, when using time domain code, a signal processing with applying Fourier transform to output data (neutron flux) is necessary to focus on the noise behavior. Additionally, in case that the noise simulator does not implement linear approximation as CORE SIM does, a use of correlation/regression coefficient as a sensitivity measure does not valid anymore, accordingly, a proper measure should be investigated (e.g., variance-based coefficient).

6.3 Concluding Remarks

This PhD study focused on building a comprehensive methodology for uncertainty analyses in neutron flux oscillating condition. The novelty of this thesis can be pointed out with the fact that most researches on uncertainty analyses for the nuclear reactor physics applications have been focusing on criticality, burnup calculation and safety-related reactor transient so far. Namely, the trial is still new and encourages further related studies by emphasizing the importance of the outcome. As it is suggested in a previous section, there still exist the points which need to be explained and improved. In addition to this, each step of the process can be optimized by considering more types of noise sources and reactors, which can enhance a flexibility that the current methodology has.

Appendix A

Distribution of Two-group Constants

This chapter summarizes distribution information of two-group constants obtained from the perturbed nuclear data at three different reactors considered in this PhD work.

A.1 CROCUS Reactor

Figure A.1~Figure A.7 are the histograms of two-groups constants based on 300 samples, which are considered in uncertainty analysis at CROCUS reactor [93].

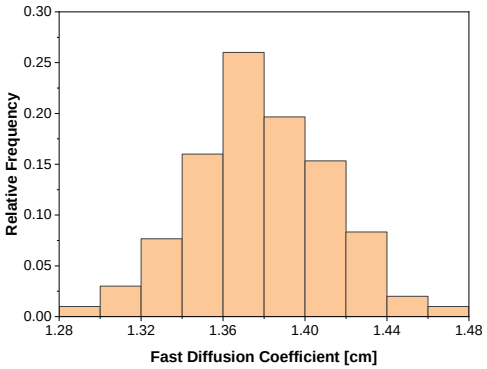

a. UO_2 region under the water level

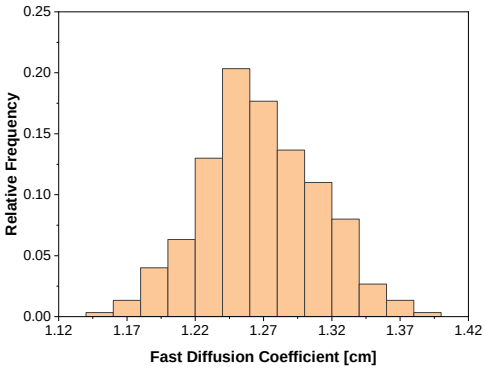

b. U_{metal} region under the water level

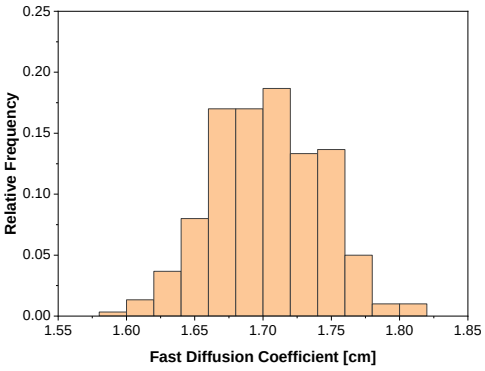

c. Control rods region under the water level

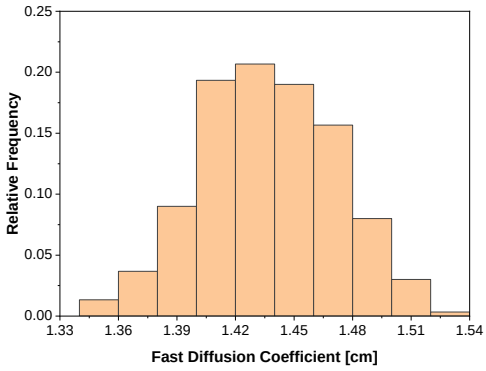

d. Reflector region under the water level

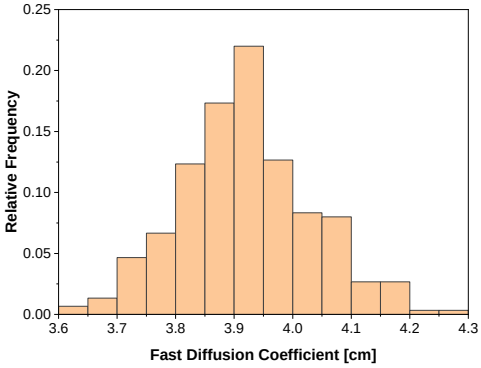

e. UO_2 region above the water level

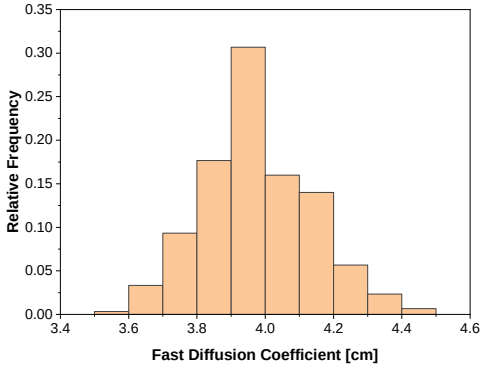

f. U_{metal} region above the water level

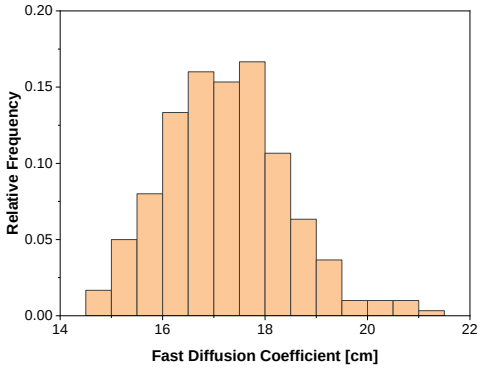

g. Control rods region above the water level

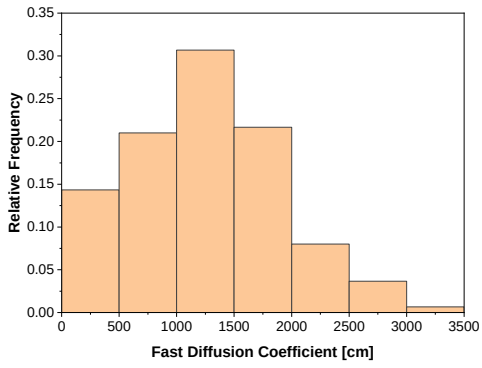

h. Reflector region above the water level

Figure A.1: The histogram of fast diffusion coefficients perturbed for 300 times

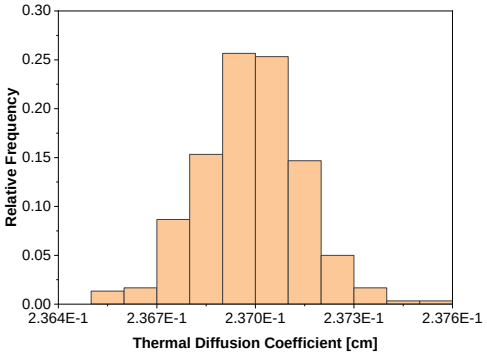

a. UO_2 region under the water level

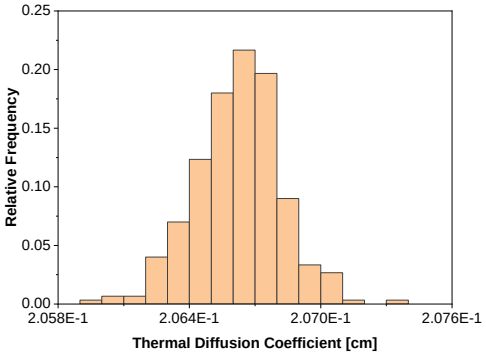

b. U_{metal} region under the water level

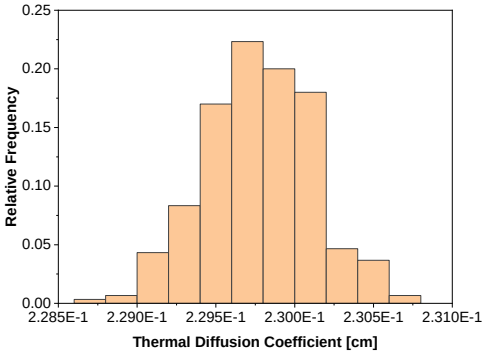

c. Control rods region under the water level

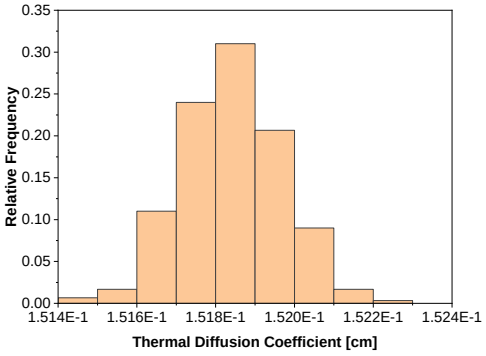

d. Reflector region under the water level

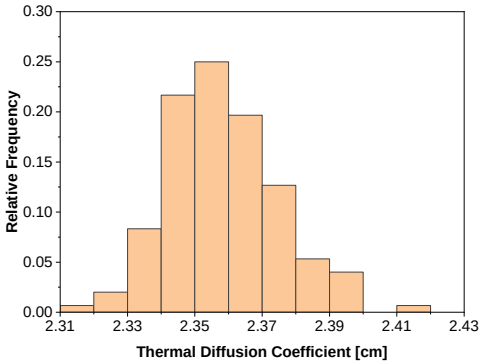

e. UO_2 region above the water level

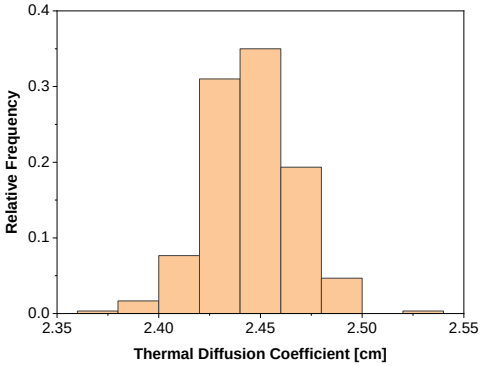

f. U_{metal} region above the water level

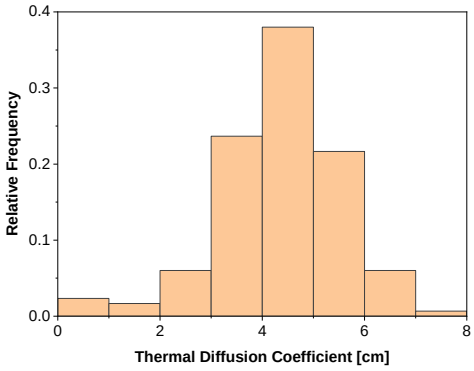

g. Control rods region above the water level

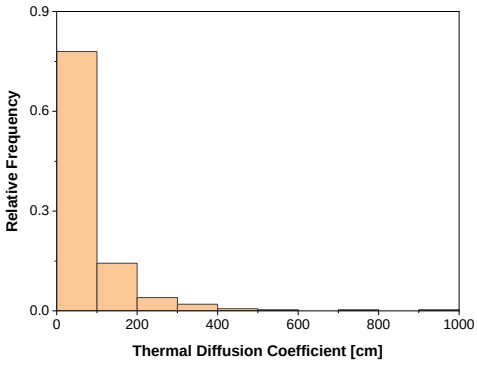

h. Reflector region above the water level

Figure A.2: The histogram of thermal diffusion coefficients perturbed for 300 times

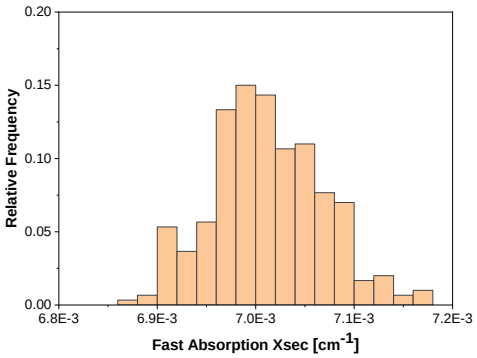

a. UO_2 region under the water level

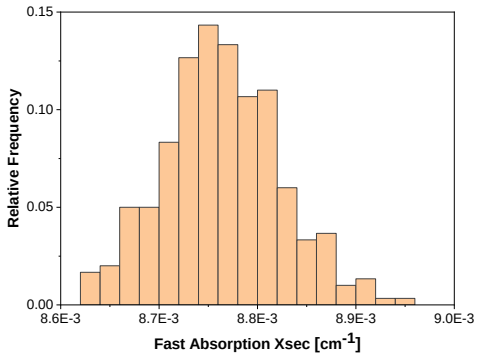

b. U_{metal} region under the water level

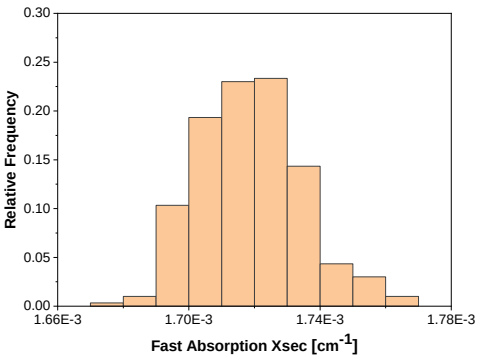

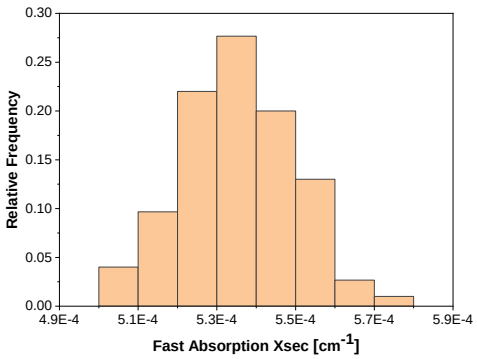

c. Control rods region under the water level

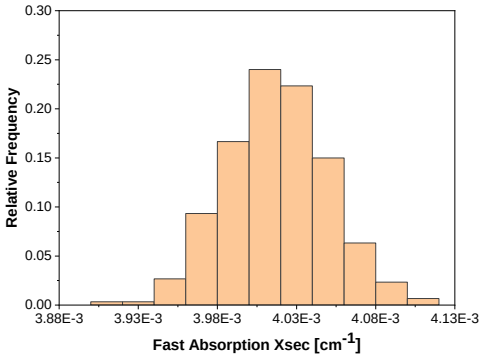

d. Reflector region under the water level

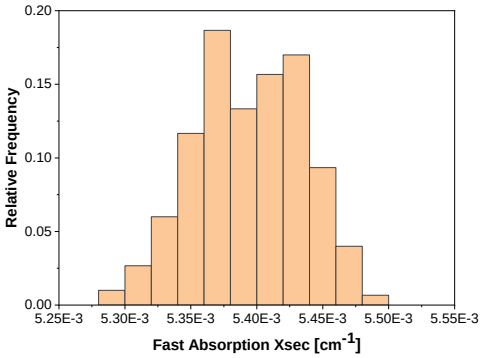

e. UO_2 region above the water level

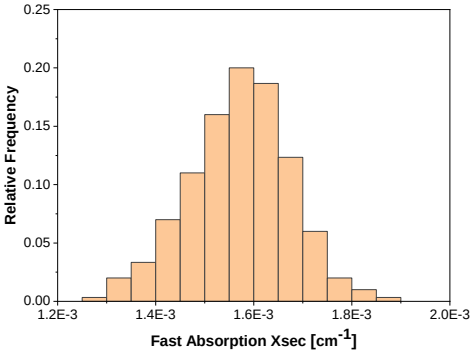

f. U_{metal} region above the water level

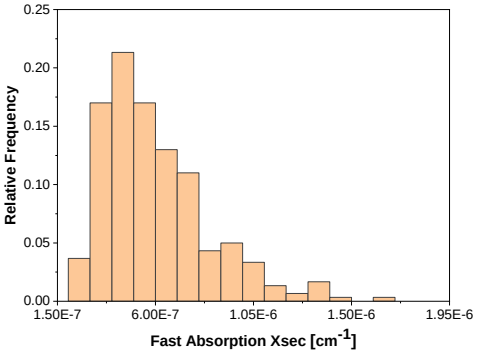

g. Control rods region above the water level

h. Reflector region above the water level

Figure A.3: The histogram of fast absorption cross-sections perturbed for 300 times

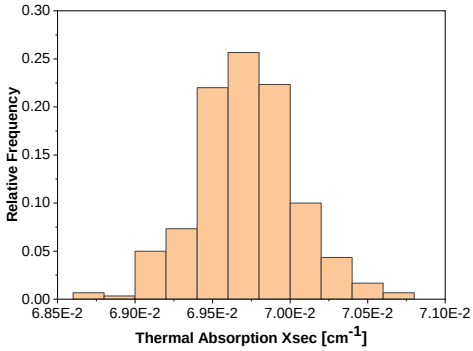

a. UO_2 region under the water level

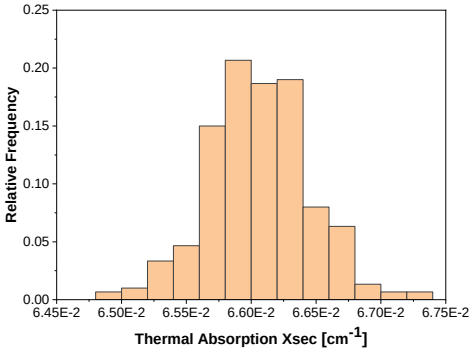

b. U_{metal} region under the water level

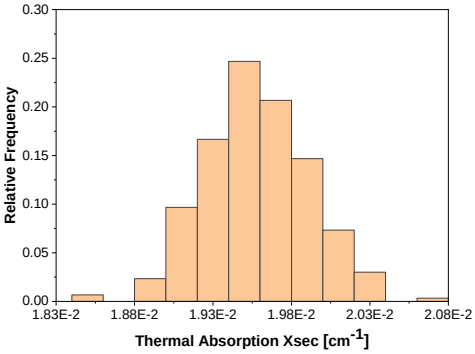

c. Control rods region under the water level

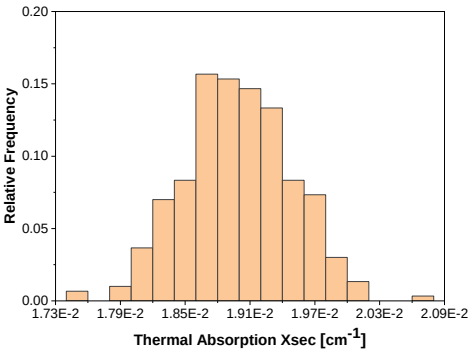

d. Reflector region under the water level

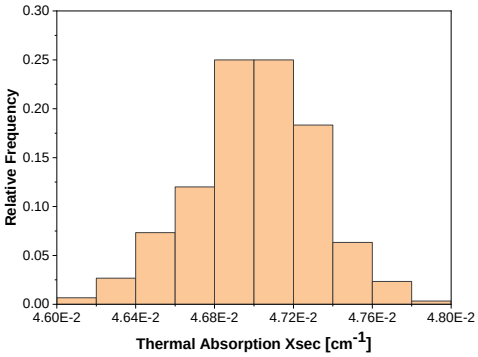

e. UO_2 region above the water level

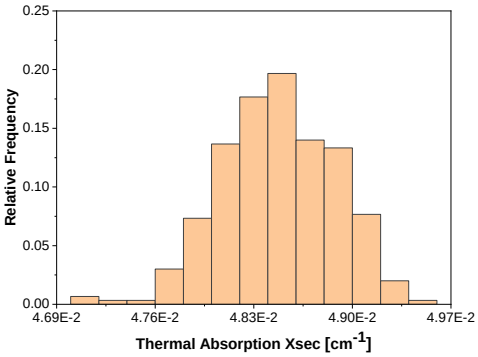

f. U_{metal} region above the water level

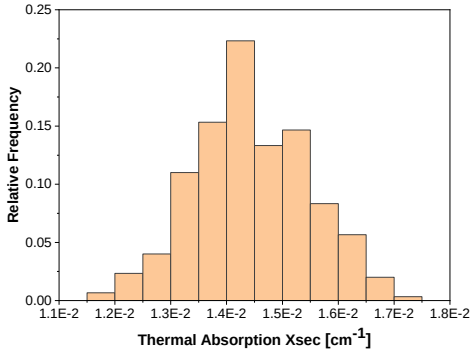

g. Control rods region above the water level

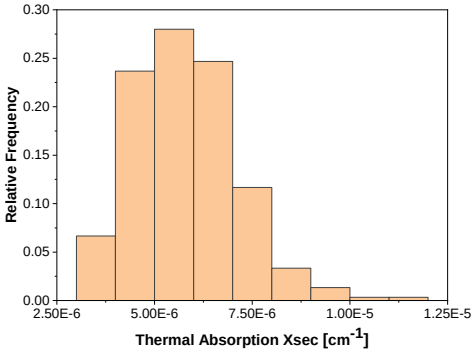

h. Reflector region above the water level

Figure A.4: The histogram of thermal absorption cross-sections perturbed for 300 times

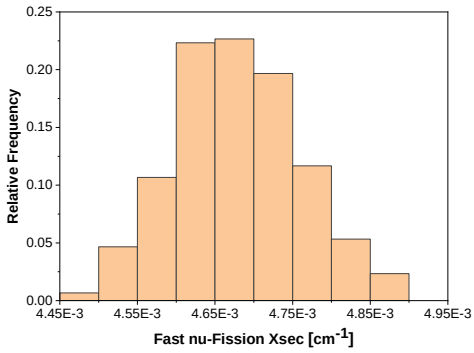

a. UO_2 region under the water level

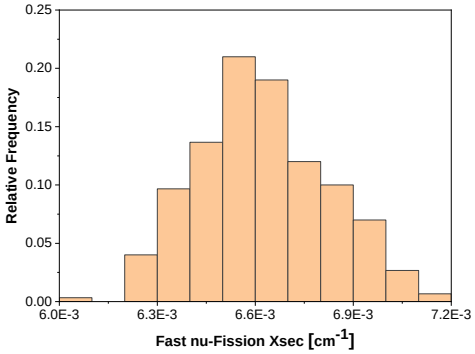

b. U_{metal} region under the water level

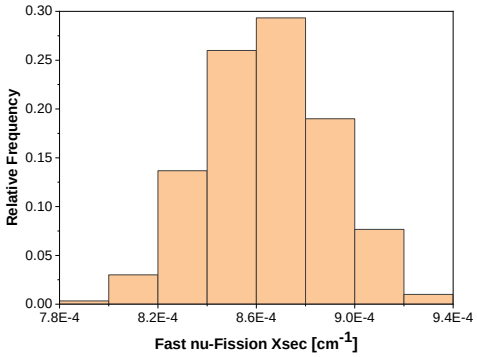

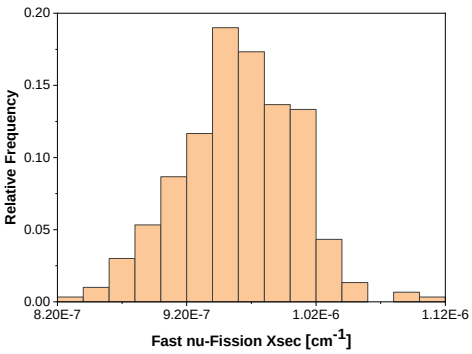

c. Control rods region under the water level

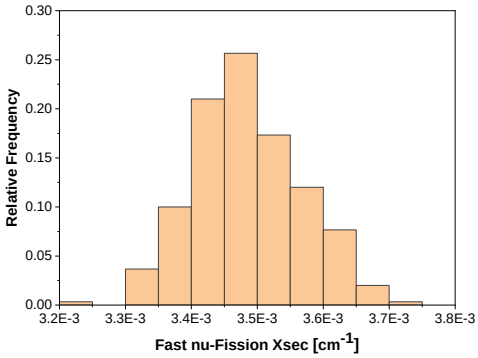

d. Reflector region under the water level

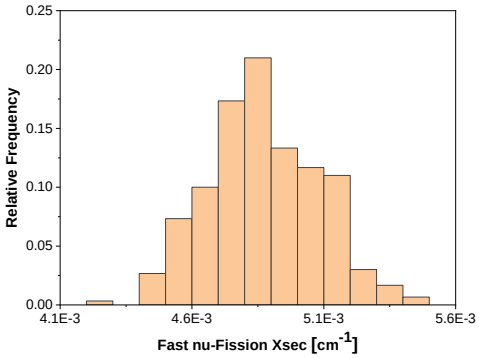

e. UO_2 region above the water level

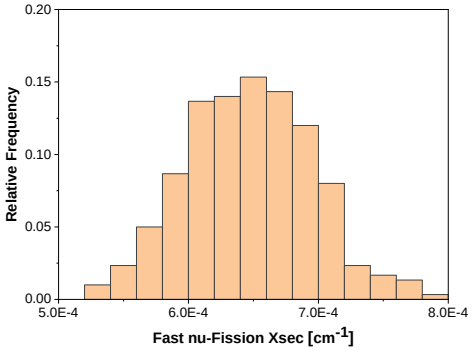

f. U_{metal} region above the water level

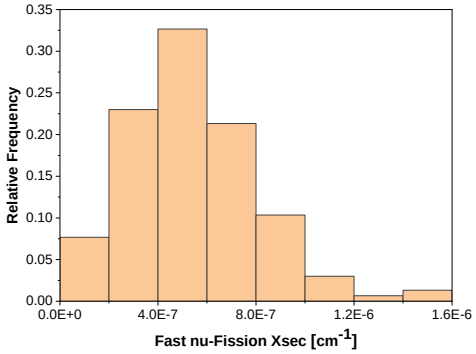

g. Control rods region above the water level

h. Reflector region above the water level

Figure A.5: The histogram of fast nu-fission cross-sections perturbed for 300 times

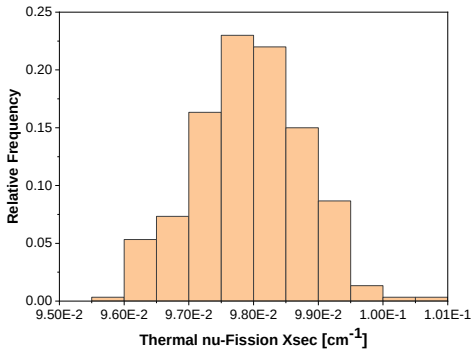

a. UO_2 region under the water level

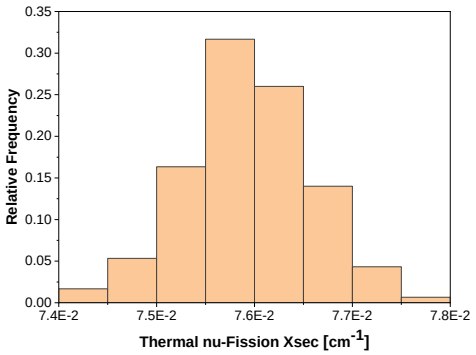

b. U_{metal} region under the water level

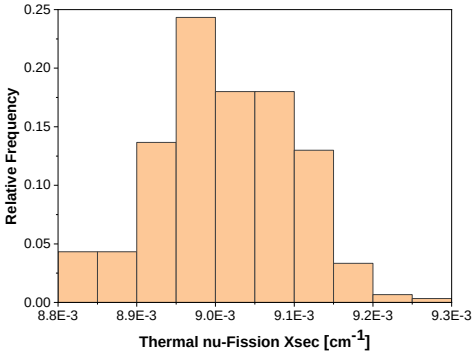

c. Control rods region under the water level

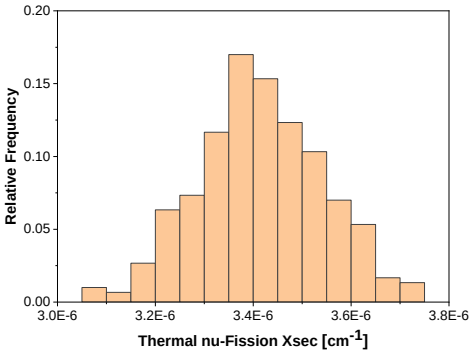

d. Reflector region under the water level

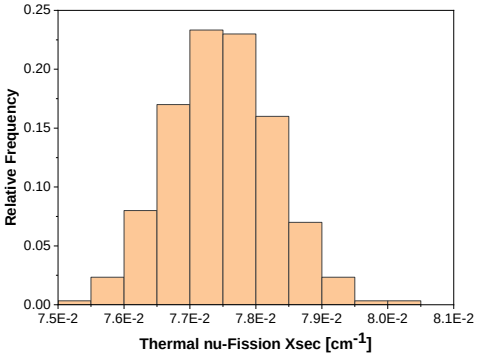

e. UO_2 region above the water level

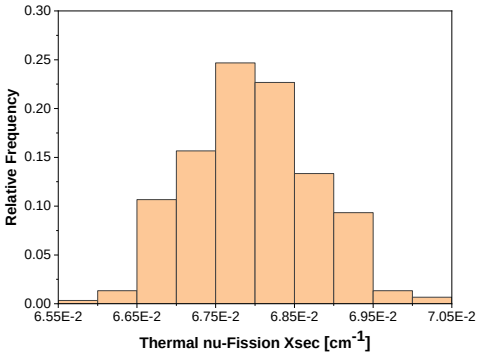

f. U_{metal} region above the water level

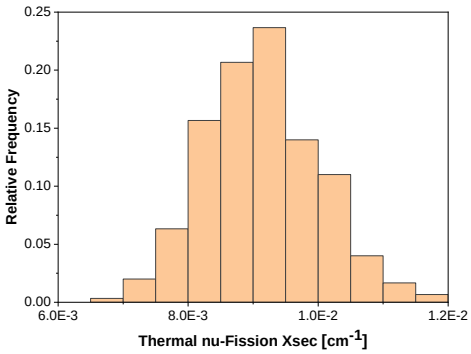

g. Control rods region above the water level

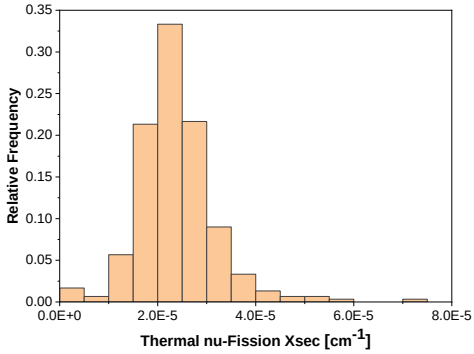

h. Reflector region above the water level

Figure A.6: The histogram of thermal nu-fission cross-sections perturbed for 300 times

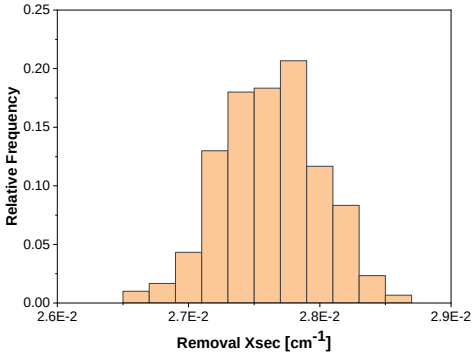

a. UO_2 region under the water level

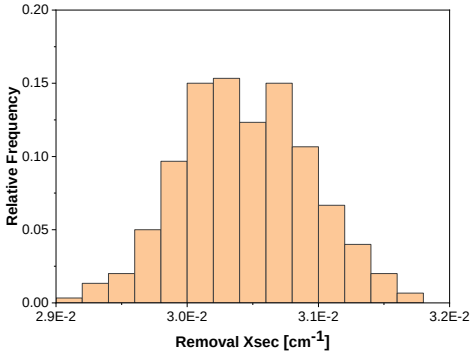

b. U_{metal} region under the water level

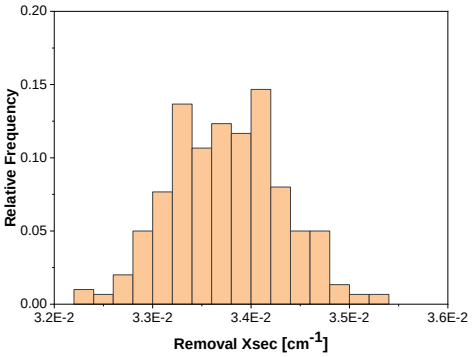

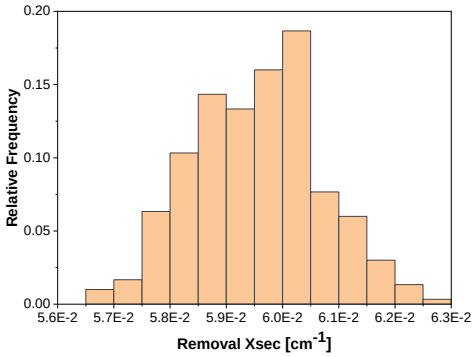

c. Control rods region under the water level

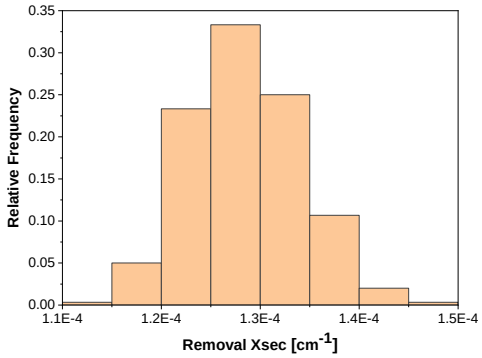

d. Reflector region under the water level

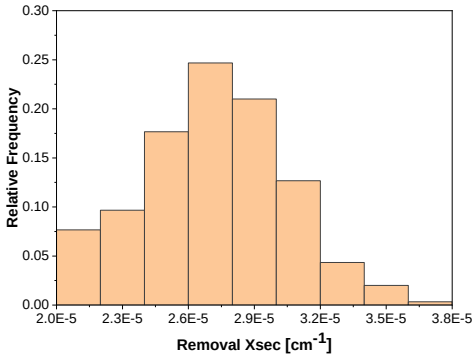

e. UO_2 region above the water level

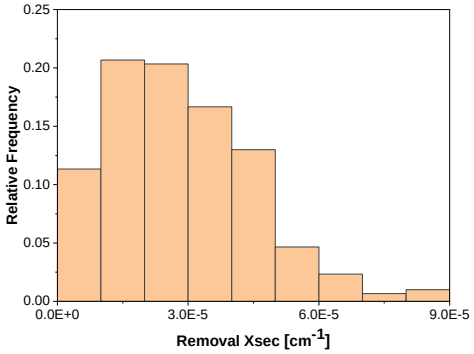

f. U_{metal} region above the water level

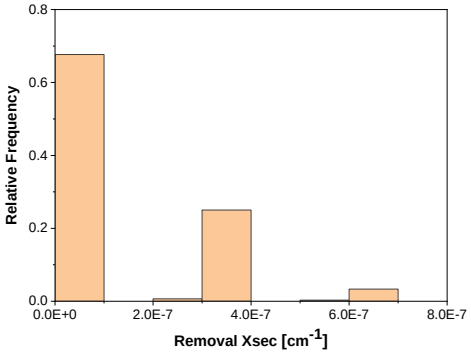

g. Control rods region above the water level

h. Reflector region above the water level

Figure A.7: The histogram of removal cross-sections perturbed for 300 times

A.2 AKR-2 Reactor

Figure A.8~Figure A.14 are the histograms of two-groups constants with 93 samples, which are considered in uncertainty analysis at AKR-2 [103]. The information of each universe is described in Figure 4.2.

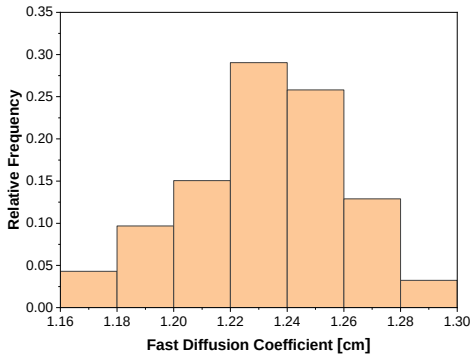

a. Universe 1

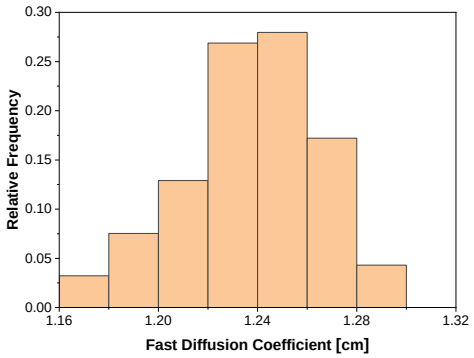

b. Universe 2

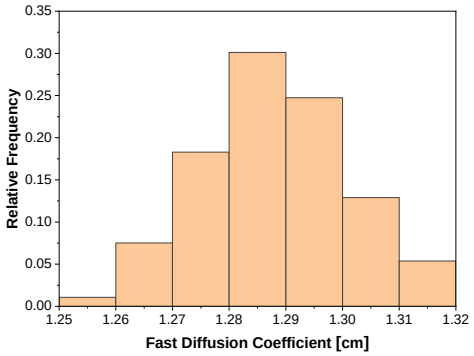

c. Universe 3

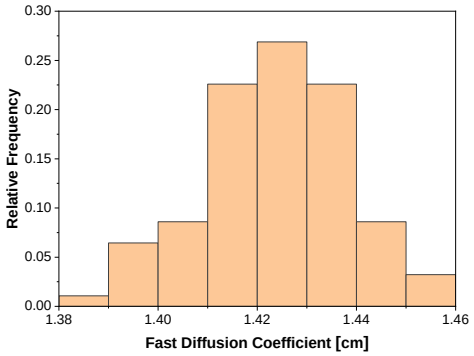

d. Universe 4

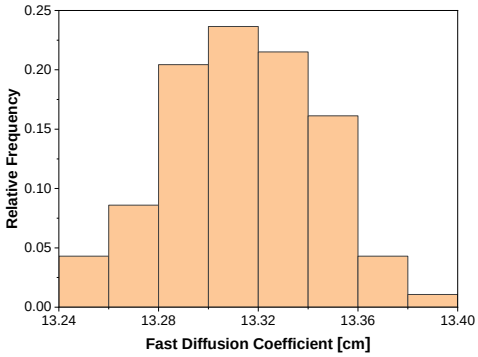

e. Universe 5

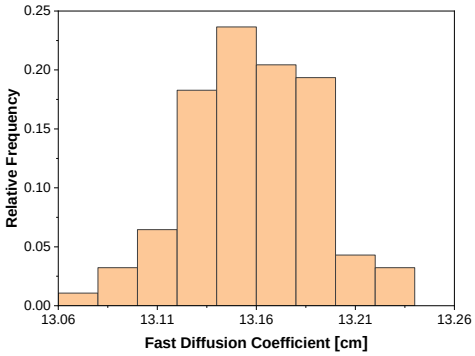

f. Universe 6

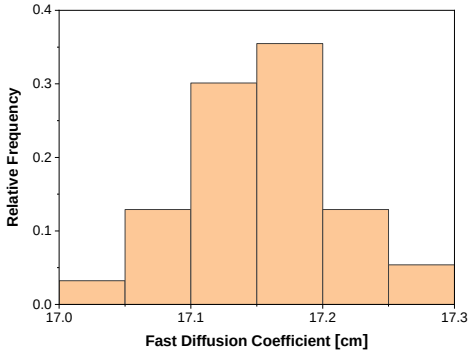

g. Universe 7

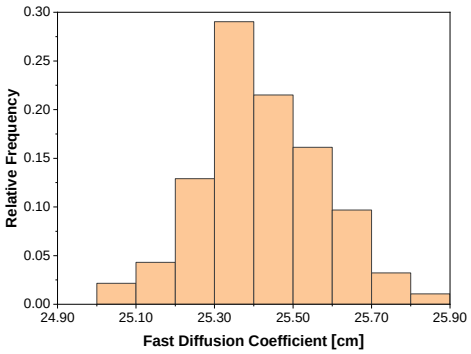

h. Universe 8

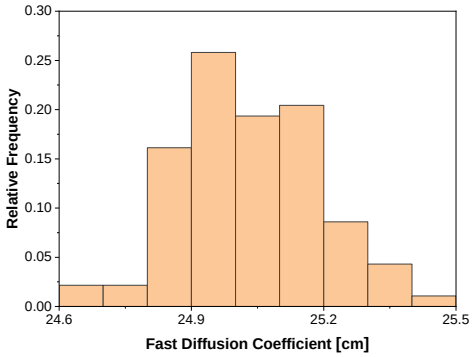

i. Universe 9

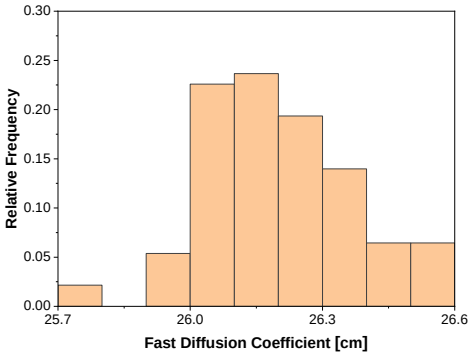

j. Universe 10

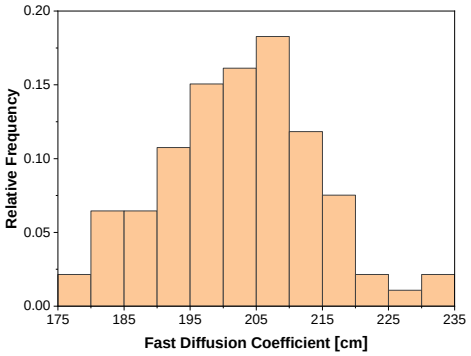

k. Universe 11

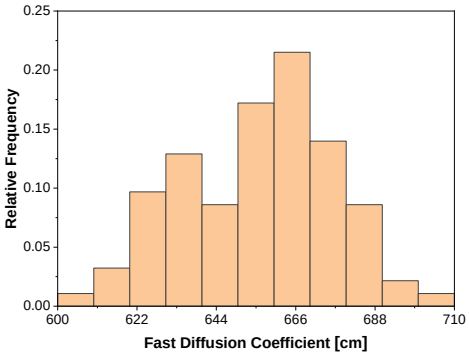

l. Universe 12

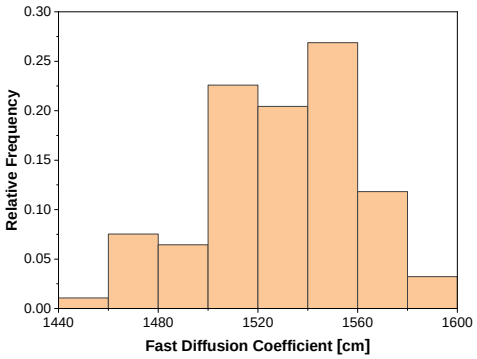

m. Universe 13

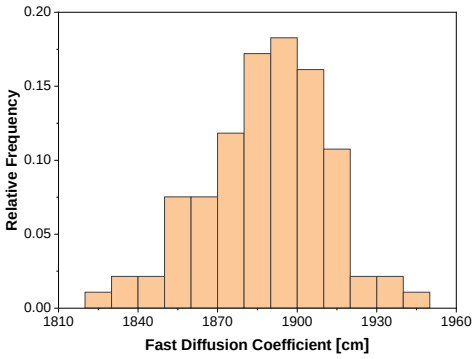

n. Universe 14

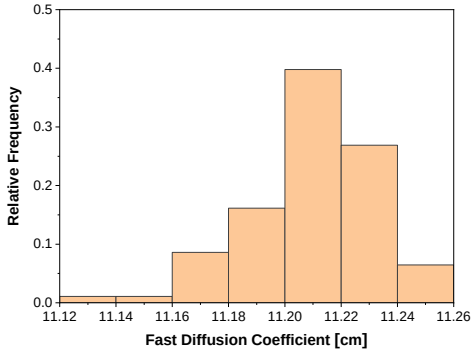

o. Universe 15

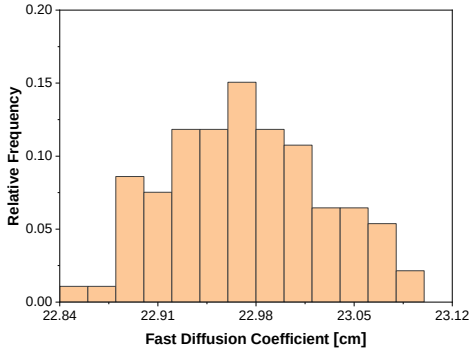

p. Universe 16

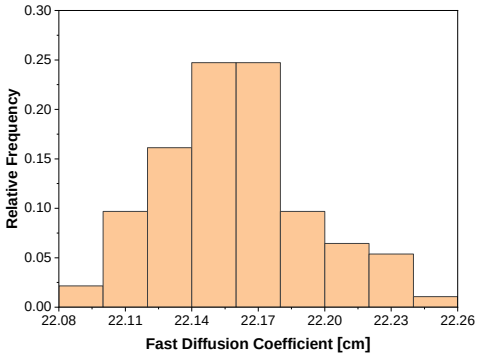

q. Universe 17

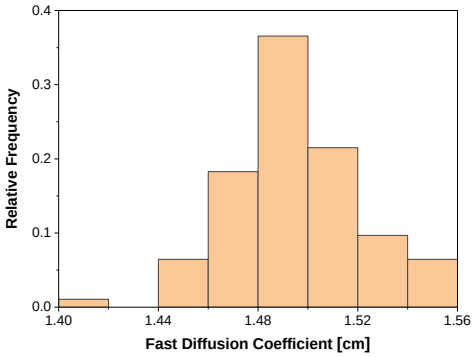

r. Universe 18

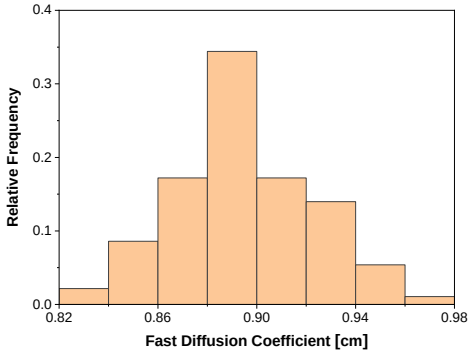

s. Universe 19

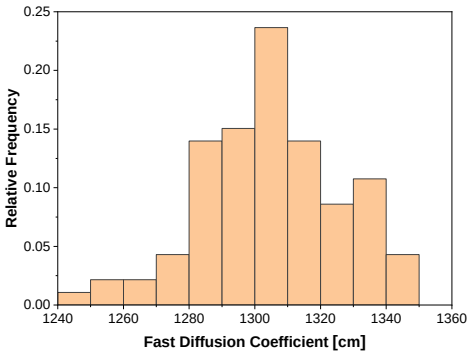

t. Universe 20

Figure A.8: The histogram of fast diffusion coefficients perturbed for 93 times

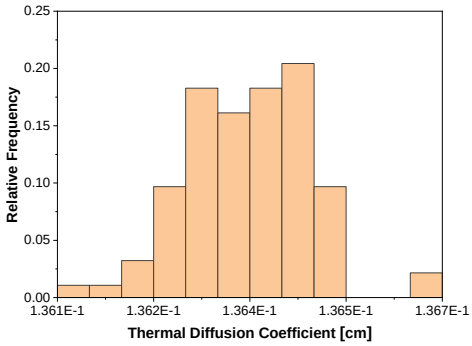

a. Universe 1

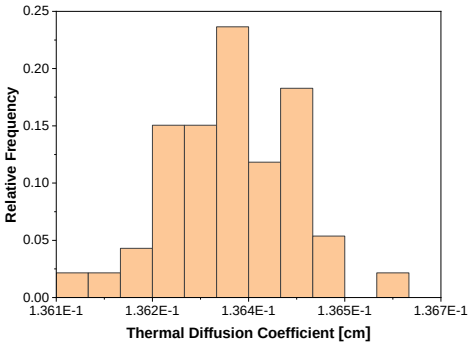

b. Universe 2

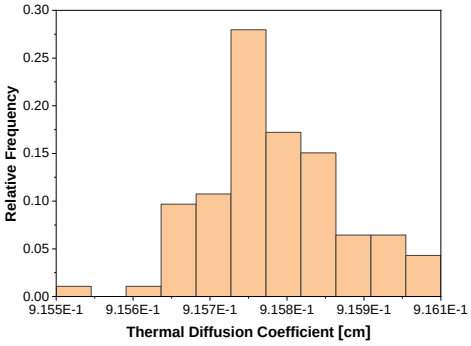

c. Universe 3

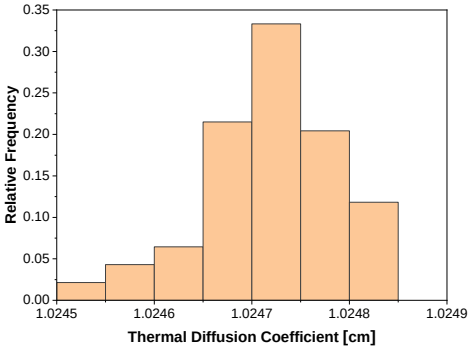

d. Universe 4

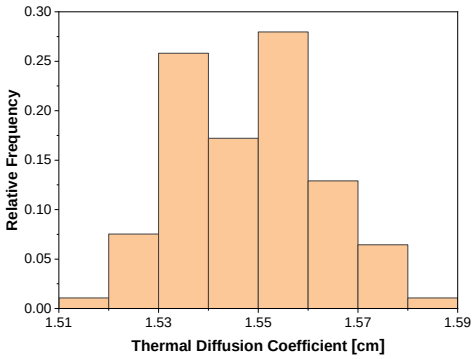

e. Universe 5

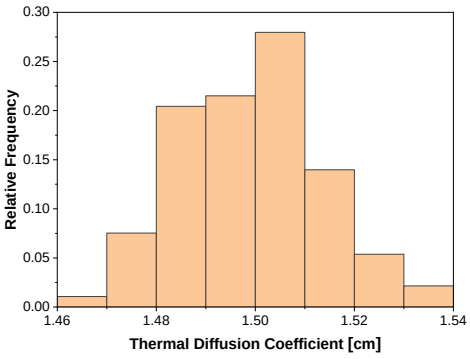

f. Universe 6

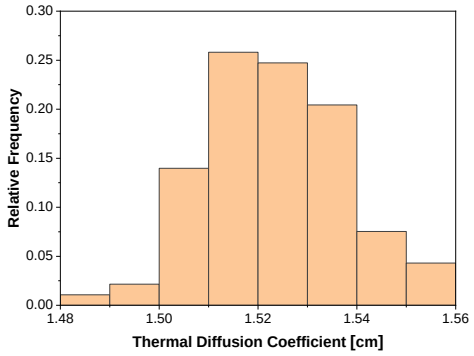

g. Universe 7

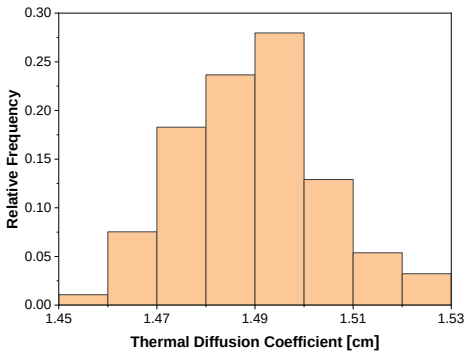

h. Universe 8

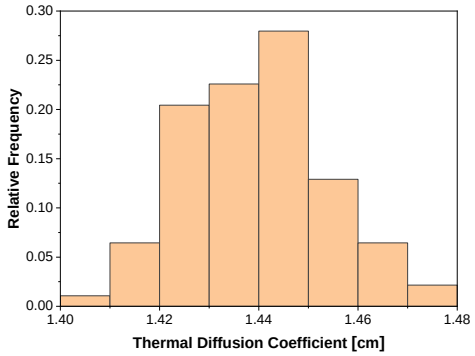

i. Universe 9

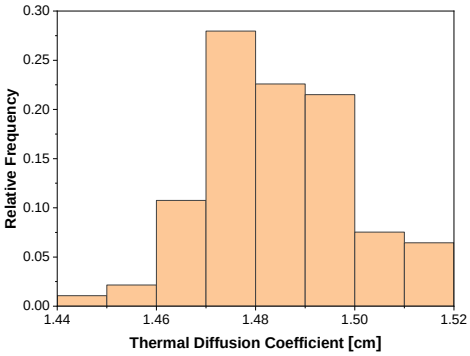

j. Universe 10

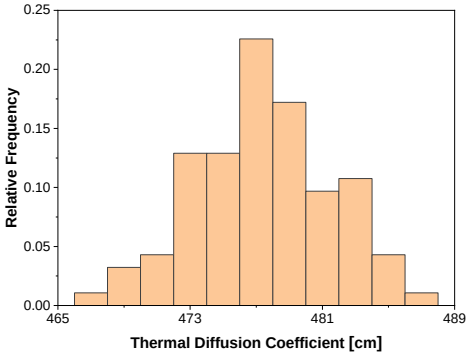

k. Universe 11

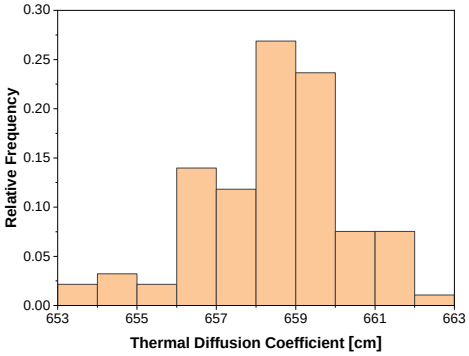

l. Universe 12

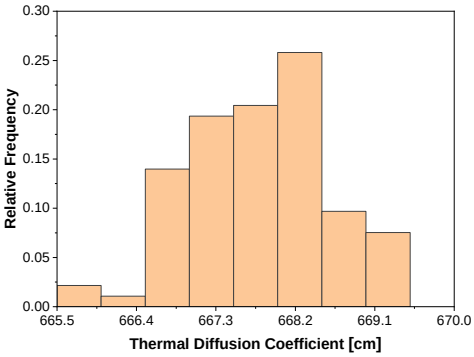

m. Universe 13

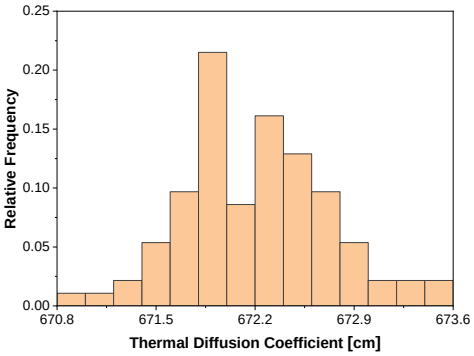

n. Universe 14

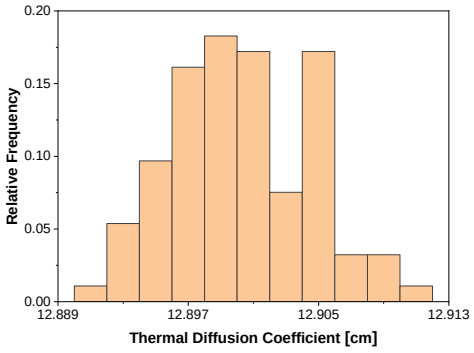

o. Universe 15

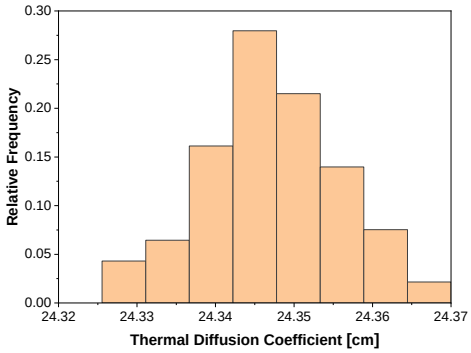

p. Universe 16

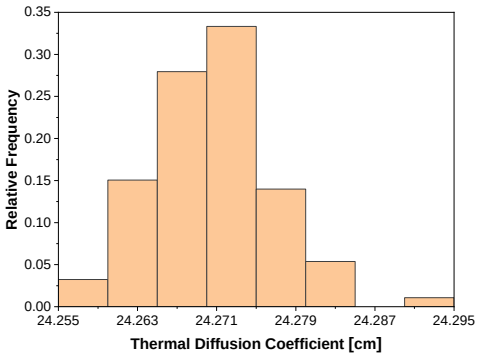

q. Universe 17

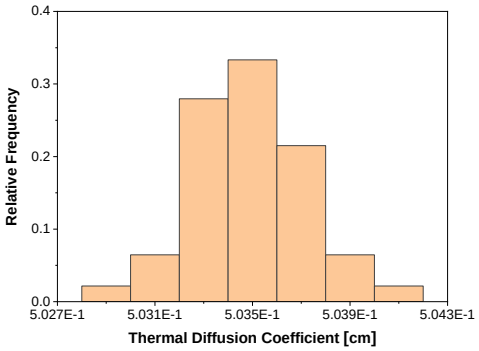

r. Universe 18

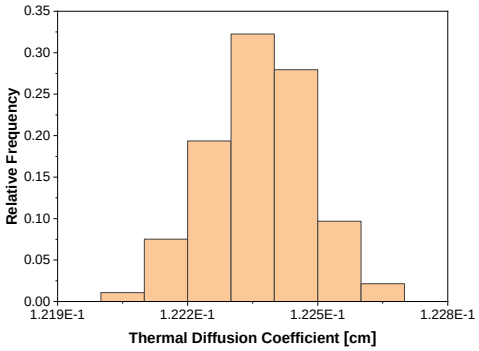

s. Universe 19

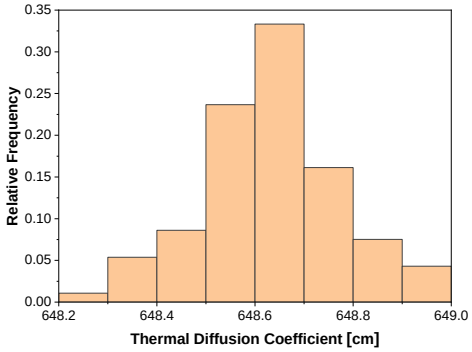

t. Universe 20

Figure A.9: The histogram of thermal diffusion coefficients perturbed for 93 times

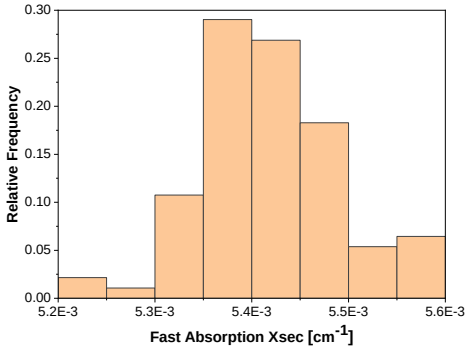

a. Universe 1

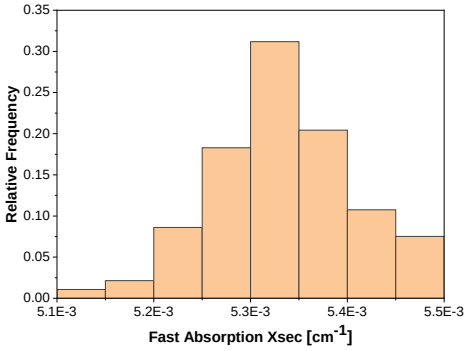

b. Universe 2

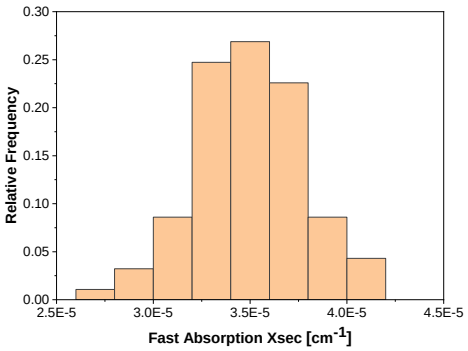

c. Universe 3

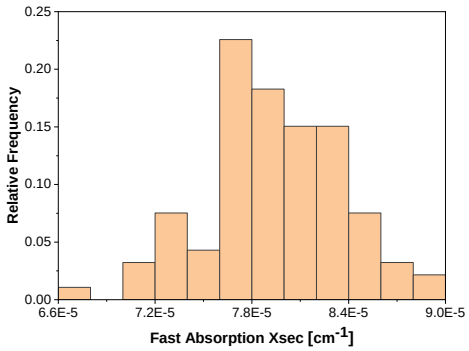

d. Universe 4

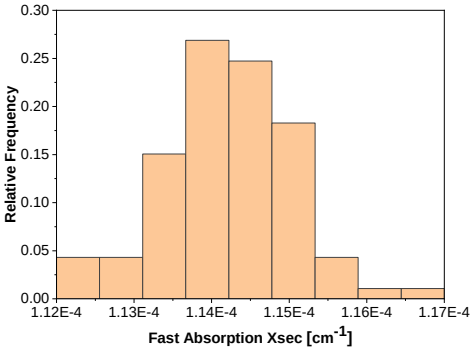

e. Universe 5

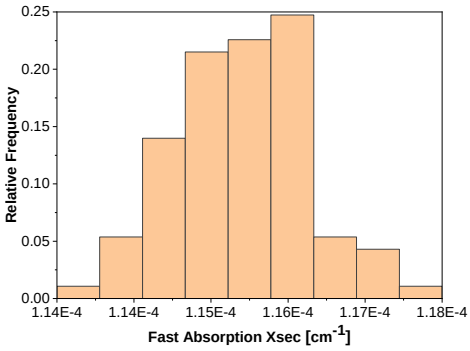

f. Universe 6

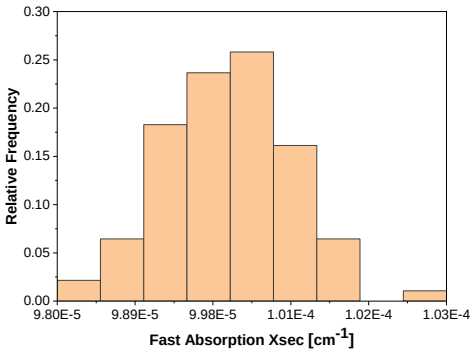

g. Universe 7

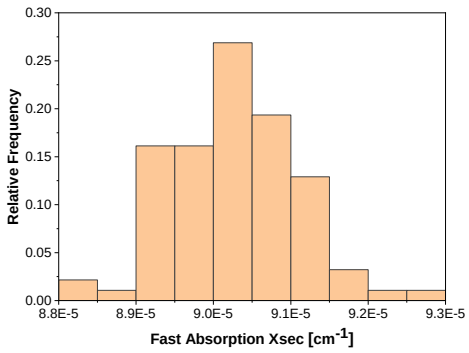

h. Universe 8

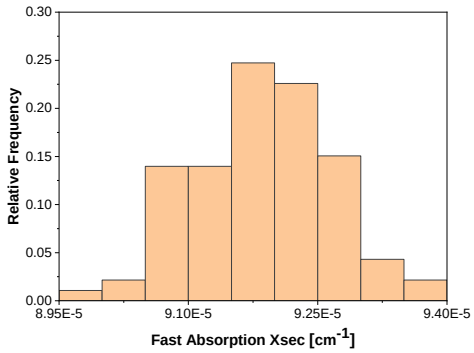

i. Universe 9

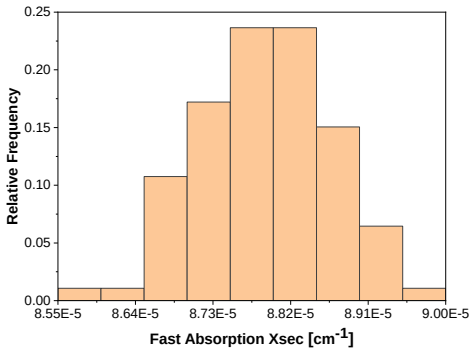

j. Universe 10

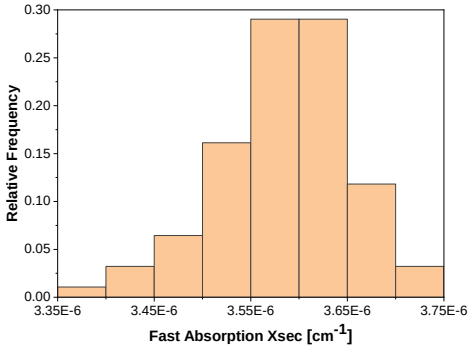

k. Universe 11

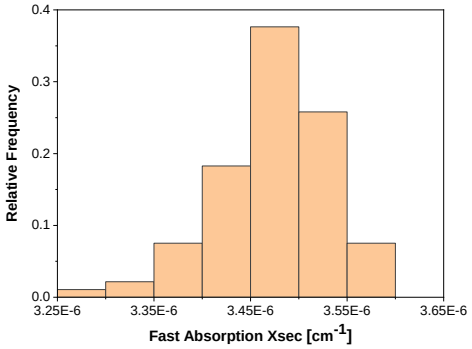

l. Universe 12

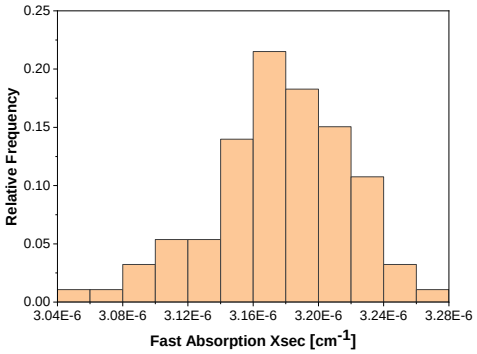

m. Universe 13

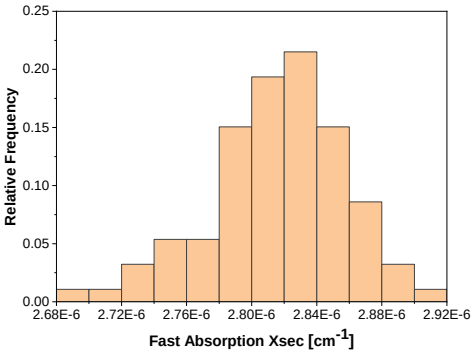

n. Universe 14

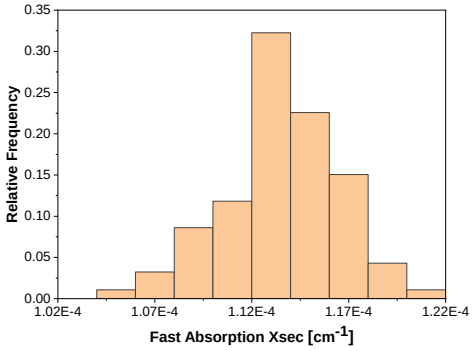

o. Universe 15

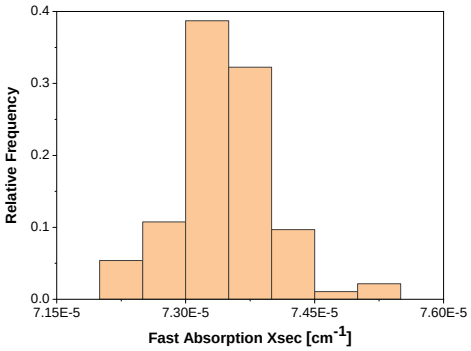

p. Universe 16

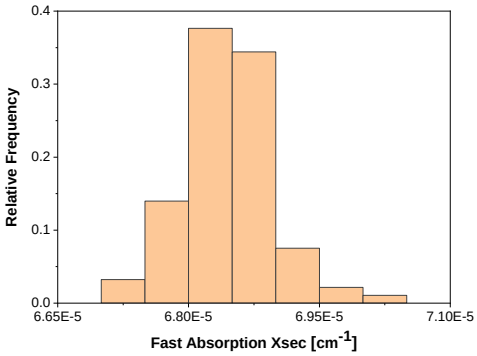

q. Universe 17

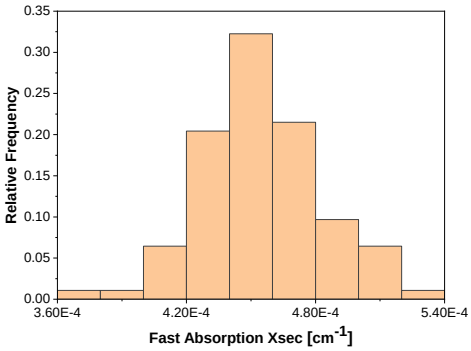

r. Universe 18

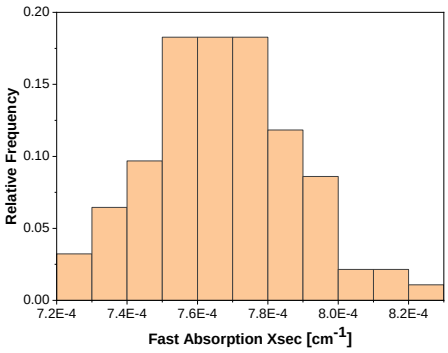

s. Universe 19

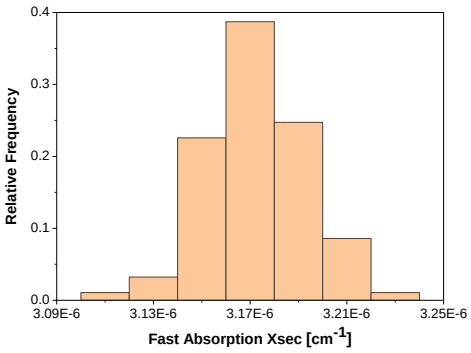

t. Universe 20

Figure A.10: The histogram of fast absorption cross-sections perturbed for 93 times

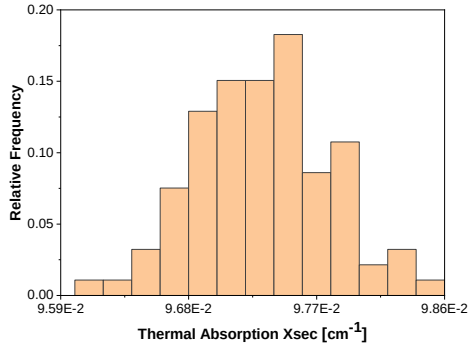

a. Universe 1

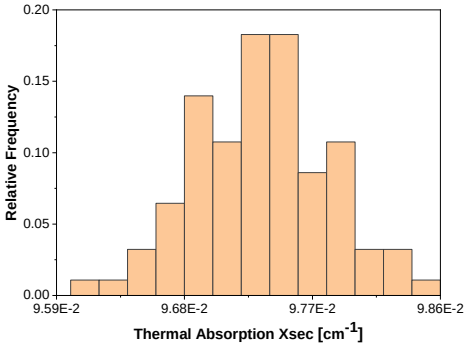

b. Universe 2

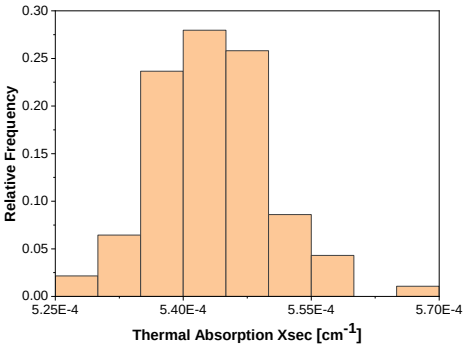

c. Universe 3

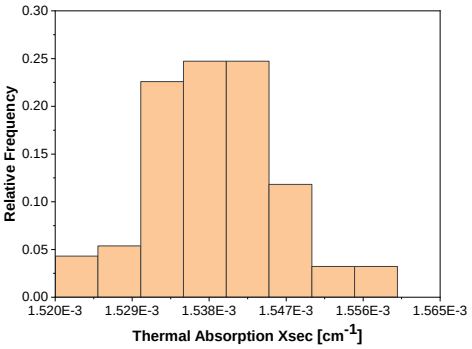

d. Universe 4

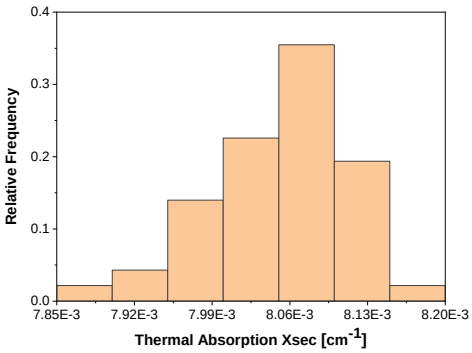

e. Universe 5

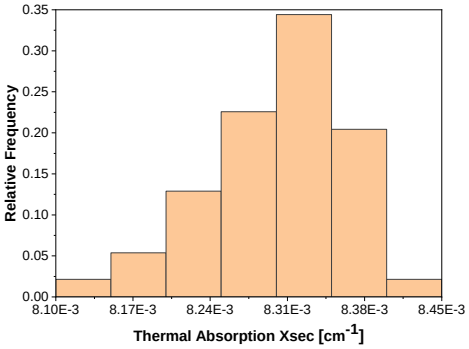

f. Universe 6

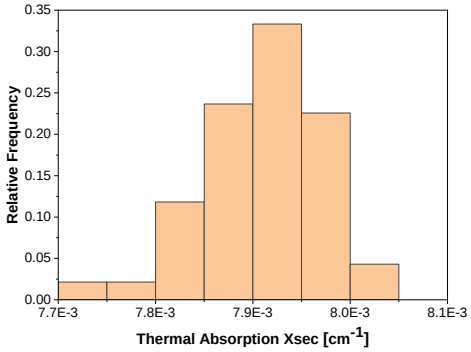

g. Universe 7

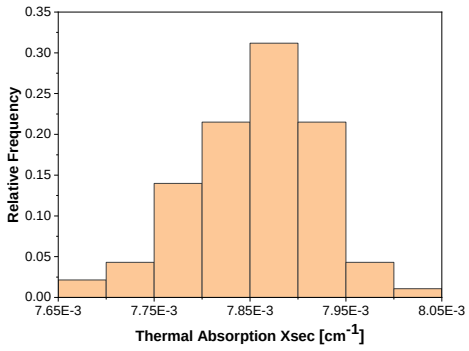

h. Universe 8

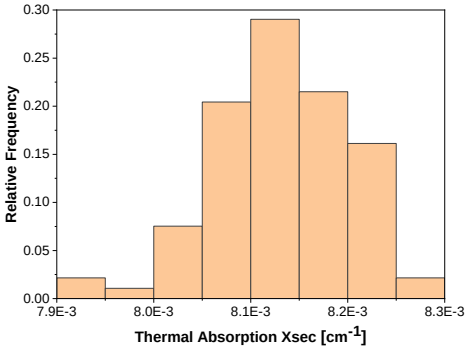

i. Universe 9

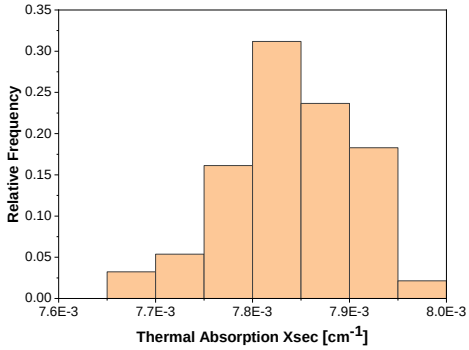

j. Universe 10

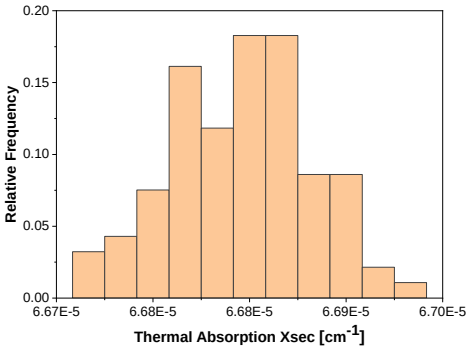

k. Universe 11

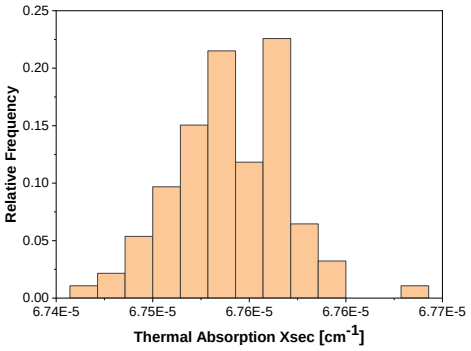

l. Universe 12

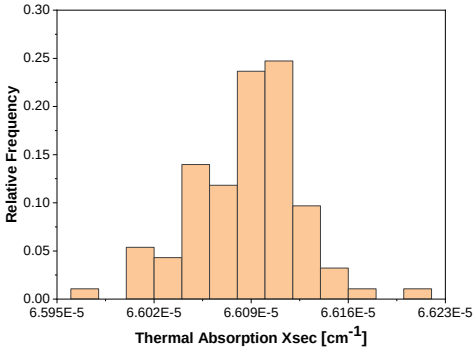

m. Universe 13

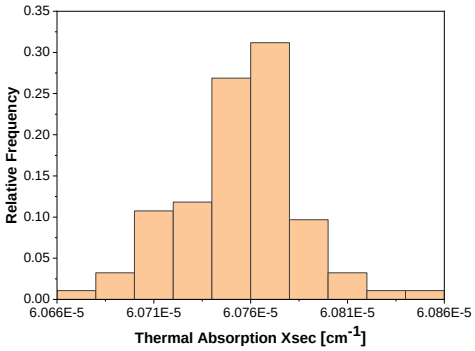

n. Universe 14

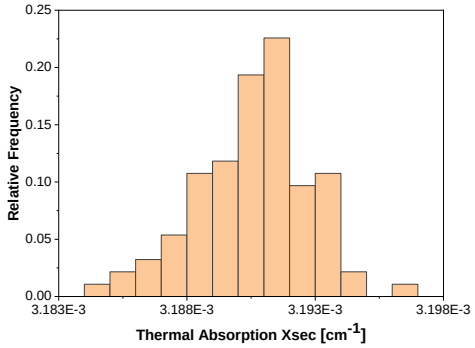

o. Universe 15

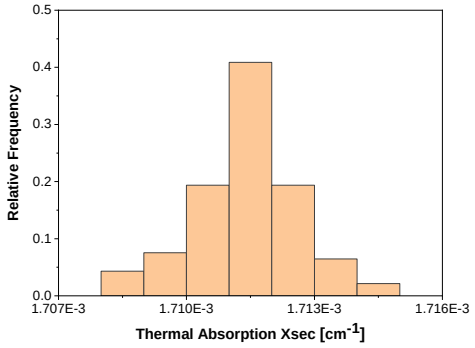

p. Universe 16

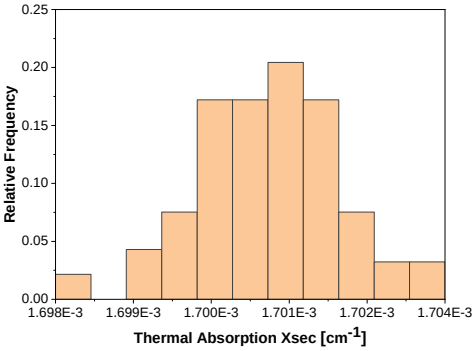

q. Universe 17

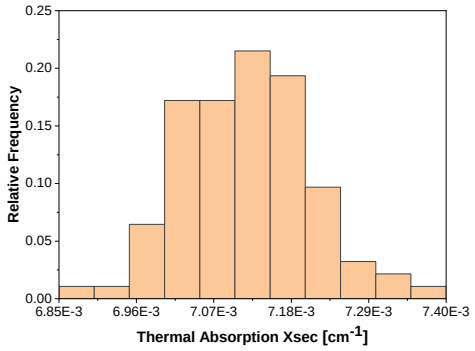

r. Universe 18

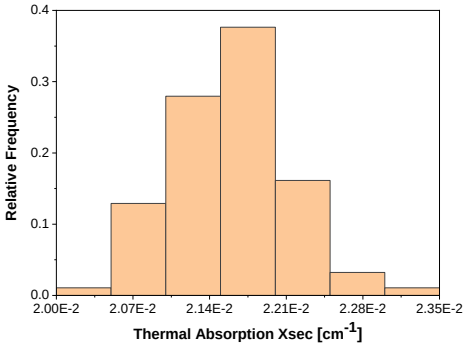

s. Universe 19

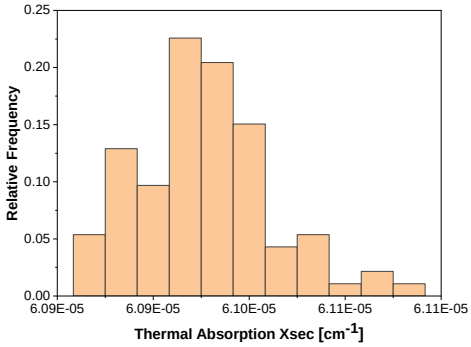

t. Universe 20

Figure A.11: The histogram of thermal absorption cross-sections perturbed for 93 times

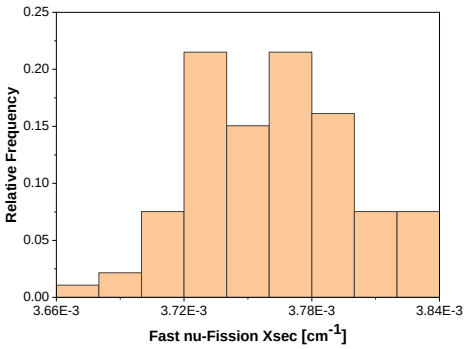

a. Universe 1

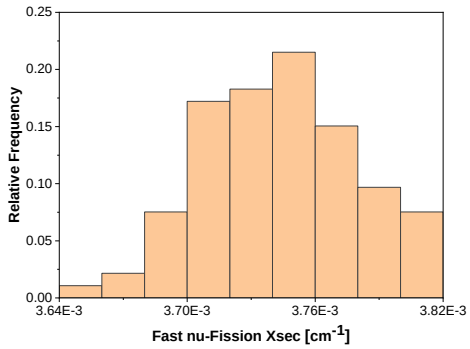

b. Universe 2

Figure A.12: The histogram of fast nu-fission cross-sections perturbed for 93 times

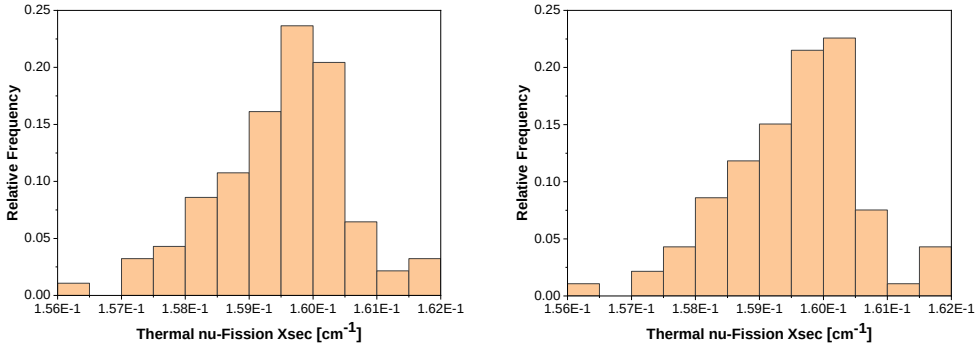

a. Universe 1 b. Universe 2

Figure A.13: The histogram of thermal nu-fission cross-sections perturbed for 93 times

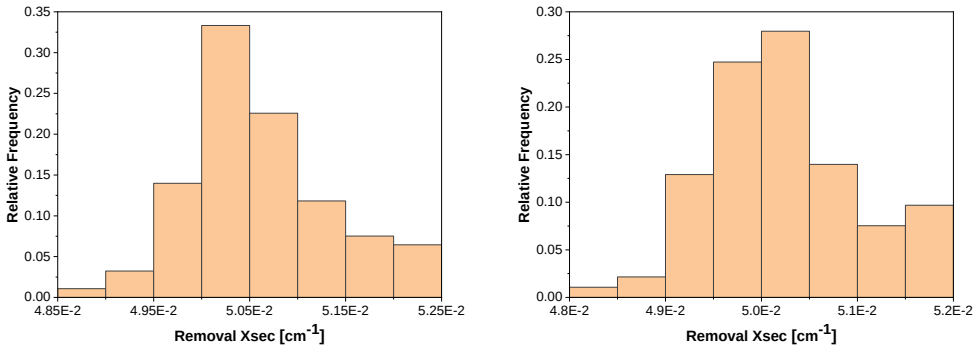

a. Universe 1 b. Universe 2

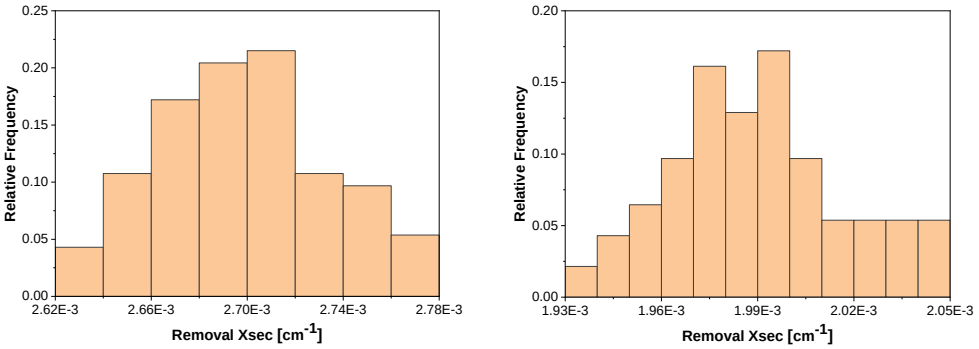

c. Universe 3 d. Universe 4

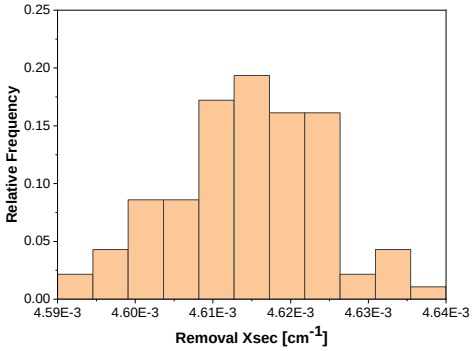

e. Universe 5

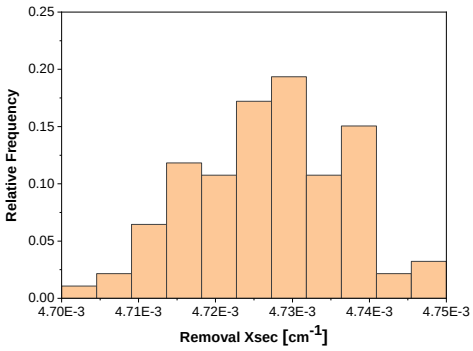

f. Universe 6

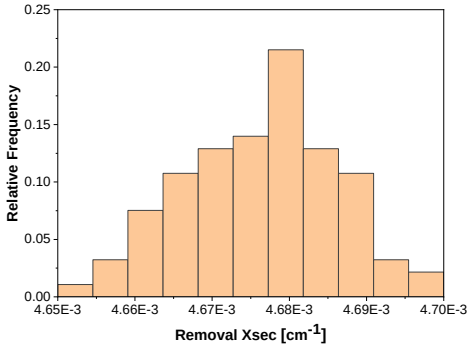

g. Universe 7

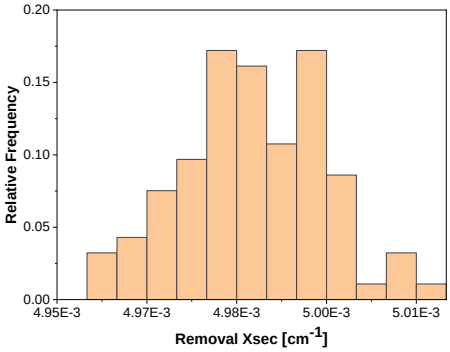

h. Universe 8

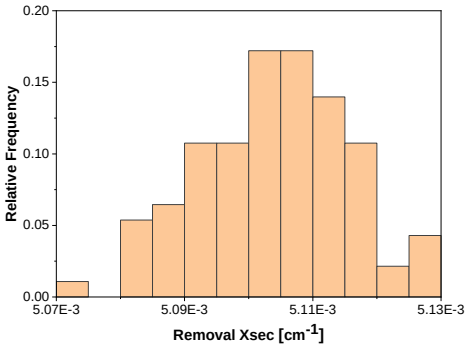

i. Universe 9

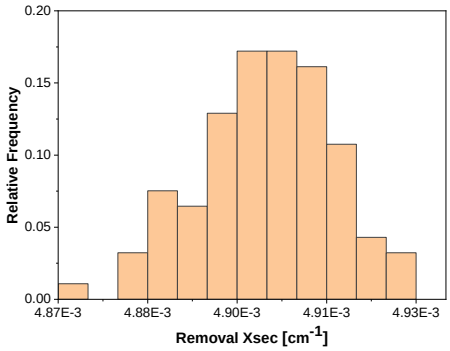

j. Universe 10

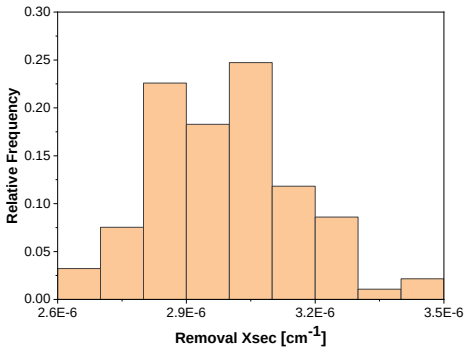

k. Universe 11

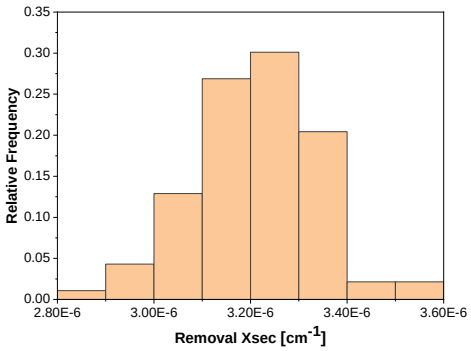

l. Universe 12

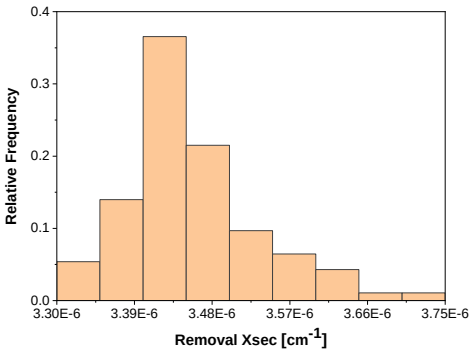

m. Universe 13

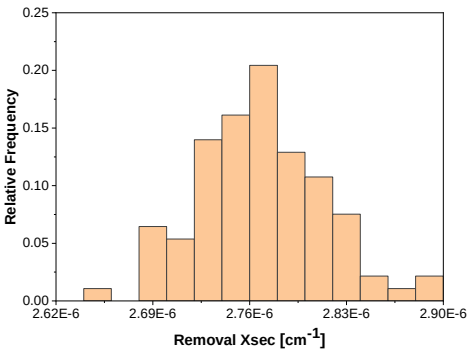

n. Universe 14

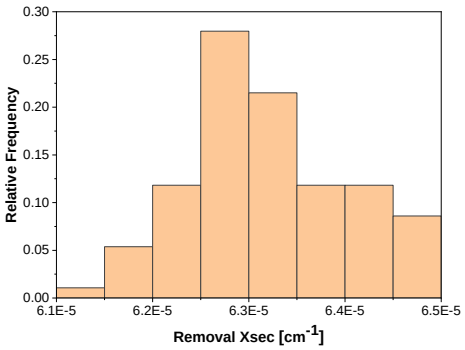

o. Universe 15

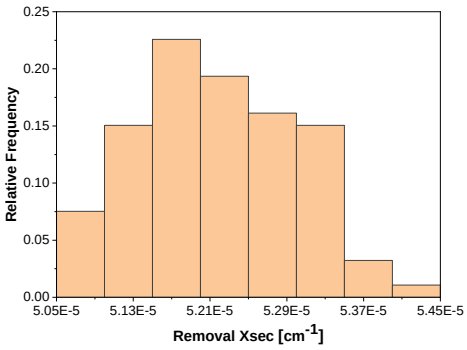

p. Universe 16

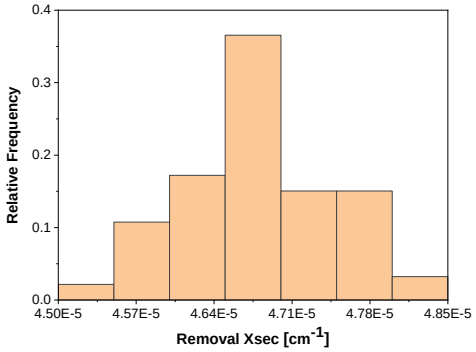

q. Universe 17

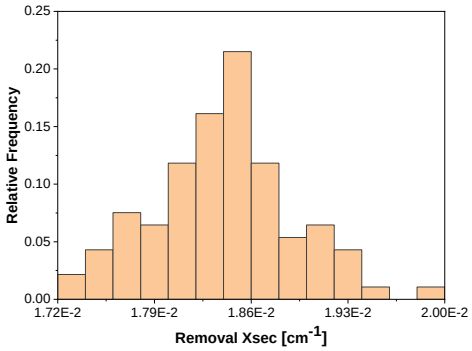

r. Universe 18

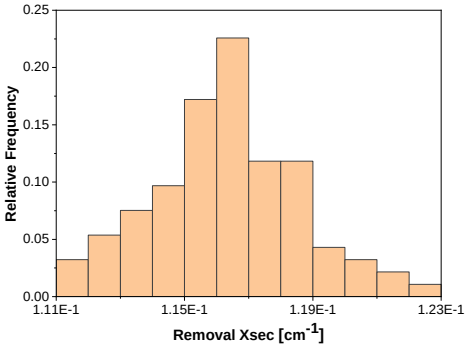

s. Universe 19

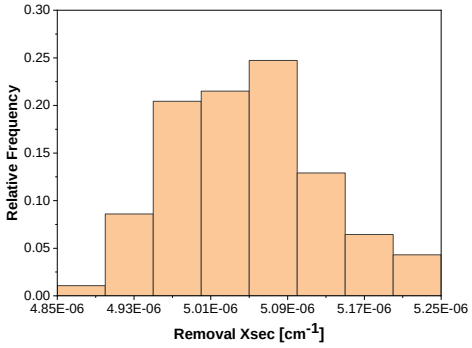

t. Universe 20

Figure A.14: The histogram of removal cross-sections perturbed for 93 times

A.3 Swiss 3-loop Konvoi Reactor

Three different core conditions are considered with various fuel enrichment and burnup condition [33]. The histograms of nuclear data, as shown in Figure A.15 ~ Figure A.17, are made with 300 data sets.

Case 1: 5.06 % – wt & 0 MWd/t

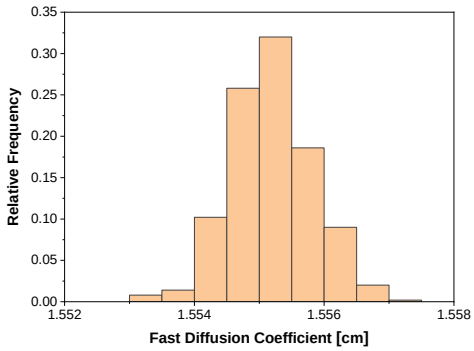

a. Fast diffusion coefficient

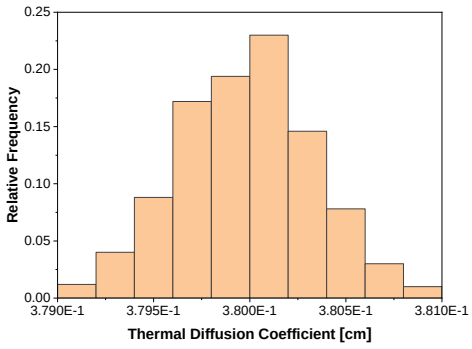

b. Thermal diffusion coefficient

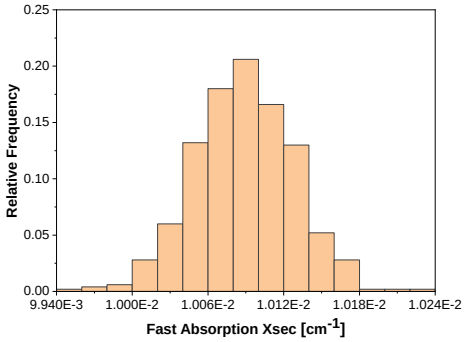

c. Fast absorption cross-section

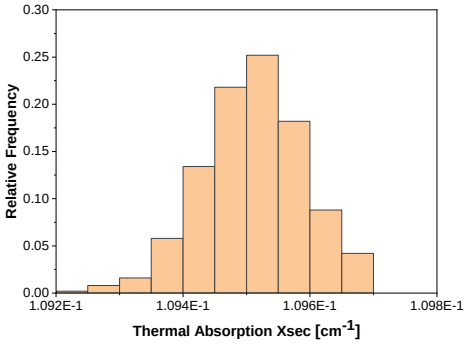

d. Thermal absorption cross-section

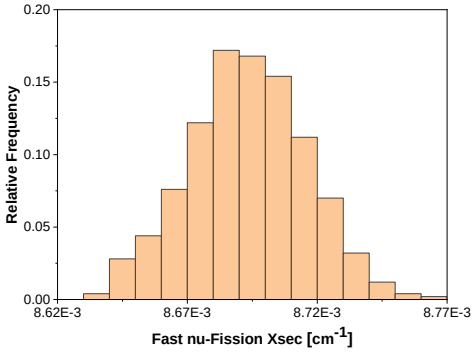

e. Fast nu-fission cross-section

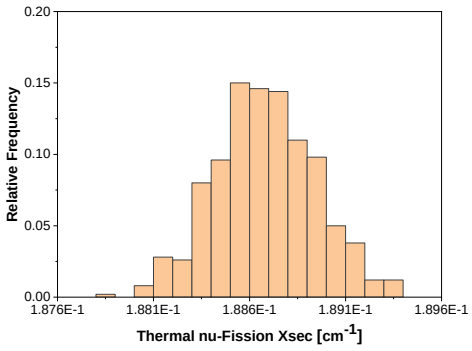

f. Thermal nu-fission cross-section

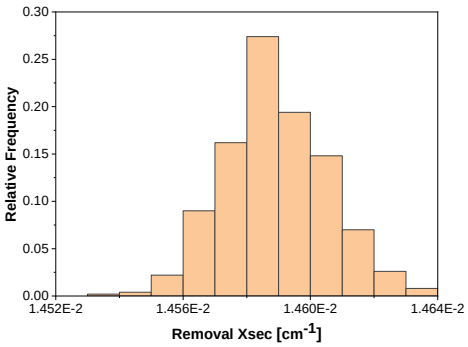

g. Removal cross-section

Figure A.15: The histogram of two-group constants at fuel condition of 5.06 % – wt & 0 MWd/t

Case 2: 5.06%-wt & 30 MWd/t

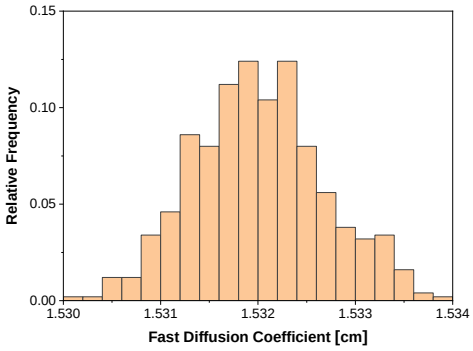

a. Fast diffusion coefficient

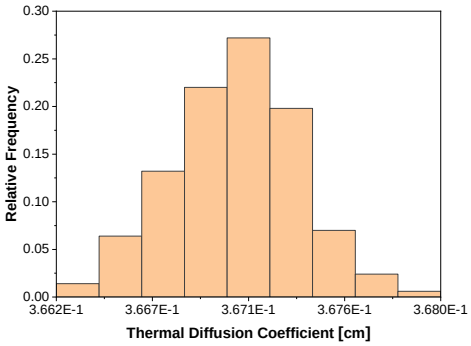

b. Thermal diffusion coefficient

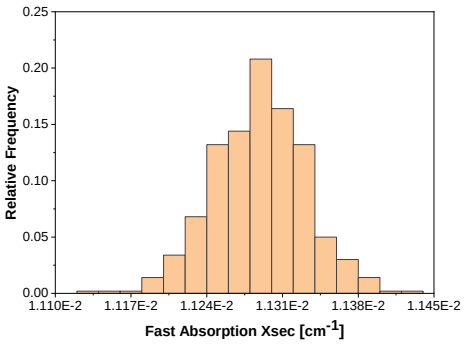

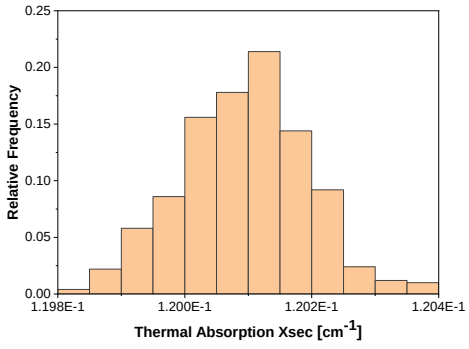

c. Fast absorption cross-section

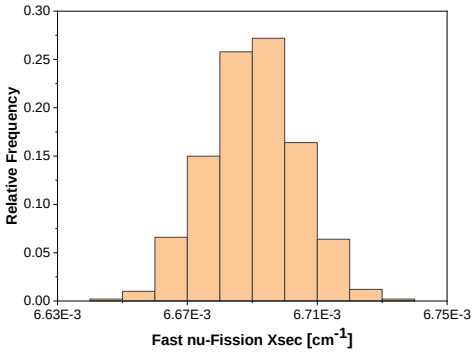

d. Thermal absorption cross-section

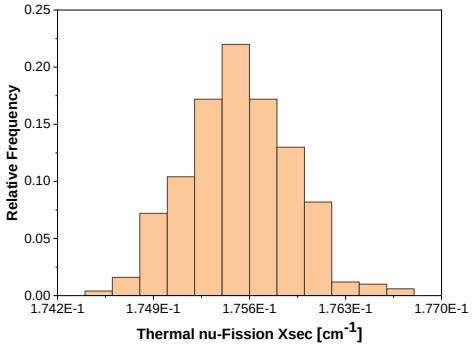

e. Fast nu-fission cross-section

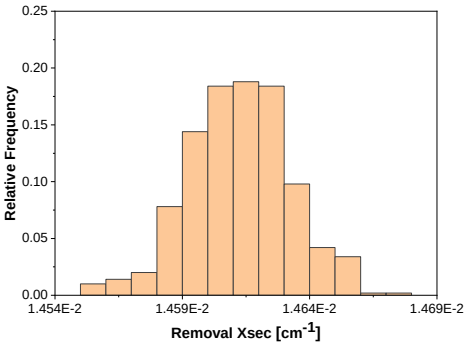

f. Thermal nu-fission cross-section

g. Removal cross-section

Figure A.16: The histogram of two-group constants at fuel condition of $5.06\ \% - \mathrm{wt}\ \&\ 30\ \mathrm{MWd/t}$

Case 3: $4.9\ \% - \mathrm{wt}\ \&\ 0\ \mathrm{MWd/t}$

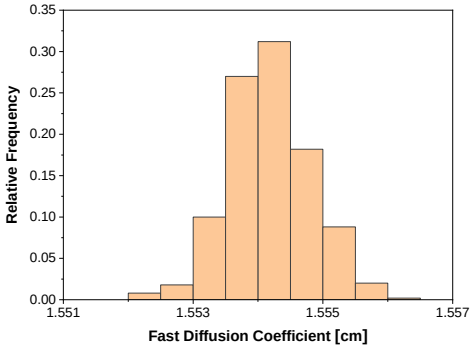

a. Fast diffusion coefficient

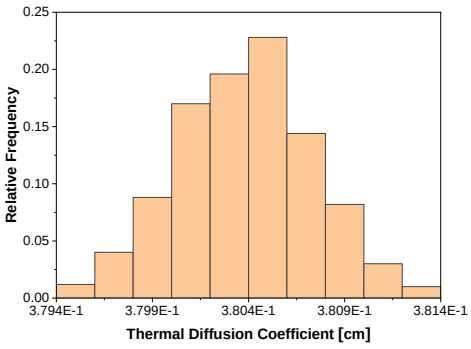

b. Thermal diffusion coefficient

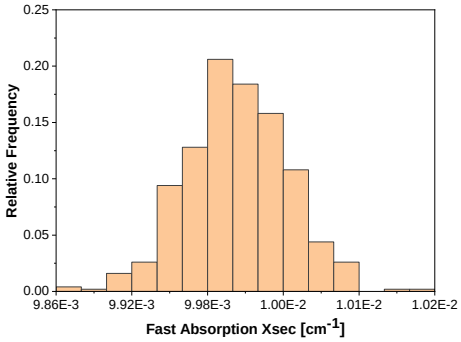

c. Fast absorption cross-section

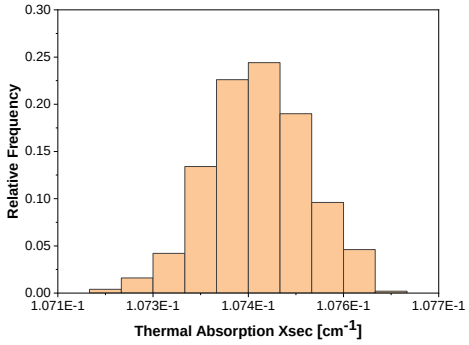

d. Thermal absorption cross-section

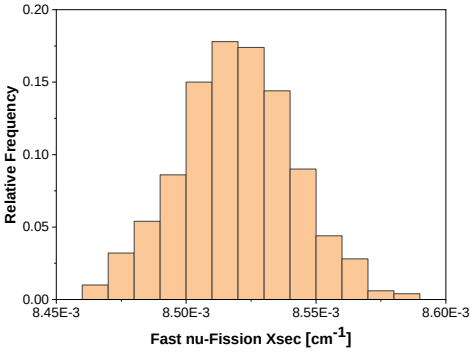

e. Fast nu-fission cross-section

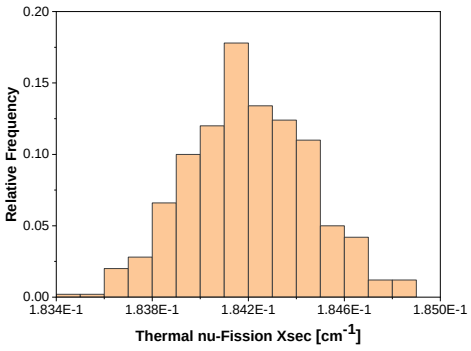

f. Thermal nu-fission cross-section

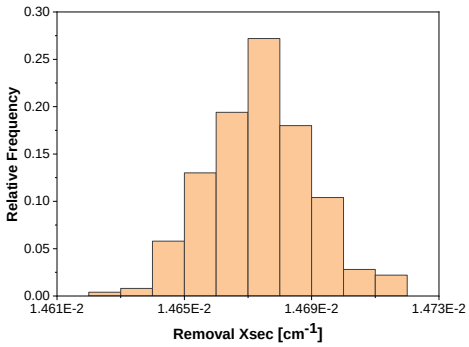

g. Removal cross-section

Figure A.17: The histogram of two-group constants at fuel condition of $4.9\% - \mathrm{wt}\ \&\ 0\ \mathrm{MWd/t}$

Bibliography

[1] H. Glaeser, “GRS Method for Uncertainty and Sensitivity Evaluation of Code Results and Applications,” Science and Technology of Nuclear Installations, 2008, pp.1-7 (2008).

[2] Bundesamt für Strahlenschutz, “Kurzbeschreibung und Bewertung der meldpflichtigen Ereignisse in Kernkraftwerken und Forschungsreaktoren der Bundesrepublik Deutschland im Zeitraum Januar 2011,“ Stand 14.12.2012 (2012) (in German).

[3] Almaraz Trillo Report, “Neutron noise status in Trillo NPP,” technical report CO-12/043, Spain (2012).

[4] CORTEX project, URL: http://cortex-h2020.eu/about-cortex

[5] W. Zwermann et al., “Nuclear data uncertainty and sensitivity analysis with XSUSA for fuel assembly depletion calculations,” Nuclear Engineering and Technology, **46**, pp.343-352 (2014).

[6] O. Buss, A. Hoefer and J.C. Neuber, “NUDUNA-Nuclear Data Uncertainty Analysis,” In Proceedings of the International Conference on Nuclear Criticality (ICNC2011), Edinburgh, UK, September 19-22 (2011).

[7] F. Bostelmann et al., “Sampling-based Nuclear Data Uncertainty Analysis in Criticality and Depletion Calculations,” In Proceedings of the ANS MC2015, Nashville, TN, USA, April 19-23 (2015).

[8] D. Rochman et al., “Nuclear data uncertainty for criticality-safety: Monte Carlo vs. linear perturbation,” Annals of Nuclear Energy, **92**, pp.150-160 (2016).

[9] M. Hursin et al., “Determination of Sobol Sensitivity Indices for Correlated Inputs with SHARK-X,” PHYSOR 2018, Cancun, Mexico, April 22-26 (2018).

[10] F. Bostelmann et al., “Uncertainty and Sensitivity Analysis in Criticality Calculations with Perturbation Theory and Sampling,” M&C+SNA+MC 2015, Nashville, TN, USA, April 19-23 (2015).

[11] H. Iwamoto, A. Stakovskiy, L. Fiorito and G. Van den Eynde, “Sensitivity and uncertainty analysis of β_{eff} for MYRRHA using a Monte Carlo technique,” EPJ Nuclear Sciences & Technologies, **4**, 42 (2018).

[12] D. Rochman et al., “Nuclear data uncertainty propagation: Perturbation vs. Monte Carlo,” Annals of Nuclear Energy, **38**, pp.942-952 (2011).

[13] L. Fiorito, “Nuclear Data Uncertainty Propagation and Uncertainty Quantification in Nuclear Codes,” Ph.D. Thesis, Universite Libre de Bruxelles, Bruxelles, Belgium, October 3 (2016).

[14] B.T. Rearden, “Criticality safety enhancements for scale 6.2 and beyond,” In Proceedings of the International Conference Nuclear Criticality Safety (ICNC2015), Charlotte, NC, USA, September 13-17 (2015).

[15] D. Rochman, A. Dokhane, A. Vasiliev, H. Ferroukhi and M. Hursin, “Nuclear data uncertainties for core parameters based on Swiss BWR operated cycles,” Annals of Nuclear Energy, **148** (2020).

[16] H. Yi, "Uncertainty and Sensitivity Analysis for Nuclear Reactor Noise Simulations," Master's Thesis in Master Program in Nuclear Science and Technology, Chalmers University of Technology (2017).

[17] V. Lamirand, M. Hursin, P. Frajtag and A. Pautz, "Future Experimental Programmes in the CROCUS Reactor," RRFM/IGORR 2016, Berlin, Germany, March 13-17 (2016).

[18] C. Demazière, "CORE SIM: A multi-purpose neutronic tool for research and education," Annals of Nuclear Energy, **38**, pp.2698-2718 (2011).

[19] Technical University of Dresden, "Training Reactor AKR-2: Technical Description and Procedure of Operation for the Reactor Facility AKR-2," (2015).

[20] A. Mylonakis et al., "CORE SIM+: A flexible diffusion-based solver for neutron noise simulations," Annals of Nuclear Energy, **155**, 108149 (2021).

[21] V. Lamirand et al., "Experimental report of the 1st campaign at AKR-2 and CROCUS," Technical Report D2.1 (2018). URL http://cortex-h2020.eu/wp-content/uploads/2019/07/CORTEX_D2_1_Experimental_Report_of_the_1st_Campaign_at_AKR2_and_CROCUS_V1.pdf

[22] V. Lamirand, G. Perret, M. Hursin, P. Frajtag and A. Rais, "Experimental prospects of the LRS," RT-100-113-15-02 (2015).

[23] A. Vasiliev et al., "Assessment of representativity of the PETALE experiments for validation of Swiss LWRs ex-core dosimetry calculations," EPJ Web of Conferences **239**, 22001 (2020).

[24] Technical University Dresden, "Training Reactor AKR-2: Experiments in Reactor Physics and Radiation Protection," (2019).

[25] Kernkraftwerk Gösgen-Däniken AG (KKG), “Technology and Operation [Brochure],” Retrieved from https://www.kkg.ch/upload/cms/user/KKG_TB_englisch_2016.pdf (2016).

[26] Gösgen, “Data compilation - Gösgen core cycles 39 & 40 – CORTEX,” BER-F-92430, Version 1 (2018).

[27] D. G. Cacuci, “Handbook of Nuclear Engineering,” Springer Science + Business Media (2010).

[28] C. Demazière et al. “Description of scenarios for the simulated data,” Technical Report D3.1 (2019). URL http://cortex-h2020.eu/wp-content/uploads/2019/07/CORTEX_D3_1_Description_of_scenarios_for_the_simulated_data_V1.pdf

[29] V. Lamirand, et al., “Neutron noise experiments in the AKR-2 and CROCUS reactors for the European project CORTEX,” EPJ web of Conferences **225**, 04023 (2020).

[30] V. Lamirand et al., “Experimental report of the 2nd campaign at AKR-2 and CROCUS,” Technical Report D2.2 (2020). URL https://cortex-h2020.eu/wp-content/uploads/2021/03/CORTEX-D2.2-experimental-report-of-the-2nd-campaign-at-AKR-2-and-CROCUS-V2.pdf

[31] A. Jonsson, H. N. Tran, V. Dykin and I. Pázsit, “Analytical investigation of the properties of neutron noise induced by vibrating absorber and control rods,” Kerntechnik 77, **5**, pp.371-380 (2012).

[32] P. Vinai et al., “Final validation report,” Technical Report D2.5 (2021). URL https://cortex-h2020.eu/wp-content/uploads/2021/09/CORTEX_D2_5_Final_validation_report_V1.pdf

[33] S. Yum and Y. Perin, “Results of the sensitivity analyses,” Technical Report D4.5 (2021). URL https://cortex-h2020.eu/wp-content/uploads/2021/08/CORTEX_D4_5_Results_of_the_sensitivity_analyses.pdf

[34] D. E. Newland, “An Introduction to Random Vibrations, Spectral and Wavelet Analysis,” Dover Publications, Incorporated (2012).

[35] P. Pathmanathan, J. M. Cordeiro and R. A. Gra, “Comprehensive Uncertainty Quantification and Sensitivity Analysis for Cardiac Action Potential Models,” Front. Physiol. 10:721. Doi: 10.3389/fphys.2019.00721 (2019).

[36] A. Saltelli, K. Chan, and E.M. Scott (Editors), “Sensitivity analysis.” John Wiley & Sons Ltd., west Sussex (UK) (2000).

[37] T. Zhu, “Sampling-Based Nuclear Data Uncertainty Quantification for Continuous Energy Monte Carlo Codes,” PhD thesis, École Polytechnique Fédérale de Lausanne, Lausanne, Switzerland (2015).

[38] T. Zhu, A. Vasiliev, H. Ferroukhi, A. Pautz and S. Tarantola, “NUSS-RF: stochastic sampling-based tool for nuclear data sensitivity and uncertainty quantification,” Journal of Nuclear Science and technology, **52**, Nos. 7-8, pp.1000-1007 (2015).

[39] S. S. Shapiro, and M. B. Wilk, “An Analysis of Variance Test for Normality (Complete Samples),” Biometrika, **52**, No.3/4, pp. 591-611 (1965).

[40] SPSS Tutorials: SPSS Shapiro-Wilk Test-Quick Tutorial with Example, URL: https://www.spss-tutorials.com/spss-shapiro-wilk-test-for-normality/#shapiro-wilk-test-what-is-it

[41] F. D’Auria and A. Petruzzi, “Background and Qualification of Uncertainty Methods,” THICKET 2008, Pisa, Italy, May 5-9 (2008).

[42] H. Glaeser, “Summary of existing uncertainty methods,” OECD/CSNI Workshop on Best Estimate Methods and Uncertainty Evaluations, Barcelona, Spain, November 16-18 (2011).

[43] E. Hofer, “Probabilistische unsicherheitsanalyses von ergebnissen umfangreicher rechenmodelle,” GRS-A-2002 (1993).

[44] B. Hallee and K. Metzroth, “Evaluation of Wilks’ One-sided Non-parametric Formula Against Analytical parametric Methods,” 2017 ANS Winter Meeting and Nuclear Technology Expo (2017).

[45] Setpoint for Safety-Related Instrumentation, U.S. NRC Regulatory Guide 1.105, Rev.3 (1999).

[46] F. Reventós, “Major Results of the OECD BEMUSE (Best Estimate Methods, Uncertainty and Sensitivity Evaluation) Programme,” THICKET-2008, Pisa, Italy, May 5-9 (2008).

[47] D. F. da Cruz, D. Rochman and A.J. Koning, “Propagation of Nuclear Data Uncertainty for a Control Rod Ejection Accident using the Total Monte-Carlo Method,” PHYSOR 2014, Kyoto, Japan, September 28-October 3 (2014).

[48] J. Toby Mordkoff, The Assumption(s) of Normality, lecture material of psychology department at Iowa University (2000).

[49] Y. Yuan, Y. Khare, X. Wang, P. B. Parajuli, I. Kisekka and S. Finsterle, “Hydrologic and water quality models: Sensitivity, American Society of Agricultural and Biological Engineers, **58(6)**, pp. 1721-1744 (2015).

[50] F. Campolongo, J. Cariboni and A. Saltelli, “An effective screening design for sensitivity analysis of large models,” Environmental Modelling & Software, **22(1)**, pp.1509-1518 (2007).

[51] W. J. Conover, “Practical Nonparametric Statistics,” 3rd ed., John wiley & Sons, New York (1980).

[52] SPSS Tutorials: Pearson Correlation, URL: https://libquides.library.kent.edu/SPSS

[53] D. E. Hinkle, W. Wiersma and S. G. Jurs, “Applied Statistics for the Behavioral Sciences,” Houghton Mifflin (1998).

[54] J. Frost, “Regression Analysis: An Intuitive Guide,” e-book URL “https://statisticsbyjim.com/regression/regression-analysis-intuitive-guide/,” 2019.

[55] T. Most, “Variance-based sensitivity analysis in the presence of correlated input variables,” In 5th international Conference on Reliable Engineering Computing (REC), pp.13-15. Brno, Czec (2012).

[56] H. Glaeser, W. Luther, and B. Krzykacz-Hausmann, “Methodoenentwicklung und exemplarische Anwendungen zur Bestimmung der Aussagesicherheit von rechenprogrammergebnissen,“ GRS Rep., no. GRS-A-3443 (2008).

[57] Mathwork, “Moore-Penrose pseudoinverse,” URL: https://www.mathworks.com/help/matlab/ref/pinv.html

[58] M. Hursin et al., “Determination of Sobol Sensitivity Indices for Correlated Inputs with SHARK-X,” PHYSOR 2018, Cancun, Mexico, April 22-26 (2018).

[59] I. M. Sobol’, “Global sensitivity analysis indices for nonlinear mathematical models and their Monte Carlo estimates,” Mathematics and Computers in simulation, **55**, pp.269-285 (2014).

[60] I. M. Sobol', "Sensitivity analysis for non-linear mathematical models," Mathematical Modeling and Computational Experiment, **1**, pp.407-414 (2013).

[61] B. Iooss, and P. LemaÎtre, "A Review on Global Sensitivity Analysis Methods," Uncertainty Management in Simulation-Optimization of Complex Systems. Operations Research/Computer Science Interfaces Series, **59**, Springer, Boston, MA. https://doi.org/10.1007/978-1-4899-7547-8_5 (2014).

[62] A. Saltelli et al., "Variance based sensitivity analysis of model output. Design and estimator for the total sensitivity index," Computer Physics Communications, **181**, pp. 259-270 (2010).

[63] M. J. W. Jansen, "Analysis of variance designs for model output," Computer Physics Communications, **117**, pp. 35-43 (1999).

[64] X. Sun, S. Roberts, B. Croke, A. Jakeman, "A comparison of global sensitivity techniques and sampling method," 22nd International Congress on Modelling and Simulation, Hobart, Tasmania, Australia, December 3-8 (2017).

[65] D. A. Becker, "Overview of advantages and drawbacks of different methods for sensitivity analysis in the context of performance assessment," 5th IGD-TP Technical Exchange Forum, Kalmar, Sweden, October 28-30 (2014).

[66] Overview of Matlab, URL: https://www.mathworks.com/products/matlab.html

[67] J. Leppänen, M. Pusa, T. Viitanen, V. Valtavirta and T. Kaltiaisenaho, "The Serpent Monte Carlo code: Status, development and applications in 2013," Annals of Nuclear Energy, **82**, pp.142-150 (2015).

[68] J. Leppänen, M. Pusa and E. Fridman, "Overview of methodology for spatial homogenization in the Serpent 2 Monte Carlo code," Annals of Nuclear Energy, **96**, pp.126-136 (2016).

[69] Information about high performance computing with LRZ, URL: https://doku.lrz.de/display/PUBLIC/Access+and+Overview+of+HPC+Systems

[70] C. Demazière, "Development of a 2-D 2-group neutron noise simulator," Annals of Nuclear Energy, **31**, pp.647-680 (2004).

[71] H. Malmir, N. Vosoughi and E. Zahedinejad, "Development of a 2-D 2-group neutron noise simulator for hexagonal geometries," Annals of Nuclear Energy, **37**, pp.1089-1100 (2010).

[72] A. Mylonakis et al., "CORE SIM+ Simulations of COLIBRI Fuel Rods Oscillation Experiments and Comparison with Measurements," PHYSOR 2020, Cambridge, United Kingdom, March 29-April 2 (2020).

[73] C. Lataniotis, S. Marelli and B. Sudret, "Extending Classical Surrogate Modelling to High Dimensions through Supervised Dimensionality Reduction: a Data-Driven Approach," International Journal for Uncertainty Quantification, **10(1)**, pp.55-82 (2020).

[74] I. Couckuyt, Email sent to S. Yum, 19th July (2019).

[75] T. Hengl, "A Practical Guide to Geostatistical Mapping," ISBN 978-90-9024981-0 (2009).

[76] O. Borries, "Surrogate Modelling using DACE," Bachelor of Science Thesis, Technical University of Denmark (2009).

[77] M. Bouhlel, N. Bartoli, A. Otsmane and J. Morlier, “Improving kriging surrogates of high-dimensional design models by Partial Least Squares dimension reduction,” Structural and Multidisciplinary Optimization, **53**, pp.935-952 (2016).

[78] S. O. Lophaven, H. B. Nielsen and J. Søndergaard, “DACE-A Matlab Kriging Toolbox, Version 2.0,” Technical Report IMM-TR-2002-12, Informatics and Mathematical Modelling (IMM)-Technical University of Denmark (2002).

[79] Y. Zhang, et al., “Uncertainty Quantification in CO2 Sequestration Using Surrogate Models from Polynomial Chaos Expansion,” Industrial & Engineering Chemistry Research, **52(9)**, pp. 3121-3132 (2013).

[80] S. Marelli and B. Sudret, “UQLab user manual – Polynomial chaos expansions,” Report # UQLab-V1.3-104, Chair of Risk, Safety and Uncertainty Quantification, ETH Zurich, Switzerland (2019).

[81] R. Schöbi, B. Sudret, J. Wiart, “Polynomial-chaos-based Kriging,” International Journal for Uncertainty Quantification, **5(2)**, pp.171-193 (2015).

[82] S. Marelli and B. Sudret, “UQLab: A framework for uncertainty quantification in Matlab,” Proc. 2nd Int. Conf. on Vulnerability, Risk Analysis and Management (ICVRAM2014), Liverpool, United Kingdom, pp.2554-2563 (2014).

[83] S. Yum et al., “Methodology for uncertainty and sensitivity analysis,” Technical Report D1.1 (2019). URL http://cortex-h2020.eu/wp-content/uploads/2019/07/CORTEX_D1_1_Methodology_for_uncertainty_and_sensitivity_analysis_V1.pdf

[84] David J. Diamond, "Experience Using Phenomena Identification and Ranking Technique (PIRT) for Nuclear Analysis," PHYSOR-2006 Topical Meeting, Vancouver, Canada, September 10-14 (2006).

[85] U. Kasemeyer et al., "Physics of Plutonium Recycling, volume IX, Benchmark on Kinetic Parameters in the CROCUS Reactor," Reports to OECD/NEA Nuclear Science Committee, ISBN 978-92-64-99020-3 (2007).

[86] A. Rais et al., "Neutronics modelling of the CROCUS reactor with SERPENT and PARCS codes," M&C 2017-International Conference on Mathematics & Computational Methods Applied to Nuclear Science & Engineering, Jeju, Korea, April 16-20 (2017).

[87] A. Rais, "PARCS code model of the CROCUS reactor," CORTEX project internal technical report (2018).

[88] J. Leppänen, M. Aufiero, E. Fridman, R. Rachamin, and S. van der Marck, "Calculation of effective point kinetics parameters in the Serpent 2 Monte Carlo code," Annals of Nuclear Energy, **65**, pp.272-279 (2014).

[89] J. Kirchner, "Data Analysis Toolkit #5: Uncertainty Analysis and Error Propagation," (PDF) Berkeley Seismology Laboratory, University of California, Retrieved April 22 (2016).

[90] N. W. Porter, "Wilks' Formula Applied to Computational Tools: A Practical Discussion and Verification," Sandia National Laboratories Report, SAND2019-1901J (2019).

[91] H. Wan, et al., "Sensitivity and Interaction Analysis Based on Sobol' Method and Its Application in a Distributed Flood Forecasting Model," Water, **7**, pp. 2924-2951 (2015).

[92] T. Zhu, A. Vasiliev, H. Ferroukhi, and A. Pautz, “NUSS: A tool for propagating multigroup nuclear data covariances in pointwise ACE-formatted nuclear data using stochastic sampling method,” Annals of Nuclear Energy, **75**, pp.713–722 (2015).

[93] M. Hursin, “PMAX_samples_update_June2020.tar,” Chalmers University FTP (core54.nephy.chalmers.se) /export/zh4/cortex/epfl/PERTURBEDXS/, Unpublished raw data (2020).

[94] P.R. Bevington and K. Robinson, “Data Reduction and Error Analysis for the Physical Sciences,” McGraw-Hill, Boston (2003).

[95] W. Wieselquist, T. Zhu, A. Vasiliev, H. Ferroukhi, "PSI Methodologies for Nuclear Data Uncertainty Propagation with CASMO-5M and MCNPX: Results for OECD/NEA UAM Benchmark Phase I", Science and Technology of Nuclear Installations, **2013**, Article ID 549793 (2013).

[96] W. Press, et al., “Numerical Recipes in C: The Art of Scientific Computing (second ed.),” Cambridge University Press (1992).

[97] S. Yum, et al., “Uncertainty Analyses of Neutron Noise Simulations in a Zero-Power Reactor,” Annals of Nuclear Energy, **174**, 109157 (2022).

[98] V. Lamirand et al., “Analysis of the First COLIBRI Fuel Rods Oscillation Campaign in the CROCUS Reactor for the European Project CORTEX,” PHYSOR 2020, Cambridge, United Kingdom, March 29-April 2 (2020).

[99] C. Demazière, “Description of the models and algorithms used in the CORE SIM neutronic tool,” Chalmers University of Technology, CTH-NT-241 (2011).

[100] N. H. Hsieh et al., "Applying a Global Sensitivity Analysis Workflow to Improve the Computational Efficiencies in Physiologically-Based Pharmacokinetic Modeling," Front. Pharmacol. 9:588. doi: 10.3389/fphar.2018.00588 (2018).

[101] F. Sarrazin, F. Pianosi, and T. Wagener, "Global Sensitivity Analysis of environmental models: Convergence and Validation," Environmental Modelling & Software, **79**, pp.135-152 (2016).

[102] S. Hübner, "AKR-2 adjusted Serpent model," unpublished document. URL https://app.lgi-consulting.org/mso/ecm/cortex-ecm-file-20812

[103] M. Hursin, "Uncertainty Analyses of Neutron Noise Simulations in a Zero-Power Reactor" Unpublished document, Email sent to S. Yum, C. Demazière, P. Vinai and R. Macián, 16th June (2020).

[104] Gösgen, "CORTEX Internal Technical Report," Gösgen Contribution to D 4.2 (2018).

[105] G. Alexandridis et al., "Results of the application and demonstration calculations," Technical Report D4.4 (2021). URL http://cortex-h2020.eu/wp-content/uploads/2020/08/CORTEX-D4.4-Results-of-the-application-and-demonstration-calculations.pdf

[106] Gösgen, "Data compilation - Gösgen core cycles 39 & 40 – CORTEX," BER-F-92430, Version 1 (2018).

[107] B. T. Rearden and M. A. Jessee, "SCALE Code System, ORNL/TM-2005/39, Version 6.2.1," Oak Ridge National Laboratory, Oak Ridge, TN (2016).